ENVIRONMENTAL GEOLOGY OF THE AVON-HEATHCOTE ESTUARY

J.M. Macpherson

A thesis submitted for the degree of Doctor of Philosophy
University of Canterbury, Christchurch, New Zealand
February 1978.

i

ABSTRACT

The Avon-Heathcote is a small, microtidal, predominantly
intertidal, weather-dominated estuary. It has experienced large
alterations to its physical environment as a result of the establishment
and growth of the adjacent Christchurch City, on what was previously a
swampy, dune-bordered coastal plain. During the period 1850-1920 the
tidal compartment decreased by 30%, then returned rapidly to its original
volume. It has since increased to about 30% more than its pre-European
volume. The inlet area progressively changed its configuration to
accommodate these alterations in volume.

An analysis of the energetics of waves and tidal currents shows
that wave-induced shear stresses predominate in this estuary, particularly
above the MTL, and are only exceeded by tidal current stresses in and
adjacent to subtidal channels, where tidal velocities exceed 60 cm/s.
Because of depth limitations the largest waves in this estuary normally
have periods of 1.4 s, amplitudes of 30 cm and lengths of 3.5 m.
Wave energy gradients are due to downfetch variations in wave frequency,
not variations in wave size.

The muddiest sediment occurs close to the entrances of the Avon
and Heathcote rivers, and patterns of mud deposition are regulated
both by rates of sediment supply and by wave energy. The sand fraction
of active surface sediment can be divided into two groups - one
consisting of a single population deposited solely from saltation, the
other consisting of a mixture of this saltation population, and material
deposited from suspension. Sand is only deposited from suspension near
the two river entrances, or on intertidal flats below the MTL, where
wave shear stresses are less than 2 dynes/cm^2.

Shallow cores reveal that a record of the history of this estuary
is preserved in its subsurface sediment. An abiologic, pre-estuarine/
estuarine pre-European/estuarine post-European sequence is recognised
beneath a 15-20 cm deep bioturbation interface. Above this interface
benthic animals have produced a homogeneous mixed layer, depleted of
suspendible fines, which is overlain by a thin and commonly quite
different active layer. The active layer exists independently of trends
in net erosion or deposition of sediment.

ACKNOWLEDGEMENTS

CONTENTS

PART THREE

BATHYMETRY

PART SIX

SUMMARY AND SYNTHESIS

Environmental Geology of the Avon-Heathcote Estuary
Corrections and Amendments

Abs   par. 1 line 2 Rivers.

p. 1   par. 1 6 km^2.

p. 3   par. 1 basin.

p. 4   par. 2 mesotidal.

p. 7   par. 2 Martins 1966, Heinemann.

p. 9   par. 1 $10^6 m^3$.

p. 13   Fig. 5 "B" missing, LH side, centre panel.

p. 18   Fig. 6 RH column consists of values > 20 knots.

p. 23   Fig. 10 directional arrows misidentified - solid arrows indicate
         the mean SW wind; sharp open arrows, the NW; and squat open arrows,
         the E wind.

p. 30   par. 3 p = fluid density.

p. 31   par. 2 orbital velocities should be in cm/s.
         par. 3 omit "geometrical optics and ".

p. 42   par. 4 final sentence should continue "...expediency, in spite
         of the further limitation that in the present case, velocities
         have not been measured 100 cm above the bed."

p. 43   tables should have $\bar{u}$, not $\bar{u}_{100}$, in LH columns.

p. 48   par. 1 sentence 2. location 3 Figure 17, not Figure 20.

p. 52   Fig. 22 Sandy Point.

p. 56   par. 4 sentence 1. Omit words in parentheses.

p. 65   sentence 1, above LWOST; sentence 4, Heathcote.

p. 66   par. 4 and onwards, Maps 3 and 4, not 2 and 3.

p. 74   Fig. 35 A is upper plot, B is lower. Sorted in caption.

p. 75   line 4 magnitude.

p. 77   2nd to last line, log.

p. 78   par. 2 modal.

p. 80   psi = $-\log_2 x$.

p.104   (and onwards), s = standard deviation, N = number of samples.

p.117   Fig. 60. Caption should continue "...subsurface sediment.
         Arrows show mean HAD values of each group."

p.118   Fig. 61. Caption should continue "...sediment. Numbered asterisks
         are group means, with b' mean unnumbered; dashed lines are linear
         regressions fitted to all group b1-b4 samples (short dashes) and
         to group means only (long dashes).

p.128   line 5 presumably.

p.129   par. 3 on not of.

p.154   par. 2 sentence 6 should read "...suspended sand (and mud)..."

p.175   par. 3 1.65 not 1.51 x $10^6 m^3$.

p.194   par. 3 Fig. 84 should be Fig. 85. In Fig. 83 data are from
         Fig. 82, not 33; and in Figure 85 data are from Fig. 84, not 35.

There are no Figures 75 and 76.

GLOSSARY OF FREQUENTLY USED ABBREVIATIONS

AHE = Avon-Heathcote Estuary

CDB = Christchurch Drainage Board

HAD = Height above (Christchurch Drainage Board) datum

HWOST = High water, ordinary spring tide

HWONT = High water, ordinary neap tide

MHW = Mean high water

MTL = Mean tide level (equivalent to mean sea level)

MLW = Mean low water

LWONT = Low water, ordinary neap tide

LWOST = Low water, ordinary spring tide

yBP = Years before present

CERC = Coastal Engineering Research Centre
(of the US Army Corps of Engineers)

LIST OF FIGURES

LIST OF MAPS

INTRODUCTION

This study consists of a detailed examination of the Avon-Heathcote Estuary (AHE), a small (area = 6 km) shallow (mean depth at HWOST = 140 cm) largely intertidal (15% subtidal) estuary surrounded by the eastern suburbs of Christchurch City on the east coast of the South Island, New Zealand (Figure 1). The AHE is a particularly suitable research area because it is a convenient size, it is readily accessible, and because its biology is fairly well known.

Purpose

The primary objective has been to investigate <u>physical</u> changes that have occurred in the AHE as a result of man's activities. This objective has been realised by making a relatively long term (130 year) retrospective assessment of the impact of Christchurch City on the estuary. Contemporary physical processes and the properties of active surface sediment were examined to identify the major sources of physical energy in the estuary, and to show how these affect the transport and deposition of sediment. Subsurface sediment was examined to test the possibility that it contains a record of past environmental conditions.

Previous work

The literature on estuaries is vast, diverse, and difficult to summarise. Good general reviews include the landmark publication edited by Lauff (Estuaries, 1967), physical oceanography texts by Ippen (1966), Dyer (1973) and Officer (1976b), collections of papers edited by Nelson (1973) and Cronin (1975), and numerous papers in scores of international journals. Volume 19(5) of Oceanus is a good review of many aspects of estuarine geology, oceanography and ecology. The innovative manual of simple oceanographic techniques by Wright (1974) is also useful.

1. Definition of an estuary. The most commonly accepted definition is that of Pritchard (1967: "An estuary is a semi-enclosed coastal body of water which has a free connection with the sea and within which sea water is measureably diluted with fresh water derived from land drainage."
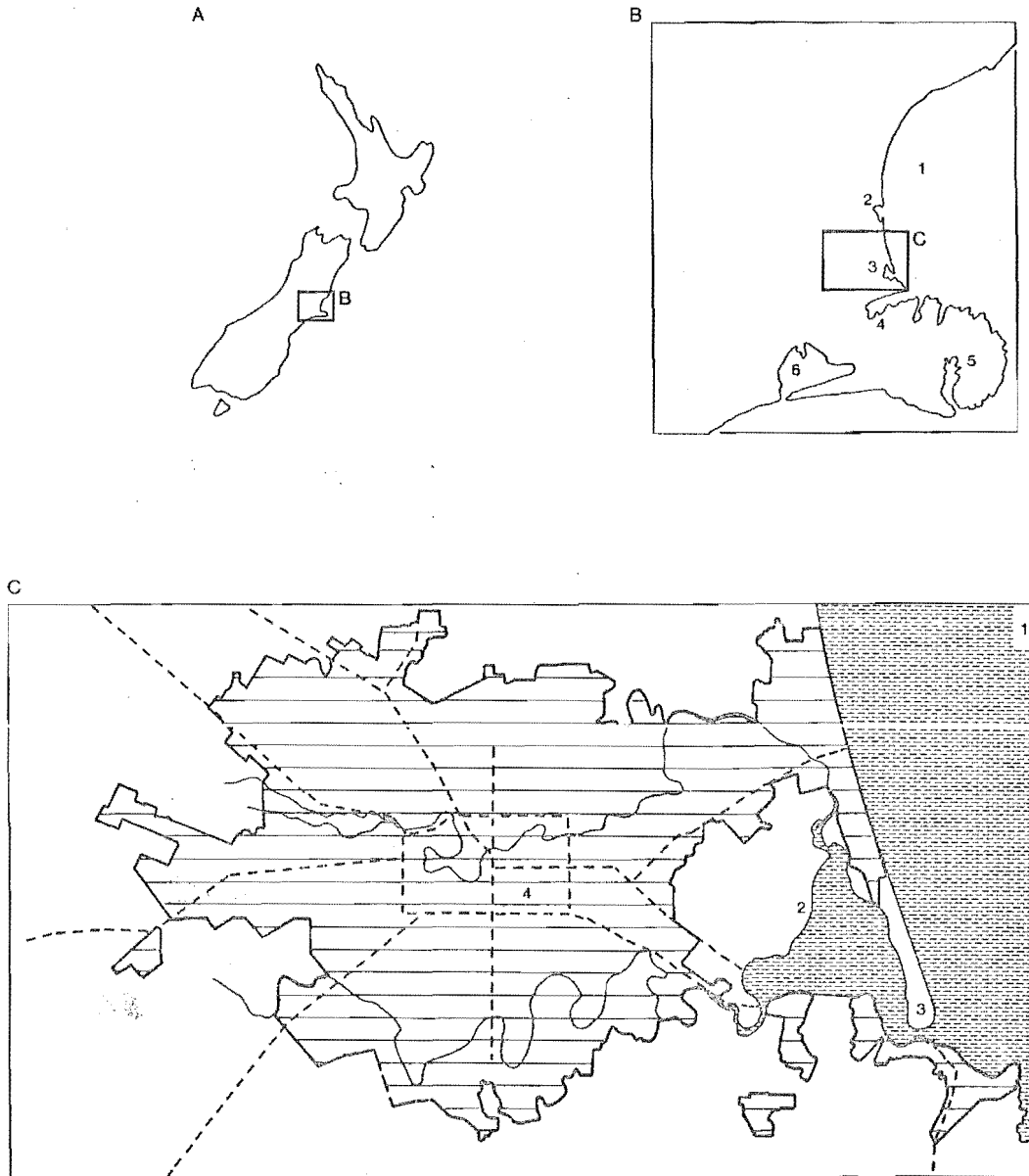
Figure 1. Location maps. A - New Zealand. B - Pegasus Bay (1), mouth of the
Waimakariri River (2), the Avon-Heathcote Estuary (3), Banks Peninsula, with
Lyttelton Harbour (4) and Akaroa Harbour (5), and Lake Ellesmere (6).
C - Detail of southern Pegasus Bay (1) and the Christchurch area, showing the
Avon-Heathcote Estuary (2), Brighton Spit (3) and the urban area (4).

2. *Classification of estuaries.* Various classification schemes for estuaries have been proposed in the past, and these can be grouped into two principal types:

(i)   Those based on the mode of formation of the basis. Thus Pritchard (1967) recognised four varieties: drowned river valleys (also known as coastal plain estuaries), fjords, bar-built estuaries, and those produced by tectonic processes (or all those not fitting the first three classes).

(ii) Those based on different degrees of mixing of fresh and salt water: circulation patterns, the intensity of vertical density stratification, and the extent of lateral homogeneity are the major variables in these classifications (Schubel, 1972; Dyer, 1973; Officer, 1976b). End members are salt-wedge estuaries, where the interface between salt and fresh water is steep and abrupt, and well mixed estuaries, where the water mass may be horizontally as well as vertically homogeneous.

3. *Discussion.* Most of the material published on estuaries is concerned with large, mesotidal, predominantly subtidal coastal plain (river valley) estuaries, where the tidal range may be considerably less than half the mean depth, and where water flowing into the estuary is usually in residence for many tidal cycles. Such estuaries are commonly either partially mixed or highly stratified (Officer, 1976b). Examples are Chesapeake Bay and the New England estuaries of the U.S. Atlantic Coast, the Thames, Tay and Severn estuaries of the U.K., and the Gironde of France.

Research in estuaries of this sort has tended to concentrate on the nature of tidal averaged (mean) flow, the location and dynamics of shoaling areas, the properties and transportation of suspended particulate matter, both organic and inorganic, and the nature and significance of poorly understood phenomena such as occurrences of ephemeral fluid mud -- heavy-metal rich, anaerobic material which may significantly alter the environmental quality of many large estuaries (for example see Officer, 1976a). The turbidity maxima which exist near the landward ends of many large estuaries, various shipping-oriented engineering problems, and environmental problems involving waste disposal are also features which have received considerable attention (for example see Cronin, 1975). Much of this material is irrelevant to the present study, because the AHE is very small,

microtidal, has an almost complete tidal exchange, and is usually
well mixed (for example see Knox and Kilner, 1973).

   4. *The influence of tidal range.* Hayes (1975) has proposed a
useful subclassification of coastal plain and bar-built estuaries
which is based in tidal range, and three classes are recognised:

   (i)   Microtidal - where the tidal range is 0 - 2 m
   (ii) Mestodial - where the tidal range is 2 - 4 m
   (iii) Macrotidal - where the tidal range is > 4 m

   Microtidal estuaries are characterised by storm-surge
and wave-built features, and may have small flood-tide deltas.
Dominant processes are wind and wave induced; currents generated
by the astronomical tide are important transporters of sediment
only at the mouth.

   The channel and shoal morphologies of tidal deltas in
mesotidal estuaries are remarkably similar from place to place,
and conform to basic models, regardless of varying local hydrodynamic
conditions (Coastal Research Group, 1969; Hayes, 1975; Reinson, 1977).
A major feature is the horizontal separation of flood and ebb currents
in the channels of the tidal deltas due to the time-velocity
asymmetry of tidal currents (Postma, 1967; Hayes, 1975). Macrotidal
estuaries are dominated by tidal currents and are usually broad-mouthed
and funnel shaped. Sand bodies are centrally located, linear, and
aligned parallel to the long axis of the estuary. Marginal muddy tidal
flats are common.

   5. *Previous work in the Avon-Heathcote Estuary.* The unpublished
compilation by Knox and Kilner (The ecology of the Avon-Heathcote
Estuary, 1973), prepared for the Christchurch Drainage Board (CDB),
contains a comprehensive summary of scientific work done in and near
the AHE prior to 1972. This work was mostly biological, much of it
directed towards an evaluation of the role of the CDB in the pollution
of the estuary. Several of the individual projects reported in this
compilation briefly examined aspects of the physical environment.
An attempt to summarise this early work would unnecessarily duplicate
Knox and Kilner's excellent review - relevant aspects of it will be
referred to where appropriate in the following report.

PART ONE

HISTORY OF THE AVON-HEATHCOTE ESTUARY

Quaternary history of the Christchurch area

Metropolitan Christchurch and the AHE are situated on a coastal
plain composed of Late Quaternary terrestrial gravels, marine and dune
sands, and estuarine peats and clays (Suggate, 1958, 1968;
Brown, 1975, in press; Wilson, in press). To the south-east, the
metropolitan area spreads on to the lower and western flanks of
Banks Peninsula, which is composed of andesitic and basaltic-andesitic
flows and red-weathering agglomerates of the Lyttelton Volcanics
(Figure 2). Yellow loess, predominantly of coarse silt, mantles the
lower flanks of the volcanic cone.

During the last 5 000 years the Pegasus Bay coastline has
migrated eastwards (D.D. Wilson, pers. comm.), leaving behind a
sequence of surface sediments which progresses from inland peat
and swamp remnants, alluvial silt and fluviatile gravels, through
sand deposits and fixed and semi-fixed dunes, to the modern beach
(Figure 2). Biggs (1947) recognised three separate dune belts
within the coastal part of this sequence (shown undifferentiated in
Figure 2); Blake (1964) dated the oldest (inland) belt at about
4 000 to 5 500 yBP, the central belt at 1 000 to 2 000 yBP, and the
youngest belt, landward of the active dunes of the modern beach, at
400 to 1 000 yBP. Dune remnants of the second belt occur west of
the AHE, while sand of the younger belt occurs to the north-east –
indicating that the estuary probably first appeared between 1 000
and 2 000 years ago. The western edge of the modern estuary is
inferred to be the approximate position of the coast at the time
of formation of the second dune belt, and Sandy Point (Map 1) is
interpreted as an abandoned spit hook, analogous to the present one
several thousand metres to the east.
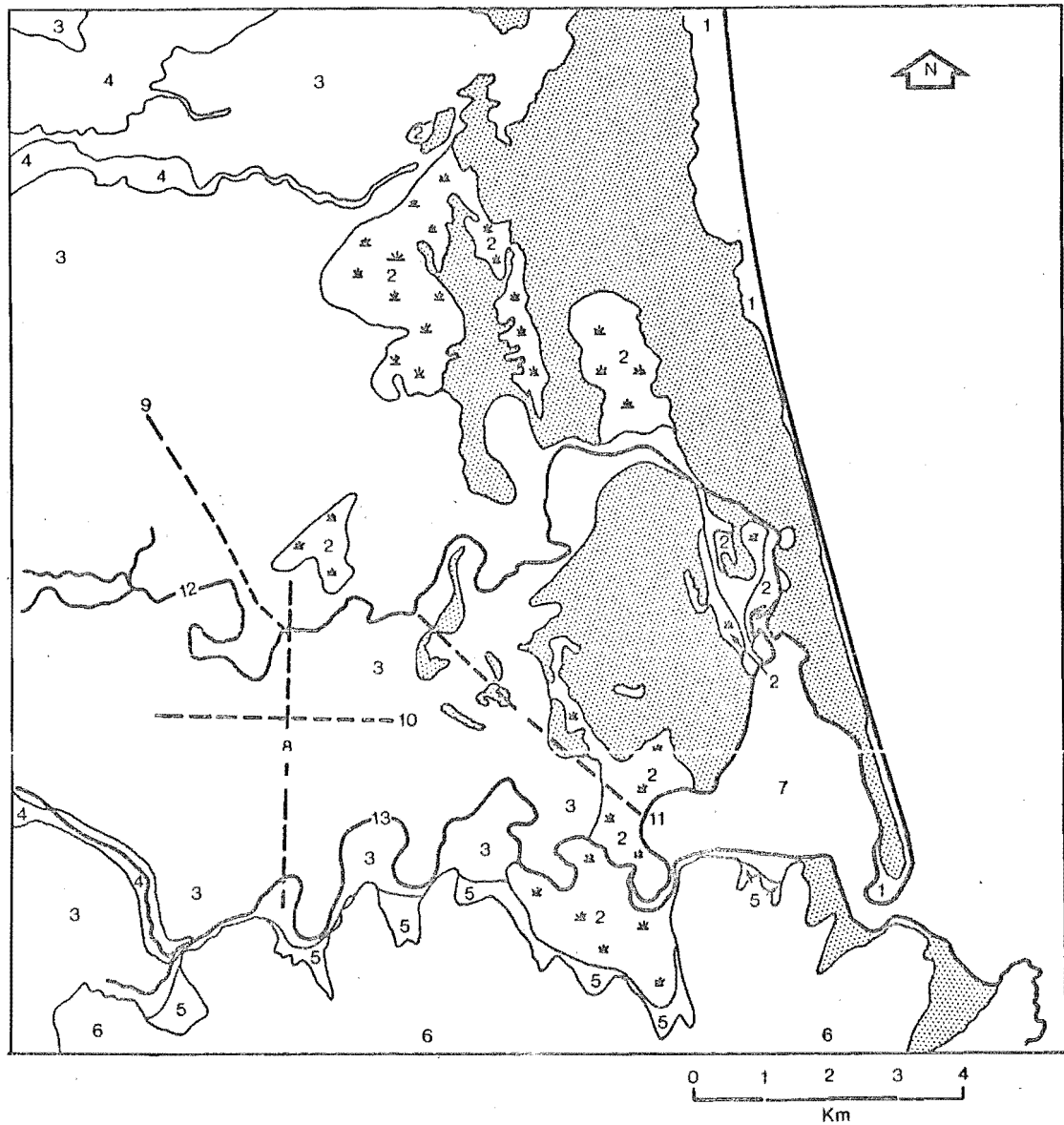
Figure 2. Geology of the Christchurch area. After Brown (1975, in press). Fixed and semi-fixed dunes and inland sand deposits are stippled. Other features include active dunes and the modern beach (1), drained peat swamps (2), alluvial silt deposits (3), fluviatile gravel of the river flood plains (4), loess areas (5) and volcanic rock of the Tertiary Lyttelton Volcanoe (6). Numbered localities include the Avon-Heathcote Estuary (7), Colombo Street (8), Papanui Road (9), Moorhouse Avenue (10), Linwood Avenue (11), the Avon River (12) and the Heathcote River (13).

Post-European history of the Avon-Heathcote Estuary

1. Introduction and discussion. The common fate of estuaries is to fill with sediment (Roberts and Pierce, 1974), and some have done so in historical times - for example the River Dee in England (Leggate, 1973). Estuaries are infilled with sediment because they are very efficient sediment sinks, accumulating almost all material entering them from both land and offshore sources (Meade, 1974). Many estuaries have filled rapidly with sediment since the beginning of the 20th Century because of landuse changes in their catchment areas (Roberts and Pierce, 1974). A major cause of accelerated infilling is the conversion of large proportions of estuarine catchments from rural to urban uses.

The effects of urbanisation on adjacent waterways are well known (Savani and Kamerer, 1961; Lindh, 1972; Guy and Jones, 1973; Heinmann and Piest, 1973). During the early urban stage - when vegetation cover is removed, some houses are built, wells are drilled and sanitary drains dug -- there is an increase in stormwater flow, an increase in soil moisture, a rise in the water table, and some waterlogging of land. As a result sediment yields increase, and sediment accumulates rapidly in nearby streams. In later stages the combination of increasing impervious cover (roofs and roads) and more efficient drainage results in increasing volumes of storm runoff and a reduction in the runoff lag time - the time between the centre of mass of a rainstorm and the centre of mass of the resulting runoff (Martins, 1968; Leopold, 1968; Detwyler, 1971).

During post-urban basin stabilisation (Guy and Jones, 1972, p.2109) sediment deposited in streams and other water bodies during early urbanisation is re-eroded, as the rate of sediment supply decreases, but runoff volumes and flood flows continue to increase. As further stabilisation occurs watercourses are stripped of sediment deposited during early development, and often increase beyond their original dimensions to accommodate the increasing flow. Sediment moving through and beyond these enlarging channels will usually be considerably coarser than sediment yielded during construction.

2. Urbanisation and drainage modifications in the Christchurch area. The first European settlers arrived in the Christchurch area in 1850, and by 1875 the population had risen to more than 10 600 (Retter, pers. comm.). Early maps of the area (known as Black Maps and held by the Lands and Survey Department, Christchurch - see Scott (1963) for a redrafted version) indicate that in about 1850 the area which is now Christchurch City was predominantly wet marshy land, with shallow ponds and shaking bogs, vegetated with rushes, flax and ferns. To the east the older parts of the dune complex were covered with grasses and Manuka, while the youngest, easternmost dunes were unvegetated. Areas of open grassland were interspersed between the swamps and sandhills.

In the earliest days of settlement surface water in the area was clear and pure in appearance, and quite suitable for drinking (Scott, 1963, p.68). However, as the population grew, the quality of the surface water declined, and after rain the area was often a "... pestilential swamp" (Hercus, 1942). Although early drainage works were undertaken by the Canterbury Provincial Council, a lack of unanimity and purpose meant that it was 1878 before the newly formed Christchurch Drainage Board (CDB) could begin an underground sewage and stormwater network. By 1901, 54 km of pipes were laid, and 3.2×10^6 gallons of effluent flowed daily to a sewage farm near the present day oxidation ponds (immediately to the west of the estuary). As a result the quality of surface water in the area improved, and in 1890 the Colonial analyst reported that water entering the estuary after passing through the new sewage farm was "... deprived of any harmfull constituents" (Hercus, 1942, p.57).

Although it was never intended to, the sewage system altered surface runoff characteristics. By 1930, a minimum of 600 gallons/acre/day of groundwater entered the sewers from the City area (Scott, 1963), reducing surface runoff from unpaved areas as a result. The significance of this effect is illustrated by the observation that in 1930, 30% of the freshwater catchment of the AHE (which covers an area of 73 miles^2 and contains 75 miles of natural watercourses) was serviced by sewers, with a total length of 152 miles (Scott, 1963).

3. Changes in the tidal compartment of the Avon-Heathcote Estuary: It is reasonable to expect that radical alterations to the hydraulics and hydrology of the freshwater catchment of the AHE, an

inevitable result of the growth of Christchurch City, would cause an accelerated rate of infilling, and a sympathetic decrease in the volume of the tidal compartment (defined as the volume of water in the estuary at high tide, minus the amount that remains at low tide). It has been possible to make a total of 10 estimates of historical volumes of the tidal compartment of this estuary, using the methods outlined in Appendix 1. Figure 3 shows the resulting trend, and also shows changes in population numbers, in the length of the sewage-stormwater system, and in the amount of effluent released into the estuary from CDB treatment works. The results summarised in Figure 3 are interpreted to mean that the tidal compartment decreased in volume from 1850 onwards, reaching a value of 4.8 to 5.0×10^6 m sometime between 1875 and 1900. This was a decrease of about 30% from the pre-European value of 7.7×10^6 m . The volume subsequently increased, quite rapidly from about 1900 to 1920, less rapidly thereafter, to reach a value of about 10.9×10^6 m in 1975 (30% more than in 1850).

Figure 3 reveals that the decreasing tidal compartment trend was reversed at about the time that the CDB began to rationalise the City drainage system (in about 1880). The subsequent rapid increase in volume was paralleled by increases in the length of the City's drainage system, suggesting that there may be a fundamental link between changes in the tidal compartment and the rate of modification of the freshwater catchment of the estuary.

4. Discussion and conclusions. Human activities which alter geomorphic systems often do so by disrupting natural steady-state or quasi-equilibrium conditions (for example, see Graf, 1977). Because fluvial systems are particularly sensitive to changes in landuse, they are especially susceptible to disruption. After the initial disturbance, they begin to change quickly, and approach new equilibria at exponentially decreasing rates. In Figure 4, two diagrammatic exponential functions are fitted to data from Appendix 1, and these show that changes in the tidal compartment of the AHE may be qualitatively modelled as two exponential functions, suggesting that the estuary has responded to two separate geomorphic disruptions. The first was due to the rapid early settlement of the area, when drainage work lagged behind urban growth, and when the volume of sediment supplied to the Avon and Heathcote Rivers probably increased steeply. This sediment was presumably deposited in the estuary, causing the decrease in the tidal compartment shown in Figure 4.

Figure 3. Christchurch and suburbs. Population, miles of stormwater and sewage pipes, volumes of effluent released into the estuary from CDB treatment works, and changes in the volume of the tidal compartment of the AHE for the period from 1850 to 1975. Circles (○) show each of the 10 estimates of the volume of the tidal compartment from Figure 79. The heavy line is fitted to mean values for about 1908 and for 1920. The low value at 1964 is predicted from the Purkert-Heath relationship, see Appendix 1.
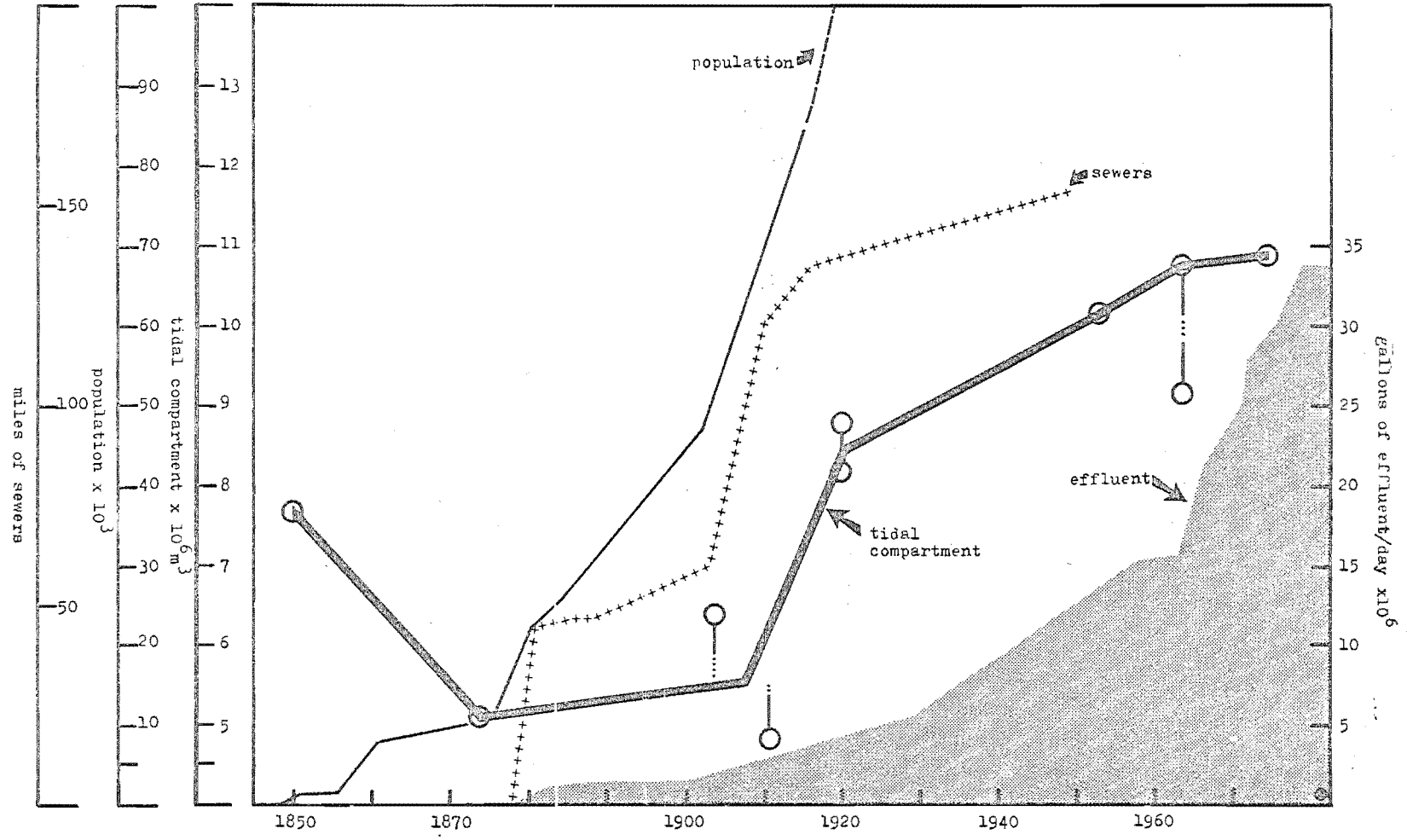
Data from Hercus (1942), Knox and Kilner (1973), Retter (personal communication), Scott (1963) and from Wigram (1916).
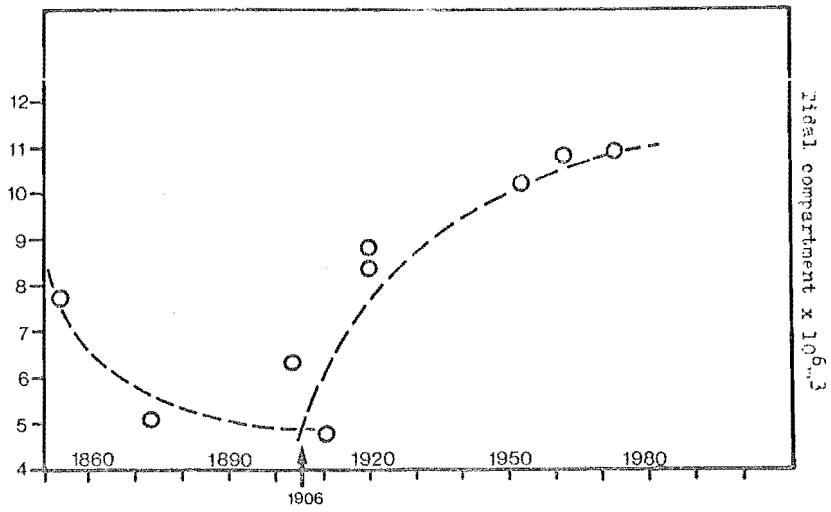
Figure 4. Diagramatic representation of exponential changes in the volume of the
tidal compartment of the Avon-Heathcote Estuary, for the period 1850 – 1980.

The second disruption, which reversed (or overwhelmed) the first, was probably a combined effect of reduced sediment supply due to drainage basin stabilisation, and of changes in both the storm- and low-flow runoff response of the area. The second curve now appears to be asymptotically approaching a new, post-urban equilibrium state.

5. *Changes at the inlet to the estuary, 1850-1975.* As well as internal volumetric changes, the estuary has experienced major changes in the configuration of its inlet area since 1850. The early maps of *HMS Pandora* (1854), Elliot (1874), McIntyre-Lewis (1904), of the Lyttelton Harbour Board survey (1920), of *HMNZS Lachlan* (1950) and of the 1970 Wallingford Report (all supplied to the writer by the CDB), provide valuable documentation of these changes. Figure 5 is a series of maps which summarise major changes that have occurred in the inlet area during the period 1854-1975. Many of these changes have been reported previously (by Pearce, 1951; Scott, 1955; Hutchinson, 1972; Knox and Kilner, 1973; and Millward, 1975), and have been interpreted as responses to inexplicable variations in onshore wave energy, longshore sediment supply, river flow, or all three.

The changes shown in Figure 5 occurred in three phases: the first, from 1850 to about 1928, saw the outlet change little, except that during the early years the arcuate southern channel carried most of the flow through Moncks Bay, and by 1928 the northern, diagonal channel carried most of the flow. The second phase, from about the mid 1920's to the mid 1950's, saw a major reorganisation occur, with most changes happening during winter storms (Pearce, 1950; Hutchinson, 1972). The principal subtidal channel migrated south into Moncks Bay, the spit grew south and west, sand was deposited on Clifton Beach (previously a rocky shore), and the ebb delta migrated north about 500 m. As the ebb delta migrated north, the wave climate of Sumner Beach changed, because the delta had previously sheltered Sumner from large waves from the east and north-east. Severe erosion of the beach threatened seaside real estate, and expensive coast protection work was necessary (Scott, 1955; Macpherson, 1976). During the third phase, from 1955 to the present, the rate of change slowed, and the result is the configuration shown in Figure 5D.

Significant changes did not occur at the outlet until the late 1920's, when the tidal compartment of the estuary first exceeded the

A

Configuration of the principal sub-
tidal channel and associated sand
bodies between 1854 and 1928. The
numbered localities are Beachville
Road (showing the position of the
present-day seawall(1)), Moncks Bay
(2), Shag Rock (3), Cave Rock (Cave
Island on early charts)(4), and
Sumner Beach (5). Note location of
the high water mark (6), the low
water mark (7), the 2 metres depth
contour (·····), the ebb tide delta
(8), the principal subtidal channel
(⟹), and the flood tide flow
pattern (⇩).

About 1935 to about 1946

C

1946 to about 1955

D

The configuration in 1975. Note the
landward migration of the 2 metre depth
contour (from 9 to 10), the northwards
migration of the ebb delta (11 to 12),
southwards migration of the principal
subtidal channel (13), the disappearance
of Sumner beach (14) and the growth of a
large new beach at Clifton (15). Note also
the presence of a well developed ebb spit
and flood ramp (16), and a flood tide
channel (17).

0   500
metres

Figure 5. Synoptic maps of changes in the inlet area of the Avon-Heathcote
Estuary for the period 1850 to 1975.

pre-European volume of about 8×10^6 m^3. Most of the changes occurred relatively quickly between 1930 and 1960, when the tidal compartment increased rapidly from 8 to 10×10^6 m^3. The writer's interpretation is that the changes shown in Figure 5 were an orderly, progressive response to accommodate the increasing volumes of water flowing through the inlet. The tidal compartment curve in Figure 4 appears to be asymptotically approaching a value of about 11×10^6 m^3, and the inlet has changed little in recent years. The 1975 configuration shown in Figure 5D has a more efficient, symetrical appearance than configurations preceding it, and appears similar in shape to high energy, mesotidal inlets associated with large bar-built estuaries, such as those on parts of the U.S. Atlantic Coast (for example, see Lynch-Blosse and Kumar, 1976).

The cross-sectional area of a stable tidal inlet (with a supply of sediment) is coupled to the flow of water through the inlet by a critical shear stress relationship, in which the maximum current speed is 1.14 m/s (Heath, 1975; Bruun and Gerritson, 1960). This is the theoretical basis of the Furkert-Heath relationship, and it means that all other things being equal, changes in the tidal compartment will cause an inlet to erode or deposit sediment to maintain a maximum throughgoing current speed of 1.14 m/s. The broad nature of this relationship is clearly illustrated in Heath's data, where 16 quite different New Zealand tidal inlets conform to the Furkert-Heath relationship, in spite of wide variations in offshore bathymetry, onshore wave energy, and rate of sediment supply (Heath, 1975, pp.453-454). Walton (1977) has recorded that in some mobile U.S. tidal inlets, there is a linear relationship between the volume of sand stored in the ebb delta (the "outer bar" of Walton), and the cross-sectional area of the adjacent inlet. This relationship is functionally analogous to the Furkert-Heath relationship, and it is interesting to note that the 1975 ebb delta in Figure 5D is larger than the ebb delta in 5A (at least, the 2 m depth contour is displaced further seaward in 1975), which probably means that it contains more sand and is acting as a depository of sand removed from the inlet as the tidal compartment increased. This interpretation lends qualitative support to the conclusion that the configuration, as well as the cross-sectional area of the inlet system has historically been regulated by the amount of water flowing through it.

It has been assumed in the past that man-induced changes in the AHE are a 20th Century event. For example, Knox and Kilner (1973) considered the first biological survey of the estuary (by Thompson, in 1929) to be a useful baseline, against which subsequent changes may be evaluated. The information in Figures 3 and 4 suggests that Thompson saw the estuary in a substantially altered state, and that the use of his observations to assay present-day features may be seriously misleading. It has also long been assumed that the estuary is filling with sediment (Knox and Kilner, 1973; J.A. Robb, pers. comm.). That the opposite is true is a surprising discovery, particularly in view of the reasonable expectation that this estuary would react to post-European changes by accumulating sediment. The discovery that both of these assumption are incorrect will fundamentally influence the following sections of this report.

PART TWO

ENERGETICS - WAVES AND THE TIDE

Introduction

From Part One it is clear that the growth of Christchurch City
has had a major impact on the Avon-Heathcote Estuary. Since the AHE
is predominantly intertidal, intertidal processes have probably
figured largely in this impact. According to Hayes (1975), microtidal
estuaries are dominated by wave generated processes, and an analysis
of wave energy is an appropriate place to begin the description of
physical intertidal processes.

Waves and wave hindcasting

Gathering statistically meaningful field data on waves is an
expensive and technically difficult process, especially in shallow
water, where waves may be influenced by local bathymetry (U.S. Army,
Corps of Engineers, 1962). A more efficient method is to predict
wave dimensions from a knowledge of the wind energy available to build
waves. This process is known as wave hindcasting (predicting waves
from past meteorological records), and the techniques, limitations and
shortcomings of the methods involved are quite well known. The
principal reference is the U.S. Army Coastal Engineering Research
Centre, Shore Protection Manual (CERC, 1973; and subsequent updates)

1. Wind characteristics. The first step in wave hindcasting
is to estimate surface wind speeds and directions. The CDB operates
a recording anemometer at Bromley, about 5 km west of the estuary.
Daily records are routinely analysed by the New Zealand Meteorological
Service, and a 5 year run of such analyses was made available by the
CDB. The 5 year record (from April 1st 1967 to March 31st 1972)
consisted of wind speeds and directions at exact hours 0100 to 2400,
NZ Standard Time, with speed in knots (where 1 knot = approximately
0.5 m/s) and directions in 10° arcs.

Since waves only occur when the tide is in, it is sufficient to
consider wind which blows for some arbitrary period corresponding to
high tide - in this study high tide ± 2 hours was chosen.

High tide times for the period covered by the wind record were obtained
from the NZ Nautical Almanack (1967-1972), with tide times for the
estuary assumed to be the times predicted for Lyttelton, plus 1 hour
(Consultants Report, 1973).

A list of high tide times (rounded to the nearest half hour)
was prepared for the 5 year period (a total of 3 586 tides). Wind
speeds and directions at each hour for 2 hours either side of high tide
were also listed, giving either 4 or 5 wind vectors, depending on
whether high tide occurred closest to a whole or half hour. Mean wind
speeds and directions were calculated for each high tide, and
variations in both speed and direction were also recorded. These pairs
of mean values are termed wind events. If the wind was calm for three
or more of the readings involved in each event, the high tide was
recorded as a calm. High tides where no data was recorded (mainly
because of instrument malfunctions) were also noted. The wind was
calm, or not recorded, for a total of 1 364 tides during the 5 year
period (38% of all events). About 10% of all events were 'no data'
events.

A wind event frequency table was constructed (Figure 6), from
which it is clear that wind events in the AHE are directionally
anisotropic, clustering about 090° (easterlies) and 260° (south-
westerlies). The purpose of a wind analysis is to determine the amount
of energy available to make waves. Thus estimates of wind stress are
also necessary. Wind stress (E_w) is defined as force/unit area acting
on the water surface, where E_w increases with increasing wind speed (U)
more rapidly than U^2, but less rapidly than U^3, so that

$$E_w \propto U^{2-3} \qquad \text{(Monk, 1955)}.$$

If E_w is assumed to increase in proportion to U^2 (for example, see
Bokuniewicz and others, 1975), then the results will be conservative
estimates of wind stress.

Multiplying U^2 by frequency for the wind speed classes in
Figure 6 yields dimensionless parameters of wind stress, which for
convenience may be recalculated as percentages (Figure 7). Low speed
wind events are more variable in both speed and direction than faster
events, and are relatively insignificant producers of waves, so wind
events with mean speeds of less than 10 knots (5 m/s) are disregarded.
The resulting distribution of effective wind stress (E_{wf}) forms the
basis of subsequent analyses.

MEAN DIRECTION   MEAN SPEED (KNOTS)

MEAN DIRECTION	2	3	4	5	6	7	8	9	10	11	12	13	14	15	16	17	18	19	20
010	0	2	3	2	1	2	1	1	3	2	1	1	1	2	0	1			
020	0	2	1	1	1	0	1	0	2	1	2	2	1						
030	0	1	2	4	3	4	2	3	2	3	2	0	0	2					
040	1	2	7	5	3	5	4	4	3	3	1	0	2	0	1	0	0	0	0	1
050	3	1	6	6	8	5	6	3	7	5	2	3	2	1					
060	6	13	7	17	10	13	4	9	6	8	6	4	1	2					
070	10	12	14	20	26	29	21	14	19	9	8	5	2	1	1	1			
080	18	15	14	26	30	34	24	22	22	14	8	3	5	2	2	0	0	0	0	1
090	14	21	15	23	18	25	24	25	24	13	12	6	4	4	1	1			
100	13	11	12	20	21	23	30	31	17	15	9	4	5	7	1				
110	6	15	17	9	7	11	9	9	11	4	6	7	1	3	1				
120	2	4	3	2	3	7	1	1	2	3	1	0	0	0	1				
130	2	0	0	2	1	1	1	2	1	0	0	0	0	0	0	0	0	0	0	1
140	2	1	0	0	0	3	0	.1	0	0	0	1							
150	1	0	1	1	1														
160	0																		
170	0	1	2	0	0	3	1	0	1										
180	0	1	1	0	2	3	2	1	1	3									
190	1	2	2	1	0	0	1	2	5	5	0	0	1						
200	2	0	1	4	6	7	4	3	9	2	3	3	5	2	0	0	1	1	
210	2	4	4	6	6	1	7	3	4	4	3	3	3	0	2	2	0	0	0	2
220	3	4	2	5	5	12	3	4	6	5	4	6	3	2	1	3	1	0	1	3
230	7	3	2	4	4	6	9	4	9	1	11	3	2	1	1				
240	9	11	7	3	6	12	4	9	8	4	0	2	0	2	0	0	0	1	
250	15	12	18	13	7	9	6	6	5	4	0	1	0	0	0	0	1		
260	9	18	12	16	23	8	4	4	2	1	2	0	0	0	0	0	0	0	1	1
270	14	12	14	13	12	6	5	4	3	0	0	1	1						
280	8	6	18	3	8	4	2	0	0	2									
290	10	4	9	7	2	2	2	0	0	0	0	0	1	3	0	0	1	0	1
300	5	5	0	3	0	1	1	1	2	0	0	3	1	3	1	0	1	1	0	1
310	1	3	1	0	1	1	2	2	1	4	1	1	2	0	1	2	1	0	0	1
320	1	4	1	1	0	1	2	2	2	0	1	1	0	0	0	1	2	0	1
330	1	4	2	0	0	2	4	1	2	0	1	2	0	2	0	1	0	0	0	1
340	1	0	0	1	3	1	1	2	2	1	1	1	1	0	0	1	1		
350	0	0	2	0	1	1	2	2	5	0	3	1	1	2	0	0	0	1	
360	2	2	3	2	1	1	2	0	0	0	3	4	3	1					
TOTAL EVENTS	177	196	203	220	219	243	192	175	186	116	91	68	48	42	14	13	9	4	4	12
PERCENT of TOTAL EVENTS	7.93	8.78	9.09	9.86	9.81	10.89	8.60	7.84	8.33	5.20	4.08	3.05	2.15	1.80	0.63	0.58	0.40	0.18	0.18	0.52

TOTAL EVENTS = 2232

PERCENT of TOTAL EVENTS = 99.10%

Figure 6. Wind event frequency table. Mean wind speed and direction for each of 2 232 high tides for the period 04 1967 to 03 1972.

DIRECTION	NUMBER OF EVENTS	PERCENT OF TOTAL EVENTS	E_w	PERCENT OF TOTAL E_w	NUMBER OF EVENTS ≥ 10 KNOTS	PERCENT OF TOTAL EVENTS	E_{wf} (≥ 10 KNOTS)	PERCENT OF E_{wf} (≥ 10KNOTS)
010	23	1.04	2185	1.44	11	1.81	1790	1.87
020	14	0.63	1302	0.86	8	1.31	1143	1.20
030	28	1.27	2157	1.42	9	1.48	1301	1.36
040	41	1.86	3096	2.05	11	1.81	1896	1.99
050	55	2.50	4156	2.75	20	3.29	2717	2.85
060	100	4.54	6482	4.28	27	4.45	3754	3.93
070	182	8.26	11846	7.83	46	7.58	6148	6.44
080	222	10.08	15009	9.92	57	9.39	7891	8.27
090	216	9.81	15438	10.21	65	10.71	8944	9.37
100	206	9.35	13655	9.03	58	9.55	8298	8.69
110	158	7.17	7510	4.96	33	5.44	4758	4.98
120	30	1.36	1701	1.12	7	1.15	963	1.01
130	11	0.50	910	0.60	2	0.33	541	0.57
140	8	0.36	414	0.27	1	0.16	169	0.18
150	4	0.18	81	0.05	0	----	----	----
160	0	----	----	----	0	----	----	----
170	8	0.36	352	0.23	1	0.16	100	0.10
180	14	0.63	916	0.60	4	0.66	436	0.46
190	20	0.91	1606	1.06	11	1.81	1301	1.36
200	53	2.41	5378	3.55	26	4.28	4196	4.40
210	56	2.54	5732	3.79	23	3.79	4518	4.73
220	73	3.31	8762	5.79	35	5.77	7273	7.62
230	67	3.04	5510	3.64	25	4.61	3985	4.17
240	78	3.54	4544	3.00	17	2.80	2433	2.55
250	97	4.40	3821	2.53	11	1.81	1477	1.55
260	101	4.58	4383	2.89	7	1.15	1793	1.88
270	85	3.86	2748	1.81	5	0.82	665	0.70
280	51	2.31	1303	0.86	2	0.33	242	0.25
290	42	1.91	2288	1.51	6	0.99	1595	1.67
300	29	1.31	3294	2.17	13	2.14	2960	3.10
310	25	1.13	3310	2.18	14	2.30	2888	3.02
320	20	0.91	2266	1.50	8	1.31	1850	1.94
330	23	1.04	2457	1.62	9	1.48	1950	2.04
340	17	0.77	1855	1.22	8	1.31	1443	1.51
350	21	0.95	2515	0.66	13	2.14	2108	2.21
360	24	1.09	2258	1.49	11	1.81	1921	2.01

Figure 7. Derivation of wind stress (E_w) and effective wind stress (E_{wf}).

Figure 8 shows the directional properties of the four distributions generated above, and from Figure 8 it is clear that three preferred directions are significant in the wind energy field of the AHE: 48% of all E_{wf} occurs between 030° and 110°, 30% between 190° and 270°, and 20% between 290° and 010°.

To simplify analyses based on the wind stress values produced above, mean values for each of the preferred directions shown in Figure 8 were calculated, using a graphical technique analogous to that used for calculating the properties of grain size distributions. Percentages of E_{wf} for each of the three wind directions were recalculated to 100 (Figure 9), and plotted on probability paper as cumulative curves. The appropriate percentiles were then read from the curves, and graphic mean values calculated.

Figure 6 shows that high speed winds are unequally distributed – south-westerlies tend to be higher velocity events than north-westerlies, which tend to be higher velocity events than easterlies. If all wind events less than 15 knots (7.5 m/s) are omitted from the calculation, easterlies produce only 28 per cent of all E_{wf}, south-westerlies 36 per cent, and north-westerlies 34 per cent. Compare this to calculations based on all data in Figure 6, which indicate that westerlies produce about 70 per cent of total E_{wf}. This means that although east winds are more persistent, they may not contribute as much energy as either of the west winds.

The CERC wave prediction method assumes that deviations from mean wind directions do not exceed 45°, and that wind speeds do not vary more than 5 knots (2.5 m/s) from mean values (CERC Manual, pp.3-27). Confidence in predicted results deteriorates significantly when deviations exceed these limits. In many hindcasting predictions, wind duration is also significant, but in small enclosed bodies of water it is unlikely to impose limits on wave estimates (Sutherland, 1977).

Inspection of instrument traces from the Bromley anemometer indicates that these constraints on speed and direction variability are probably only exceeded in one of every 12 or 15 events, and the effect of limited duration (when the wind blows for less than half the 4 hour high tide period, for example) is only significant in perhaps one event in every 30. Since the simplified hindcasting method employed in this project will be accurate within 20% for only about two thirds of the time (CERC Manual, pp.3-33), it has been assumed that

Figure 8. Frequency distributions of wind stress, effective wind stress, percent total wind events, and percent total wind events greater than or equal to 10 knots (5m/s).

96.21% of all E_{wf} is accounted for in three 90° sectors; 030–110°, 190–270°, 290–010°, distributed about the three mean directions shown.

Percent of total (all wind events)

Percent of total (events ≥ knots)

Direction (10° arcs)

21
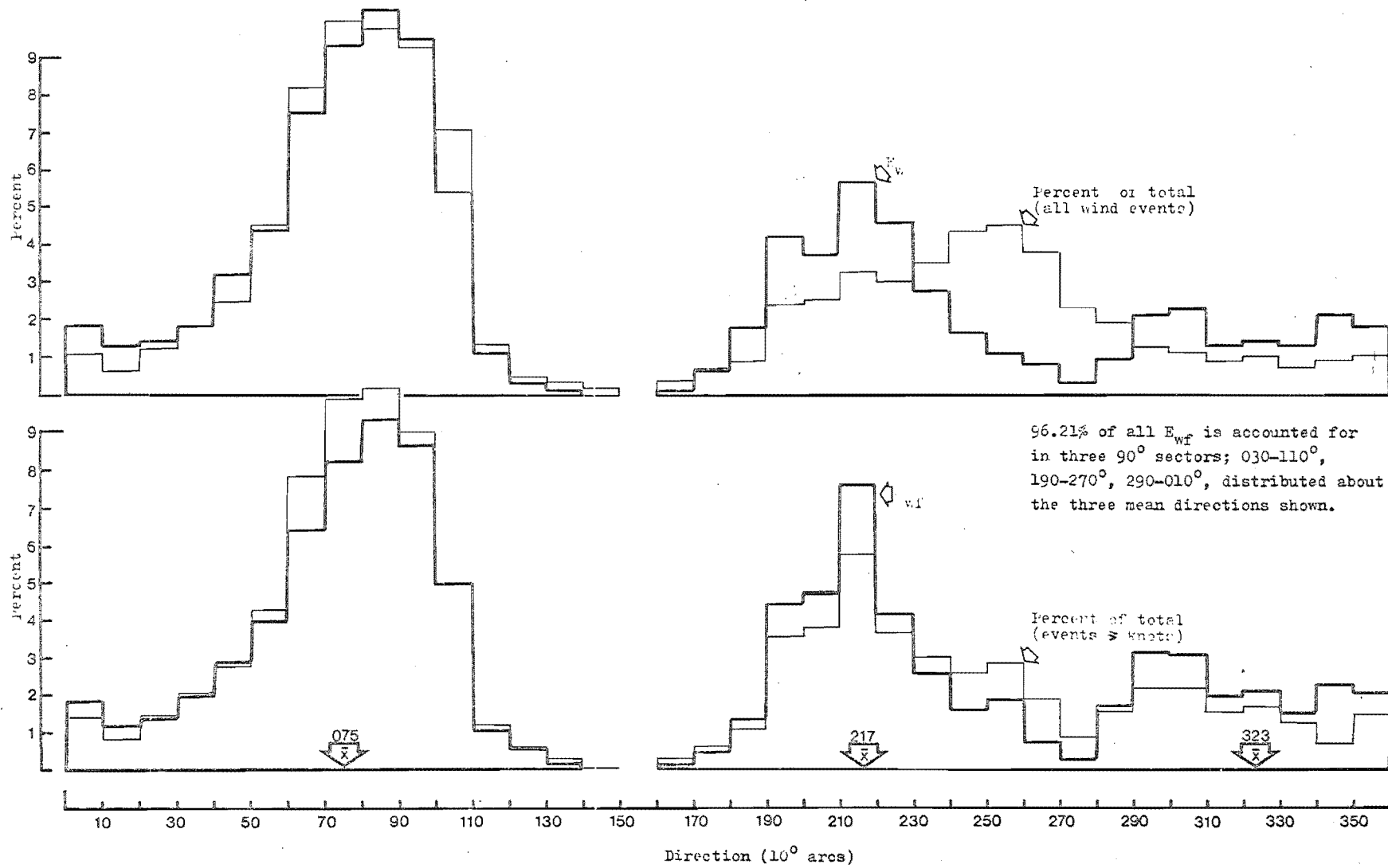
CUMULATIVE PERCENT CURVES FOR THE
THREE PREFERRED DIRECTIONS
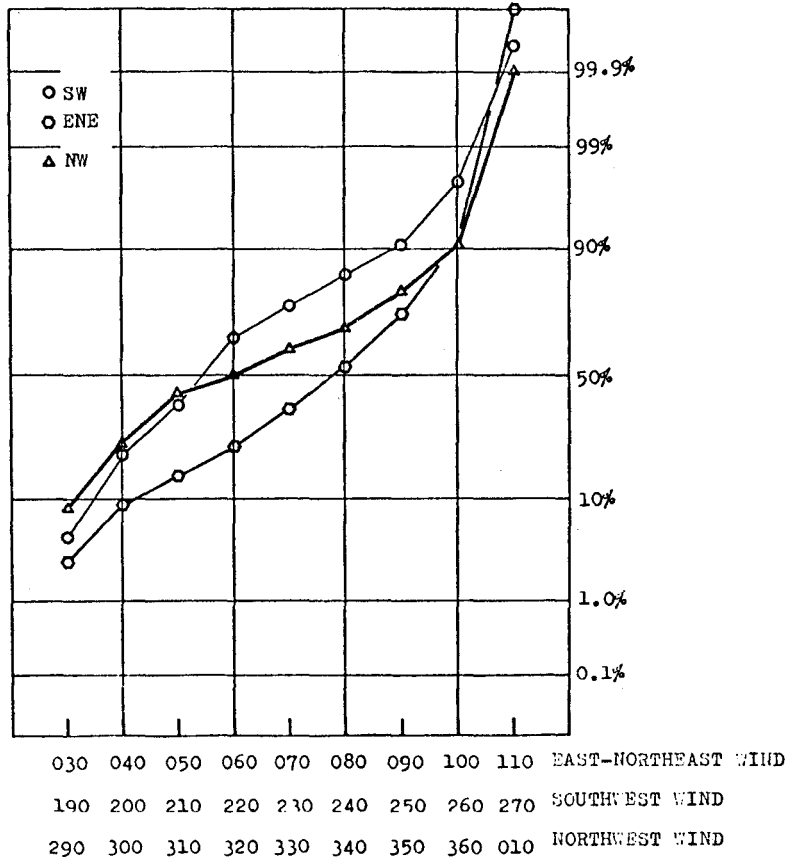
030	040	050	060	070	080	090	100	110	EAST-NORTHEAST WIND	
190	200	210	220	230	240	250	260	270	SOUTHWEST WIND	
290	300	310	320	330	340	350	360	010	NORTHWEST WIND	

	E_{wf} PERCENT	CUMULATIVE PERCENT		E_{wf} PERCENT	CUMULATIVE PERCENT		E_{wf} PERCENT	CUMULATIVE PERCENT
030	2.846	2.846	190	4.88	4.88	290	8.62	8.62
040	4.148	8.994	200	15.75	20.63	300	15.99	24.61
050	5.944	14.938	210	16.95	37.58	310	15.60	40.21
060	8.213	23.151	220	27.29	64.87	320	9.99	50.20
070	13.453	36.604	230	11.20	76.07	330	10.54	60.74
080	17.264	53.688	240	9.13	85.20	340	7.80	68.54
090	19.568	73.436	250	5.54	90.74	350	11.39	79.93
100	18.154	91.590	260	6.73	97.47	360	10.38	90.31
110	10.409	101.999	270	2.49	99.96	010	9.67	99.98

Mean direction 075°
East-northwest wind

Mean direction 217°
Southwest wind

Mean direction 323°
Northwest wind

Figure 9. Directional distribution of effective wind stress (E_{wf}).
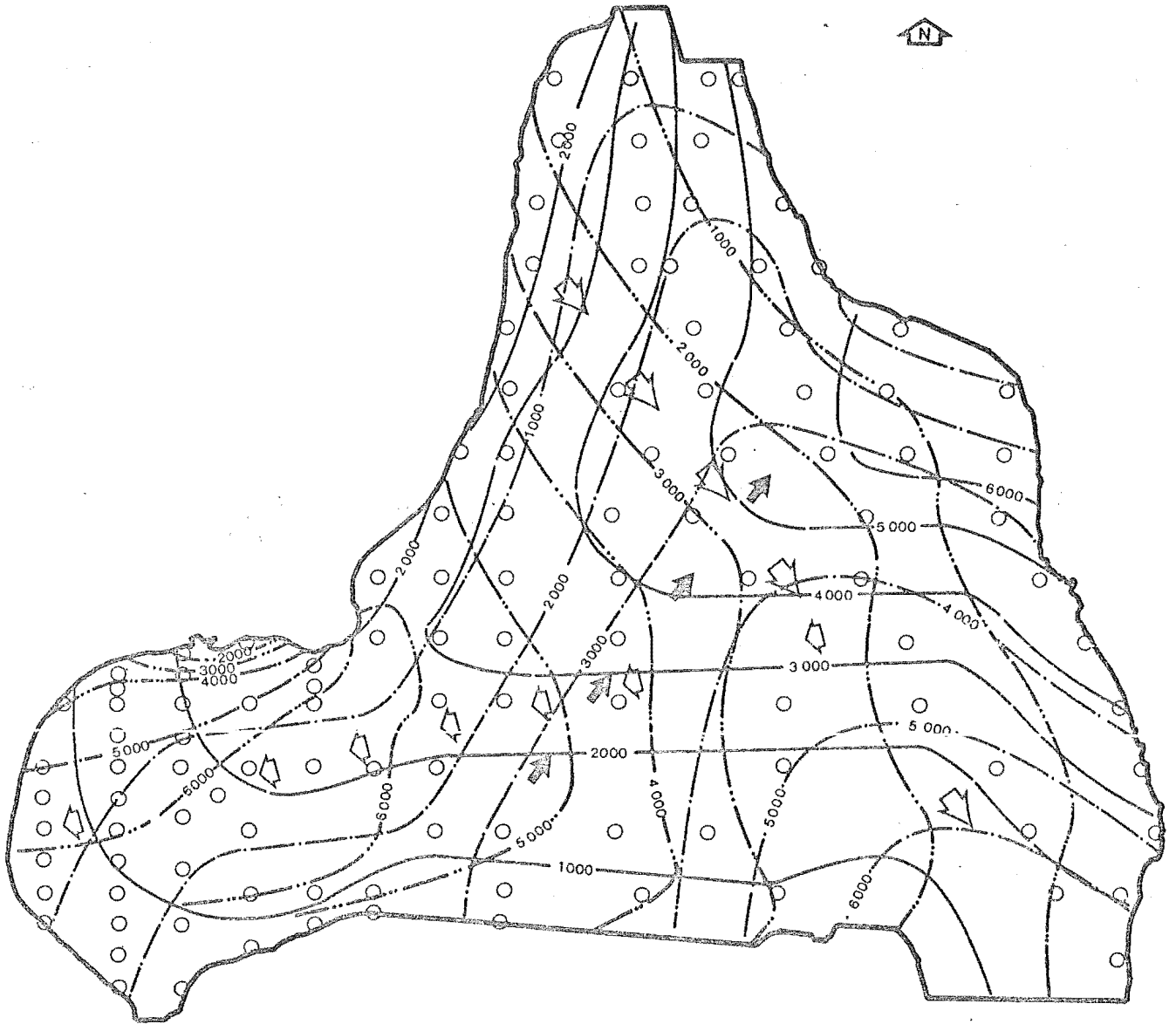
Figure 10. Effective fetch map of the Avon-Heathcote Estuary.

Contours of equal effective fetch (in thousands of feet). Calculated according to the method of the US Army Shore Protection Manual, pp 329-332. Solid line = south west wind at a mean direction of 217 degrees (squat open arrows), line with one dot = north west wind at 323 dgrees (sharp open arrows) and line with two dots = east wind at 075 degrees (solid arrows). Circles are data points.

incorporating the few events with high variability into the analysis will not materially alter the reliability of the results.

2. *Delineating a fetch.* The second step in the hindcasting procedure is to choose a fetch over which wind is reasonably constant in speed and direction, and to measure its length. The three mean directions from Figure 9 delineate appropriate fetch directions.

Fetch width may be significant in enclosed bodies of water, placing a restriction on fetch distances, in such a way that the less the width/length ratio, the shorter will be the effective fetch. The CERC procedure (pp.3-30 to 3-33) was used in this study, and effective fetch values for the relevant wind directions were calculated for about 110 stations in the AHE.

Figure 10 shows contours of effective fetch for the three mean wind directions; in the AHE, few areas have fetches exceeding 1 800 metres (6 000 feet), and long fetch winds are distributed quite uniformly around the east, south, and south-west shores. Areas in the north-west experience only short fetch east winds. The pattern of fetch contours is most complex in the south-west, where fetch width is more limiting than elsewhere in the estuary.

3. *SMB wave predictions.* Once mean wind speeds and directions have been established, and effective fetches calculated, wave parameters may be read directly from prediction graphs. The CERC graphs are based on procedures developed by Sverdrup and Munk (1947), with revisions by Bretschneider (1958) and subsequent modifications, and the prediction scheme is known as the Sverdrup-Munk-Bretschneider (SMB) technique. Replotted versions of SMB curves from the CERC Manual are presented as Figure 11. With these graphs, wave heights and wave periods may be estimated for winds of 10, 15 and 20 knots, for given fetches from 1 000 to 8 000 feet (300 to 2 400 metres). The curves in Figures 11A and 11B are for wave generation in water 5 feet (1.5 metres) deep (Figure 3-21, CERC Manual, pp.3-47).

4. *Limitations on wave dimensions.* Water depth affects wave generation. In water where the relative depth d/L is greater than 1/2 (d = depth below still water level, L = wave length), wave characteristics are virtually independent of water depth, and waves are unaffected by the bottom.
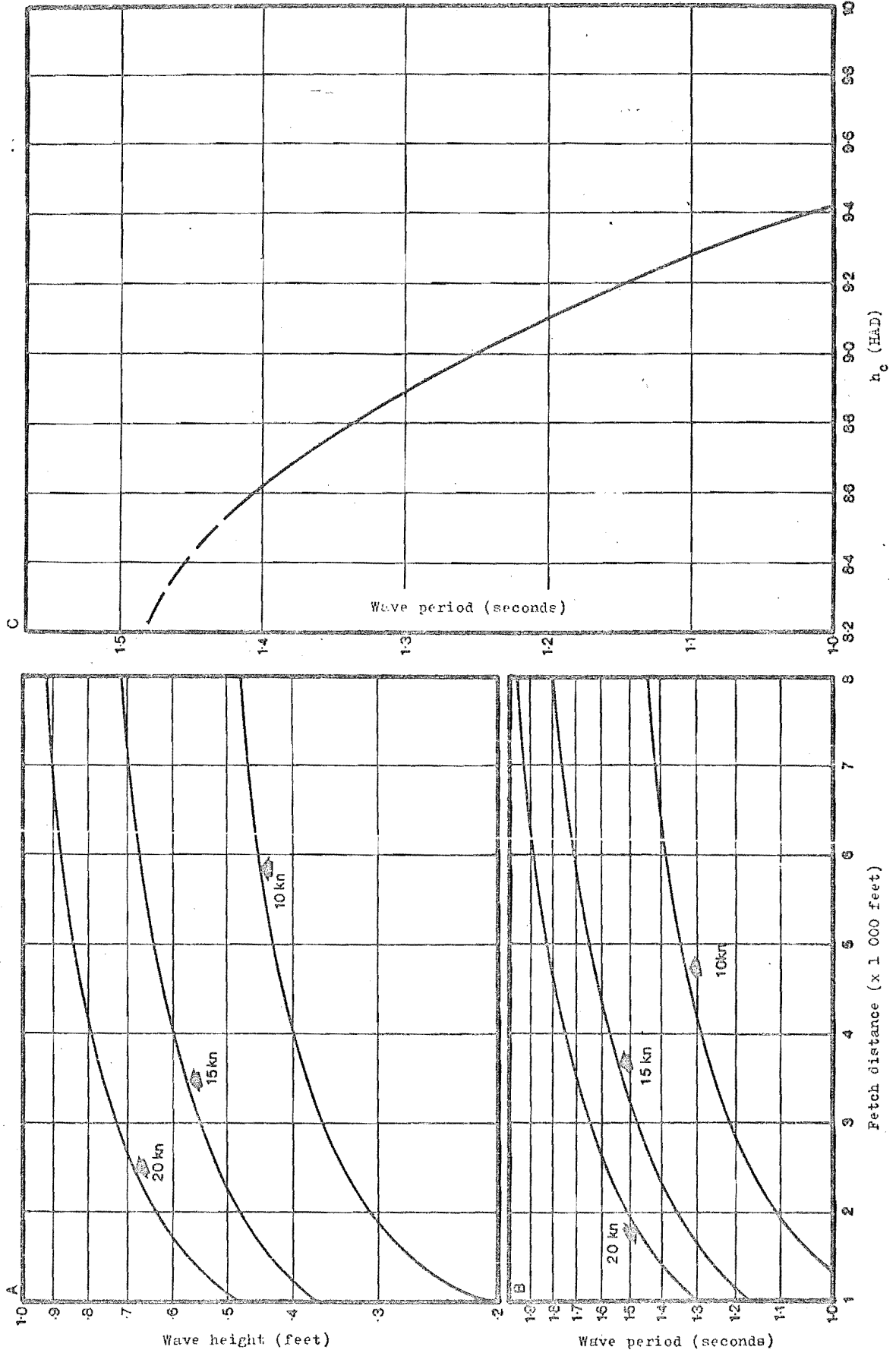
Figure 11. Wave prediction curves for water 5 feet deep (1.5m) for winds of 10, 15 and 20 knots (5m/s, 7.5m/s, 10m/s). A - Wave height curves. B - Wave period curves. C - Height above datum of half deepwater wave length (h_c) v wave period, for the Avon-Heathcote Estuary.

As waves propagate into shallow water, or grow downfetch in water of constant depth, they begin to feel the bottom and bottom sediment starts to feel the waves, as oscillatory water motions associated with the waves exert a shear stress on the bottom.

Where d/L is less than 1/25, waves are in shallow water, and depths from 1/2 to 1/25 are defined as transitional (Madsen, 1976; CERC Manual, 1973). Significant alterations to wave properties begin when waves propagate into water shallower than d/L = 1/2 (a water depth referred to as h_c). Since wavelength varies with decreasing depth in shallow water, h_c is calculated from wave period (T), which remains constant according to

$$h_c = 2.56 \ T^2 \ .$$

For example, a 1.2 second wave has an h_c value of about 1 metre, and interacts with the bottom in water shallower than 1 metre.

Inspection of Figure 11B shows that for winds from 10 to 20 knots, and for fetch distances from 1 000 to 6 000 feet, wave periods in the AHE will vary from about 1 s to 1.9 s. However, if h_c values are recalculated as height above datum values (by subtracting h_c from a still water level of 10.22 m, which is HWOST) it is found that when wave periods reach about 1.35 s to 1.4 s, they have h_c values of about 8.7 m HAD (Figure 11C). This means that in water deeper than 8.7 m HAD, 1.4 s waves will be interacting with the bottom. Map 1 shows that only small areas of the AHE are deeper than 8.7 m HAD; thus waves with periods greater than 1.4 s will be rare in this estuary. This conclusion is supported by two observations:

(i)   When ripples form on the higher intertidal flats they are of uniform size and spacing -- regardless of the mean wind speed, direction or fetch distance during the preceding high tide -- and so were presumably made by waves of similar uniform sizes.

(ii) On days when the mean wind speed exceeds about 10 knots, high tide wave trains contain a high proportion of spilling waves (Cokelet, 1977) - that is, many waves in the train have reached a limiting steepness (a maximum size) and have begun to break. Yachtsmen also record that waves larger than about 1 foot (30 cm) are rarely encountered in the AHE, regardless of wind strength or fetch distance (G. Coates, pers. comm.).

5. *Wind event frequencies*. The preceding analysis has shown
that regardless of fetch distance or wind velocity, the waves which
form at about high tide in the AHE rarely have periods which exceed
1.4 s. This means that the best method of assessing the relative
wave-making importance of the three mean winds is to calculate wind
event frequencies, not total effective wind stress. From Figure 7
the appropriate frequencies are:

Direction	Number of events	Percentage of total events
075	327	56
217	166	28
323	94	16

These data indicate that the east wind is the dominant wave producer,
as east winds are twice as frequent as south-west winds, and four
times as frequent as north-west winds.

6. *Discussion*. The particular significance of sections 4
and 5, above, is demonstrated in Figure 12. Wave-generated shear
stress exerted on the bottom of the estuary increases downfetch
because with increasing fetch, a greater number of wind events are
capable of building waves which feel the bottom. If downfetch
energy gradients occur, they are a product of a greater number of
wave events, each of which builds waves of a similar size, not a
result of increasing wave size. A further conclusion is that if
much of the wind blowing down a particular fetch occurs as high
velocity events, most waves will bottom near the proximal end of the
fetch, and wave energy will tend to be distributed uniformly down
fetch. If much of the wind blows as low velocity events, at or near
10 knots, then the bottoming zone is spread down the fetch, and
there is more likely to be a downfetch energy gradient. Obstructions
such as shoals or sand mounds which are significantly shallower than
water on their upfetch side will cause equilibrium waves to break,
and if the breaking zone is shallow enough to cause the complete
breakdown of approaching waves, it will act as the origin of a
second fetch, further homogenising downfetch energy distribution.

Figure 12. Diagramatic illustration of the relationships between wave generation and water depth in the Avon-Heatcote Estuary.

800   0

metres

East wind

HWOST

10.0m HAD

Waves break on central shoals, new wave train is generated

x

h_c 15 knot wind

h_c 10 knot wind

h_c 10 knot wind

Central sand mound

h_c 15 knot wind

9.0m HAD

z

bottom

p

y

n

o

m
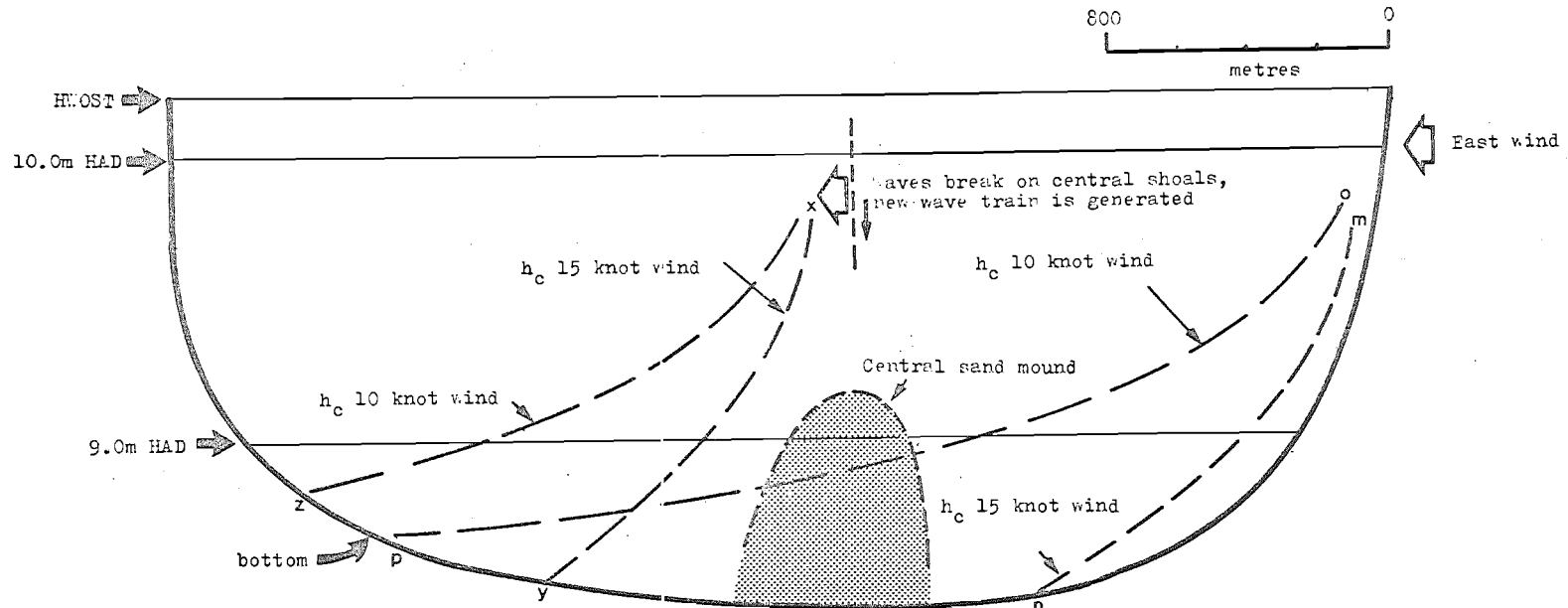
Explanation

1. A 15 knot east wind begins to generate waves at m; as the wave train progresses downfetch, wavelength increases until n, where water depth is equivalent to half the wavelength, and waves effectively enter shallow water.

2. A 10 knot east wind begins to generate waves at o; which reach a water depth equivalent to half their wave length at p, and effectively enter shallow water.

3. As waves approach shallow central sandy mounds, increasing steepness causes breaking by spilling, and the wave train may break down. New generation begins at x, and half wavelength depths follow paths x - y, x - z.

h_c = half wavelength depth, below still water line (where SWL = HWOST)

Near bottom velocities and shear stresses

As waves enter water shallower than $d/L = 0.5$ they begin to
exert shear stresses on the bottom. To the first approximation
the motion involved is purely oscillatory – there is no net transport
(Madsen, 1976). From Airey wave theory (see the CERC Manual for an
excellent discussion of wave theory) it is possible to calculate wave
properties associated with this oscillatory motion, including horizontal
near bottom velocities, amplitudes of near bottom wave orbits, and the
maximum near bottom shear stresses. Madsen (1976) has presented a
useful summary of these applications, and the following analyses are
substantially derived from that summary.

Maximum horizontal near-bottom velocity (u_b): For waves with T_o
= 1.4 s, H_o = 14 cm, and L_o = 3.56 m (where T = wave period, H = wave
height, L = wave length, and the subscript o indicates deep water
conditions), the following values are calculated:

h	h/L_o	u_b
0.5 m	0.14	22.12 cm/s
1.0 m	0.28	14.38 cm/s
1.5 m	0.42	9.95 cm/s

These values demonstrate the large increases in near bottom velocity
that occur as waves propagate into shallow water, producing steep energy
gradients along the bottom in the transition zone between deep and
shallow water.

Orbital amplitudes: As waves shoal, the originally circular
orbits become elliptical, and the amplitude of motion near the bottom
(A_b) increases according to $A_b = u_b/w$; where w = radian frequency,
$2pi/T$. The following values are calculated from the above figures:

u_b	A_b
22.12 cm/s	4.93 cm
14.38 cm/s	3.21 cm
9.95 cm/s	2.92 cm

Wave Reynolds Number (RE), relative roughness (d_s) and the
friction factor (f_w): The maximum near bottom shear stress is related
to the square of velocity by a wave friction factor, f_w.

For turbulent flow the wave friction factor is a function of relative bottom roughness and the wave Reynolds number, $u_b A_b/v$; where v is the kinematic viscosity of the fluid (10^{-1} cm^2/s). Where bottom roughness is contributed by ripples, the equivalent sand roughness (d_s) may be quite high (0.5 to 1.5 cm). Where the bottom is smooth, d_s may be as low as 1.5×10^{-3} cm (fine sand sized), or even as low as 1.5×10^{-4} cm (silt sized). Thus relative roughness values (A_b/d_s) may vary from about 10 to about 3 200 for h = 0.5 m, and from 2 to about 2 000 for h = 1.5 m.

The wave friction factor is a function of both relative roughness and RE, and may be obtained from a friction factor diagram (Madsen, 1976, Figure 8; after Jonsson, 1965). The following values have been calculated:

Water depth	d_s	A_b/d_s	f_w
0.5 m	0.5 cm	10	7×10^{-2}
0.5 m	0.015 cm	330	0.15×10^{-2}
1.0 m	0.015 cm	214	0.02
1.5 m	0.5 cm	6	0.1
1.5 m	0.015 cm	195	0.015

Maximum near bottom shear stress ($t_{b,max}$): Knowledge of f_w permits evaluation of the maximum bottom shear stress, which is proportional to the product of the friction factor and the square of the bottom velocity.

$$t_{b,max} = \tfrac{1}{2} f_w \, p u_b^2 \, .$$

For water depth of 0.5 m, with roughness contributed by ripples 0.5 cm high,

$$t_{b,max} = 17.13 \text{ dynes/cm}^2 .$$

If roughness is fine sand sized,

$$t_{b,max} = 3.67 \text{ dynes/cm}^2 .$$

For water which is 1.0 m deep, with 0.015 cm bottom roughness,

$$t_{b,max} = 2.07 \text{ dynes/cm}^2 .$$

For water which is 1.5 m deep, with 0.5 cm bottom roughness,

$$t_{b,max} = 4.95 \text{ dynes/cm}^2,$$

and if bottom roughness is fine sand sized,

$$t_{b,max} = 0.5 \text{ dynes/cm}^2.$$

These figures emphasise that waves exert very much more stress on a rippled bottom in water 0.5 m deep, than on a smooth fine sandy bottom in 1.5 m deep water – the difference is about 1.5 orders of magnitude.

Threshold of sediment motion under waves

Komar and Miller (1975) present a set of curves relating bottom orbital velocities to grain diameters for varying wave periods for the threshold of sediment motion, and from this figure the values below were obtained.

wave period = 1.4 seconds,

water depth	orbital velocity	approximate maximum grain diameter potentially entrained by waves
0.5 m	22 m/sec	0.5 mm (1.0 phi)
1.0 m	14 m/sec	0.25 mm (2.0 phi)
1.5 m	10 m/sec	0.15 mm (about 3 phi).

Considering that there have been relatively few studies of sediment movement under waves, and that more data may alter the empirical relationships which form the basis of the equations governing Komar and Miller's (1975) threshold diagram, better approximations than these are not possible at present.

Wave refraction

1. *Introduction*. Many waves in the AHE feel the bottom along much of their traverse across the estuary, and it is reasonable to assume that their passage is significantly altered by the configuration of the bottom. One result of this feedback is that waves are refracted, tending to approach the shore normal to the bottom contours. Refraction may be analysed graphically, with the theoretical basis developed from geometrical optics and Snell's Law (CERC Manual, pp.2-65), by tracing the

passage of wave rays (orthogonals to crests) across a sloping bottom as a sequence of straight line increments. This method is labour intensive, and numerical methods have been developed as a more efficient alternative (Wilson, 1966). A version of Wilson's computer program has been adapted for the University of Canterbury Burroughs B7600 computer by A.J. Sutherland (Department of Civil Engineering), and this program was used to obtain the data summarised in Figure 13, which shows the results of a number of computer runs for mean south-west and east winds.

The method involves drawing an arbitrary grid over the estuary, and reading off water depths at grid intersections (where depth is assumed to be depth below HWOST). The resulting lists, combined with wave period and deepwater crest orientations form the input data for the program. Results are plotted as wave rays, which may be replotted on to the original bathymetric base.

2. *Discussion.* Refraction analyses are usually undertaken for oceanographic or engineering purposes, or as a method of evaluating longshore differences in wave energy, where variations in beach alignment, or of offshore bathymetry, may variously modify deepwater waves as they approach the shore. In such studies it is usually assumed that waves entering the coastal zone have travelled from a generating area some distance away, and that the only modifications that occur as waves run in towards the coast are those produced by the shoaling transformation. Little work appears to have been done in shallow enclosed basins where deepwater conditions may only apply for short sections of the total fetch, and where there is a continuing interaction between the forcing wind and the restraining limitation of shallow water. It may well be that the assumptions built into the numerical method do not apply in such circumstances (CERC Manual, pp.2-65); in particular the assumptions that waves are long-crested, constant period, small amplitude, and monochromatic. For this reason the information in Figure 13 probably only has qualitative applications - attempts have not been made to calculate the effects of the shoaling transformation on wave properties.

3. *Results.* Figure 13 indicates that east wind waves are little modified by the bottom north of line 12 (Map 1), until running into water shallower than mid tide levels (9.0 m HAD - water shallower than 1.20 m).
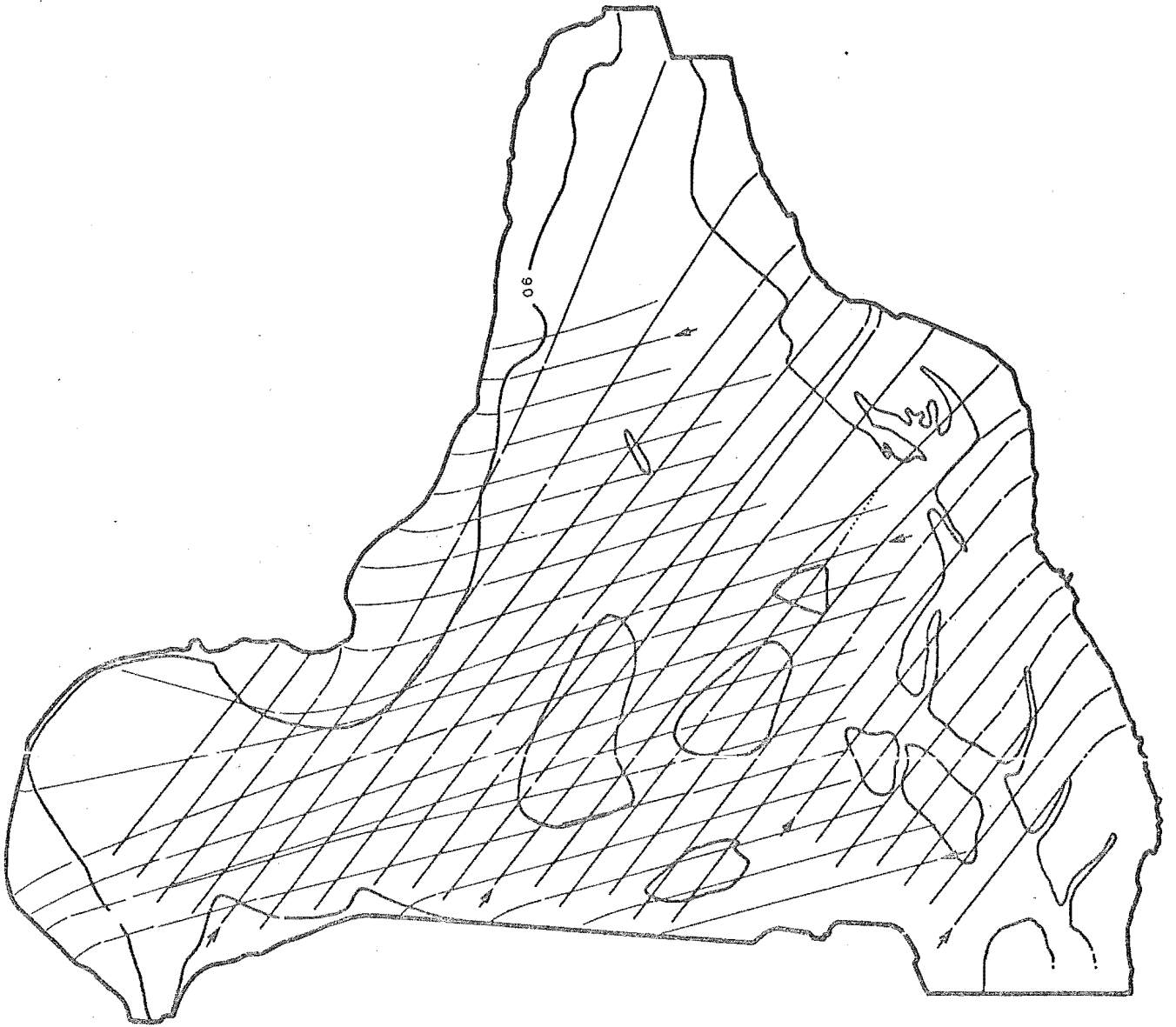
Figure 13. Southwest wind (217°) and east wind (075°) wave refraction diagram. Wave period 1.4 seconds. Arrows show directions of wave propagation in deep water, assumed parallel to the wind directions. Lines are wave rays (orthogonals to crests).

Central bathymetric highs and shallow marginal areas act as lenses,
converging wave rays (as in the south Heathcote Basin) or causing rays
to diverge (as in north Heathcote Basin). Where rays converge, waves
will become steeper, and if the train is close to a limiting steepness,
breaking will occur, probably as slightly more vigorous spilling.
Where rays diverge, energy is spread along greater crest lengths,
and wave heights should decrease. The overall effect is probably that
refraction acts as a further homogeniser of wave properties in
converging areas, producing uniform wave fields where many individual
waves are close to a maximum steepness. In diverging areas, maximum
wave sizes may be less than the mean equilibrium size.

The refraction pattern for the mean south-west wind indicates
that Sandy Point tends to shade the upfetch western shore from waves,
while the central highs tend to homogenise wave properties, and produce
a uniform wave climate along the eastern shore the estuary. A few trial
runs for the mean north-west wind showed an analogous pattern,
indicating that north-west wave energy is spread uniformly along the
south and south-east shores.

Wave-generated bedforms

1. Introduction. When the wind during a preceding high tide
exceeds about 10 knots, intertidal flats uncovered at low tide show
widespread trains of strikingly parallel straight transverse
asymmetrical ripples (Figure 14). Such ripples have been widely
reported on tidal flats (i.e. Allen, 1968; Reineck and Singh, 1974;
Tanner, 1967) and are thought to be produced by shoaling waves that
generate an asymmetrical oscillatory motion at the bed. In the
Avon-Heathcote Estuary these ripples rarely occur below the mean tide
level (9.0 m HAD), and are usually only found in clean sand. They
often form lanes several metres wide (Allen, 1968, p.92) and may occur
in isolated patches surrounded by smooth sand. In very shallow water
(less than about 20 cm) around the edges of the estuary, very
asymmetrical lingoid or barchan-shaped ripples may occur, merging
offshore into straight ripple trains, or occasionally occurring as
isolated ripple patches. If succeeding high tides are calm, newly
formed ripple trains are destroyed by rounding of the crests and by
bioturbation of the soft sediment surface (especially by the abundant
mudflat snail *Amphibola* - Figure 14F), so that after about 4 to 6 calm
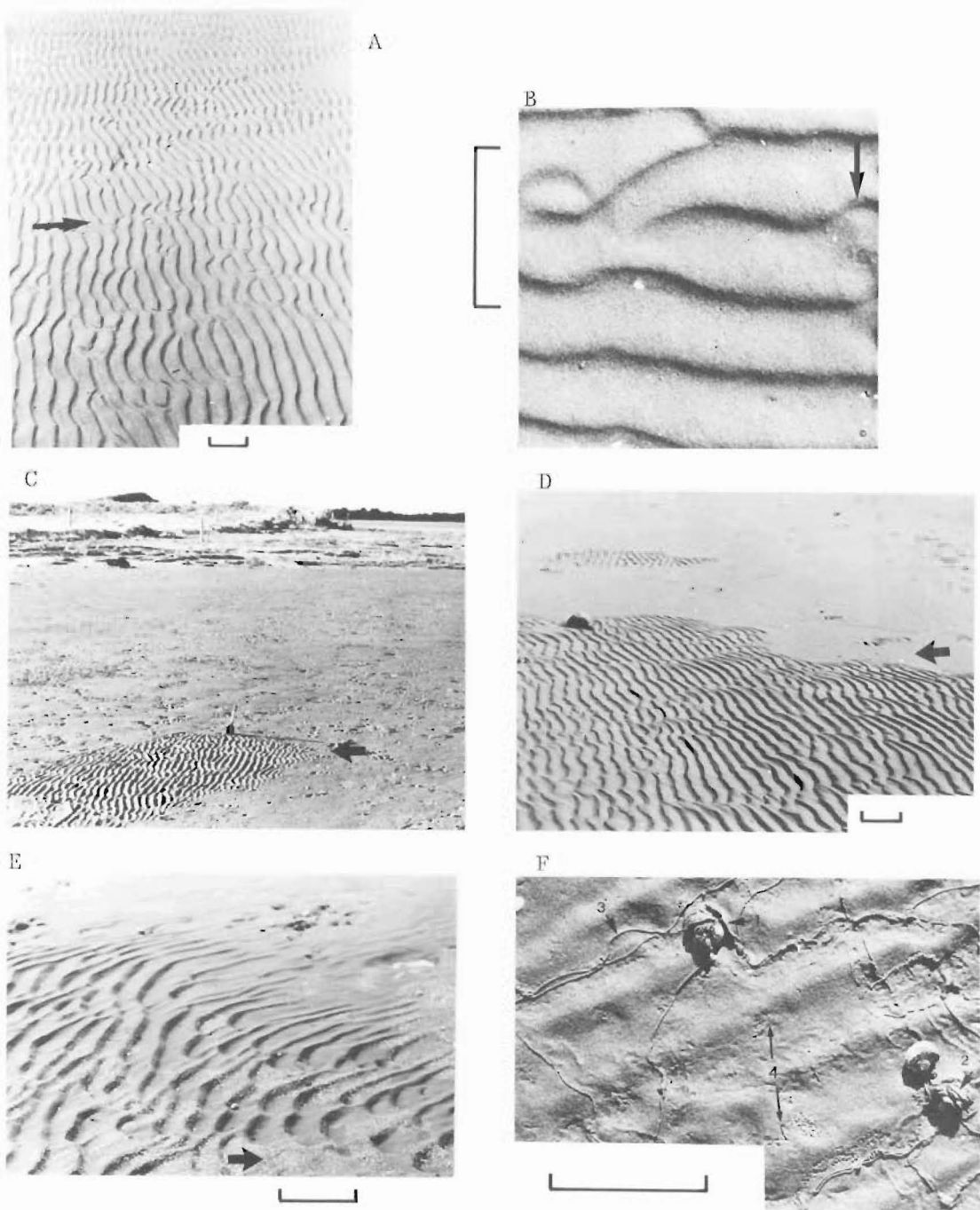
Figure 14. Wave formed ripples of the Avon-Heathcote Estuary. A - Parallel almost straight asymmetrical ripples typical of eastern high tide (9.5m) slopes. Scale is 10cm, arrow shows direction of wave propagation, which was to the north east. View is to the north. B - Detail of ripples in A, scale is 10cm, arrow shows wave direction. C - Isolated patch of almost straight asymmetrical ripples near the HW mark at Sandy Point (bone tip in background). Arrow shows wave direction. D - Detail of part of an isolated ripple patch on the eastern hiih tide slope. Note abrupt transition from smooth to rippled sand. HW mark is to the left, view is south, scale is 10cm. E - Barchan-shaped very asymmetrical ripples at the HW mark (landward of D, above). Arrow shows wave direction, scale is 10cm. F - Detail of rippled surface after one calm high tide, showing the smoothing activities of Amphibola crenata, burrowing into the surface at (1) and (2), and packaging surface sediment into fecal strings (3). Note the characteristic birds-foot shaped feeding trace of the bivalve M. liliana (4). Scale is 10cm. Also see Figures 65 and 66.

Figure 15. Distribution and orientations of wave-formed ripples on September 4 1976 (west side) and September 8 1976 (east side). Arrows show mean wind directions during the preceding high tides, numbers are ripple crests/m, thick lines show crest strike directions at each site.
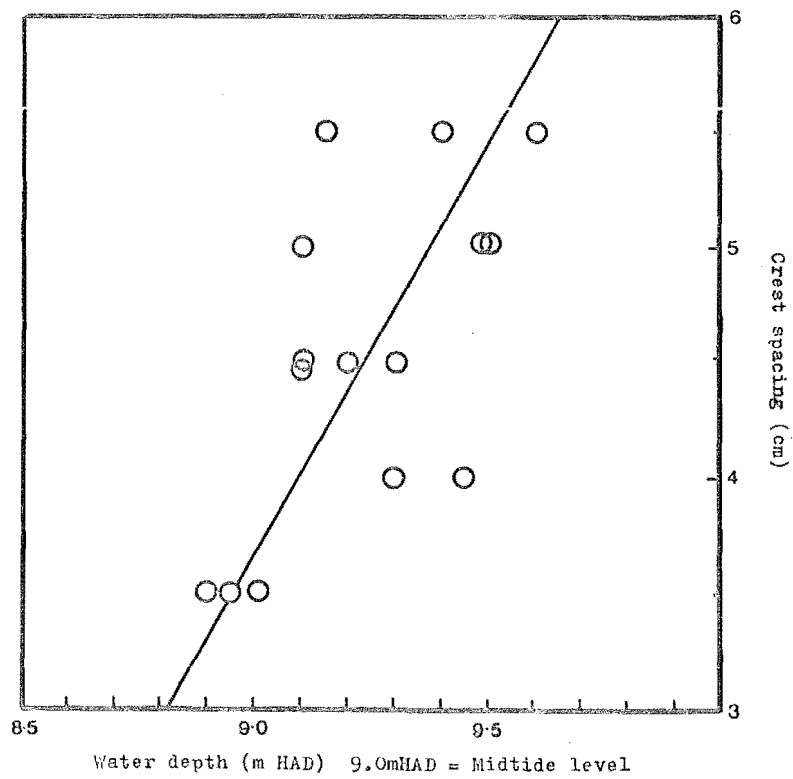
Figure 16. Ripple crest spacing vs water depth (as height above datum), western slopes, September 4 1976.

high tides the flats are quite smooth.

    2. *Ripple orientations and dimensions*. Ripples were measured at low tide on opposite sides of the estuary on September 4th and September 8th 1976. Winds of 12 knots (6 m/sec) from 070 degrees, and 14 knots (7 m/sec) from 252 degrees, respectively, blew during high tides which preceded the two visits, and the state of preservation of both ripple sets indicated that they formed during the preceding high tide.

    In both areas (Figure 15) crest spacing was quite uniform on the higher flats (at about 20/m, measured normal to crests), regardless of fetch. Ripples formed in deeper water tended to be smaller, especially on the western side of the estuary, where up to 30 crests per metre were occasionally measured (Figure 16). Mean values were:

	Mean crest spacing	Mean crest strike	Angle between preceding mean wind and mean ripple crest strike	Standard deviation	Number of measurement
East side	4.53 cm	028°	55°	0.72 cm 7.50°	15 15
West side	4.58 cm	285°	42°	0.20 cm 25°	6 9

In small bodies of water, ripple wavelength is usually about 4/5ths of the amplitude of the waves (Inman, 1957; Komar, 1974, quoted *in* Komar, 1976). If this relationship holds in the AHE, the waves which formed the ripples in Figure 15 had near-bottom amplitudes ranging from 4.16 cm to 6.82 cm (from 30/m to 18/m). In section 7 above, predicted amplitudes for water of 1.0 m deep and 1.5 m deep were 3.21 cm and 4.93 cm. The predicted values are about 30% too small, which seems to indicate that the relationship between wave size and ripple amplitude is not generally applicable. However, few of the data used to establish the relationship were from natural conditions, and those which were scattered widely about mean values (Inman, 1957).

Tides

1. *Introduction.* In an intertidal estuary, the semi-diurnal tide contains considerably more kinetic energy than the waves which develop on windy days (Bukuniewicz and others, 1975), yet in typical microtidal estuaries tidal currents are only important transporters of sediment near the inlet, where tidal velocities are highest (Hayes, 1975). Wind-induced processes (waves and wind tides) predominate throughout the remainder of typical microtidal estuaries.

Although wave motion may be the principal initiator of sediment movement (on the Continental Shelf), net sediment transport is usually accomplished by a superimposed current (Madsen, 1976). Carter and Heath (1975) have demonstrated the importance of superimposed currents on the New Zealand Shelf, as have Channon and Hamilton (1976) for part of the Shelf off Southwest Britain.

In developing an understanding of the intertidal sedimentation of the AHE, the present analysis began by considering wave energy; the observations above suggest that the next step is to assess tidal current energy.

2. *Previous work.* Linzey (1944) described the general characteristics of tidal movements in the AHE, and collected some current-velocity data. Bruce (1953) and Webb (1972) added to this early work (see the summary in Knox and Kilner, 1973). Mawson (1972) has calculated river and other non-tidal flows for various discharge conditions and tidal ranges, and has usefully summarised the hydrological properties of the estuary and its freshwater catchment.

The Wallingford Report (1970) contains data on tide levels and current velocities at the inlet to the estuary (at Shag Rock and at the Sumner Lifeboat Station), at Ferrymeade Bridge, and at Bridge Street Bridge. These data were supplied to the Wallingford investigators by consultants to the CDB, to be used for the scaling and evaluation of a large (30m × 30m) physical model of the estuary. According to the Wallingford report, maximum tidal velocities in the principal subtidal channel at Shag Rock reach 1.52 m/s during flood tides and 1.83 m/s during the ebb (in both cases measurements were made 1 metre below the surface). These velocities are almost twice those measured by Bruce (1953), who reported a maximum ebb velocity of 1.10 m/s at Shag Rock. Notes on the *HMS Pandora* chart (1854) indicate that maximum currents were about 2 knots (1.0 m/s) in the vicinity of Shag Rock.

Heath (1975) has shown that maximum tidal velocities in mobile inlets in theory should be about 1.14 m/s.

Linzey (1944) measured a flood tide maximum of 0.46 m/s at Ferrymeade Bridge, and an ebb maximum of 0.3 m/s. The Wallingford Report indicates that the CDB consultants recorded 0.6 m/s in both cases. At Bridge Street Bridge Linzey recorded 0.3 m/s maxima for both the ebb and flood tides, while the consultants recorded 0.6 m/s and 0.8 m/s respectively. It appears that the consultants obtained values about twice those reported from other sources. This may have been a result of misreading the current meters used to obtain the data, or perhaps a drafting error if the consultants supplied the Wallingford investigators with graphed rather than tabulated results. Certainly at least one Figure in the Wallingford Report is plotted upside down (part of Figure 6, Part I), so the second option is quite plausible. Yet it is difficult to believe that the Wallingford investigators would accept a mistake of that order, and the build it into their model!

The only available information on current velocities from intertidal areas is that supplied by Knox and Kilner (1973) and summarised in Figure 17. Current velocities deduced from dye tracers (or from drogues, or any other free submerged or semi-submerged objects) as in Figure 17, are known as Lagrangian velocities (where, in effect, a parcel of water is tracked along a stream-line for a measured time and an average velocity is calculated). Lagrangian velocities are not necessarily comparable to Eulerian velocities (measured as the rate of flow past a fixed point) because the two techniques resolve turbulence in moving water in different ways - the meters used to obtain Eulerian velocities introduce significant flow disturbances, and they are insensitive to higher frequency fluctuations (Byrne and Boon, 1973). The Lagrangian velocities shown in Figure 17 are likely to be conservative, and perhaps less than equivalent Eulerian measurements, because the method of estimating distances assumes that dye slugs travelled linearly from point to point within the estuary - which may not be the case. Figure 17 indicates that Lagrangian velocities in the subtidal channel several hundred metres downstream from Bridge Street Bridge are about 15 cm/s shortly after high tide, and reach 62 cm/s in the principal subtidal channel 3.5 hours after high tide. Lagrangian velocities of 83 cm/s were recorded in Figure 17 in the subtidal channel off Beachville Road. These are similar to the values of Linzey (1944) and Bruce (1953), but considerably less than the Eulerian velocities reported by the consultants to the CDB.
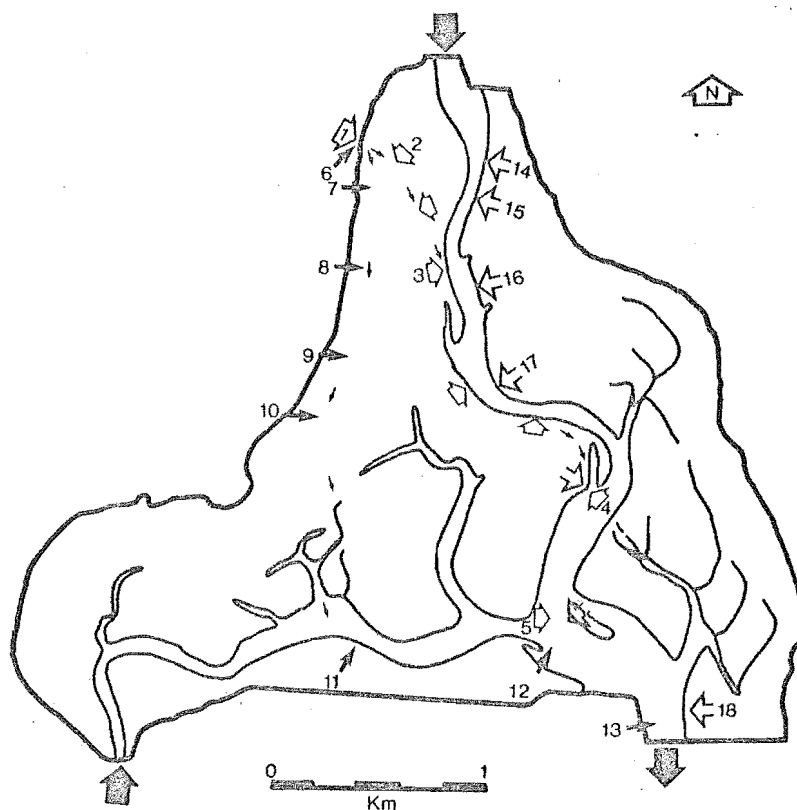
Experiment 1. December 6, 1972. Flat calm conditions, Rhodamine dye. Dye released at position 1 above; locations at 30 minutes (2), 43 minutes, 61 minutes (3), 105, 124 and 163 minutes (4) and at 178 minutes (5), are shown by the series of large squat arrows above (▽).

Calculated velocities for the leading edge of the dye slug are; 0-30 minutes, 0.05m/sec; 0-43 minutes, 0.15m/sec; 0-61 minutes, 0.34m/sec; 61-105 minutes, 0.23m/sec; 105-163 minutes, 0.24m/sec; and 164-178 minutes, 0.75m/sec.

Experiment 2(A). February 1973. North east wind at 5-10 knots, light water chop, Rhodamine dye. Dye released at 6; locations at 40 minutes (7), 65 minutes (8), 105 minutes (9), 135 minutes (10), 230 minutes (11), 250 minutes (12) and 265 minutes (13), are shown by smaller black arrows above.

Calculated velocities for the leading edge of the dye slug are; 0-40 minutes, 0.05m/sec; 0-65 minutes, 0.12m/sec; 0-105 minutes, 0.15m/sec; 0-135 minutes, 0.15m/sec; 135-230 minutes, 0.18m/sec; 230-250 minutes, 0.62m/sec; 250-256 minutes, 0.83m/sec.

Experiment 2(B). As for 2(A), except dye (Fluoresceine) was released directly into the Avon sudtidal channel at 14. Locations at 20 minutes (15), 70 minutes (16), 130 minutes (17), 170 minutes,(190 minutes, and 210 minutes (18), are shown by open arrows above (⟁).

Calculated velocities for the leading edge of this dye slug are; 0-20 minutes, 0.15m/sec; 0-70 minutes, 0.13m/sec; 0-1 0 minutes, 0.10m/sec; 0-170 minutes, 0.18m/sec; 0-190 minutes, 0.21m/sec; 190-210 minutes, 0.62m/sec.

Figure 17. Intertidal and subtidal current velocities in the Avon-Heathcote Estuary. From dye tracking experiments reported by Knox and Kilner (1973).

In view of the above discussion, the Wallingford Report data is discounted, and the values below have been adopted as probable maximum values, based on Figure 17, and both Linzey (1944) and Bruce (1953).

	Maximum·velocity
Higher intertidal flats	5 cm/s
Intermediate intertidal flats	20 cm/s
Lower intertidal flats	35 cm/s
Intertidal channels	60 cm/s
Subtidal channels	90 cm/s
Principal subtidal channel	114 cm/s

3. *Shear stress*. The movement of sediment under unidirectional currents has received considerable attention – much of it to do with the transport of sediment in rivers and artificial channels, but an appreciable amount involving the transport of sandy sediment on the Continental Shelf and in nearshore waters (see Sternberg, 1968, 1972; Ludwick, 1975).

Komar (1976 a,b) has presented a particularly useful summary of the properties of boundary layers of natural unidirectional currents, and of the derivation of the quadratic stress law,

$$t = c_{100} \, p(\bar{u}_{100})^2 \, ,$$

where t = boundary shear stress, c_{100} = drag coefficient from measurements made 100 cm above the bottom, p = fluid density, $\bar{u}_{100}$ = mean velocity 100 cm above the bottom. The quadratic stress law establishes a proportionality between the boundary stress exerted by a fluid flow and the square of the mean velocity of the flow, so that by assuming or establishing c_{100}, only $\bar{u}_{100}$ need be known to evaluate t.

Sternberg's (1968, 1972) measurements of c_{100} in Puget Sound, U.S.A., indicate that $c_{100} = 3 \times 10^{-3}$. This result has been supported by Channon (again for Shelf conditions, in Channon and Hamilton, 1971) and McCave (in Komar, 1976b). Thus

$$t = 3 \times 10^{-3} \, p(\bar{u}_{100})^2 \, .$$

There are limitations on the use of this average value of c_{100} (Komar, 1976b, pp.100-102; Ludwick, 1975), but considering the levels of approximation involved in the estimates of tidal velocities, the assumption of Sternberg's value is probably a reasonable expediency.

The following magnitudes for near bottom shear stresses are obtained for the tidal velocities tabulated above:

$\bar{u}_{100}$	90	60	35	20	5 cm/s
shear stress	25	11	3.8	1.24	0.08 dynes/cm^2.

The two or three lower values are order-of magnitude estimates at best, especially since the flow boundary may not be hydrodynamically rough when $\bar{u}_{100}$ is less than about 15 cm/s (Komar, 1976b).

These figures support the observation of Madsen (1976), that shear stresses generated by waves tend to be an order of magnitude greater than stresses generated by unidirectional flows of equivalent velocity — the shear stress under a 1.4 s wave in 50 cm of water is 17 dynes/cm^2 for an orbital velocity of 22 cm/s; a tidal flow of 20 cm/s exerts a shear stress on the bottom of about 1.2 dynes/cm^2.

4. Sediment entrainment. As the velocity of fluid flow over a bed of sediment increases, a stage is attained when the fluid exerts sufficient stress on the particles making up the bed to cause them to move from the bed and be transported. This stage is the threshold of sediment movement, or the critical stage for erosion or entrainment (Komar, 1976b, p.108). Miller and others (1977) have recently reviewed the subject of sediment threshold, and re-evaluated a variety of methods for deriving threshold conditions. Their Figure 7 (p.519), relating critical shear stress to grain diameter of quartz-density material in water at 20°C, yields the following values:

$\bar{u}_{100}$ (cm/s)	shear stress (dynes/cm^2)	threshold grain diameter		
		mm	phi	size class
90	25	3.5	-2.0	granule
60	11	2.0	-1.0	vc sand
35	3.8	0.8	0.25	c sand
20	1.24	0.09	3.4	vf sand
5	0.08	0.01	6.0	silt

5. *Entrainment into suspension.* Bagnold (1966) has shown that sediment is entrained directly into suspension if upward-directed turbulence in the boundary layer contains velocity fluctuations which exceed the settling velocity of sediment grains. Bagnold's (1966) suspension criterion indicates that sediment finer than 0.17 mm (2.5 phi) will be entrained directly into suspension immediately after threshold conditions are exceeded. McCave (in Komar, 1976b) considered that sediment finer than 0.23 mm (2.0 phi) would be entrained directly into suspension.

6. *Current-generated bedforms.* If threshold conditions are exceeded by a gradual increase in current velocity, the first evidence of sediment movement is the construction of bedforms, which progress through a hierarchical sequence as shear stress increases. The literature on current=formed bedforms is very large (see Simons and others, 1965; Guy and others, 1966; Allen, 1968, 1970; Boothroyd and Hubbard, 1974, 1975; and the useful summary and review of Reineck and Singh, 1975). The properties of bedforms are one of the two key responses used to infer sediment transport patterns in many marine studies (Swift and Ludwick, 1976), because bedforms often indicate a sense of transport as well as a transport mode (the other response is the sediment grain-size frequency distribution).

Current-formed ripples are absent from the intermediate and higher intertidal flats of the AHE - here tidal currents reach maximum velocities of 20 cm/s, and are only capable of entraining silt and very fine sand. On lower intertidal flats, where current velocities may reach 35 cm/s, isolated lingoid ripples and small patches of strongly undulatory straight ripples (sinuous ripples of Allen, 1968) do occur, but are restricted to channel edges (Figure 18A). Lingoid ripples occur on the floors of intertidal channels and on point bars adjacent to subtidal channels (Figure 18B) and are widespread on the flood delta and superimposed on larger bedforms in the inlet area (Figure 18C,D).

Weakly undulatory and almost straight-crested ripples occur sporadically on lower intertidal flats, and may occur on the eastern slopes of the eastern central sand mound, where they display a flood-oriented asymmetry. They may also occur on the higher intertidal slopes of the eastern flats, south of line 15, where they are ebb-oriented. Some occurrences of almost straight-crested ripples in the
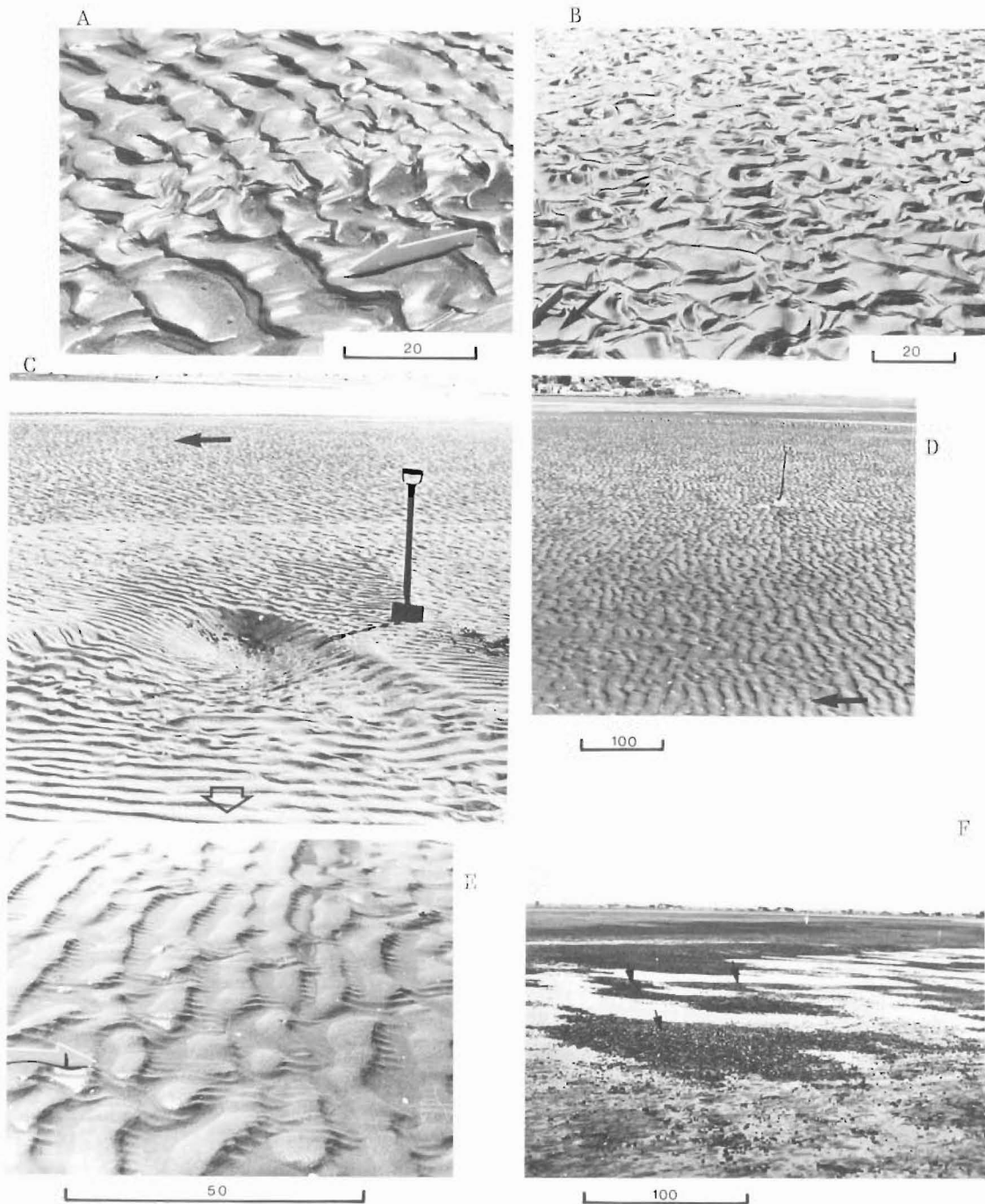
Figure 18. Current-formed ripples in the Avon-Heathcote Estuary. A - Undulatory ripples. Arrow shows (ebb) flow direction, subtidal channel edge, northern margin of southern slopes (Figure 20). Scale is in cm. B - Lingoid ripples from the tidal delta south of line 16. Arrow shows (ebb) flow direction. Scale is in cm. C - Weakly undulatory and almost straight ebb-oriented ripples south of line 16, with an incipient lunate megaripple in the foreground. Spade is 1m high, arrows show (ebb) flow direction. D - Weakly undulatory ripples opposite Beachville Road (background) as in C, above. Scale in cm. E - Almost straight-crested shore-normal current ripples with superimposed shore-parallel wave ripples, south eastern high tide slopes, south of line 15. Current from left to right, wind which formed the wave ripples blew towards the observer. Scale in cm. F - Irregular metre-scale possible incipient megaripples in channel off the Causeway, south of the Heathcote subtidal channel. View is north east, flood-tide flow direction is to the left, scale is in cm. Ripples consist of fluidal mud and abundant cockles.

last two locations have the appearance of wave ripples; they are
distinguished from wave ripples by their size (they are usually about
twice as large, with crest spacings of 8 to 10 cm), and by their
orientation, which is shore-normal (at right anlges to the shore-
parallel tidal currents) rather than shore-parallel. They often show
superimposed wave ripples with a different orientation (Figure 18E).

Visible megaripples, with crest spacings of 60 cm to 6 m, and
sand waves, with crest spacings greater than 6 m (scheme of Boothroyd
and Hubbard, 1974) only occur on the sides of the inlet channel south
of line 15 (Map 1); where they are particularly well developed on the
ebb spit and flood ramp in Moncks Bay (Figure 19). Some larger
intertidal channels contain ebb-oriented slightly asymmetrical mounds
of coarse shelly debris (Figure 18F) which may be 15 to 20 cm high,
and vary from a few centimetres apart to more than 10 metres apart.

The AHE is predominantly intertidal, and the bathymetry is
dominated by intertidal flats which are shallower than the midtide level
(which is 9.0 m HAD in Map 1; also see Part 3). The above discussion
illustrates that tidal currents do not entrain sediment on flats
shallower than the midtide level, and only sporadically entrain sediment
on the lower intertidal flats, in areas adjacent to the intertidal or
subtidal channels. Larger bedforms are restricted to the inlet area
south of line 15, where current velocities probably exceed 60 cm/s .

Wind-driven currents

On shallow continental shelves, prevailing winds may increase
(or decrease) the velocity of tidal currents by a factor equivalent
to 1.5% or 2% of the wind speed (Caston, 1976). Some data from the
North Sea indicate that above a threshold wind velocity, variously
estimated at from 10 knots (5 m/sec) to 25 knots (12.5 m/sec), near
surface currents may respond to wind by as much as 4 per cent of the
wind speed (Caston, 1976). Hellstrom (1940), Norrman (1964) and
Kjerfve (1975), among others, have shown that in shallow, enclosed
basins, wind stress on the surface tends to pile water against the
downwind shore (wind setup) with the result that water levels fall
at the upwind shore (wind setdown). The phenomenon is known as a
wind tide, and it may generate quite strong currents as water flows
away from the setup end.

Figure 19. The intertidal configuration of the ebb-tide delta of the Avon-Heathcote Estuary (in Moncks Bay) in mid 1975 (top) and mid 1977 (below). Notice the seperation of ebb (1) and flood (2) channels in 1975, flood-oriented megaripples (3), and sandwaves (4), and ebb-oriented sand waves on the flood ramp (5) (see Hayes, 1975; Coastal Research Group, 1969; and Allen, 1968 for terminology). By mid 1977 the ebb spit had grown east towards the entrance at Shag Rock (6), and been breached by the ebb flow (7). Notice the ebb-oriented sand waves (8, 9), ebb-oriented megaripples (10), and flood-oriented slightly undulatory sand waves (11). Both photographs by Frank McGregor

Knox and Kilner (1973) have described the pattern of water
movements on the eastern side of the estuary on both windy and calm
days (their observations are summarised in Figure 17), and the writer
made similar observations - on days when a moderate to strong easterly
blows, turbid water entering the estuary from the CDB outfalls near the
western end of line 6 (Map 1) flows south along the western shore of
the estuary on the ebbing tide, and enters the Heathcote channel in the
eastern Heathcote Basin. On calm days the turbid plume flows obliquely
offshore, entering the Avon channel at location 3, Figure 20. This is
interpreted as evidence that the east wind influences the circulation
of water across the western flats, and generates a long-shore current
which flows down the western shore of the estuary.

A predictable result of increasing depths of water over the
intertidal zone of the AHE is that maximum wave sizes will increase,
more stress will be exerted on the water mass by winds, and setups
will be more likely to occur. There is some evidence that a coincidence
of spring high tides and strong south-west winds may cause more than
normal supratidal flooding in the north-east corner of the estuary
and upstream in the Avon River (P.J. McWilliam, pers. comm.), probably
as a result of wind setup.

It is concluded from the above observations that both east and
south-west winds influence the circulation of water on an estuary-wide
scale during the period around high tide, and the speculative model
presented as Figure 20 is an attempt to predict the effects of these
influences. The overall results are that Avon River water will tend to
flow more across the western than the eastern intertidal flats in the
north; Heathcote River water will tend to be ponded in the Heathcote
Basin, and flow slowly seawards, and sediment suspended from the eastern
and central flats will tend to be transported west across the estuary by
advection (in suspension in a moving water mass).

Apart from the brief qualitative observations outlined above,
these possible effects are unexplored in the AHE; yet they may be quite
significant - a 20 knot wind which produced a current equivalent to 5%
of wind speed would be generating a 50 cm/s current. Added to an
ebbing tide, such a current could more than double normal tidal
velocities, and so significantly alter the ability of tidal currents
to entrain sediment.
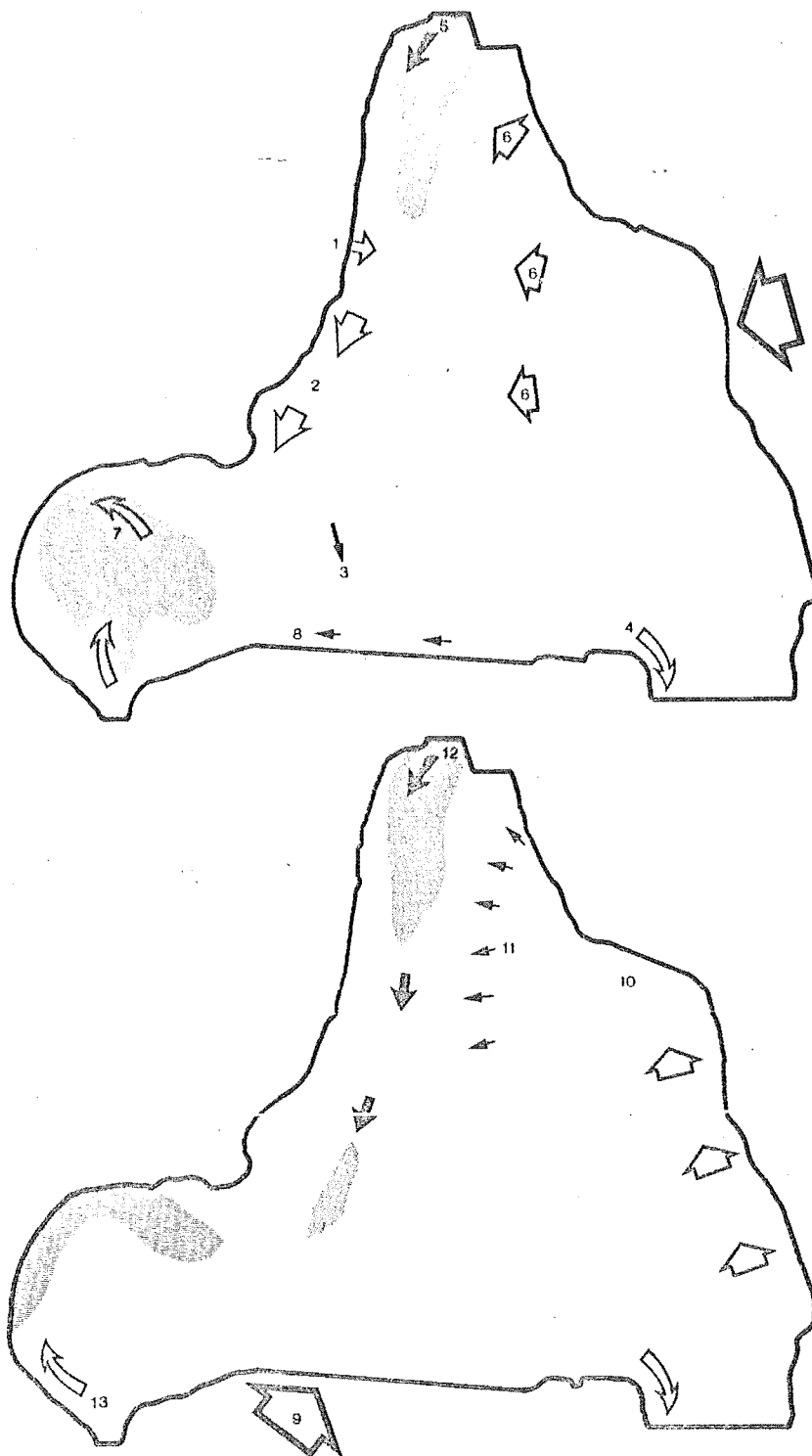
Figure 20. Possible wind-driven advective circulation of the Avon-Heathcote Estuary.

On days when the east wind exceeds about 10 knots (5m/s), effluent discharged from CDB outfalls at (1) shortly after high tide, flows as a turbid plume down the west side of the estuary (Figure 18)(2) to enter the Heathcote Channel at (3) after about 170 minutes. By 300 minutes the leading edge of the plume may be at Beachville Road (4).

Water entering the estuary from the Avon River may be directed westwards (5) as water entrained by the east wind flows downwind across the central flats. Water on the eastern flats will tend to flow north and west for some time after high tide (6), producing a flood-oriented flow assymetry over the eastern flats.

Water entering from the Heathcote River may be ponded in the Heathcote Basin (7) and flow slowly eastwards against the east wind setup 8

When southwest winds blow (9) water may be forced northwards along the eastern shore to contribute to a setup in the northern end of the estuary (10). Water may flow westward away from the setup surge (11), diverting Avon River water west across the western slopes and flats (12), as on easterly days.

Heathcote River water may flow northwards away from the southwest sitdown at (13) and be ponded in the Heathcote Basin, as on easterly days.

Map 1

INTERTIDAL BATHYMETRY of the AVON-HEATHCOTE ESTUARY

Contours are height above Christchurch Drainage Board datum in metres (1), based on surveying done in late 1975, 1976 and early 1977. Contour interval is 10cm. Map is not planimetrically correct - contouring is based on interpolation between surveyed lines, guided by uncontrolled vertical air photographs. Subtidal channels are not contoured - see Appendix 2 for details.

Tidal levels with reference to CDB datum		Water depth with reference to CDB datum	
Highest high tide (HHT)	10.79m HAD	Depth below HWOST	HAD
High water ordinary spring tide	10.21		
Mean high tide (MHT)	9.87	0	10.20
High water ordinary neap tide	9.54	20	10.00
		40	9.8
Mean tide level (MTL)	8.99	80	9.4
Low water ordinary neap tide	8.20	100	9.2
Mean low tide (MLT)	8.12	120	9.0
Low water ordinary spring tide	8.05m HAD	140	8.8
		180 cm	8.6 m HAD

Land margins are classified as seawall (2), rip-rap shore protection (3), sandy beach at HWOST level (4), man-made earth works (5), or cliffed and eroding salt marsh (6). Numbered circles (7) indicate permanent (usually concrete) markers at the ends of surveyed lines 2-16.

Surveying controlled by Tom Cleary (CDB), map drafted by J. K. Macpherson, drawn by Lee Leonard in December 1977.
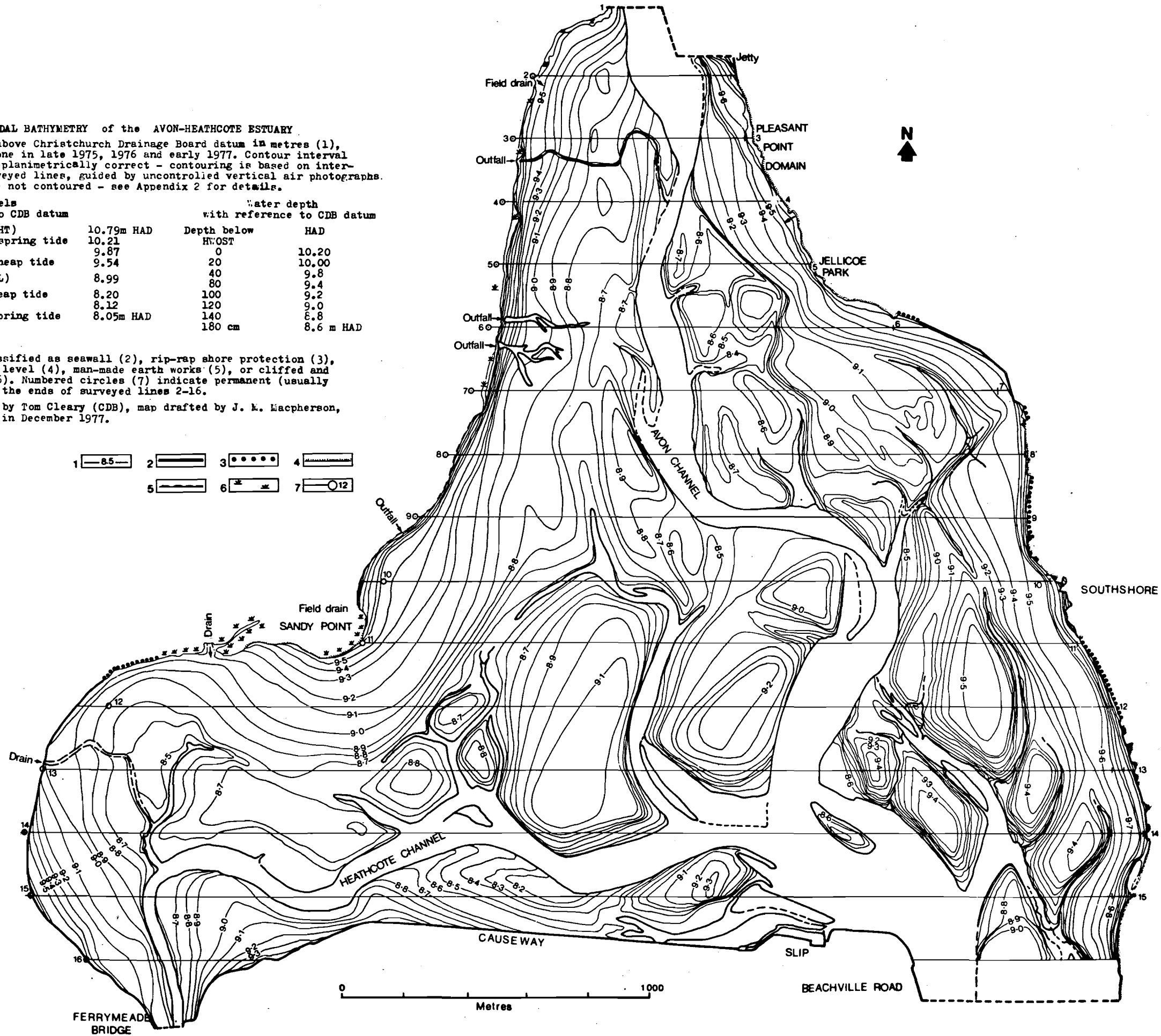
PART THREE

BATHYMETRY

Introduction

An examination of the profiles in Appendix 2 indicates that the intertidal zone of the AHE can be separated into a small number of bathyforms - intertidal landforms - which are characterised by consistent heights above datum, shape and orientation; and which show uniform and predictable patterns of erosion and deposition of sediment over the period 1962-1975/77. A scheme which subdivides the AHE into 12 such bathyforms is presented in Figure 21.

Descriptions and interpretations

1. Eastern high tide slopes.

(i) The eastern high tide slopes (bathyform 1 in Figure 21) extend from the high water mark to the first intertidal or subtidal channel, and occur along the complete length of the eastern side of the estuary. The shoreline along this eastern side may consist of a sandy beach, a cliff eroded into salt marsh deposits, a seawall, or riprap shore protection (Figure 22). Offshore, these eastern slopes are usually low angle convex upwards features, commonly with a break in slope at about 9.5 to 9.6 m HAD - for example see profiles 5, 6, 8, 9 and 10, Figure 23. Occasionally there is an upper slope, above 9.5 m, which is steeper and concave offshore, as in profile 10, Figure 23.

(ii) Wave-induced, near-bottom shear stresses are highest in water which is shallower than 0.5 m in the AHE, and we have seen (in Part 2), that wave formed ripples often occur on intertidal flats and slopes above 9.0 m HAD. If wave energy has any influence on the bathymetry of this estuary, it should be easiest to identify this influence in the area of the eastern high tide slopes, where maximum shear stresses occur.

Figure 25 shows a plot of steepness (defined as the horizontal distance from the high water mark to the 9.6 m contour, measured along bathymetric profiles 2 - 15) vs south-west wind fetch distance.
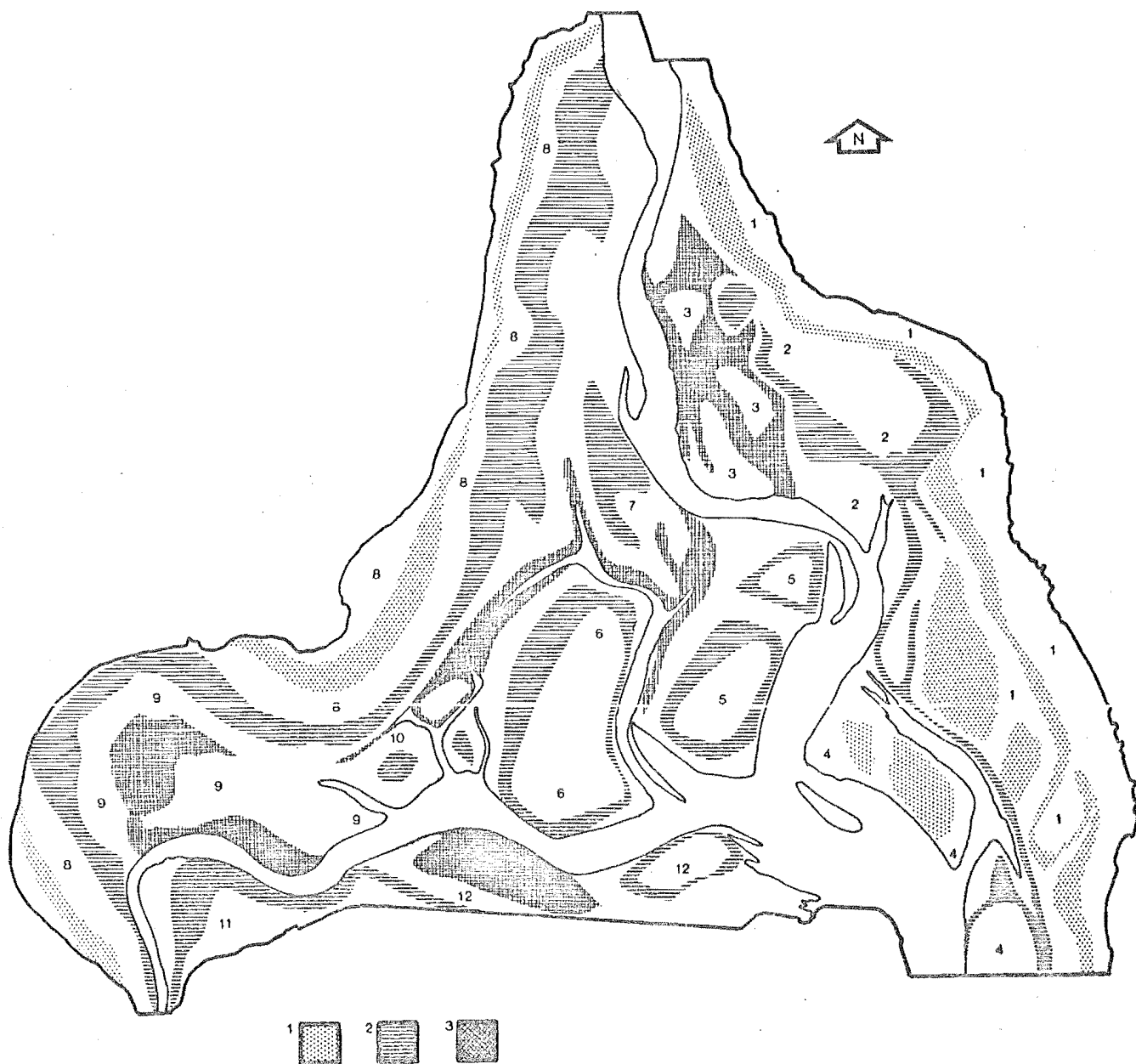
Figure 21. Intertidal bathyforms of the Avon-Heathcote Estuary.

1. - Eastern high tide slopes. 2. - Eastern mid tide shelf.
3. - Eastern low tide flats. 4. - Flood tide delta. 5 to 7. - Central
mounds. 8. - Western slopes and flats. 9. - Heathcote Basin.
10. - Central low tide flats. 11. - Southern mid tide flats.
12. - Southern slopes and flats, McCormacks Bay channels. Shading
indicates zones between 9.2 and 9.4m HAD (1), between 8.8 and 9.0m
(2), and below 8.6m (3). This figure is summarised from Map 1.
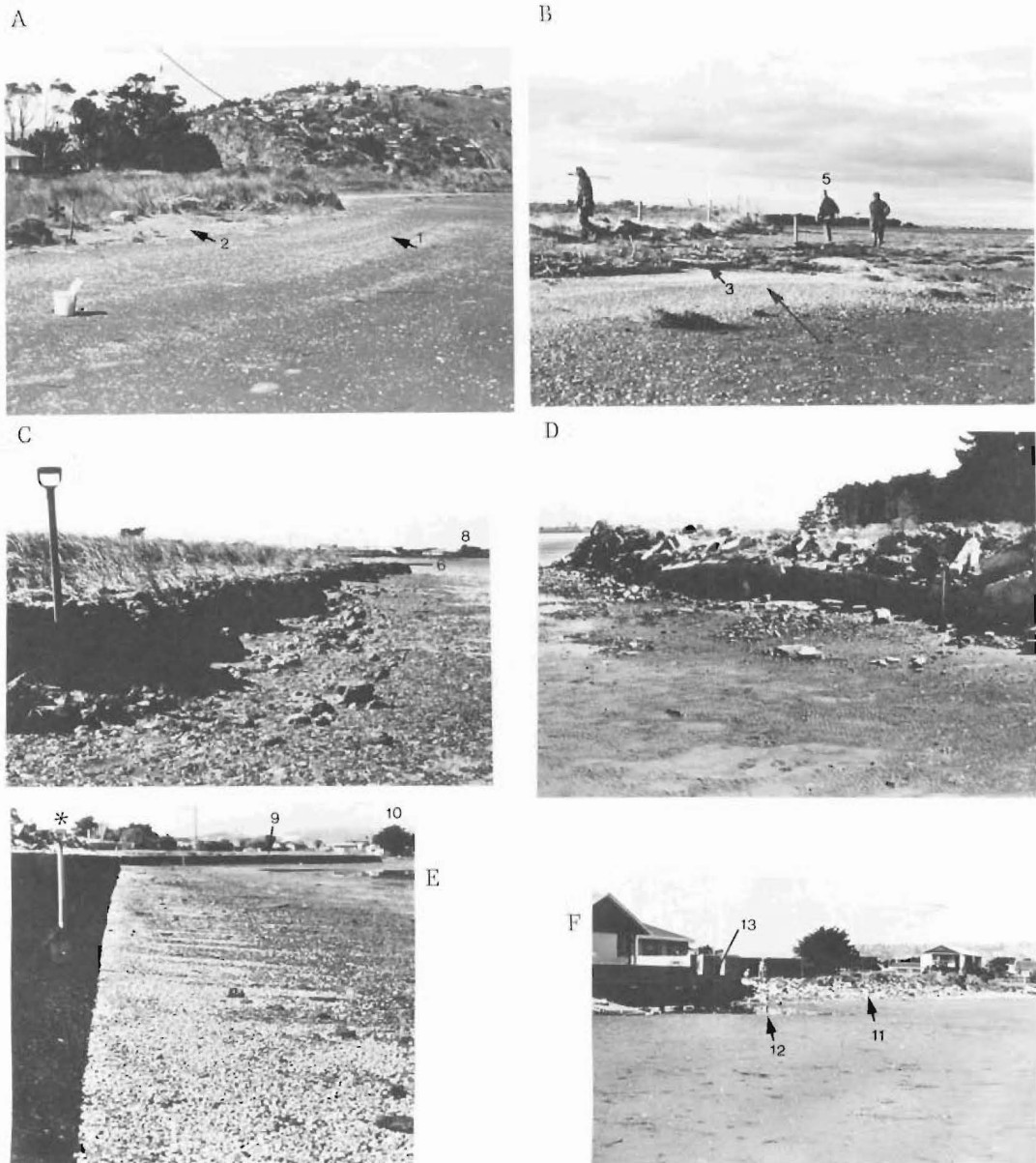
Figure 22. Shorelines of the Avon-Heathcote Estuary. A, B - Sandy and shelly
HW mark beaches. Note swash marks (water level marks) (1 and 4), and the line
of debris along the HWOST mark (2 and 3). A is near east end of line 16, Map 1,
B is south side of Sndt Point. Spade (1 metre high, *) and CDB survey crew
(5) give scales. C - Eroding salt marsh, south Pleasant Point area, near the
east end of line 6, Map 1. Note HWOST level (6) and boulder sized mud particles
(7)eroded from cliffed marsh deposits. Spade for scale, view is east south east,
location (8) is similar to location (10) below. D - Coarse riprap shore
protection, immediately west of C, above. Spade for scale (*). E - Seawall at
east end of lines 6 and 7, Map 1. Spade for scale (*). F - Fine riprap shore
protection (11), Southshore area, near the east end of line 13, Map 1. Note
shallow pond (12) in front of a vertical concrete block seawall (13), probably
due to reflection of waves at high tide.

looking north
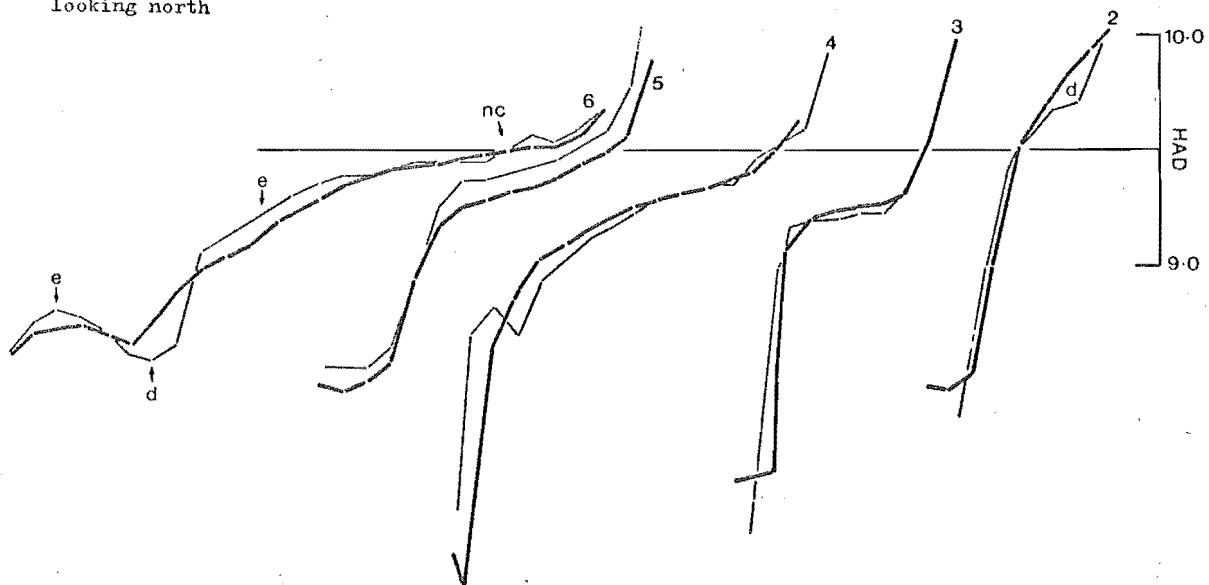
Heavy lines are profiles surveyed in 1975 and 1976 ('75),
lighter lines are profiles surveyed in 1962 ('62).

e = erosion, nc = no change,
d = deposition.

Vertical scale is height above datum
in metres, where 10.21m HAD = HWOST.

Refer to Appendix 2 and Map 1
for location details.
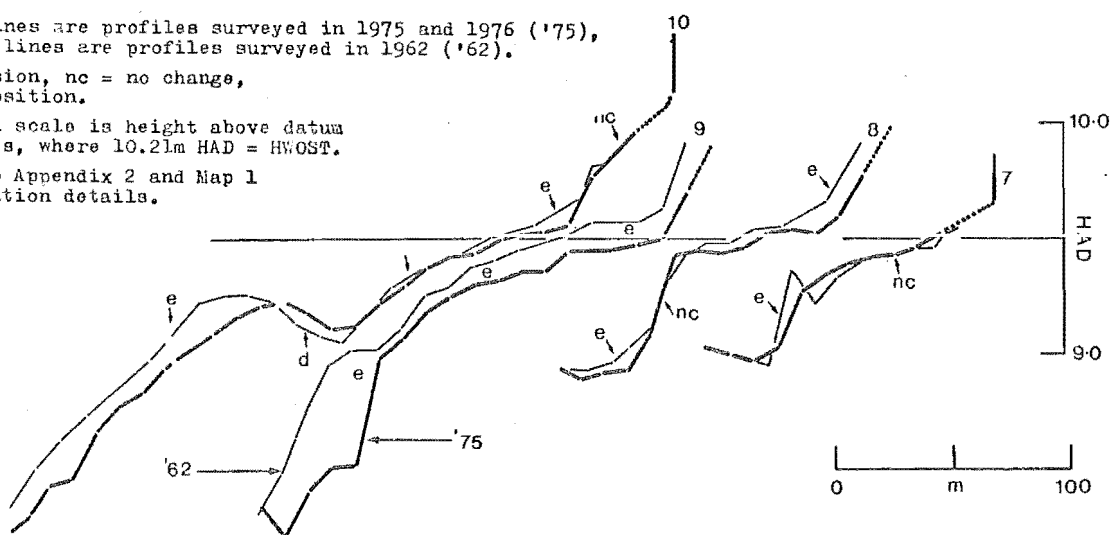
Figure 23. Bathymorphic profiles. Eastern high tide slopes, lines 2-10.

looking north
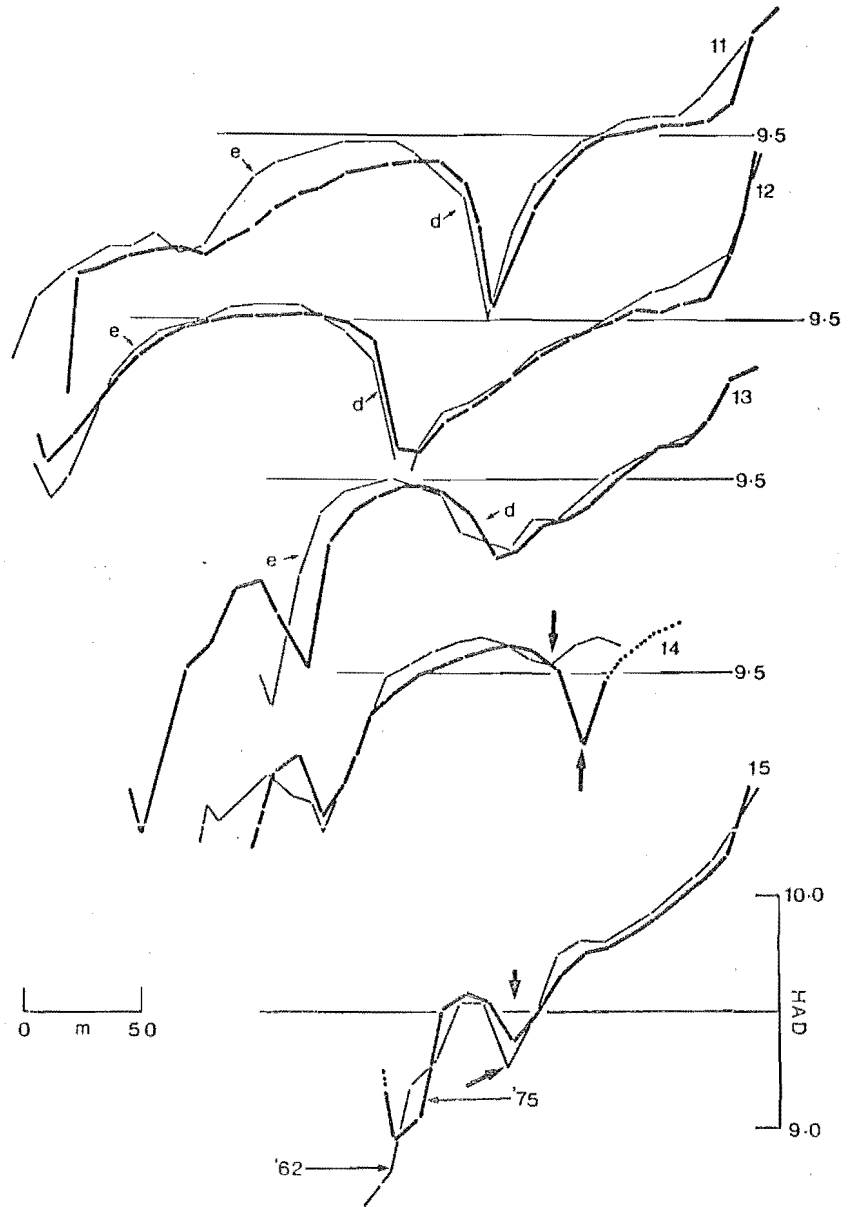
Figure 24. Bathymorphic profiles. Eastern high tide slopes, lines 11-15. Legend as in Figure 23.
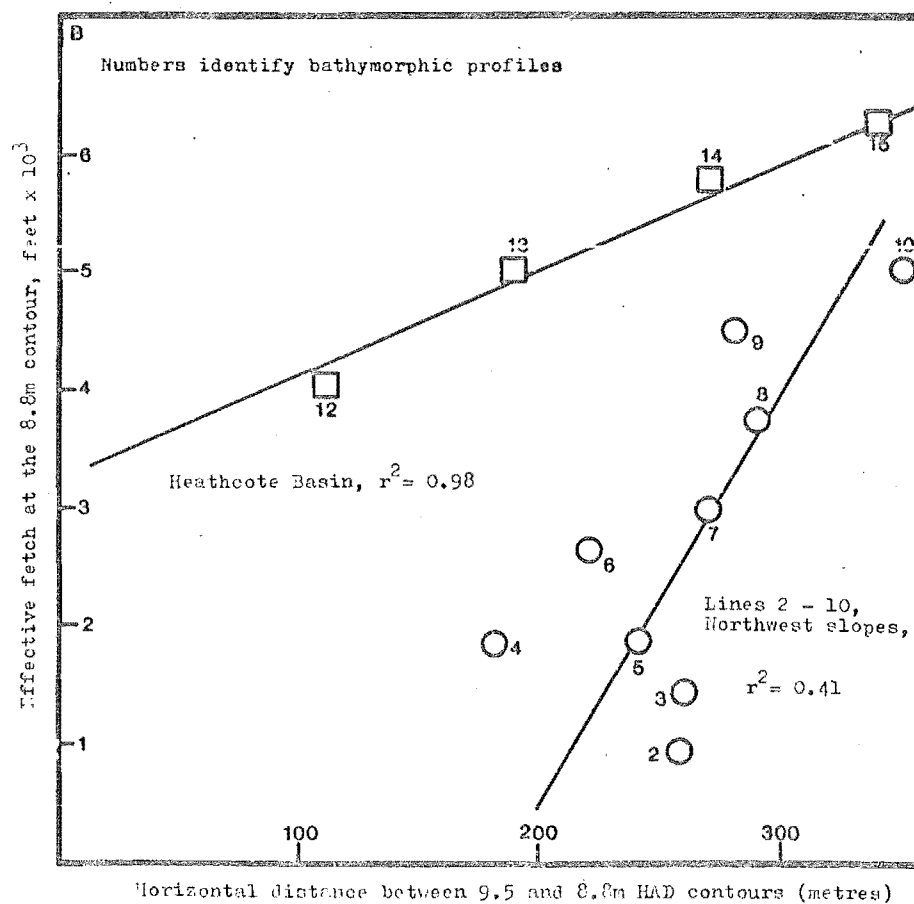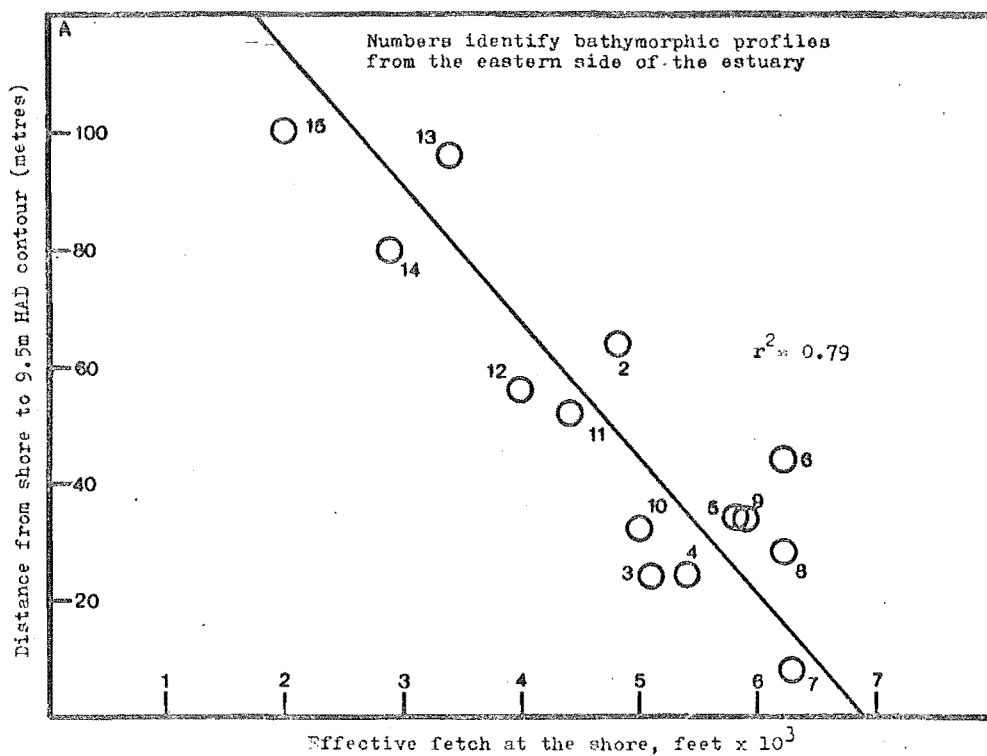
Figure 25. Bathymorphic response to wave energy. A – Distance from high water mark to the 9.6m HAD contour vs effective southwest fetch, crosslines 2-15, eastern high tide slopes. B – Steepness of the western high tide slope (defined as the shore-normal distance between the 9.5m and 8.8m HAD contours) vs effective east fetch, lines 12-15, Heathcote Basin, and lines 2-10, northwest high tide slopes.

The good linear fit between steepness and fetch distance (and thus wave energy) indicates that the configuration of these upper eastern slopes is significantly influenced by wave energy.

(iii) Between lines 10 and 16 the eastern slopes are separated from a flight of offshore mounds by three deeply incised arcuate intertidal channels. In this area north-west winds have maximum fetch distances, and the offshore mounds and channels appear to be aligned normal to the direction of the mean north-west wind. In the north, from lines 5 to 9, the bathymetry appears to be aligned normal to the south-west wind. Figure 26 indicates that these effects are probably responses to a vector product of the two west winds, and that the eastern high tide slope is responding to wave energy by orienting itself normal to the dominant wave approach direction. Rosin (1975) has demonstrated an analogous (but more striking) response in a microtidal estuary in the U.S.A. (Nantucket Harbour) where shoreline features display a long-term equilibrium configuration governed largely by the direction of wave approach.

The patterns of erosion and deposition shown in Figures 23 and 24 indicate that where profiles have changed over the period 1962-75, the general shape has been conserved, and the trend is towards a uniform concave-convex configuration. Where deposition has occurred it has been in the lee of bathymetric highs (lines 6, 10, 11, 12 and 13). Slopes with no upwind bathymetric high have almost all experienced some erosion. Thus the intertidal channels south of line 9 are migrating landwards, as they line up across the mean incoming wave train (see line 14 especially). Note that the higher ends of lines 6, 7 and 8 changed little over the 12 year period, indicating that here, where wave energy is highest, the bathymetry has achieved a quasi-stable form. The higher ends of lines 12, 13 and 14 show similar stability, presumably for the same reason, but with respect to the north-west wind.

2. *Eastern mid tide shelf and low tide flats.* Between the foot of the high tide slope and the Avon channel, the eastern intertidal flats are separable into a midtide bathyform (number 2 in Figure 27), and a low tide bathyform (number 3 in Figure 27), with mean heights above datum of about 9.0 m and 8.75 m respectively.

(i) Figure 27 shows that in bathyforms 2 and 3, westward facing slopes were usually eroded between 1962 and 1975, whereas east facing slopes usually accumulated sediment.

West facing slopes in the lee of bathymetric highs showed little change, and intertidal channels have maintained their positions.

(ii) The stability over the 12 year period of relatively steep slopes, particularly at the landward edges of these bathyforms, indicates that unlike the high tide slope, these flats are not attempting to orient themselves with respect to prevailing or vector wave approaches. The analysis in Part 2 has shown that in water 1.5 m deep, over a smooth bottom, the orbital motion of 1.4 s waves exerts only 0.5 dynes/cm^2 on the bottom, and the above observations indicate that this is not sufficient to significantly influence the configuration of the intertidal zone at depths below the midtide level (below 9.0 m).

3. Western slopes and flats. Figures 28 and 29 show the east-facing bathymorphic profiles of the western intertidal zone. This side of the estuary is influenced predominantly by east wind waves (Figure 10) and effective fetch increases progressively from north to south. There is a corresponding decrease in the steepness of the intertidal zone (Figure 25B), indicating that the higher flats on this side of the estuary are also responding to wave energy.

(i) Downfetch (higher wave energy) west side profiles resemble those from the higher energy sector of the opposite shore (compare the western and eastern ends of profile 10, Appendix 2); this is interpreted to mean that the trend visible in Figures 28 and 29 is towards a universal form, stable at the energy levels associated with fetch distances of about 6 000 feet (1 800 m). In this estuary, wave energy gradients are a result of increasing shear stress frequencies, not increasing wave size – since maximum waves are of uniform size throughout the estuary. Thus the equilibrium bathymetry demonstrated above is a response to more frequent stress, not to changes in absolute levels of stress. As effective fetch distances increase from north to south, the total amount of sediment involved in erosion and deposition over the period 1962-1975/77 decreases. This may mean that the rate of response to wave energy is also related to shear stress frequency, and that given sufficient time, the north-west slopes may also adopt a stable configuration similar to that in the south-west. This conclusion has significant implications, especially where shoreward erosion of salt marsh may soon threaten stopbanks on the eastern edges of CDB oxidation ponds.
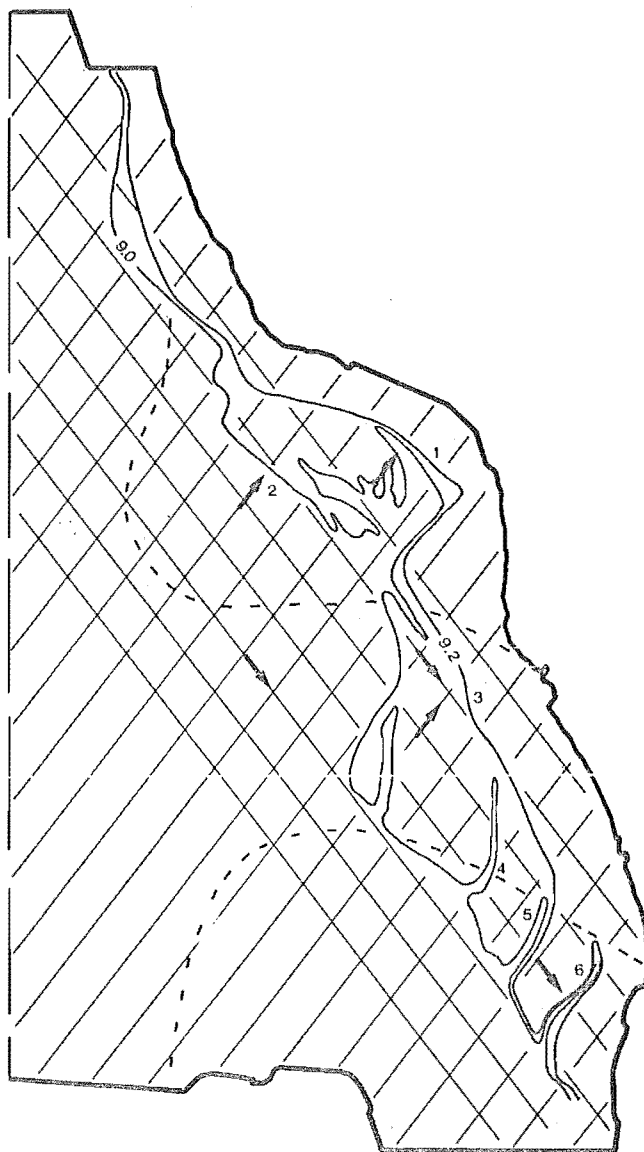
Figure 26. Summary bathymetry and wave energy distribution of the eastern side of the AHE. Contours are 9.0m and 9.2m HAD, and 5 000 feet effective fetch (--). Straight lines indicate mean south west (217°) and north west (323°) wind directions (⟶) from Figure 10. Notice alingment normal to longest-fetch south west winds at 1 and 2, and an alignment normal to a probable vector product of the two winds, at 3. Notice also an increasing tendency for the 9.0 to 9.2m bathymetry to align itself normal to the north west wind where effective fetch distances approach 5 000 feet, from 4 to 6.

Lines 7 and 8   Eastern mid tide shelf   looking north
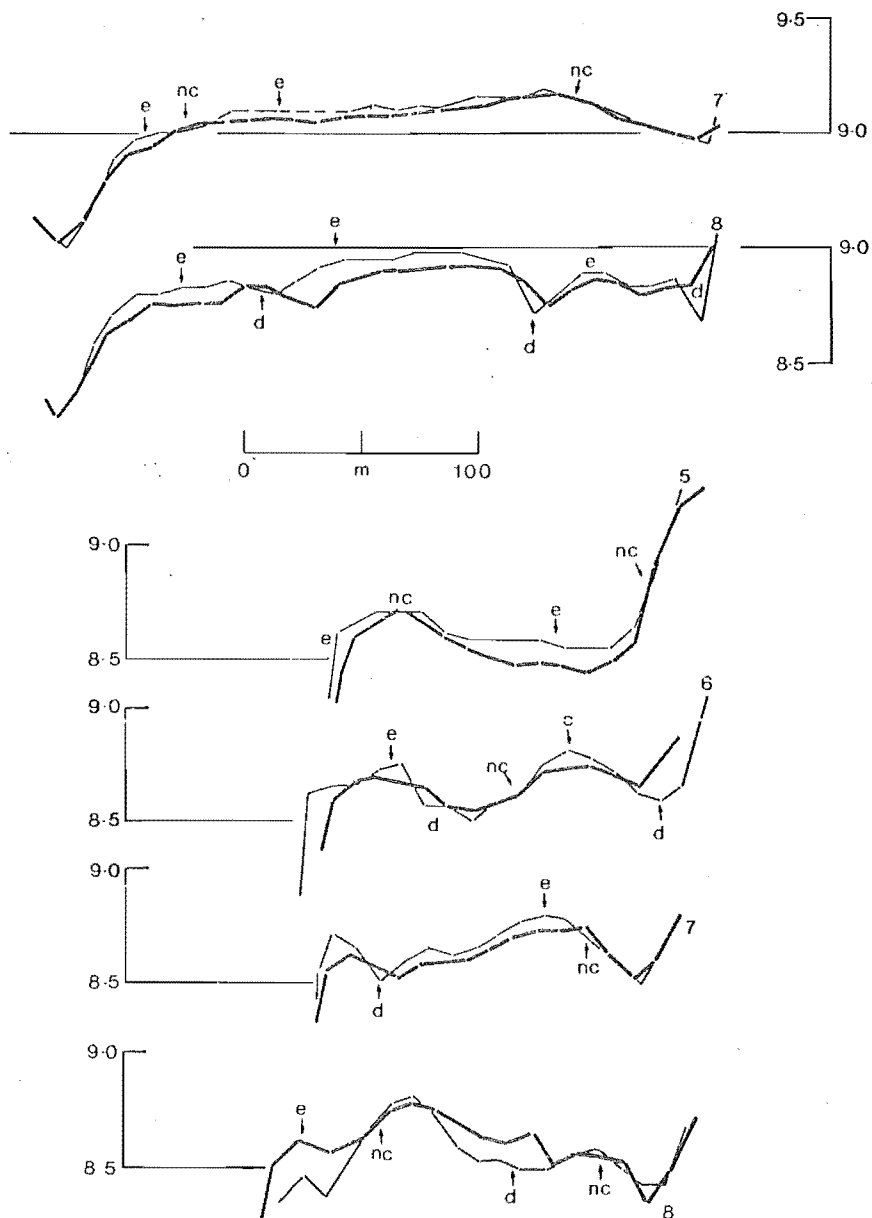
Figure 27. Bathymorphic profiles. Eastern midtide shelf, lines 7 and 8. Eastern low tide flats, lines 5-8. Legend as in Figure 23.
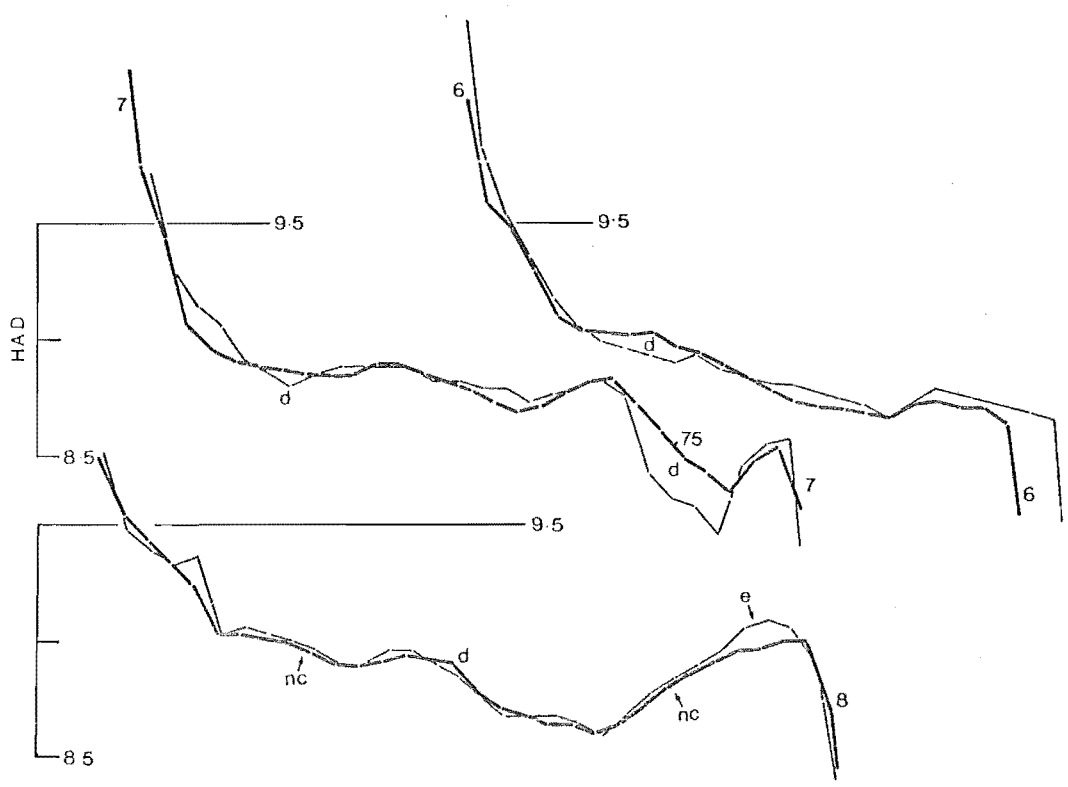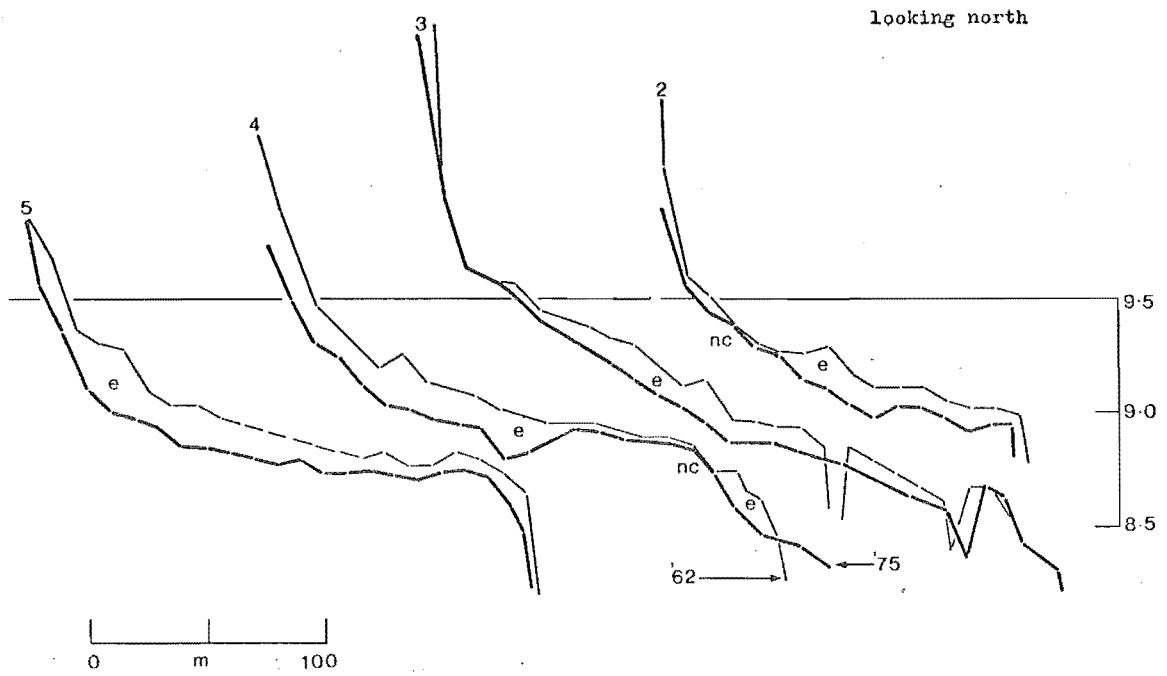
Figure 28. Bathymorphic profiles. Western slopes and flats, lines 2-8. Legend as in 23.

looking north

$$ \vdash\!\dashv $$

0   m   100

9·5

d

d

9

9·5

9·5

d

10

'62   d   '75

11

15

14

9·5

13

12

HAD

d

8·5
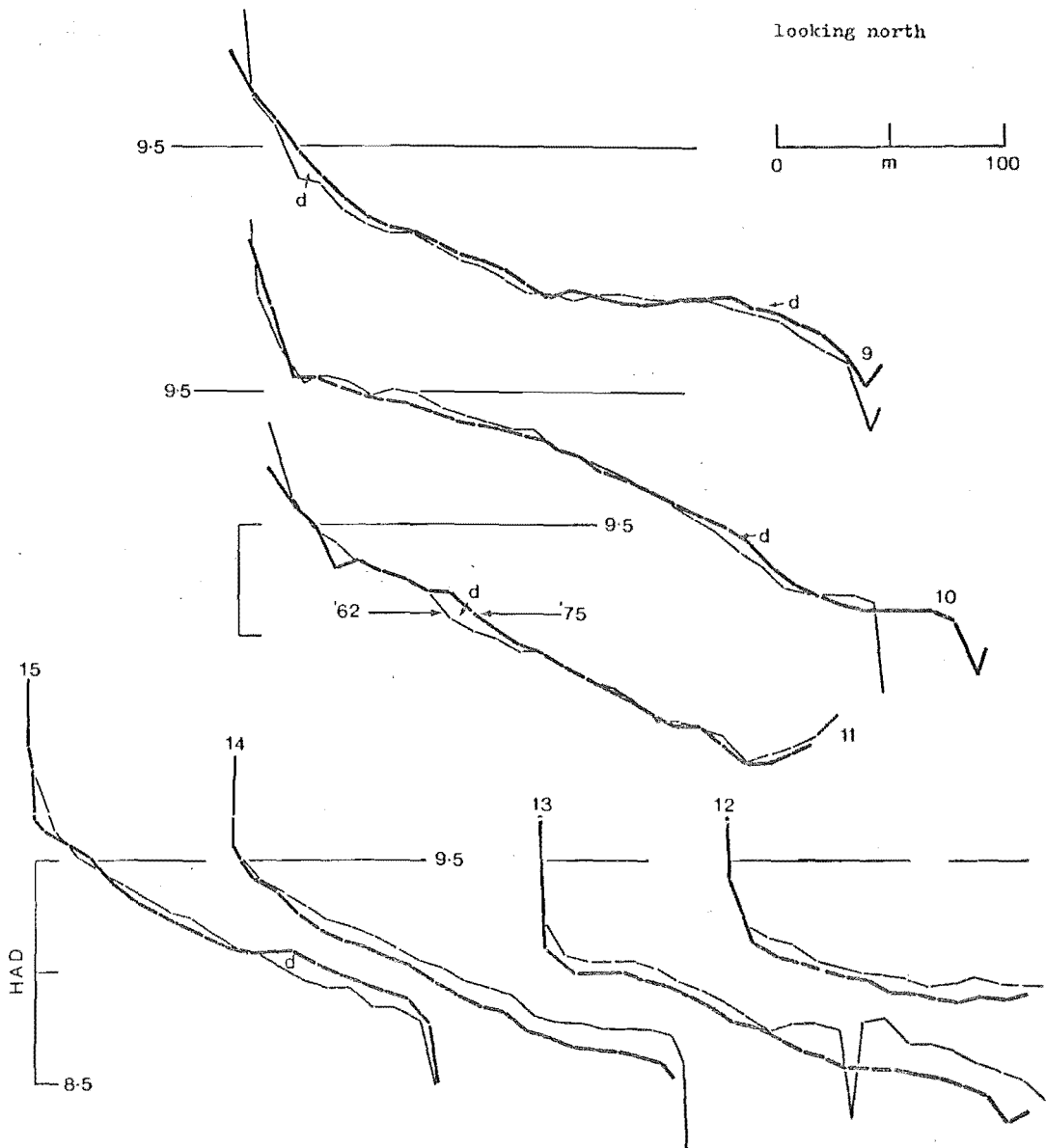
Figure 29. Bathymorphic profiles. Western slopes, lines 9–15. Legend as in Figure 23.
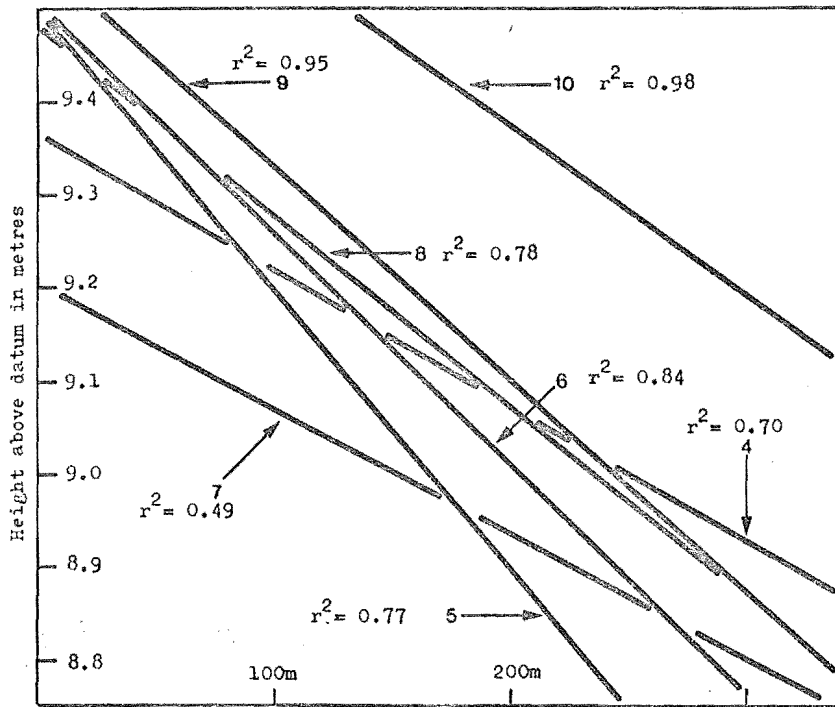
A. Linear regressions fitted to height above datum vs distance offshore for survey lines 4 through 10, west side. Higher coefficients of determination indicate straighter survey lines.
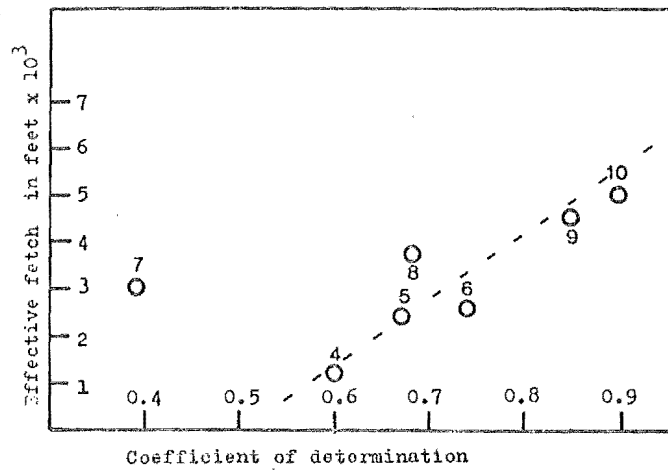
B. Profile straightness (from A) vs effective fetch at the 8.8m HAD contour, for survey lines 4 through 10, west side.

Figure 30. Bathymorphic response to wave energy. A - Profile straigtness. B - Profile straighness vs effective fetch. Lines 2-10, western slopes.

(ii)   The steepness trend demonstrated in Figure 25B is accompanied by a parallel trend towards profile straightness - line 11, for example, is quite straight. This straightness trend can be illustrated by plotting distance offshore (from the 9.5 m contour to the 8.8 m contour) against HAD, for survey stations along each of the western profiles. The regression lines and their coefficients of determination are plotted in Figure 30A, and in 30B, coefficients of determination are plotted against effective fetch, showing clearly that apart from profile 7, coefficients are higher (lines are straighter) as fetch increaes.

4. *The Heathcote Basin*. Because fetch width has a relatively large influence on effective fetch values in the narrow Heathcote Basin, patterns of increasing wave energy (with respect to the east wind) are difficult to predict. Notice however that profiles 12, 13, 14 and 15 (Figure 29), all of which end at the Humphreys Drive seawall, are quite uniform in appearance, steepening slightly to the north. Figure 25B indicates that this is probably a response to increasing fetch, and that these four profiles are slight variations on a straight, high energy profile.

5. *Central mounds*. Bathyforms 5, 6 and 7 (Figure 31); rounded, regularly shaped mounds in the centre of the estuary, show patterns of erosion and deposition which are dominated by the lateral migration of major intertidal and subtidal channels. For example, between 1920 and 1962 a subtidal channel around the northern edge of bathyform 6 was abandoned (see line 10, Appendix 2), and the channel between bathyforms 5 and 6 eroded laterally about 50-60 m over the period 1962-1975/77 - from location 1 to 2 in Figure 31. Away from the major channels relatively little erosion and deposition occurred between 1962 and 1975/77.

6. *Throughgoing subtidal channels*. For convenience, only the Avon and Heathcote throughgoing channels are termed subtidal. Minor contributory-distributary channels may be at least partly subtidal, or subtidal only during neap tides; since they always originate on, or flow across, the intertidal flats, they are termed intertidal. Where the two subtidal channels meet - off Beachville Road, Figure 5 - they become the principal subtidal channel, which flows out to sea.

looking north

9·0

8

9·0

11

9·0

12

0   m   100

HAD

9·5

9·0

8·5

13

a

b

e

2

d

stc

'62

'75
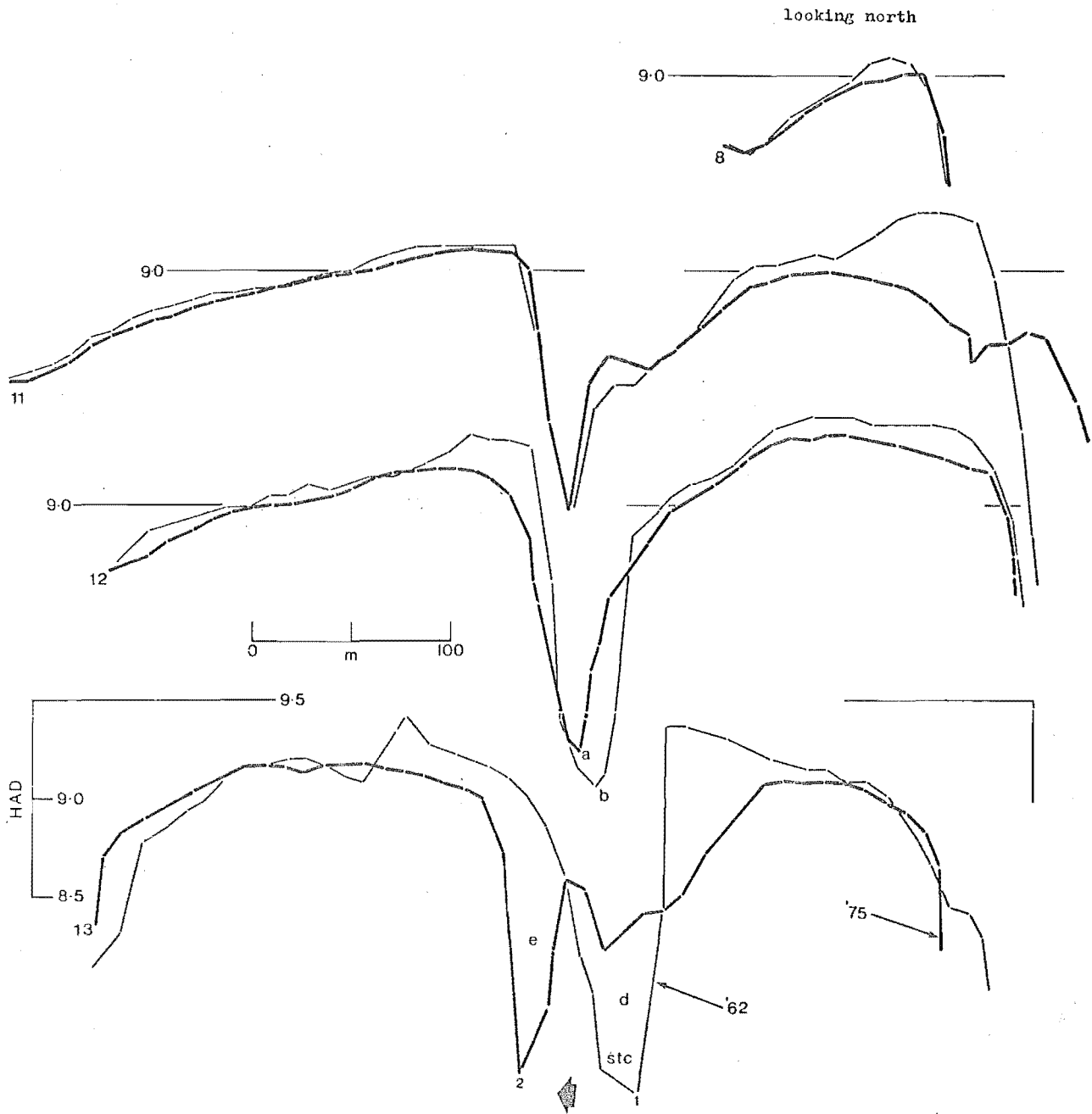
Figure 31. Bathymorphic profiles, Central sand mounds, lines 8, 11-13. Legend as 23.

Both intertidal and subtidal channels are steep sided features (Appendix 2), with a break in slope at the edge of the intertidal flats at about 8.5 to 8.6 m HAD (50-60 cm above HWOST, 30-40 cm above HWONT). Thus flow is wholly within the channels for about 2-4 hours around low tide, and they become extensions of their respective rivers until some time after the tide turns. Very little standing or slow-moving water remains on the intertidal flats once they are uncovered on the ebb tide. The Avon and Heatchote channels are quite shallow where they enter the estuary (at Bridge Street Bridge and Ferrymeade Bridge) averaging about 1.0 m to 1.5 m below LWOST, with deeper pools down to 2.5 m below LWOST. As they approach their confluence, and the start of the common channel, they deepen to about 2.5 m to 3.0 m below LWOST, and from the beginning of the common channel, water depth increases rapidly, to a maximum of about a metre above datum (7 or 8 metres deep), just upstream from Shag Rock (Royds and Sutherland, 1962).

The profiles in Appendix 2 reveal that few major changes have occurred in the positions or depths of the subtidal channels since 1920. They do tend to be slightly deeper and straighter than in 1920, and some lateral adjustments have occurred. For example, see lines 2 and 6, Appendix 2, where the Avon has abandoned the channel it preferred in 1920 and eroded a new one, resulting in a straighter configuration. Historical evidence for changes over the period 1850-1920 is sparse, although there is agreement that both the Avon and Heathcote channels widened and straightened their courses over that period (Hutchinson, 1972; Knox and Kilner, 1973). Knox and Kilner record that the Avon channel would not have been navigable by a boat with a 2 foot draft at low water in 1858.

These widening and straightening trends are interpreted to be an adjustment to the increasing tidal compartment, and to be analogous to changes in the configuration of the principal subtidal channel, which has also adjusted to changes in the volume of the tidal compartment (Part One).

Discussion

(i) No attempt has been made to describe the sedimentology or bathymetry of the inlet area (the ebb and flood deltas south of line 16) for two reasons: because it was recognised early in the project that intertidal processes within the body of the estuary were probably more

important in its post-European evolution, and because tidal deltas have been quite well documented in the literature, and delta processes are well known (for example see Coastal Research Group, 1969; Klein, 1970; Boothroyd and Hubbard, 1974; Hayes, 1975; Allen and Friend, 1976).

(ii)   Resio and others (1977) have analysed the bathymetry of the shallow continental shelf off the Atlantic and Gulf Coasts of the U.S.A.   They found that offshore profiles could be divided into two segments;   a curvilinear, concave upwards, nearshore segment, and a linear (straight) offshore segment.   They interpreted this configuration to be predominantly wave influenced.

The striking similarity between higher energy profiles from the AHE and typical shelf profiles figured by Resio and others (1977, Figure 1) is intriguing, and suggests that some sections of the AHE may resemble, on a smaller scale, the North American east coast shelf. Perhaps the 'universal' equilibrium configuration of some of the higher intertidal flats of the AHE is a feature of all weather-dominated shelf-like sea floors.

Patterns of erosion and deposition

The 1975/77 resurvey of the AHE was intended to quantify changes which might have occurred since 1962, and the 1920 data was assessed for similar reasons (J.A. Robb, pers. comm.).   The aim was to detect patterns of erosion and deposition, and in particular to provide evidence concerning the role of effluent discharged by the CDB in both local and estuary-wide deposition.   Maps 2 and 3 in Appendix 1 are the first attempts to synthesise data from the three surveys.

Map 2 shows areas of net erosion and deposition for the period 1920-1962 for the area north of line 10 (data were sparse south of line 10, and direct comparison with the 1962 survey was not possible). Landward erosion of supratidal salt marsh has occurred along most of the north-west shore of the estuary (also see Harrison, 1967).   This erosion is continuing, and Millward (1975) considered that tens of metres may have been removed from much of the north-west shore over the past twenty or so years.   Sediment has accumulated on the intertidal flats adjacent to the salt marsh in the north-west corner of the estuary and also in a broad intertidal zone which becomes an intertidal channel (north of area 2) to the south.   Sediment also accumulated where subtidal channels were abandoned between 1920 and 1962 (areas 3 and 4,

Map 2; possibly also area 2).. In general, erosion of sediment from the intertidal flats was widespread, with almost a metre of material removed in some areas (Appendix 1).

Map 3 shows patterns of erosion and deposition for the whole estuary over the period 1962-1975. Inspection of Map 3 and the profiles in Appendix 1 indicates that much smaller volumes of sediment were involved in net movements during this period. Sediment accumulated at all of the major entrances to the estuary: at the Ferrymead Bridge; south of the Jetty in the far north-east; on the flats in the inlet area opposite Beachville Road; and off the outfalls along the western flats north of Sandy Point (see Map 1 for location details). All of these locations are point sources of inflowing water, and it is a reasonable conclusion that sediment deposited adjacent to each, was from external sources. In particular the accumulation of about $60\,000\,m^3$ of sediment in areas 2 and 3, downstream from the CDB outfalls, may indicate that they have been responsible for the deposition of large volumes of sediment.

Figures 28 and 29 show that this material accumulated either in shallow water – for example at about 9.0 m HAD on line 6, and between 9.0 and 9.5 m HAD on lines 9 and 11 – or in deeper water, usually on lee slopes, at the offshore ends of lines 7 - 11. Thus some of this material accumulated in areas sheltered from wave activity, but quite significant amounts accumulated on otherwise stable slopes subjected to high levels of wave activity.

There is no evidence of preferential deposition close to the outfalls – in deeper water the thickness of accumulated sediment seems to be related more to the extent of shelter from east wind waves than to distance from the outfalls (see profile 7, Figure 27). Apart from their proximity to the outfalls, there is no bathymetric evidence that the accumulations of sediment on lines 6 - 11 are related to the release of effluent from the oxidation ponds.

Some sediment deposited near the western end of line 6 has been supplied by the erosion of plunge pools and channels near the outfall pipes, but this redeposition has involved 100s rather than 1 000s of cubic metres of sediment, and is probably insignificant in the overall sediment budget.

An energy-bathymetry model for the Avon-Heathcote Estuary

Figure 32 is a generalised semi-quantitative model of the bathymetric distribution of wave- and tidal current-induced near bottom shear stress in the AHE. The model is based on the simplifying assumption that the bottom may be classified into three depth zones; 9.5 m slopes, flats, and mounds; 9.0 m flats; and 8.75 m flats. Intertidal areas consisting of more or less straight slopes which deepen offshore at constant rates are for convenience considered to be special cases, where the straight horizontal lines in Figures 32B and 32C may be replaced with sloping or curved lines, while the essential relationships remain unchanged.

The modelled energy distribution in Figure 32 is from data in Part 2; for wave energy the simplifying assumption is that shear stress values are 17 dynes/cm on 9.5 m slopes, 2 dynes/cm^2 on 9.0 m flats and mounds, and less than 0.5 dynes/cm^2 on 8.75 m flats. For tidal current energy the corresponding figures are; less than 0.1 dynes/cm^2, 1.2 dynes/cm^2, and 4 dynes/cm^2. In the intertidal channels shear stress values of 12 dynes/cm^2 are assumed.

Figure 32 illustrates three features which are particularly important in the energetics of this estuary:

(i) Areas characterised by high wave energy and high tidal current energy tend to be mutually exclusive.

(ii) At HWOST, wave stresses are an order of magnitude higher in water which is 0.5 m deep (on 9.5 m flats and slopes), than in water which is 1.0 m deep (on 9.0 m flats). The figures are 17 dynes/cm^2 vs about 2 dynes/cm^2.

(iii) Tidal shear stresses are greater than wave-induced shear stresses on the deeper intertidal flats, and reach maximum values in intertidal and subtidal channels.
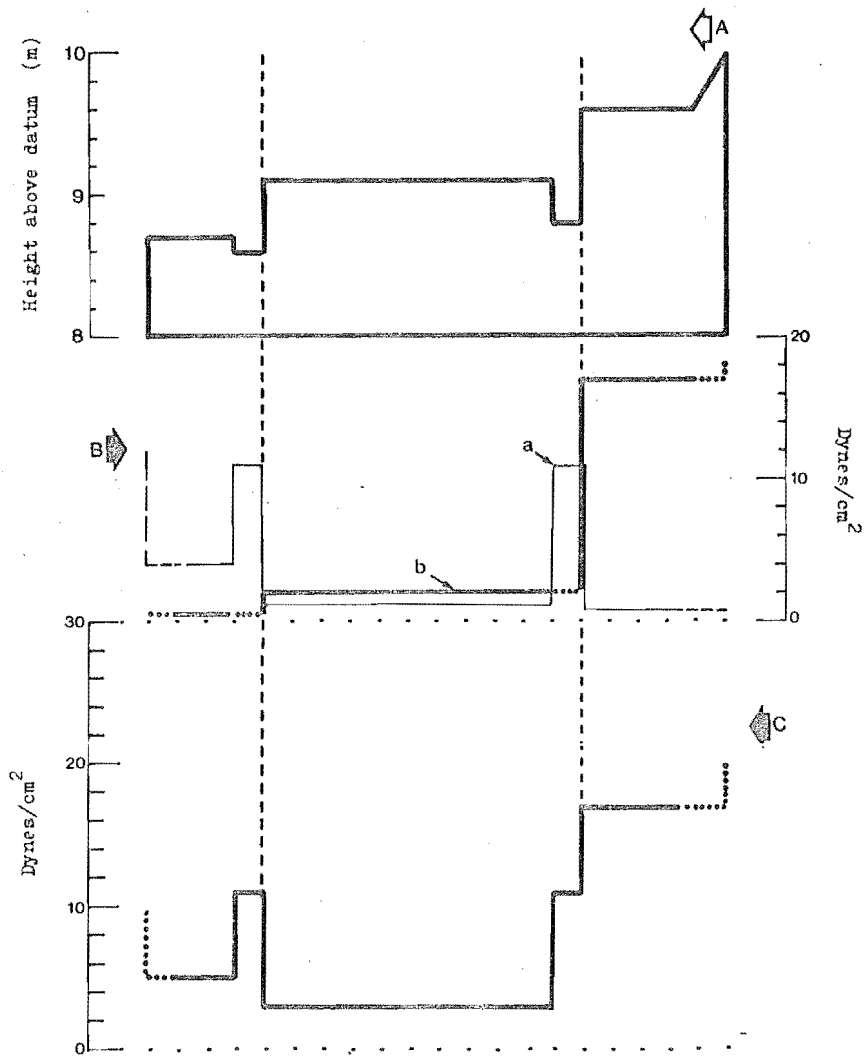
Figure 32. Bathymetry/Energy model of the intertidal slopes and flats of the Avon-Heathcote Estuary. A - Bathymetry model, consisting of 9.5m slopes, 9.0m shelves, and 8.75m HAD low tide flats, with intermediate intertidal channels. B - Modelled distribution of tide induced (a) and wave-induced (b) near bottom shear stress. C - Combined wave and tidal current shear stress, produced by summing (a) and (b) from B.

PART FOUR

SURFACE SEDIMENT

Introduction

Much of the research effort in this study concentrated on surface sediment, because this material potentially bears the imprint of its depositional environment. It may exhibit process-specific properties imprinted on it during transport or deposition, as well as trends which develop in response to local or regional energy gradients.

The theoretical approach to sampling and analysing surface sediment, and the sampling design, sampling methodology and analytical procedures adopted for this study are detailed in Appendix 3. In brief, the need for a reliable, representative and environmentally meaningful sample suite was satisfied by sampling only active, uppermost surface sediment, by performing size analyses only on the sand fractions of surface samples and by using a sedimentation instrument – a Woods Hole-type Rapid Sediment Analyser (RSA) to determine these size distributions. The development and verification of a sampling philosophy led to the preparation of a short paper (Macpherson and Lewis, in prep.) and the arguments presented in that paper are given in an expanded form in Appendix 3. Also included in Appendix 3 are the results of a comparison of size analyses performed by both sieving and sedimentation, and results of tests to examine the reliability of the methods used to measure sediment muddiness, and those used to measure sand fraction granulometrics by sedimentation. An evaluation of the variability likely to be present at or near sampling sites is also presented in Appendix 3.

Mud

Sand and mud sized sedimentary particles are transported and deposited according to different physical laws (see Appendix 3), and their properties and distributions should be considered separately.

1. Observations and interpretations. The muddiest sediment in the AHE occurs in the Heathcote Basin, where an area of about $600\,000\,m^2$ (defined by the 40% mud contour, Figure 33) has a mean muddiness of 60%

(s = 16%, N = 37), and maximum values up to 90%. Sediment with more than 40% mud also occurs along the western intertidal flat, and in the north-west corner of the estuary, where an area of 240 000 m² has a mean muddiness of 50% (s = 11%, N = 31). Two shallow subtidal ponds on the eastern low tide flats are the only other areas with more than 40% mud. The two largest muddy areas will be referred to as the Heathcote and Avon Mud Depositories.

Figure 33 shows that the Heathcote Depository occurs on the lower flats adjacent to the Heathcote River entrance, and that the Avon Depository similarly occurs adjacent to the Avon River entrance. On the central western flats muddy sediment occurs as an elongate zone which becomes narrower and less muddy with increasing distance from the river entrance.

In 1965, automatic turbidity meters were installed in the Avon River (near Gloucester Street) and the Heathcote River (near Buxton Terrace) by the consultants to the CDB (the Wallingford Report, 1970). Both ran for about 12 months, and the results indicate that during 1965, 900 tons (dry weight) of suspended solids was transported down the Avon River (2.5 tpd) and 11 000 tons down the Heathcote (30 tpd). Records for a period of high river flow in April 1968 indicate that values for suspended solids in the Heathcote River were 10 times higher than in the Avon (1 275 ppm vs 135 ppm), and Heathcote flood flows may normally carry an order of magnitude more suspended solids than the Avon.

In Figure 34, all samples from Lines 2 to 11 (Map 1) on the western slopes are grouped into areas of approximately equal size. Regressions of sediment muddiness on to HAD for all samples from each area show that there is an offshore trend towards muddier sediment in deeper water in each of the four areas, that the trends steepen offshore from north to south, and that sediment at equivalent depths tends to be less muddy in the south.

Tidal current velocities and shear stresses increase as water depth increases towards subtidal channels in this estuary (Part Two), so it is unlikely that the patterns of sediment muddiness shown in Figure 33 are significantly influenced by tidal currents - if they were, sediment muddiness would decrease with increasing depth, which is clearly not the case. It is probable that these patterns are influenced both by variations in wave energy, which increases from north to south as east wind fetch distances increase, and by preferential deposition, with the muddiest sediment deposited closest to the source of supply,
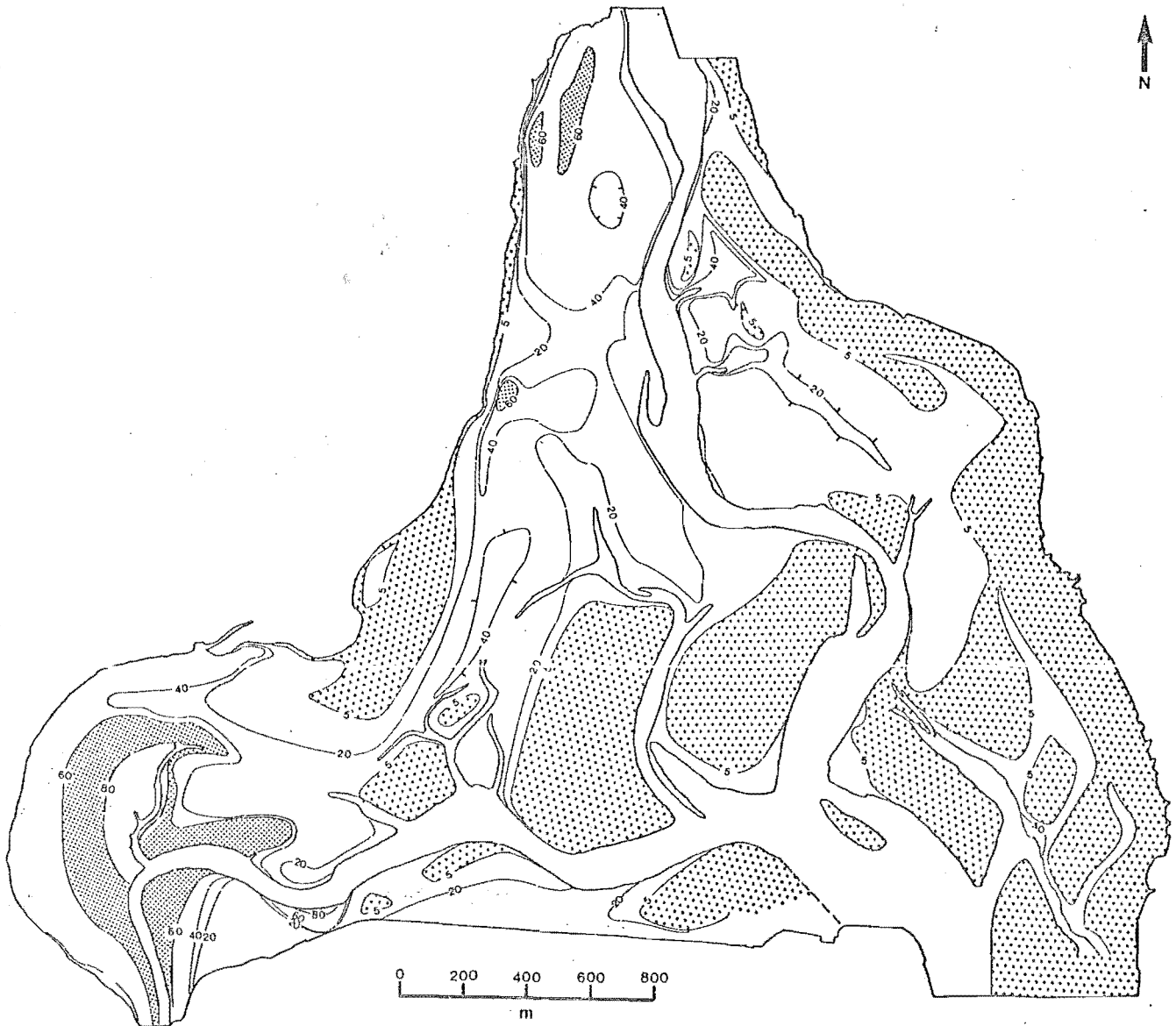
Figure 33 Muddiness of surface sediment of the Avon-Heathcote Estuary. Contoured at 5%, 20%, 40%, 60% and 80%. Closed contours with outer hachures contain higher values within, inner hachures indicate lower values within.
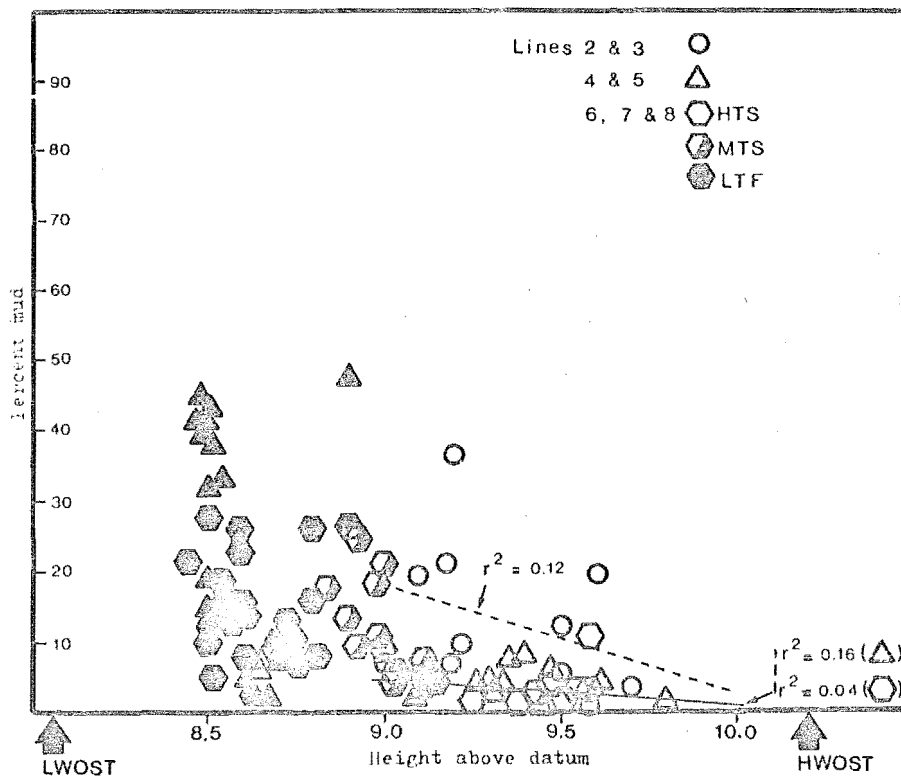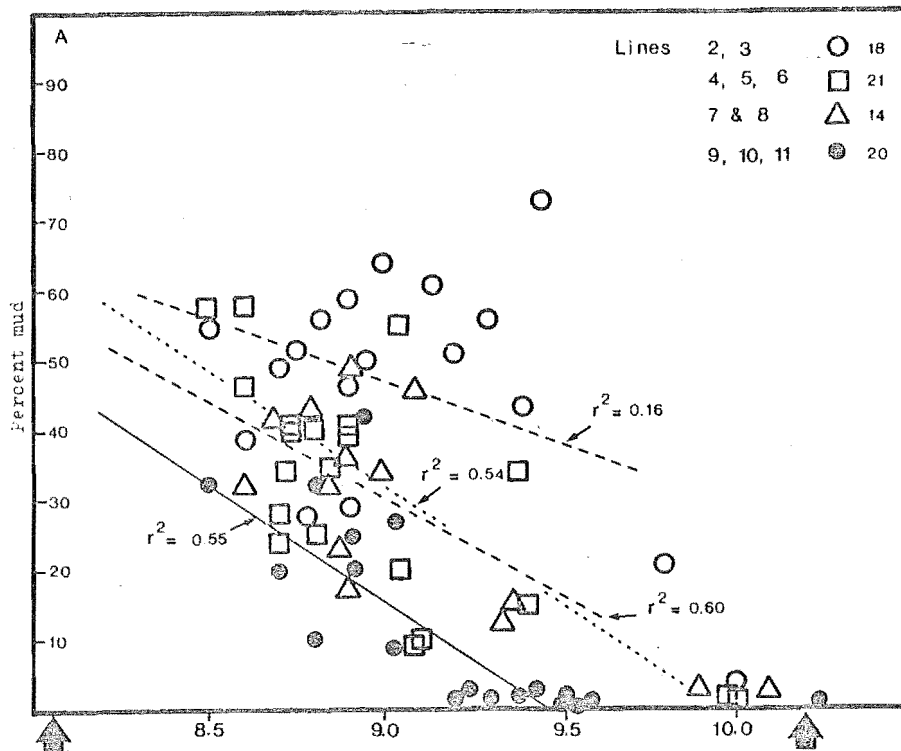
Figure 34. Sediment muddiness vs water depth (as HAD). A - Samples from the western slopes and flats of bathyform 8, lines 2-11. B - Samples from the eastern slopes and flats of bathyforms 1, 2 and 3, lines 2-8. Empty symbols represent high tide slope (HTS) samples, half blacked symbols represent mid tide shelf (MTS) samples, and fully blacked symbols represent low tide flat (LTF) samples.
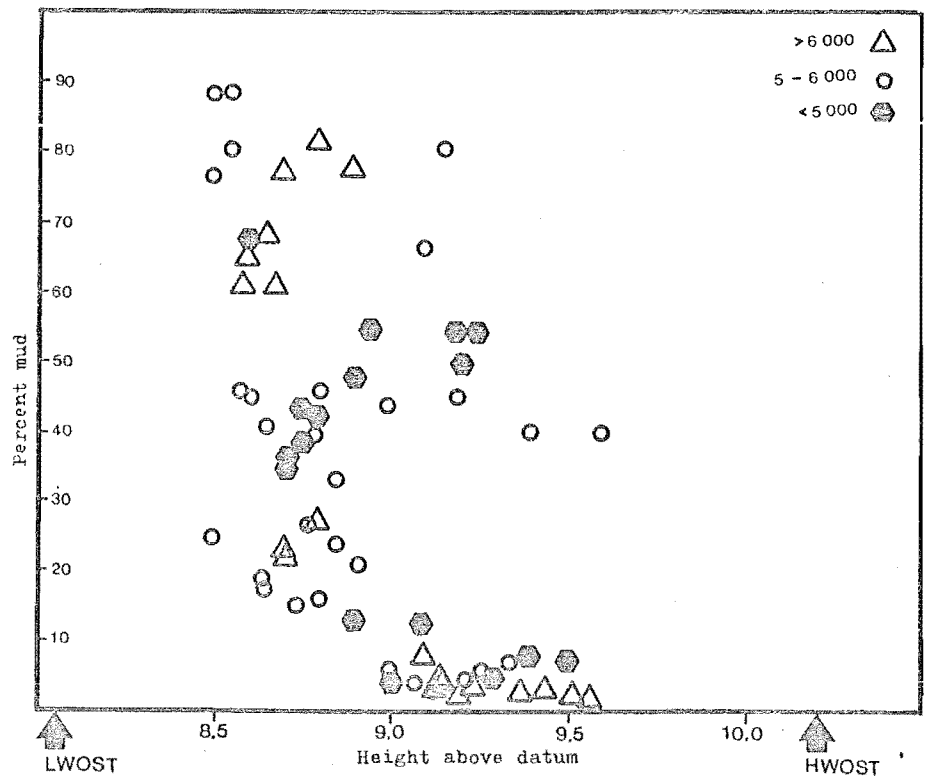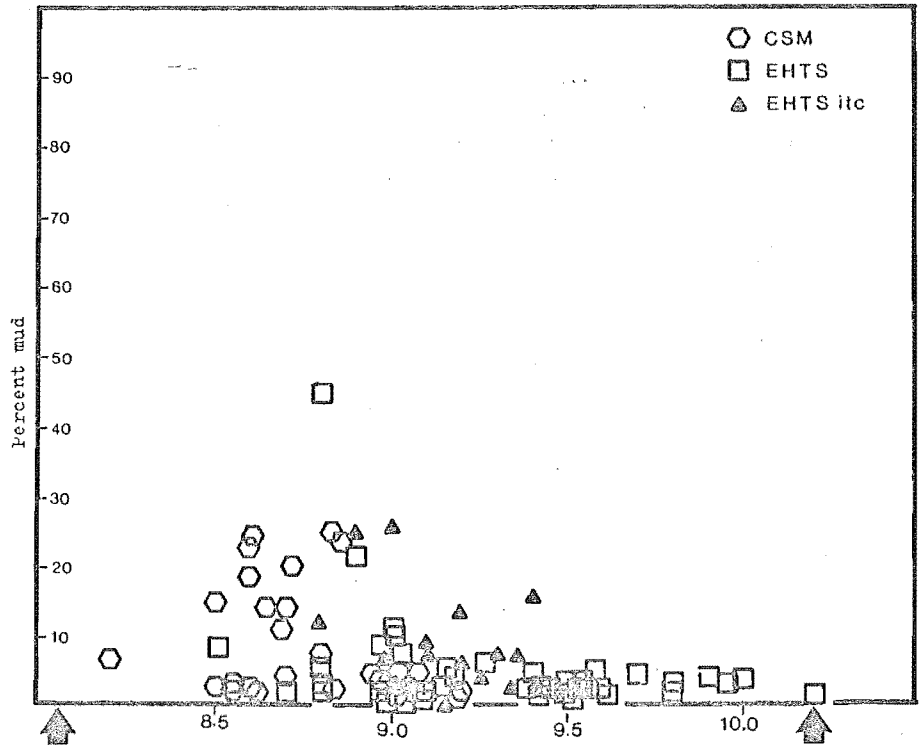
Figure 35. Sediment muddiness vs water depth (as HAD). A — Samples from central mounds (CSM), eastern high tide slopes (EHTS) and intertidal channels within and adjacent to the eastern high tide slopes (itc). B — Samples from the Heathcote Basin, bathyforms 8(lines 11 and south), 9 and 10. Samples are sotred into three effective fetch classes.

the Avon River.

On the north-eastern flats, at equivalent distances from the river entrance and at equivalent water depths, sediment is about an order of magnitudes less muddy than on the western slopes (Figure 35B). There is a weakly developed longshore trend visible in the data from these eastern slopes, but south of Line 3 (Map 1), sediment above the MTL is uniformly mud free. There is also a poorly developed tendency for sediment muddiness to increase with increasing depth below the MTL, and the lowtide flats (at about 8.5 to 8.8 m HAD) are clearly muddiest at equivalent depths in the north (lines 2 and 3). The significantly lower muddiness of these eastern flats may be due to higher wave energy, or to the frequent westward diversion of muddy Avon River water by a wind induced circulation (Figure 20). That muddy sediment does not occur above the MTL in areas exposed to longfetch waves is interpreted to result from higher levels of shear stress, which increases steeply above the MTL.

Figure 35B shows per cent mud plotted against water depth (as HAD) for the northern and western flats of the Heathcote Basin, with samples grouped into three fetch classes. Figure 35B indicates that in the Heathcote Basin, sediment muddiness is partly independent of water depth. It is likely that wave energy exerts an insignificant influence on the distribution of mud in this area, and that processes related to preferential deposition (close to the Heathcote River point-source) dominate.

2. *Discussion.* The evidence for nearly complete retention of fluvial sediment in many estuaries is incontestable (Schubel, 1971; Meade, 1974; Drake, 1976). If it is assumed that a minimum of 80% of the 12 000 tons/year supplied to the AHE is permanently deposited in the two muddiest areas, this would represent an accumulation of 0.01 tons/m^2/year of sediment, or about 1 cm/year (assuming 1 ton = 1 m^3). However the data and discussions presented in Part One indicate that the AHE has been a net exporter of sediment since about the turn of the century. This apparent paradox will be returned to, and examined in more detail, in Part Five.

The pattern of sediment muddiness shown in Figure 33 is not similar to the patterns of erosion and deposition shown in Map 4, indicating that deposition and erosion of sediment, and sediment muddiness, are independent and that much of the mud in this estuary is

deposited in areas undergoing net erosion. This indicates that very little mud is permanently deposited, and it is probable that the residence time is short for mud particles entering this estuary. Since mud sized particles are important in the fluxes of many agents of pollution through estuaries, this is a conclusion with broad environmental significance (see Goldberg, 1976).

A reasonable extension of the conclusions arrived at above is that any external source of fine sediment will have a mud depository at its entrance to the estuary. The CDB has been concerned that the release of treated effluent at the point sources shown in Map 1 may be contributing to the deposition of organic-rich fine sediment in the north end of the estuary (J.A. Robb, pers. comm.). Knox and Kilner (1973) record an extensive area of fine sediment "... in front of the sewage oxidation ponds" (p.64), and by implication the release of effluent here was considered to be the source of this sediment. The present study indicates that in 1975/77 this zone of fine sediment did not exist, and that the distribution of mud on the north-west intertidal flats can be adequately related to an Avon River source. Thus there is no evidence that the release of effluent contributes to the deposition of mud in this area.

Sand

Of the two response characteristics used to infer patterns of sediment transport - sediment textures and substrate bedforms - the former has greater potential in the present study, because bedforms are absent or ephemeral in most intertidal areas in this estuary (see Part Three).

1. Introductory discussion. Numerous attempts to identify and model environment-specific sediment textures have been reported in the literature. Historically two lines of investigation have been followed. The first utilises various bivariate combinations of grain-size parameters, in the hope of arriving at genetic textural classifications (Folk and Ward, 1957; Mason and Folk, 1958; Stewart, 1958; Sahu, 1964; Friedman, 1976; Moiola and Wieser, 1968; Hails and Hoyt, 1969). Passega (1957) introduced the CM diagram (first percentile vs median) in an attempt to refine the bivariate method, and to relate textures directly to sedimentary processes. Subsequent work by Passega (1964),

Rizzini (1968) and Passega and Byramjee (1969) led to the use of other plots (F/M, L/M, A/M; where F, L and A are weight percentages finer than 125, 31 and 4 microns respectively). There is little to be gained from this bivariate approach in the present study. While it is convenient to illustrate sediment properties with bivariate plots, and to characterise sediments in terms of summary statistics (Folk and Ward, 1957), it is naive to expect such characterisations to lead to universally applicable genetic classifications of sediment textures. Bivariate plots are frequently subjective and ambiguous oversimplifications of the real world, and they often produce contradictory results (in particular see the recent work of Siemers, 1976; and Amaral and Pryor, 1977).

The second line of investigation is based on the physics of sedimentation, and offers much more promise - it follows from early work by Udden (1914), Doeglass (1946) and Inman (1949). Here the organising principle is that the size-frequency distributions of sand samples tend to be log-normal (Krumbein, 1934). It is now part of the conventional wisdom that log-normal distributions, defined by their means and standard deviations, are signatures of depositional events (Swift and Ludwick, 1976), and that deviations from log-normality reflect both the provenance and subsequent hydraulic history of a sediment.

When plotted on a probability scale, log-normal size distributions appear as straight lines. However, most natural distributions are s-shaped and may be resolved into three straight-line segments, each of which represents subpopulations within distributions. Different interpretations of the significance of these subpopulations have led to the development of two schools of thought:

(i) Straight line segments may be the result of mixing of two or more overlapping log-normal subpopulations (Tanner, 1959, 1964; Spenser, 1963). The processes involved may be simply mixing (adding together of two or more basic components), or may be more complex, due to the censoring, filtering or truncation of components, or a combination of these (Tanner, 1964). It is mathematically and physically feasible to derive any given log-probability curve from mixtures of a variety of other curves, so this first interpretation is quite valid (Tanner, 1964; Reed and others, 1975; Sagoe and Visher, 1977), but if correct, it severely limits the interpretive power of lob-probability grain size analysis, because the processes involved cannot be retrieved from the

resulting distribution, and the meaning of the curve remains a mystery.

(ii) The second school bases its interpretation of size distributions on the work of Moss (1962, 1963, 1972), even though some writers appear to be reluctant to acknowledge this debt (see Tanner, 1964; Middleton, 1976). Moss recognised that many s-shaped cumulative curves are due to the presence of three subpopulations of grains. A framework subpopulation makes up the bulk of most sediments, with a model diameter which is related to the hydraulics of the flow. A finer interstitial subpopulation consists of grains fine enough to filter into the gaps between the framework grains. Moss recognised a relationship between grain subpopulations and transport mechanisms (surface creep or traction, saltation and suspension) and showed that the most exactingly selected particles, the framework population, are deposited from a carpet of saltating grains. Coarse grains are transported by sliding or rolling along the depositional surface, and so must be transported over a bed of relatively low grain roughness, and are always coarser than the grains deposited from saltation. Fine grains of the interstitial subpopulation are deposited from suspension.

A contemporary application of Moss's concepts is that of Visher (1969, 1972). Here the basic assumption is that any s-shaped cumulative curve can be subdivided into straight-line segments, each of which represents a truncated normal subpopulation, deposited from a particular transport process, and that the breaks (inflections and truncated segments) are environmentally diagnostic. According to this approach a coarse subpopulation (coarser than 0.0 to -1.0 phi) usually consists of grains transported by traction, a predominant central subpopulation consists of grains deposited from saltation, and a fine subpopulation (usually finer than 2.0 to 3.0 phi) consists of grains deposited from suspension. Visher further proposed that within broad limits, cumulative curve shapes are diagnostic of their depositional environment, with different curve shapes a product of different combinations of sorting and mixing of subpopulations.

A major problem with the Visher approach is that it lacks experimental respectability - very little evidence is available to prove or disprove the basic assumptions (Middleton, 1976; Sagoe and Visher, 1977). It remains attractive mainly because it is potentially the most useful tool in the area of research which aims to extract information

on depositional sedimentary processes from textural responses.

Reed and others (1975) have evaluated some of the assumptions contained in the Moss-Visher approach to grain-size analysis. They found that by generating hypothetical grain-size distributions and mixing them in different proportions, they could produce realistic looking probability plots consisting of straight-line segments intersecting at oblique angles. They also found that by dissecting representative curves from the literature, they could identify distributions which were also mixtures of normal, untruncated distributions, some which were combinations of truncated distributions, and some which were apparently not combinations of normal curves, either mixed or truncated. They concluded that sieved grain-size distributions may well be mixtures of log-normal distributions, but they may equally well be truncated mixtures, or other unidentifiable functions. Thus the conclusions of the first school, above, are quite justified.

Reed and others then investigated the significance of settling velocity distributions, and discovered that this technique, in combination with multivariate statistics, provided a reliable method for discriminating between depositional environments. They decided that sands are truly composed of log-normal subpopulations, probably attributable to the traction, saltation and suspension modes of grain movement, but that it is settling velocities, not sieved grain sizes, that are log-normally distributed.

Three major conclusions which result from the above discussion are: (i) Separate straight-line segments in settling velocity distributions of sand probably represent log-normal subpopulations. (ii) Segments coarser than 0.0 phi represent material transported by traction, those finer than 3.0 phi represent material transported in suspension, and predominant central segments represent material transported by saltation. And (iii), while sieved size distributions may or may not be signatures of particular depositional events, the evidence of Reed and others (1975) suggests that *settling velocity* distributions are usually process-specific signatures, and usually do consist of mixtures of log-normal subpopulations.

2. Numerical procedures. A major requirement of an analysis of large numbers of experimental results is a simplification which reduces the data to a manageable form, yet obscures as little useful information as possible. In the present project this requirement has been

accomplished by ordering the samples into like groups with a Q-mode
cluster analysis (program on tape supplied by M. McClennan, New Zealand
Forest Research Institute, Christchurch). Q-mode cluster analysis is
a technique which groups samples which are most similar (which have a
high coefficient of similarity - in this case a modified Sorensons
coefficient), and then orders them at successively lower levels
with other groups (see Davis, 1973, pp. 456-472). The result is a
hierarchical classification that is both objective and unambiguous.

The sorting process had to be conducted at two levels, since
about 480 samples were involved. Initial clustering runs were conducted
using all of the samples from each of the bathyforms identified in
Figure 20, so that these first runs involved between 50 and 150 samples.
Input data were the seven psi percentiles coded from the Rapid Sediment
Analyser (RSA) cumulative curves (see Appendix 3).[*] From the resulting
dendrograms, groups of samples with coefficients of similarity greater
than 0.99, and with both mean diameter and sorting standard deviations
less than 0.05, were identified. These groups were then represented by
the individual sample with sorting and mean diameter values closest to
the group mean. Representative samples were then run again, and the
resulting dendrogram is presented as Figure 36.

3. Cluster analysis results and interpretations. Inspection
of Figure 36 shows that the dendrogram may be subdivided into equivalent
groups at various levels of similarity. For example a subdivision at a
similarity of about 0.96 to 0.97 results in the six groups labelled A to
F in Figure 36. This classification proved to be a good compromise
between simplification and a minimum loss of information, and has been
adopted for further analysis. Sample lists and the input data which
form the basis of this classification are included in supplementary
material filed in the University of Canterbury Department of Geology
Library. Representative cumulative curves for each cluster group are
plotted in Figures 37 and 38, and these are replotted on common axes
as curve envelopes in Figure 39.

Figures 40 and 41 illustrate some of the summary properties of
the 480 samples involved in the classification.

---

[*] In this report psi $= \log_2 x$, where x = the sedimentation diameter,
defined in Appendix 3. This transformation is analogous to the
size-scale phi transform of Krumbein (1934); after Middleton (1967),
as used by Reed and others (1975).
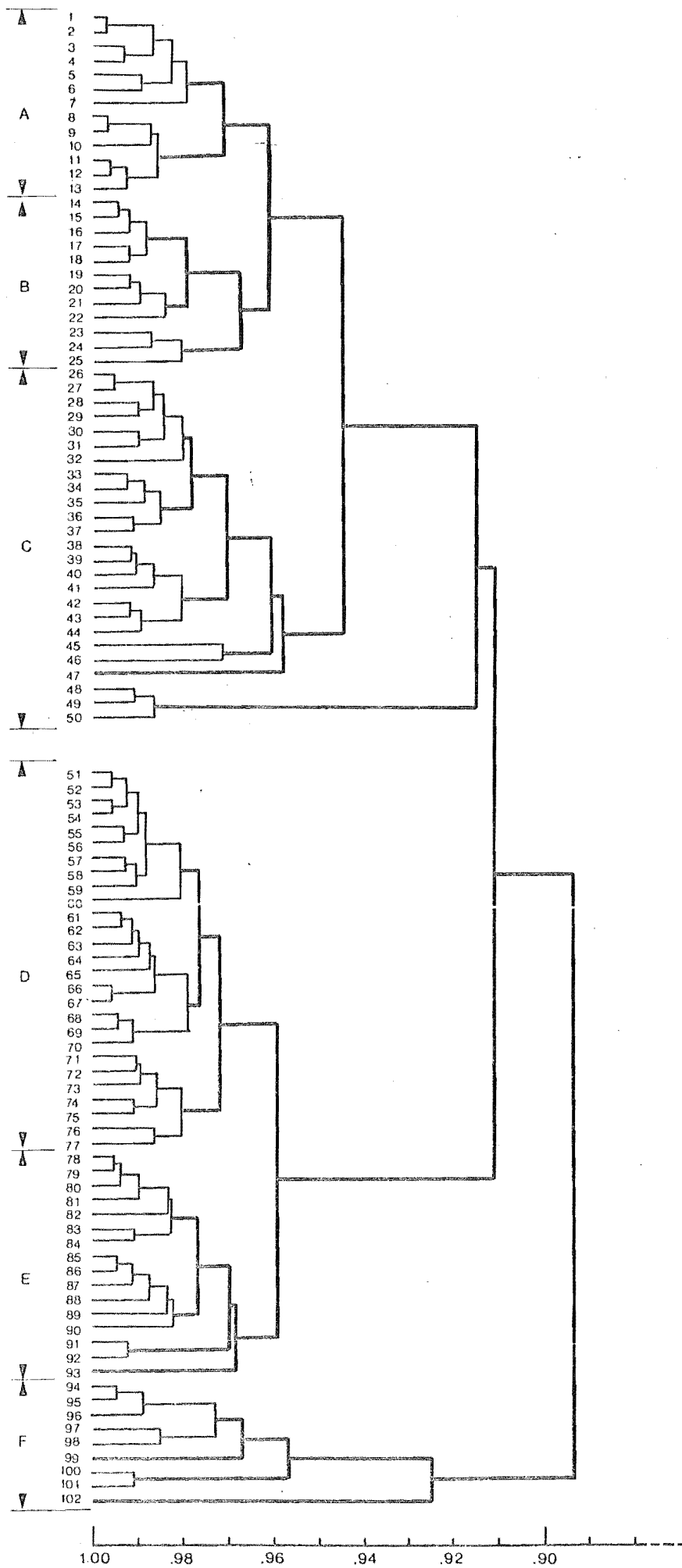
Figure 36   Dendrogram resulting from cluster analysis of 102 representative samples
of surface sediment from the Avon-Heathcote Estuary. Similarity scale is a modified
Sorrensons Coefficient . Groups A-F represent a 6-fold grouping of the 102 samples.
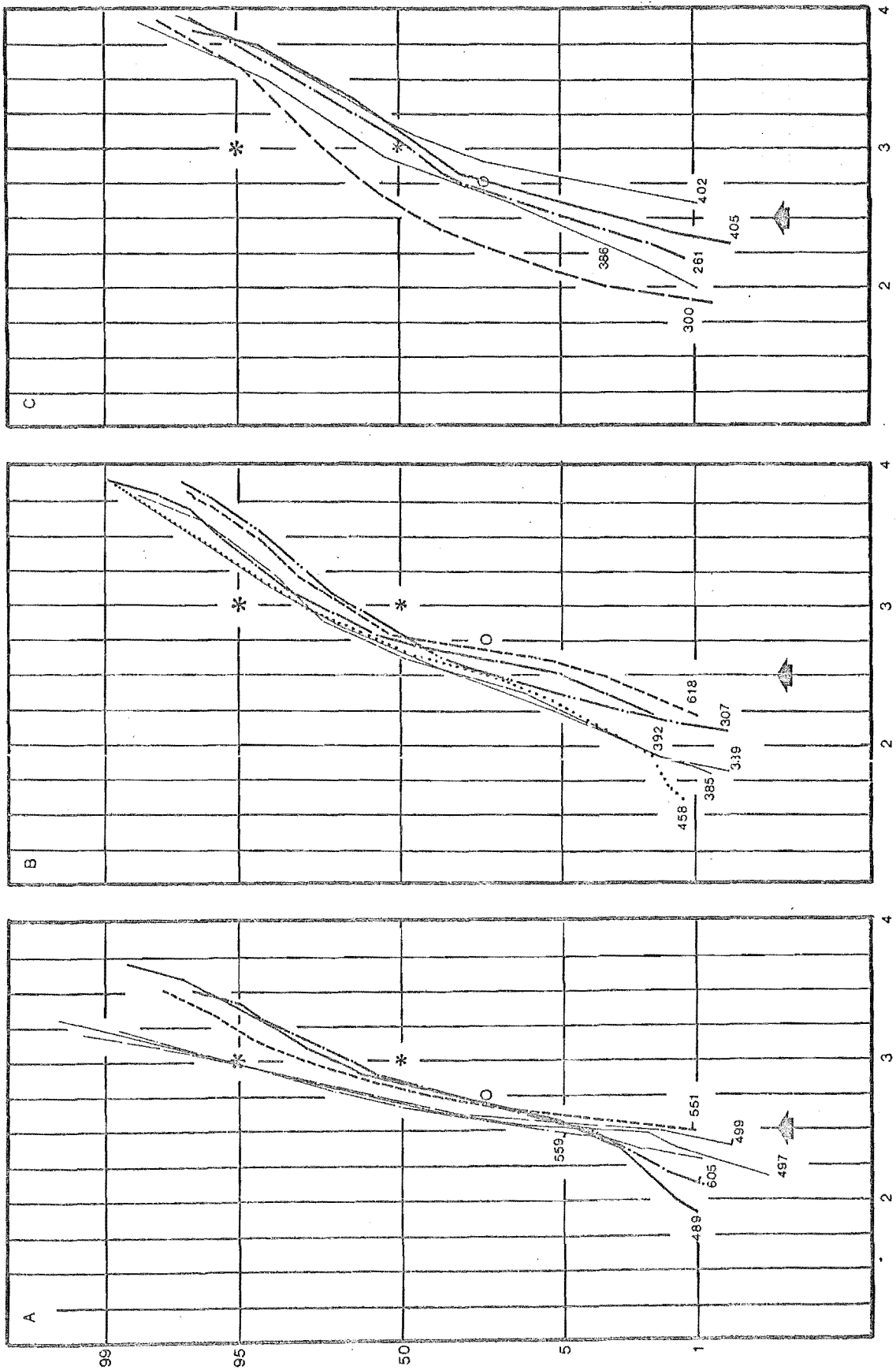
Figure 37. Representative cumulative probability curves of sample from cluster groups A, B and C.
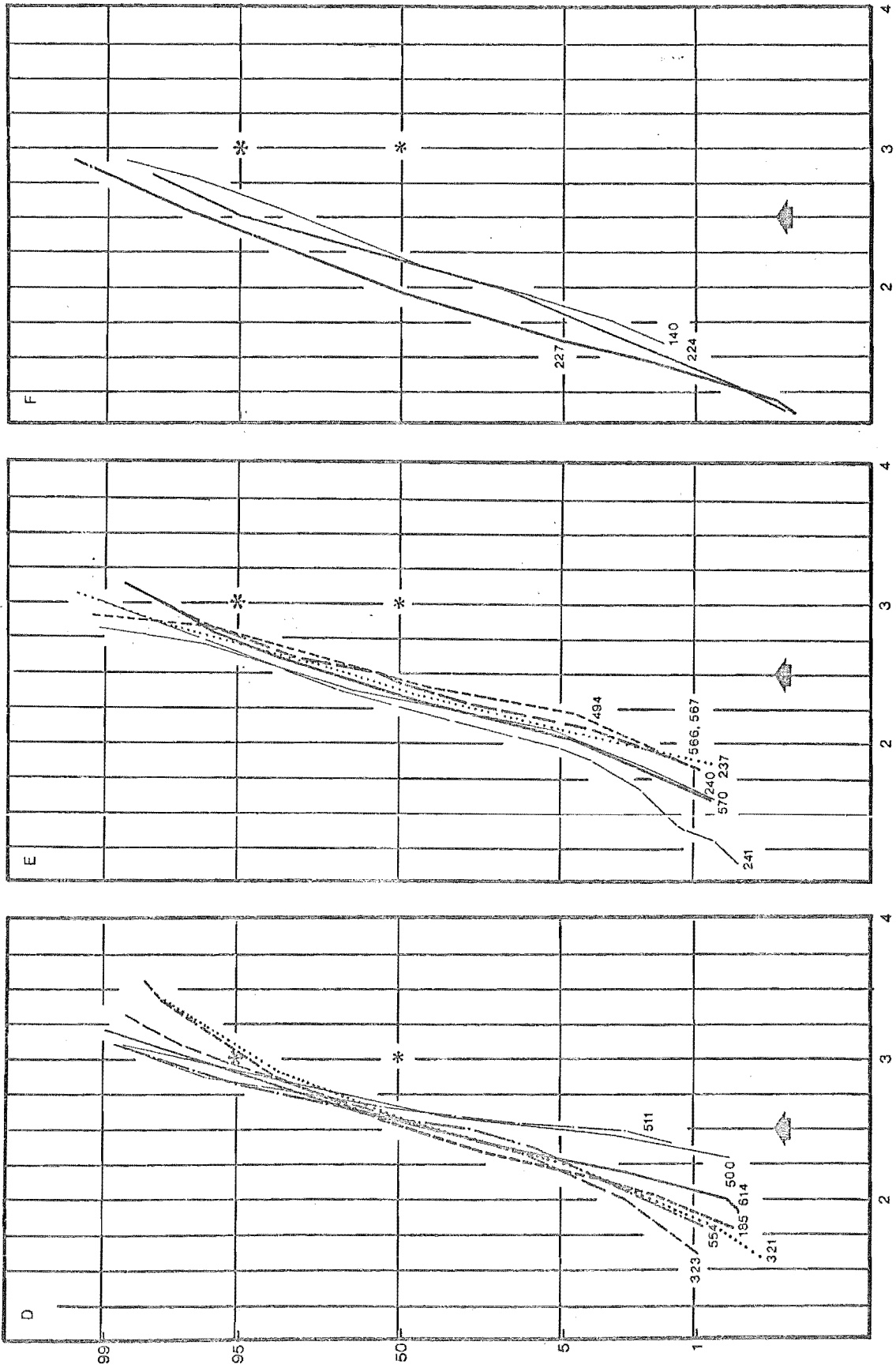
Figure 38. Representative cumulative probability curves of samples from cluster groups D, E and F.
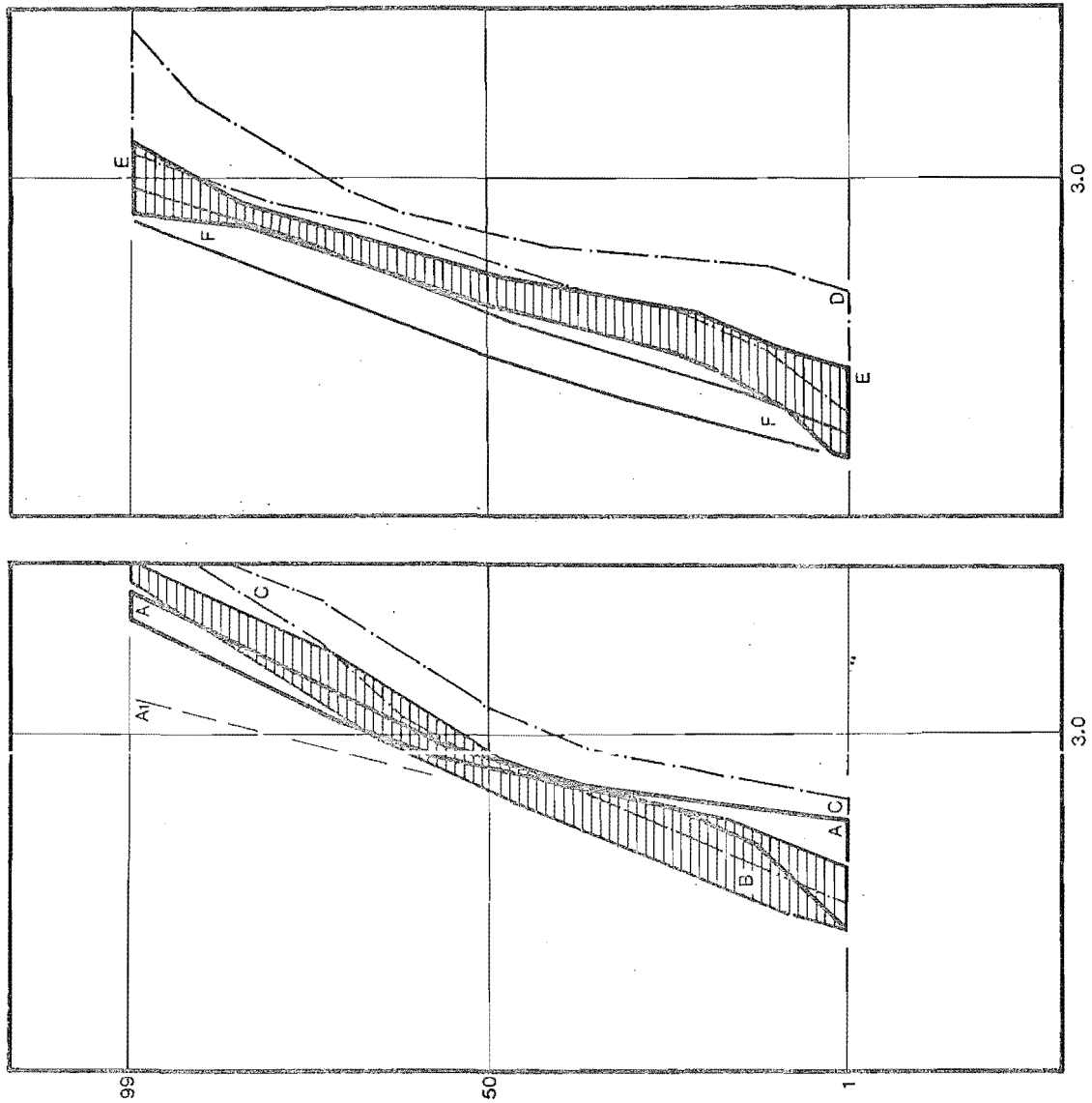
Figure 39. Cumulative curve envelopes (from Figures 41 and 42) of cluster groups A-C and D-F, plotted on common axes.

In Figure 40 the most commonly used Folk and Ward (1957) graphic statistics (mean size and sorting) are plotted together, and in Figure 41 the 5th and 95th percentiles, from the Folk and Ward input data, are plotted. In both Figures 40 and 41 sample groups overlap, and samples tend to be uniformly distributed within their sectors of the plots. This is interpreted to mean that the six groups in Figure 36 are subdivisions of a continuous spectrum of size distributions, and that the cluster grouping is an arbitrary subdivision of this spectrum (an artificial ordering of the input data into like groups), not a recognition of six discrete natural clusters.

A convenient standard scheme for describing cumulative curve shapes has been adopted, and three basic shapes are recognised: (1) Straight or monolinear. (ii) Bilinear or trilinear (with 2 or 3 straight-line segments). And (iii) Curvlinear (with no break in slope). Groups A to C contain size distributions which are characteristically bilinear or s-shaped curvilinear, with a marked inflection (break in slope) at about 3.0 psi/50%. The two linear segments in these curves are interpreted as two log-normal subpopulations; it may be that samples with curvilinear size distributions contain untruncated mixtures of these same two populations, and sharp inflections represent truncated mixtures. However there is no way ot testing this possibility (Reed and others, 1975; Clark, 1976).

Following the introductory discussion, above, the two straight-line subpopulations are interpreted to represent material deposited from saltation (the coarse population) and from suspension (the fine tail). Notice that the coarse halves of these size distributions are uniformly steep, and cover similar size ranges, indicating that sorting within the coarse saltation population is similar, and that differences between saltation populations are due largely to variations in population mean size. However the suspension populations become both finer and poorer sorted from A to C, suggesting that the saltation and suspension populations have granulometric properties that are at least partly independent; for example in Figure 41 there is a slight tendency for coarser psi 5 values to correspond to coarser psi 95 values (where psi 5 and psi 95 are assumed to be representative of the saltation and suspension populations respectively), but the two are largely independent.

Groups D to F consist of samples which are generally better sorted and coarser than A to C, and which are characterised by straight
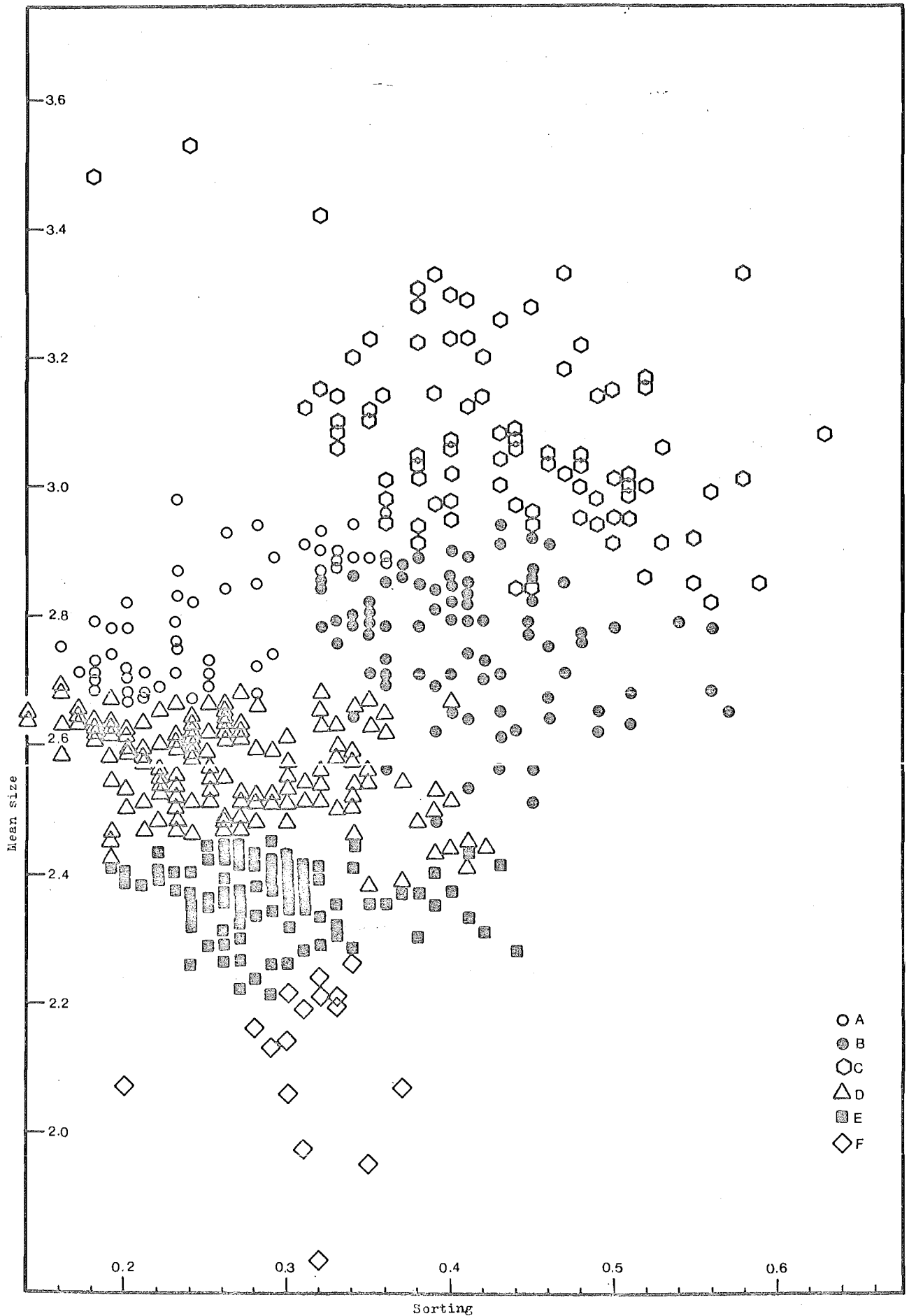
Figure 40. Scatter plot of mean size vs graphic standard deviation (sorting) of 480 samples fromcluster groups A-F.
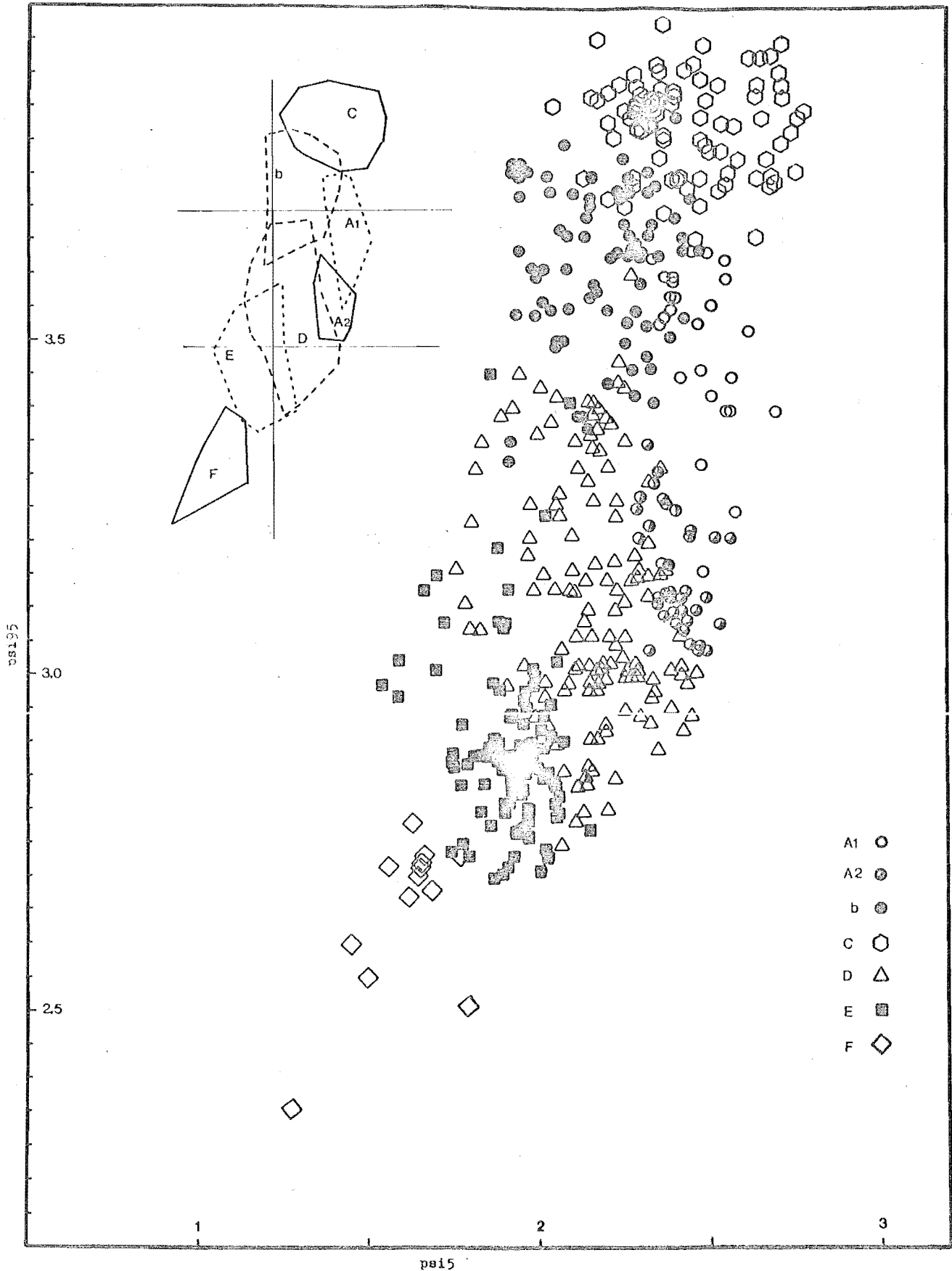
Figure 41. Scatter plot of 5th percentiles (psi5) vs 95th percentiles (psi95) of 480 samples from the cluster groups A-F.

or slightly curvilinear cumulative curves (Figure 39). Except for some samples in Group D, fine subpopulation material is apparently absent from these samples – they are interpreted to consist of a single log-normal population, probably deposited from saltation.

There is a slight tendency for sorting to worsen from D to F, with a marked coarsening trend, and in general terms it is reasonable to interpret all Group D-F samples as similarly sorted, with most of the difference between them due to variations in mean grain size. An examination of Figure 39 indicates that Group D-F sediment may be physically identical to the saltation populations of Group A to C samples.

General conclusions which result from these data and analyses are that the sand fractions of surface sediment in the AHE consist of material deposited solely from saltation, or of a mixture of material deposited from both saltation and suspension. The uniformly well sorted saltation population has granulometric properties that are largely independent of those of the suspension population. Most of the variation between samples is due to the presence or absence of the suspension subpopulation (which if present makes up about 50% of the sample), and to variations in the mean size (but not the sorting) of the saltation population.

4. *Height above datum preferences of groups A to E.* Histograms of HAD vs frequency for samples from each of the cluster Groups A to E are presented in Figure 42. Two observations are particularly significant:

(i) The two Groups A to C and D to E have distinctly different HAD preferences. About 75-80% of all Group A to C samples were from below the MTL (below 9.0 m HAD), only 0.5% were from above 9.5 m HAD, and there were none above 10.0 m. Groups D and E prefer shallow water – about 60% of all Group D samples were from above the MTL, and 80% of Group E samples were from above the MTL. However, the depth distributions of D and E are bimodal; there is a small peak in the histograms between 8.5 m and 8.75 m, and a much larger peak between 9.0 m and 9.25 m. Thus sediment belonging to Groups D and E is found in two environments – on the deepest intertidal flats (flats deeper than 8.5 m HAD are uncommon), and on intertidal flats above the MTL.

(ii) The three Groups A, B and C show markedly similar depth preferences.
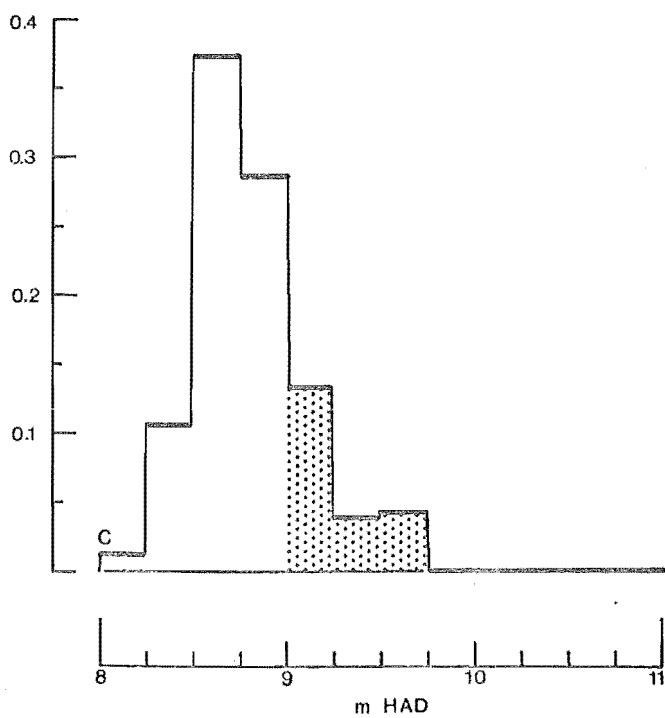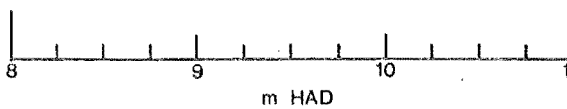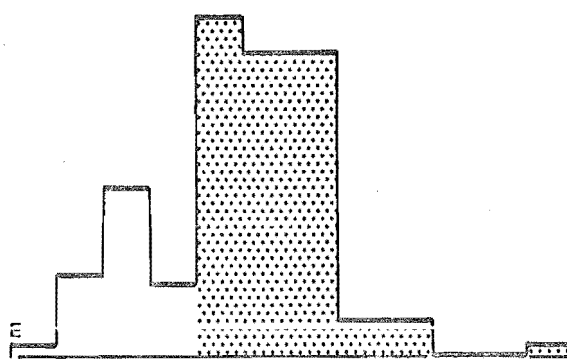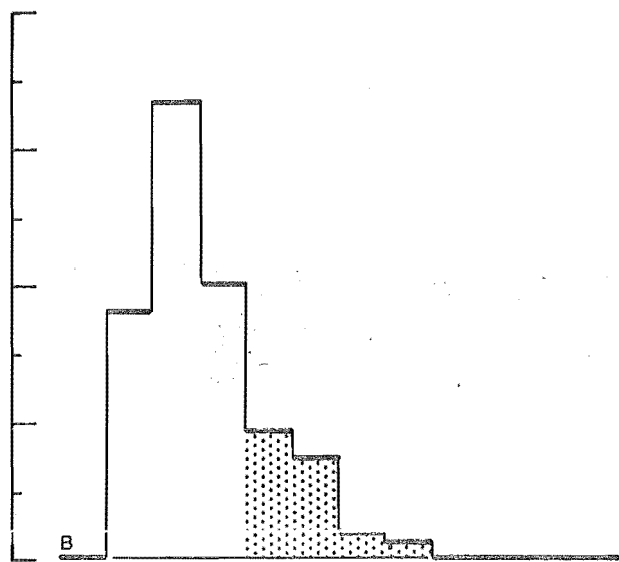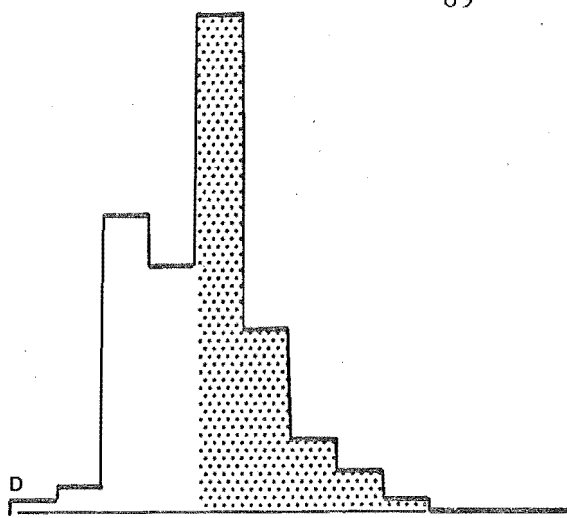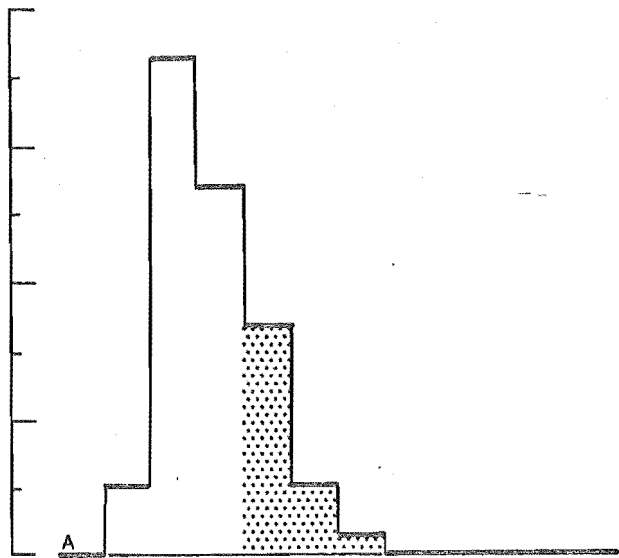
Figure 42. Histograms of sample frequency vs sample HAD for cluster groups A-E.

General conclusions which result from these observations are
that sediment is only commonly deposited from suspension below the MTL,
in water deeper than about 1.2 m below HWOST. However the absence of
a suspension subpopulation is not depth-diagnostic, because sediments
without the population also occur on the deeper intertidal flats, below
the MTL. Processes which are responsible for the differences between
Groups A, B and C are independent of depth, since the three groups have
almost identical depth preferences.

5. *Regional distribution patterns*. Map 2 shows the regional
distributions of the six cluster Groups A to F. The following features
are visible in this map:

(i) In the Heathcote Basin the largest area of Group C sediment in
the estuary occurs close to the river entrance, and there appears to
be a progression from Group C to B to A with increasing distance from
the entrance. This progression is shown in a simplified diagrammatic
form in Figure 43. In the sequence C-B there is a slight coarsening
of the saltation population, and in C-B-A there is a clear trend towards
a coarser, better sorted suspension population.

(ii) Large areas of the higher intertidal flats around the edges of
the AHE consist of Groups D and E sediment. Group E is distributed
along the entire length of the eastern high tide slopes, and in an
intermittent strip down the western high tide slopes, becoming more
abundant south of line 6 (Map 1). In general there is also an offshore
trend across the higher intertidal slopes and flats, from F to E to D.
These patterns are also shown diagrammatically in Figure 43.

(iii) An assemblage of Groups D and A occurs on midtide (9.0 m) slopes
and flats in the centre of the estuary, and along the eastern flats.
On the eastern midtide flats Group A1 sediment occurs only in the
intertidal channels.

(iv) The north end of the western slopes and the low tide flat
east of the Avon channel are characterised by a mixed assemblage,
where sediment of Groups A to C occurs in an apparently disorganised
pattern, with poorly developed depth preferences. In this north-western
corner of the estuary sediment of groups D to F is restricted to narrow
irregular zones along the upper and lower margins of the intertidal
flats.

Map 2. Distribution of samples belonging
to cluster groups A to F. Contours are
8.6m, 8.8m and 9.0m, from Map 1. Shading
and hatching indicate the distributions of
the groups and assemblages identified below.

Predominantly group A

Predominantly group B

Predominantly group C

Assemblage of groups D+A

Predominantly group E

Disordered assemblage of A+B+C

Assemblage of D+B+E

Subgroup A1 samples

Cluster group

A
B
C
D
E
F
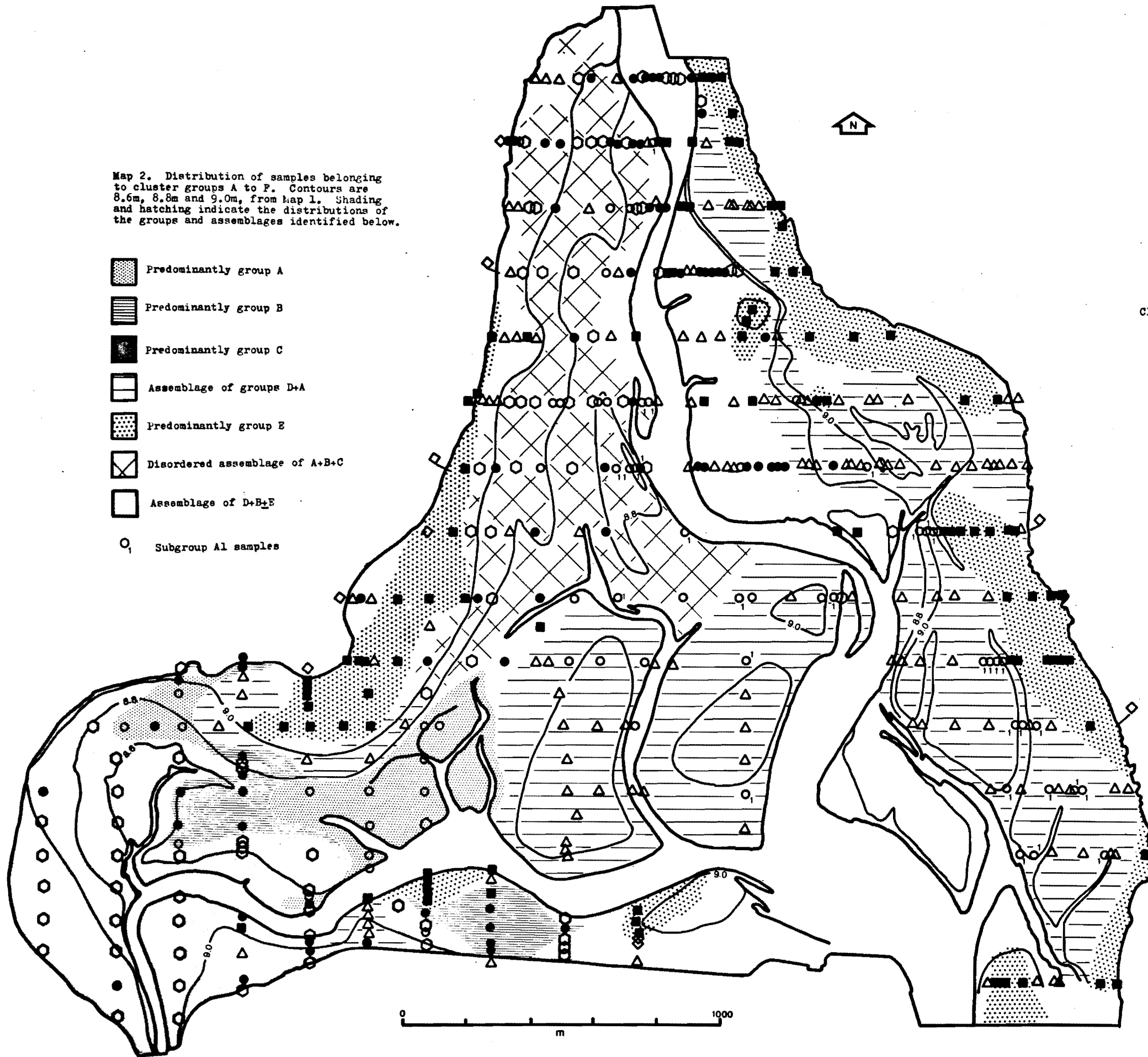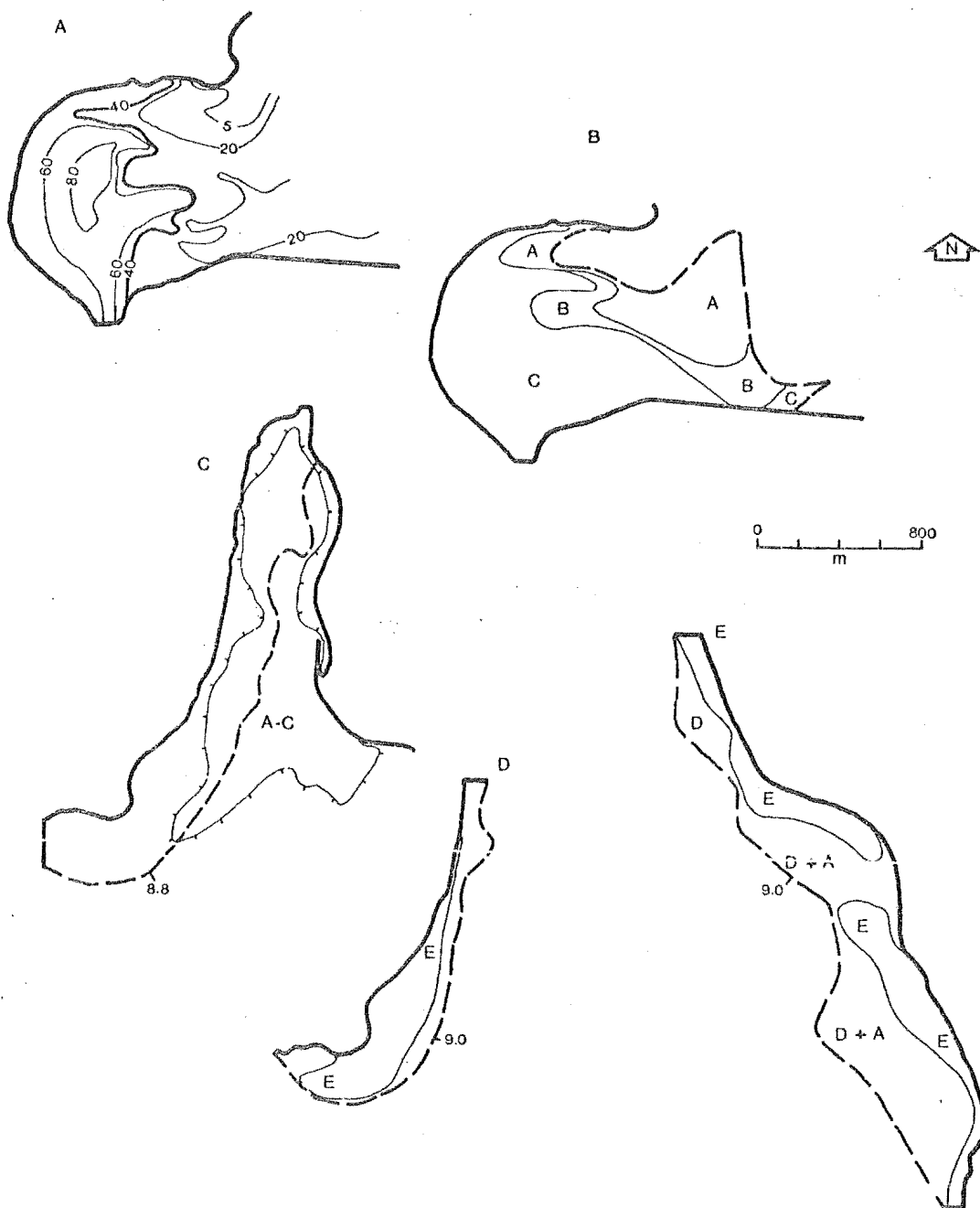
Figure 43. Diagrammatic distribution patterns of sediment cluster groups. A - sediment muddiness from Figure 37, for comparitive purposes. B - Generalised pattern of distribution of samples from groups A, B and C in the Heathcote Basin. C - Occurrence of assemblage A+B+C in the north west of the estuary, 8.8m HAD contour shown for reference. D - Distribution of group E sediment on higher western slopes.
E - Distribution of group E sediment and the assemblage D+A, on the eastern high tide slopes. 9.0m HAD contours shown for reference. See Map 4 for the original patterns.

6. Interpretations.

(i)   The pattern of mud deposition in the Heathcote Basin (shown in summary form in Figure 43A) is the result of a compromise between processes which supply mud to the AHE, and those which influence its deposition. Similarly, the distribution of sand of Groups A to C sediment in this basin is a compromise between the two sets of processes. Close to the river entrance, only Group C sediment is deposited, regardless of water depth (Figure 43B). With increasing distance from the river entrance, Groups B and A occur.

The major differences between A, B and C are in the mean size and sorting of the suspension subpopulation, which becomes coarser and better sorted with increasing distance from the river entrance. The sequence C-B-A is interpreted to be a preferential deposition feature, perhaps related to suspended sediment concentrations – which must be highest in fresh river water, and which decrease as river water is mixed into cleaner, more saline estuary water.

One result of this pattern of deposition is a negative selective sorting effect, where the suspended sediment subpopulation is finest and poorest sorted close to the source, the mean size of the subpopulation increases with increasing distance 'downstream', and whole sample sorting values worsen rather than improve with increasing distance from the source.

(ii)   Above the 9.0 m HAD contour (in water shallower than 1.2 m below HWOST), the distribution of sediment consisting of a single saltation population (Groups D, E and F) is influenced by both water depth and fetch distance. For example in Figure 43D, Group E sediment occurs in progressively deeper water as east wind fetch distances increase from north to south. Since downfetch energy gradients are due to higher frequencies of similar sized waves in this area (see Part Two), this pattern is interpreted to be a result of increasing shear stress frequency, rather than increasing absolute levels of shear stress. However the observation that Group E sediment is found in progressively deeper water from north to south, while mean size and sorting values remain constant, is interpreted to mean that the granulometric properties characteristic of Group E sediment are a response to constant absolute levels of shear stress, and are independent of shear stress frequency. As fetch distances increase, shear stress frequencies necessary for the formation of Group E sediment occur in progressively

deeper water, and as maximum values of about 1 800 m are approached, the Group E zone approaches depths of about 1.2 m below HWOST (9.0 m HAD).

The wave climate of the eastern side of the AHE is more homogeneous than the climate of the western side, and as a result Group E sediment occurs along almost the full length of the eastern high tide slope (Figure 43E).

(iii) The widespread group D ± A assemblage – commonest on 9.0 m flats – is interpreted to form in areas of relatively low near bottom shear stress, relatively far from the two river entrances.

(iv) The northern zone of mixed A to C sediment, shown diagrammatically in Figure 43C, is interpreted to be an area where no single environmental factor is sufficiently dominant to exert an organising influence on the active layer. Fine sediment is supplied to these western slopes by the Avon River in relatively small amounts, so there is not a clearly visible distribution pattern, as there is in the Heathcote Basin. East wind fetch distances are short, the area is protected from long-fetch southerlies, and as a result it is only in the shallowest water that shear stress frequencies are high enough to influence sediment properties in a consistent manner.

(v) In this estuary, active sediment cumulative curve shapes, recognised and sorted into like groups by the clustering operation, are not process-specific. The energy/bathymetry model proposed in Figure 32 indicates that wave stress is energetically dominant in shallow water, while tidal currents dominate in deeper water, yet Group E sediment occurs in both environments. It appears that curve shapes may be shear stress-specific, regardless of how the stress is applied.

(vi) The presence of large areas of active sediment with remarkably uniform properties is interpreted to mean that most of the surface sediment in this estuary is in equilibrium with the physical environment. The gradient from C to A in the Heathcote Basin presumably also represents a dynamic equilibrium, between processes which supply the sediment and those which distribute it.

(vii) A comparison of Map 2 and Maps 3 and 4 indicates that there is no apparent relationship between the cluster group pattern and patterns of erosion and deposition.

    7. Graphic statistics. It is instructive to compare Map 2 with traditional granulometric maps (Figures 44 and 45) which show patterns of mean size and sorting in the AHE. Predictably there are similarities, since all three maps are based on the same size distributions. Notice however that there is considerably less information in the two graphic statistics maps, partly because the sediment in this estuary shows little size or sorting variation, and partly because graphic statistics are insensitive to minor variations in size distributions. In effect, the cluster map combines the four graphic statistics of mean size, sorting, skewness and kurtosis in one variable.

    Figures 44 and 45 emphasise that mean size variation is greater than sorting variation in the AHE. Mean size values range from coarser than 2.0 psi (0.25 mm, medium sand) to finer than 3.0 psi (0.125 mm, very fine sand), with minimum recorded values of about 3.5 psi (about 0.09 mm). However sand from this estuary is either well sorted or very well sorted, with values ranging from 0.14 psi to 0.50 psi. Natural sediments may be as poorly sorted as 8 or 10 phi (Folk, 1968), which emphasises the uniformly good sorting in this environment.

    Earlier work (see Figure 32) has shown that it is possible to realistically model the bathymetry and the distribution of energy in the AHE in relatively simple terms. It is clear from the results above that surface sediment granulometrics are poorly related to this process model in some areas, and below the MTL, sediment properties are a compromise between the rate of supply of sediment, and the ability of physical processes to sort it into depth-specific assemblages.

    In an attempt to test the systematics of the relationship between bathymetry and sediment granulometrics a number of representative bathymorphic profiles were plotted at a constant horizontal scale, and sediment samples collected along each profile were also plotted at the same scale. The advantages of a constant scale approach are that it is easier to compare trends along sample lines within bathyforms, and to compare different bathyforms of various sizes.

    The results are shown in Figures 46 to 48, and summarised in model form in Figure 49. These diagrams show that on the western slopes, from Lines 2 to 11 (Map 1), both longshore and offshore trends occur. The bathymetric analysis in Part Three has shown that these western slopes become progressively less steep and straighter with increasing wave energy, and the constant scale diagram in Figure 46A
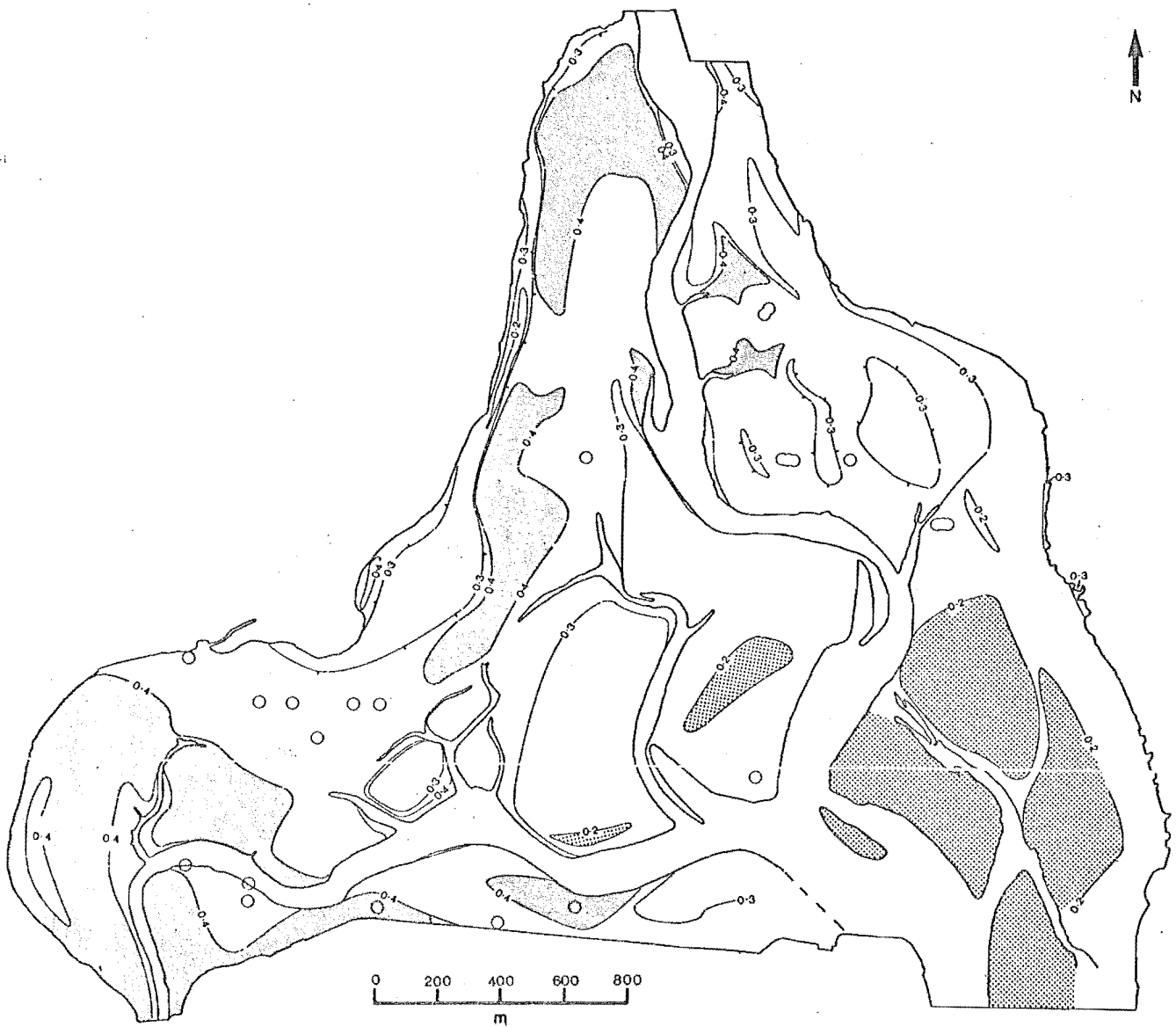
Figure 44. Surface sediment of the Avon-Heathcote Estuary. Sand fraction graphic
standard deviation (sorting), contoured at 0.2psi, 0.3psi and 0.4psi. Small circles
enclose samples not within the indicated sorting classes. Closed contours with outer
hachures contain higher values, inner hachures indicate lower values within.
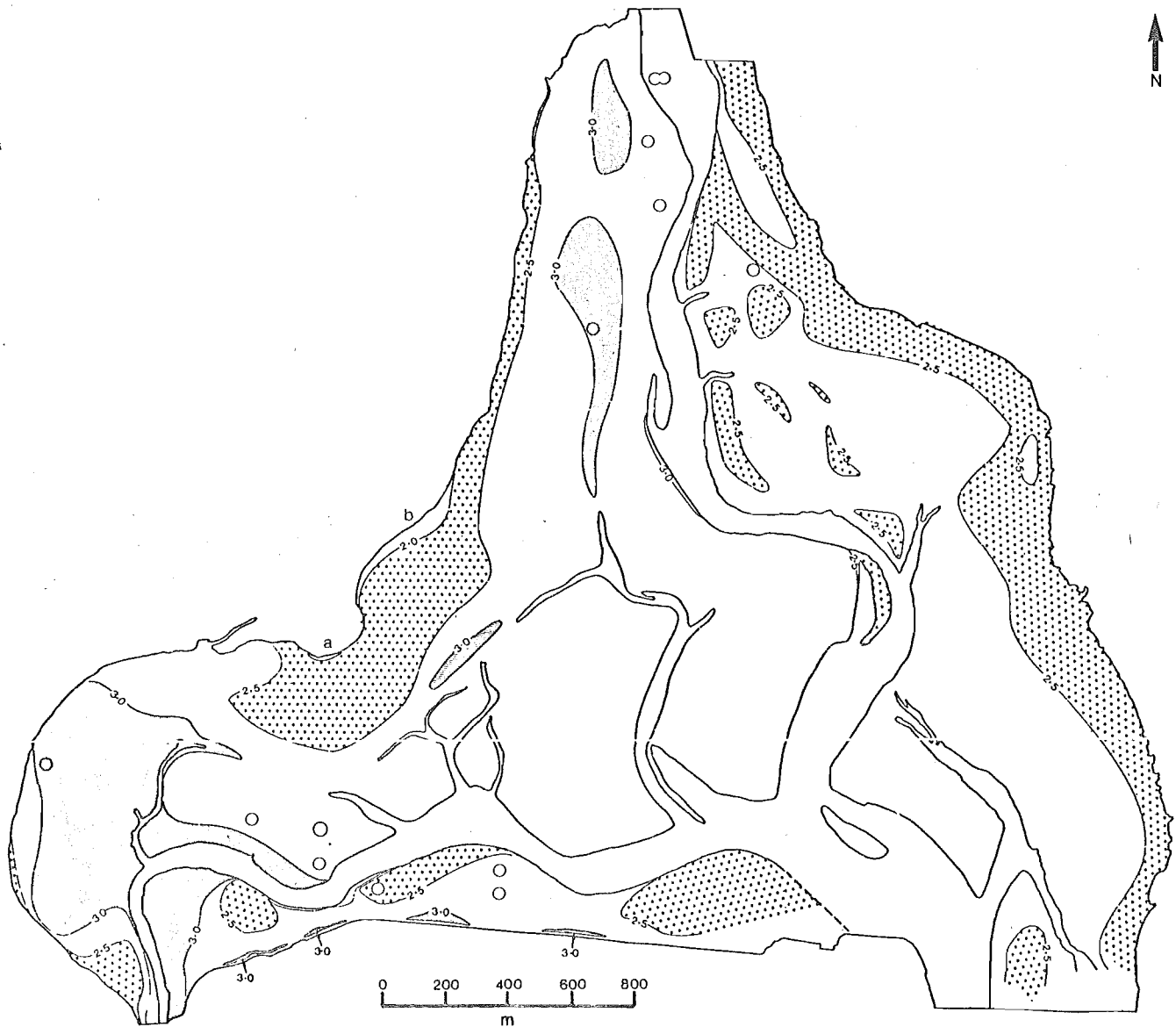
Figure 45. Surface sediment of the Avon-Heathcote Estuary. Sand fraction graphic
mean diameter, contoured at 2.0psi, 2.5psi and 3.0psi. Sediment with mean sizes
coarser than 2.0psi occurs only at (a) and (b). Small circles enclose samples not
within the indicated size class.
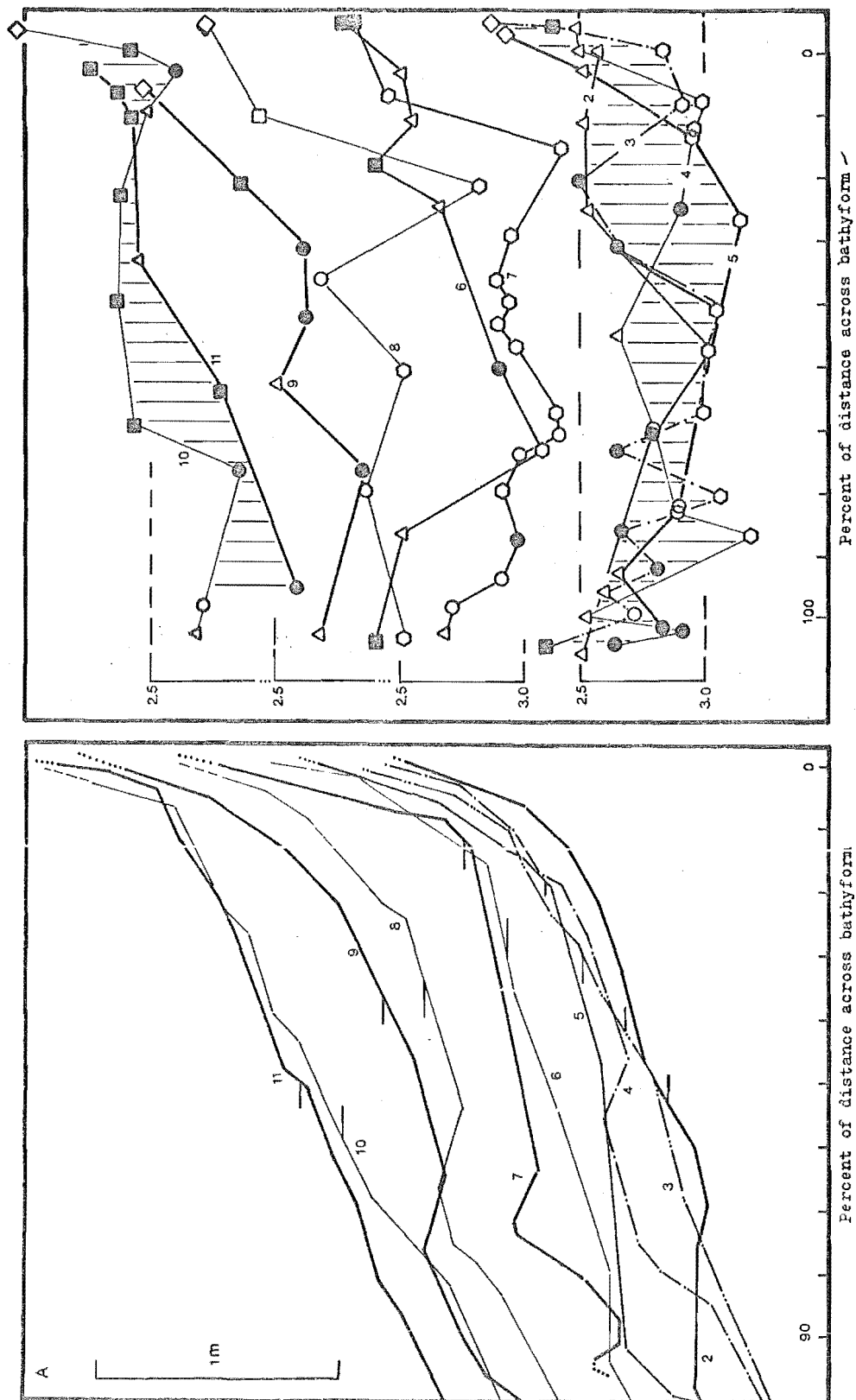
Figure 46. A — Constant-scale bathymorphic profiles, lines 2–11 from the western slopes and flats. Horizontal reference marks are at 9.0m HAD. B — Trends in sand fraction graphic mean diameter plotted at the same constant scale. Cluster group symbols as in previous figures. Profiles are plotted on seperate vertical axes in four groups (2-5, 6+7, 8+9, 10+11) for easier comparisons.

emphasises these progressive changes. The profiles plotted on separate vertical axes in Figure 46A fall into four groups: 2 to 5, 6 and 7, 8 and 9, and 10 and 11. The northernmost profiles are distinctly curvilinear, while the southern profiles are distinctly straight.

The mean sedimentation diameter trends in Figure 46B also show progressive changes. Profiles 2 to 5 have broadly similar characteristics, with Group D, E or F sediment at the landward edge, a central zone consisting predominantly of A to C sediment, and a channel margin zone of D and E (± B) sediment. Profiles 6 and 7 are similar, with a broad central zone of finer sediment and coarser sediment of cluster Groups D and E at the landward and channel margins. Profiles 8 to 11 end offshore in shallow intertidal channels – where tidal velocities are lower – and here there is a simple fining offshore trend, with coarsest sediment at the landward edge, and with relatively little sediment of Groups A to C.

The close parallels between bathymetry and sand fraction trends in Figure 46 indicates that wave energy is the primary control on sand fraction properties. However the trends along profiles 2 to 5 are clear evidence that in deeper water, adjacent to subtidal channels, tidal currents may exert the primary influence on sand fraction properties.

With increasing fetch distances the relationships between bathymetry and sediment granulometrics become simpler and easier to predict (compare Line 11 in Figures 46A and 46B). In general sorting improves, skewness values approach zero (indicating perfectly symmetrical size distributions) and kurtosis values approach 1 (indicating perfect Gaussian size distributions) as mean diameters approach values of about 2.5 psi.

Figure 46 demonstrates the relationships between bathymetry and mean size on representative low tide (8.75 m) flats. The profiles in 46A change progressively through the sequence 6-7-8-5-2, and the corresponding mean size trends do likewise (46B). However the grain size response is not related only to water depth, and trends along individual profiles appear to be a compromise between tidal energy, wave energy, and the rate of sediment supply.

Figure 47 shows constant scale bathymetric and mean grain size trends across representative 9.0 m flats and mounds, and representative eastern 9.5 m slopes. Both the bathymetry and grain size profiles are markedly uniform, with as much grain size variation between profiles as along profiles, and no visible relationships between profile
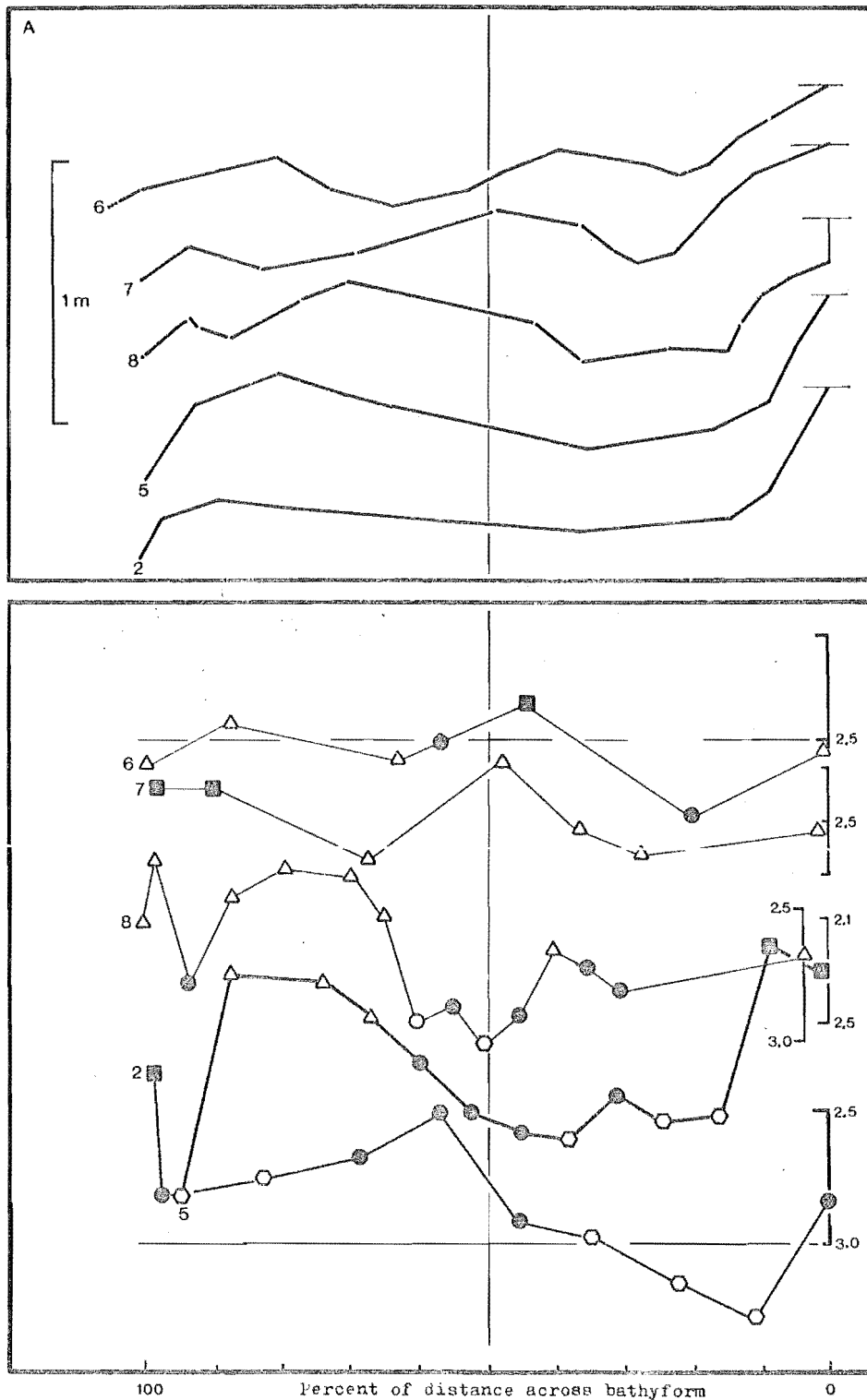
Figure 47. A — Constant-scale bathymorphic profiles, lines 2, 5, 6-8 from the eastern low tide flats . Horizontal reference marks are at 9.0m HAD. B — Trends in sand fraction graphic mean size.

configurations and the corresponding grain size trends. Figure 49 demonstrates that above the MTL, sediment properties are uniform and independent of HAD, with coarsest sediment at the landward margins of bathyforms. Finest sediment occurs in deeper water adjacent to the intertidal channels, and there is a slight mean grain size difference between 9.0 m and 9.5 m bathyforms, shown diagrammatically in Figure 49.
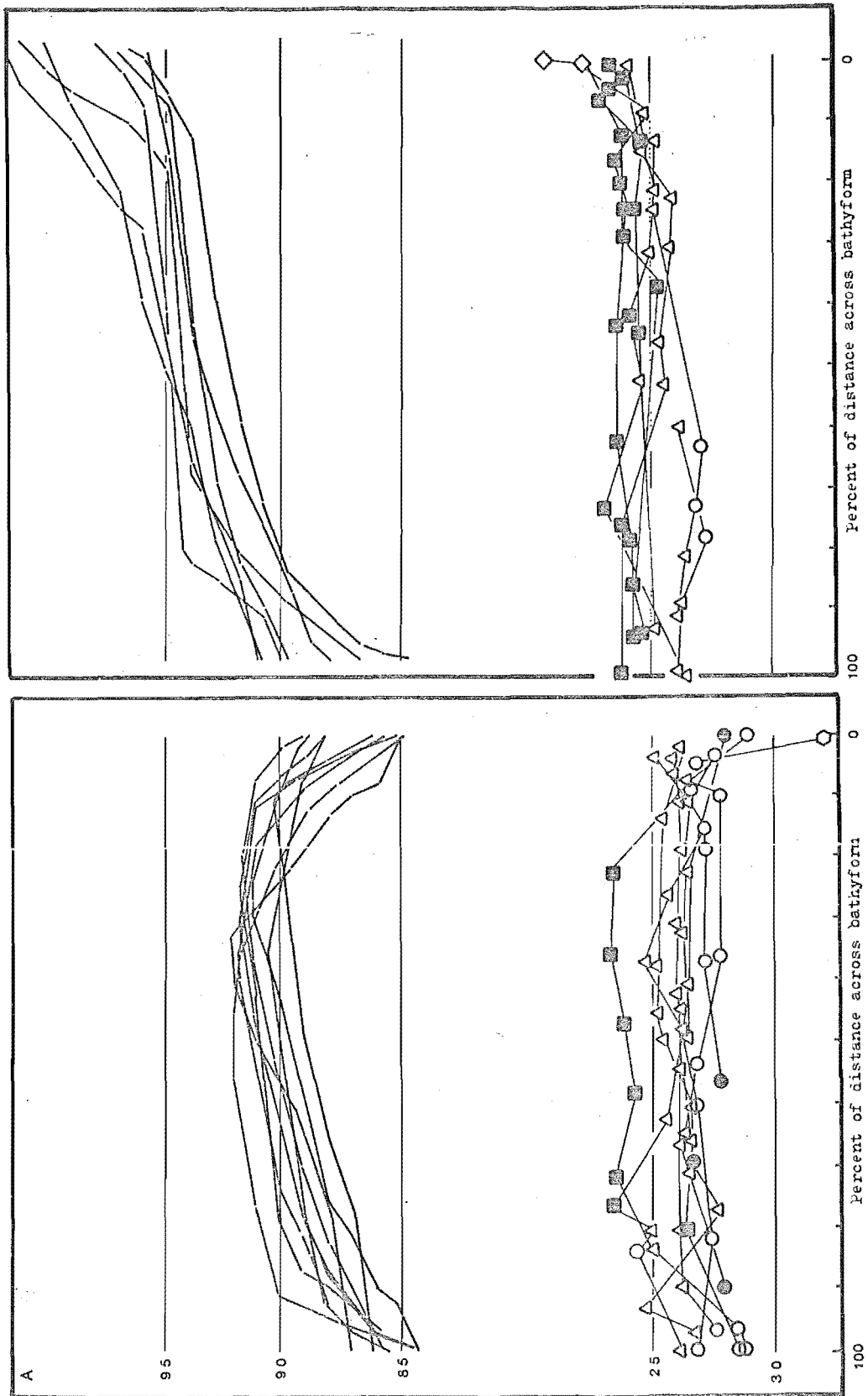
Figure 48. A – Constant-scale bathymorphic profiles across 9.0m HAD flats and shelves, plotted on common axes, and with trends in sand fraction graphic mean diameter shown below. Profiles viewed looking north or east. B – Constant scale bathymorphic profiles across representative eastern high tide slopes, plotted on common axes, and with sand fraction trends as in A.
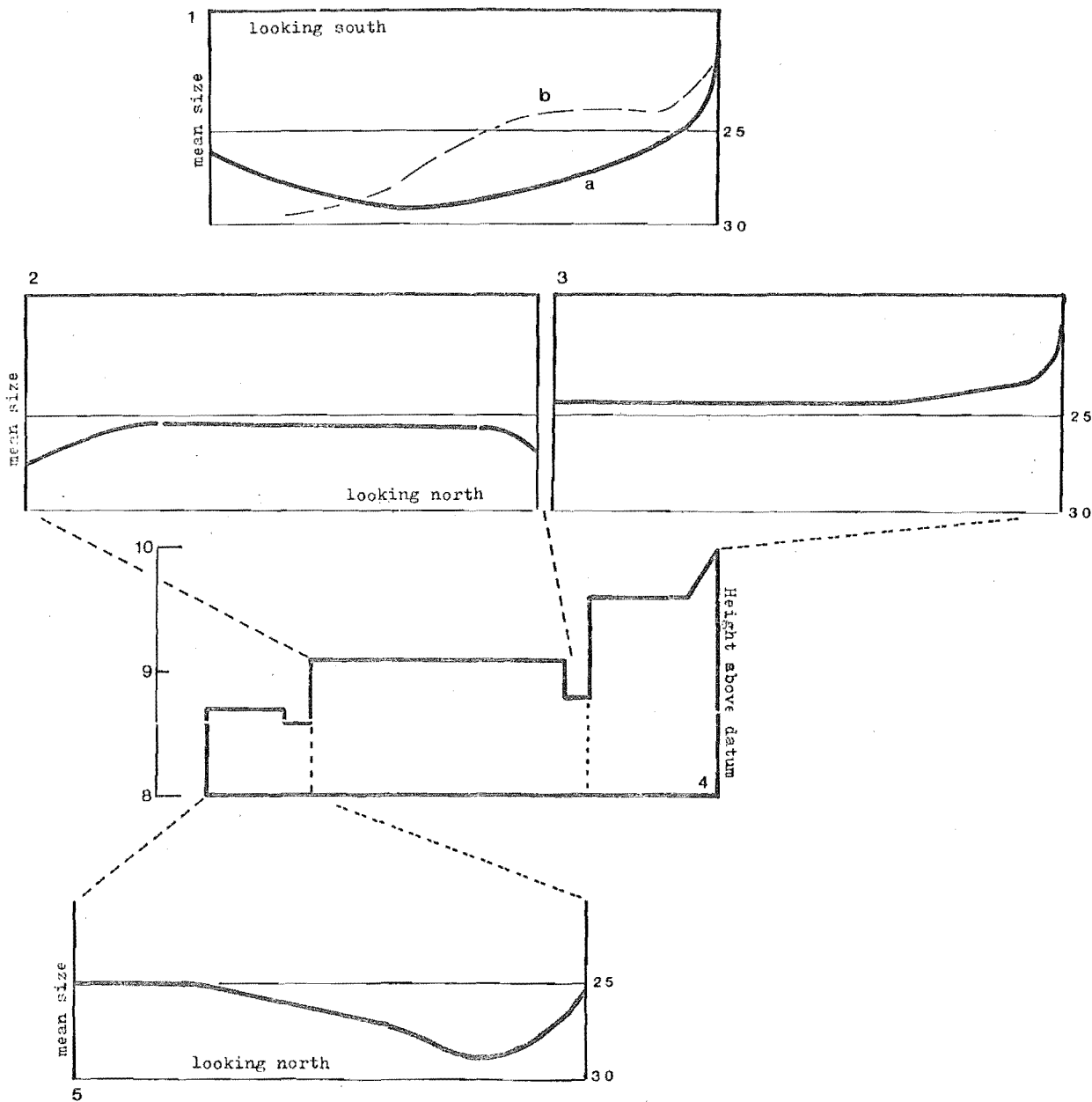
Figure 49. Graphic mean size/ bathymetry model of the surface sediment of the Avon-Heathcote Estuary. Mean diameter trends are from Figures 45 to 47.

1 - Shore-normal trend where the bottom slopes regularly offshore (as on the western slopes and flats, showing a generalised trend (a) and a long-fetch, straight-profile trend similar to those on lines 10 and 11 (b).

2 and 3 - Shore-normal trends across mid tide shelves and high tide slopes.

4 - Bathymorphic model (from Figure 32). 5 - Trend across low tide flats.

PART FIVE

SUBSURFACE SEDIMENT

Introduction

An analysis of subsurface sediment from the AHE was undertaken to evaluate a number of outstanding problems. In particular the active layer assumption, which formed the basis of the sampling method used to collect surface sediment, required testing. The nature and significance of processes which maintain equilibrium distribution patterns in the face of continuing erosion need to be evaluated, and the probability that there may be a stratigraphic record of the response to early urbanisation outlined in Part One, also requires evaluation.

Methods

To obtain the maximum information from subsurface sediment it is necessary to collect undisturbed stratigraphic sequences. Two methods were adopted in this study:

(i) Short lengths of thin-walled plastic drain pipe (internal diameter 60 mm, outer diameter 64 mm) were pushed by hand into the sediment, then lifted or dug out. Tubes were sealed with plastic bags, returned immediately to the laboratory and opened with a sharp knife.

(ii) Longer cores were collected with thicker-walled tubing (internal diameter 53 mm, outer diameter 60 mm) cut into 1.5 m and 2 m lengths. The tubes were hammered into the sediment with the flat back of a spade. Before use the top end was squared off to avoid splitting, and a shallow cutting face was bevelled on to the leading edge. The tubes could often be driven 1.5 m to 1.8 m into the sediment, and were then dug out. Recovery problems were only encountered where sediment in the tube was predominantly mud free; in most cases muddy layers near the tops of filled tubes acted as natural plugs, preventing the loss of sediment from the bottom end of the core. These thicker tubes were opened in the laboratory by cutting a slice of plastic from opposite sides with an electrical band saw, leaving a thin layer which was subsequently cut through with a knife.

In both methods, once the tubes were cut open, the top half was lifted off, exposing an almost undisturbed sequence of sediment for description and analysis. A total of 47 cores were recovered using the two methods. All were logged immediately after opening - while still wet, and before oxidation destroyed layering and mottling due to the presence of chemical layering (Hayes, 1964). Samples were analysed exactly as were surface sediment samples.

Results and interpretations

Detailed core logs are presented in Appendix 4. An examination of these logs reveals that four distinctly different stratigraphic units are present in the subsurface sediment of the AHE. There is an upper zone of dark grey and black mottled, bioturbate sediment, inhabited by a number of burrowing animals, and separated from underlying sediment by a bioturbation interface. Beneath this surface there are three units: a basal massive sand unit - unit (a); an intermediate layered muddy unit - (b); and an uppermost, thin, massive, muddy unit - (c). The stratigraphic relationship of these units are summarised in Figures 50 to 53.

Sediment from beneath the bioturbation interface

1. *Unit (a).* Several of the deeper cores finished in massive, dark grey, friable, clean, coaser fine sand (with mean diameters from 2.0 to 2.5 psi) or medium sand, with rare wood fragments, and sparse coarse shelly debris. Unit (a) sediment was uniformly low in mud (mean muddiness was 3.47%, s = 1.66%, N = 8). Sand fraction graphic statistics, input data, and probability cumulative curves are shown in Figures 54 and 55, where it can be seen that apart from two unusual samples from core 42 (830 and 831), unit (a) sand is uniformly well sorted, although spanning a wide size range. Cumulative curves of unit (a) sand are either almost straight, or slightly curvilinear, and are interpreted to represent a single saltation population, similar to Groups D to F in the surface sediment scheme. Figure 55B indicates that there is no relationship between grain size and HAD in this unit. If the tidal range has remained unchanged since the deposition of unit (a) sand, then Figure 55B indicates some of it was probably deposited in subtidal conditions, and all of it was deposited below the MTL.
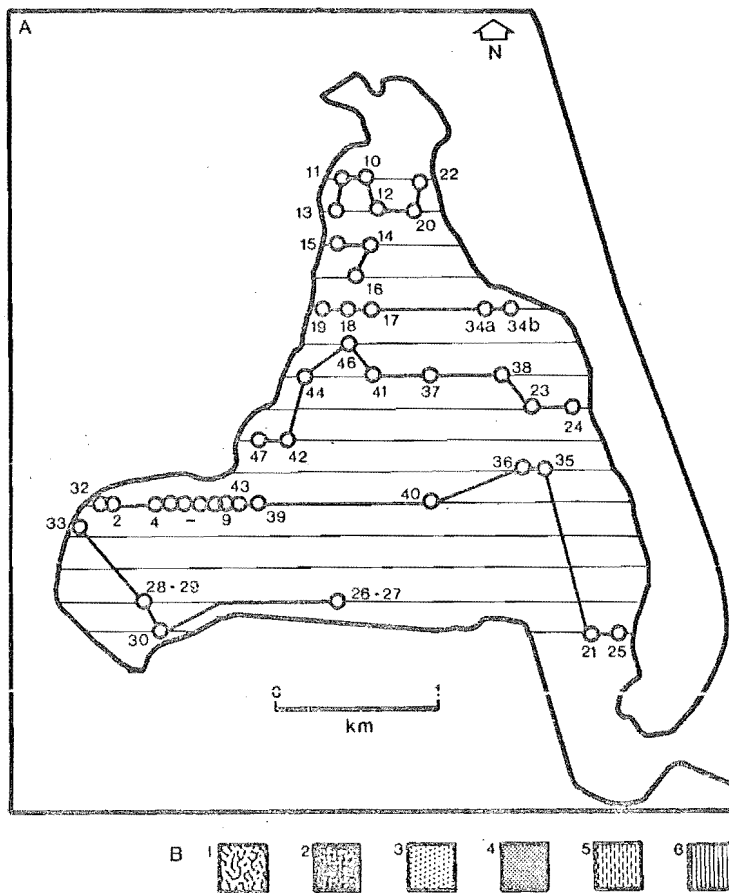
Figure 50. Stratigraphic sections and summary graphic logs. A - Core locations.
B - Simplified descriptive sedimentology of cores. 1 - Bioturbate (mottled) sediment.
2 - Olive grey plastic mud. 3 - Friable massive dark grey fine sand. 4 - Massive
dark grey and grey-black muddy fine sand and very fine sand. 5 - Weakly laminated
very fine sand and muddy very fine sand. 6 - Well laminated very fine sand, very fine
sandy mud and mud.
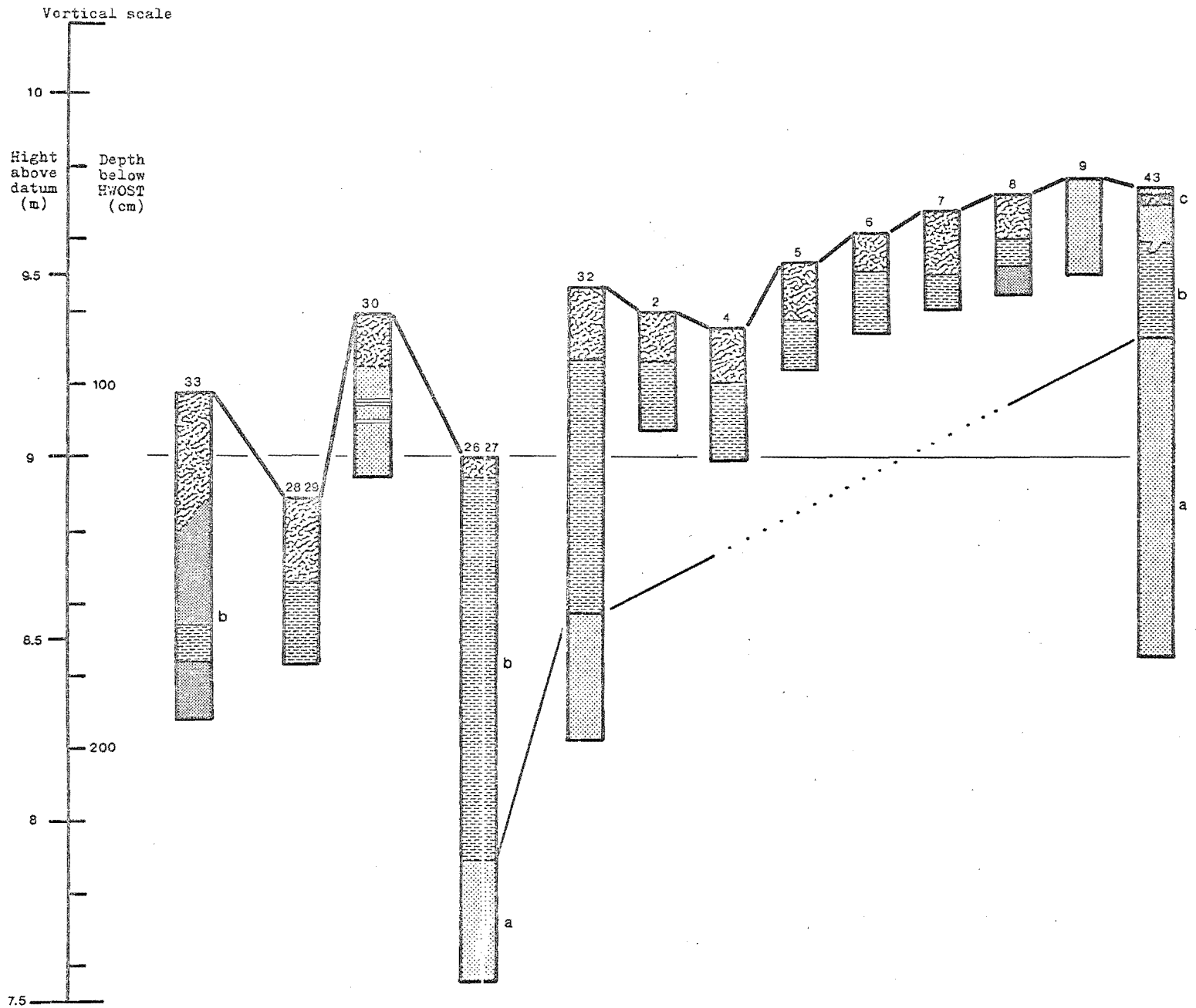
Figure 51. Summary stratigraphy based on detailed logs in Appendix 4. See Figure 50 for locations of cores and sediment descriptions. Letters (a), (b) and (c) refer to stratigraphic units described in text.
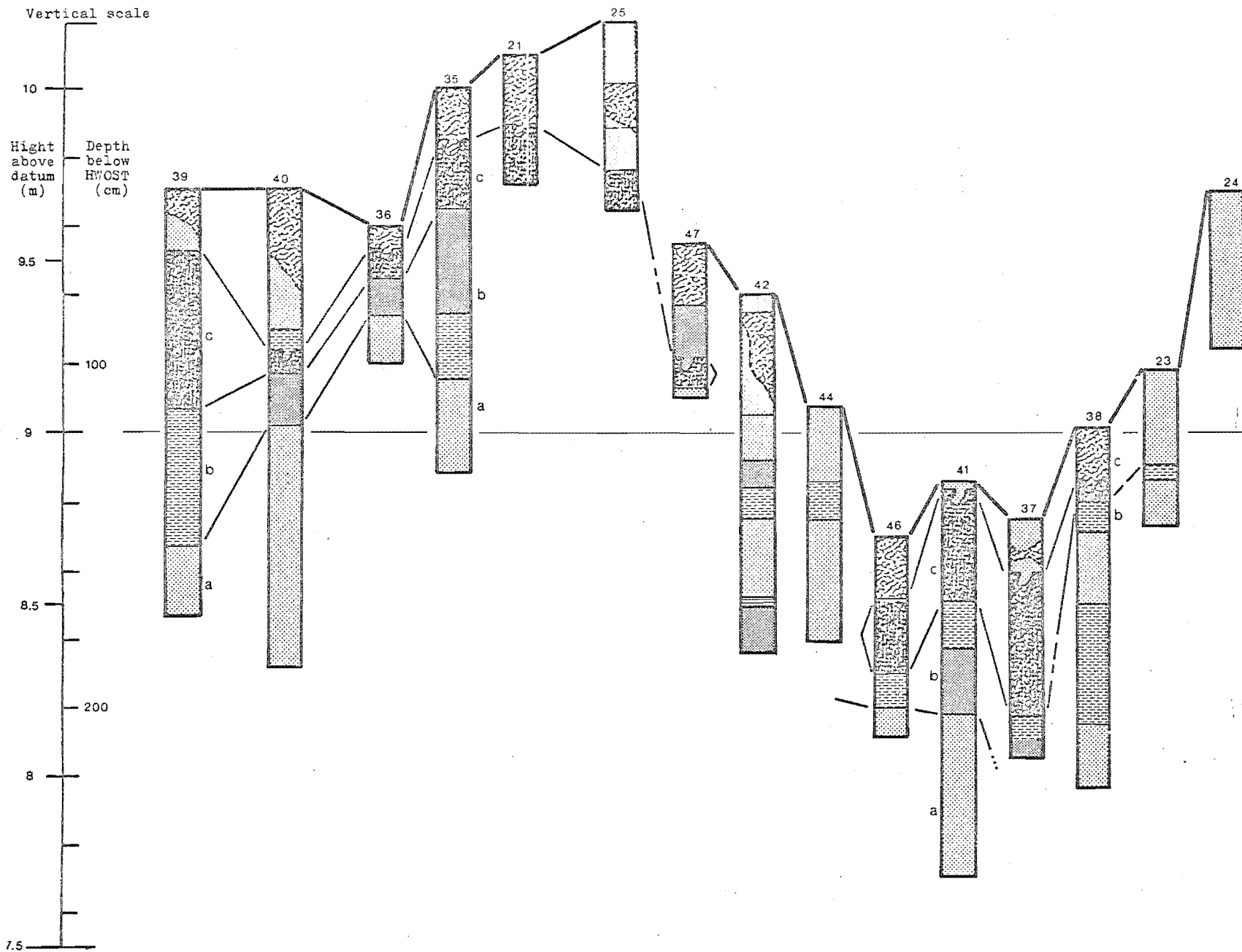
Figure 52. Explanation as for Figure 51.
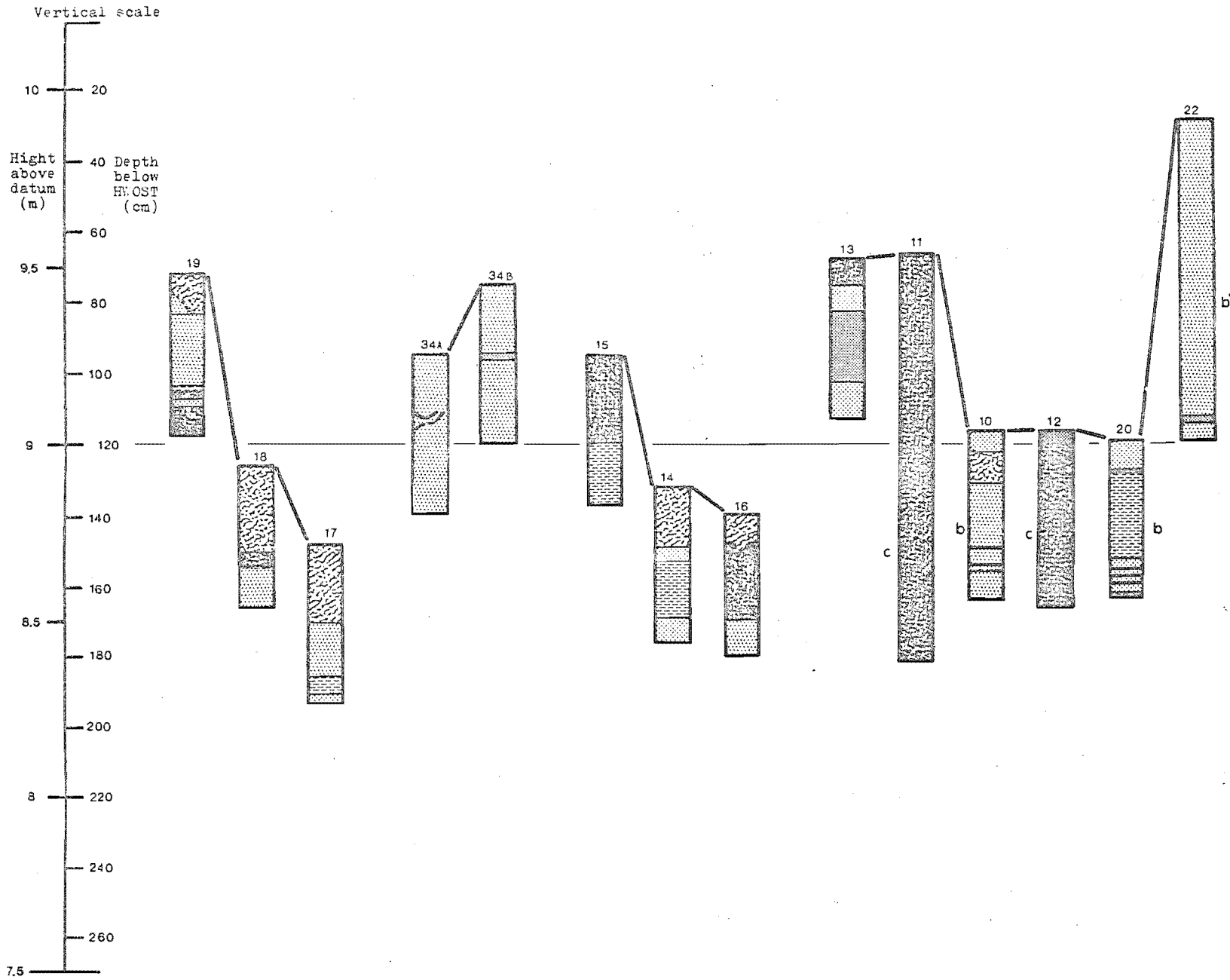
Figure 53. Explanation as for Figure 51.
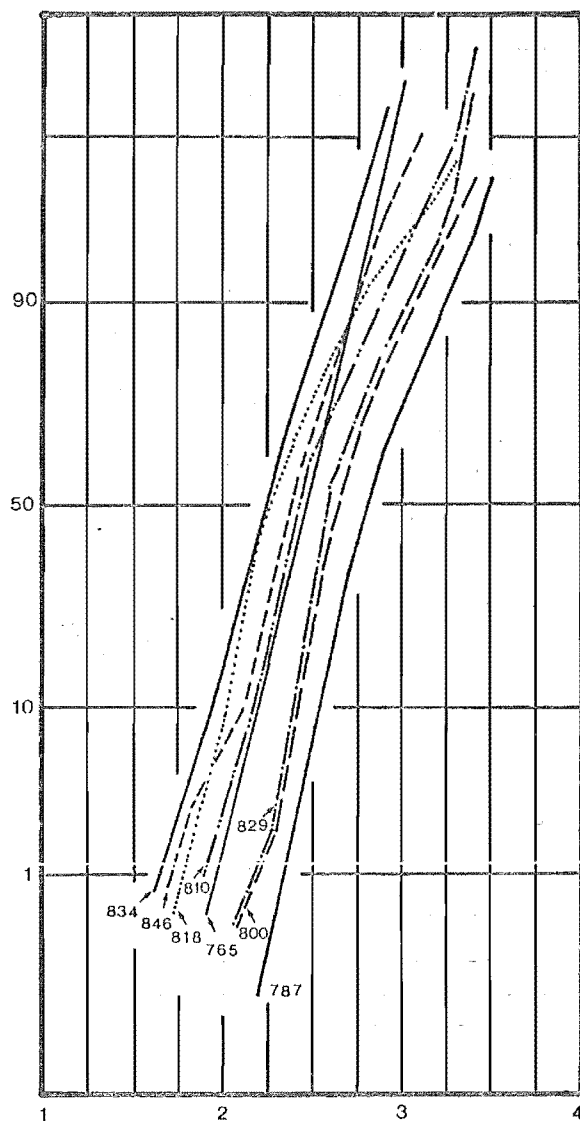
SAMPLE NO.	GR. MEAN	ST. DEV.	SKEWNESS	KURTOSIS	PHI5	PHI16	PHI25	PHI50	PHI75	PHI84	PHI95
787	2.35	0.28	0.25	0.97	2.47	2.60	2.65	2.81	3.04	3.15	3.39
800	2.68	0.25	0.30	1.22	2.35	2.47	2.53	2.64	2.82	2.94	3.21
810	2.48	0.28	0.25	1.05	2.09	2.24	2.28	2.44	2.65	2.77	3.04
818	2.32	0.30	0.33	1.07	1.93	2.06	2.10	2.26	2.50	2.63	2.97
829	2.64	0.25	0.43	1.16	2.35	2.44	2.49	2.58	2.79	2.91	3.20
830	3.16	0.51	0.08	0.79	2.30	2.65	2.78	3.10	3.61	3.73	3.90
831	3.17	0.51	0.10	0.79	2.30	2.66	2.78	3.10	3.61	3.74	3.91
834	2.25	0.25	0.07	1.09	1.81	2.02	2.09	2.23	2.41	2.50	2.66
846	2.41	0.25	0.04	1.19	1.95	2.19	2.25	2.40	2.56	2.65	2.85
852	1.86	0.24	0.29	1.07	1.54	1.65	1.70	1.82	2.01	2.12	2.35

Figure 54. Representative cumulative probability curves, graphic statistics and percentile input data, unit (a) subsurface sediment.

Figure 55. Scatter plots of graphic mean diameter vs graphic standard deviation, and graphic mean diamter vs HAD, unit (a) subsurface sediment.

Figure 56 shows contours drawn on top of unit (a). The data used to construct Figure 56 were derived by calculating the HAD of the upper contact of unit (a) for all core locations where unit (a) sand was recovered. If the assumption that the upper contact of unit (a) sediment represents a synchronous surface is justified, then Figure 56 may indicate that immediately before deposition of overlying sediment the unit (a) surface consisted of a western mid to low tide slope, separated from an eastern low tide flat by a broad subtidal channel.

Drillers logs, supplied to the writer by the CDB, and information from D.D. Wilson (pers. comm., 1977), indicate that typical sequences of sediment encountered during subsurface investigations near the AHE pass through an upper layer of fine muddy material, from 1 to 2 m thick, and then through at least tens of metres of monotonous, massive, dark grey sand. Cores figured by Brown (1975, in press), indicate that this sand – the Christchurch Formation of Suggate (1958) – is up to 50 m thick beneath the estuary. Unit (a) is interpreted to represent the uppermost few decimetres of this sand, and to be uppermost Christchurch Formation sediment.

Unit (a) is interpreted to be pre-estuarine, open ocean sediment for two reasons. Firstly because of the similarity between unit (a) sediment and monotonous, supposedly marine sediment beneath it (Suggate, 1968). Secondly, because of the textural evidence in Figure 54 – present day sand with nearly straight cumulative curves and uniformly excellent sorting only occurs in shallow water (above 9.0 m HAD) where wave energy is relatively high. The presence of similar sand in deeper water (down to 8.0 m, Figure 55B) may indicate a regime of larger waves – and perhaps oceanic conditions.

2. *Unit (b)*. In almost all cores, massive clean friable unit (a) sand is overlain by muddy, stratified sediment. The contact is invariably sharp and abrupt, and represented by a significant textural discontinuity. This stratified sediment is commonly plane-laminated muddy very fine sand, often with centimetre or decimetre scale interbeds of massive muddy fine sand and muddy very fine sand. Where relatively thick (as in core 41), this sequence may contain one or more decimetre-scale fining upwards sequences, with individual units typically beginning at an erosional and textural discontinuity as clean fine sand, grading up into weakly laminated finer fine sand (2.5 to 3.0 psi), muddy laminated very fine sand, and massive very fine sandy mud or mud (more
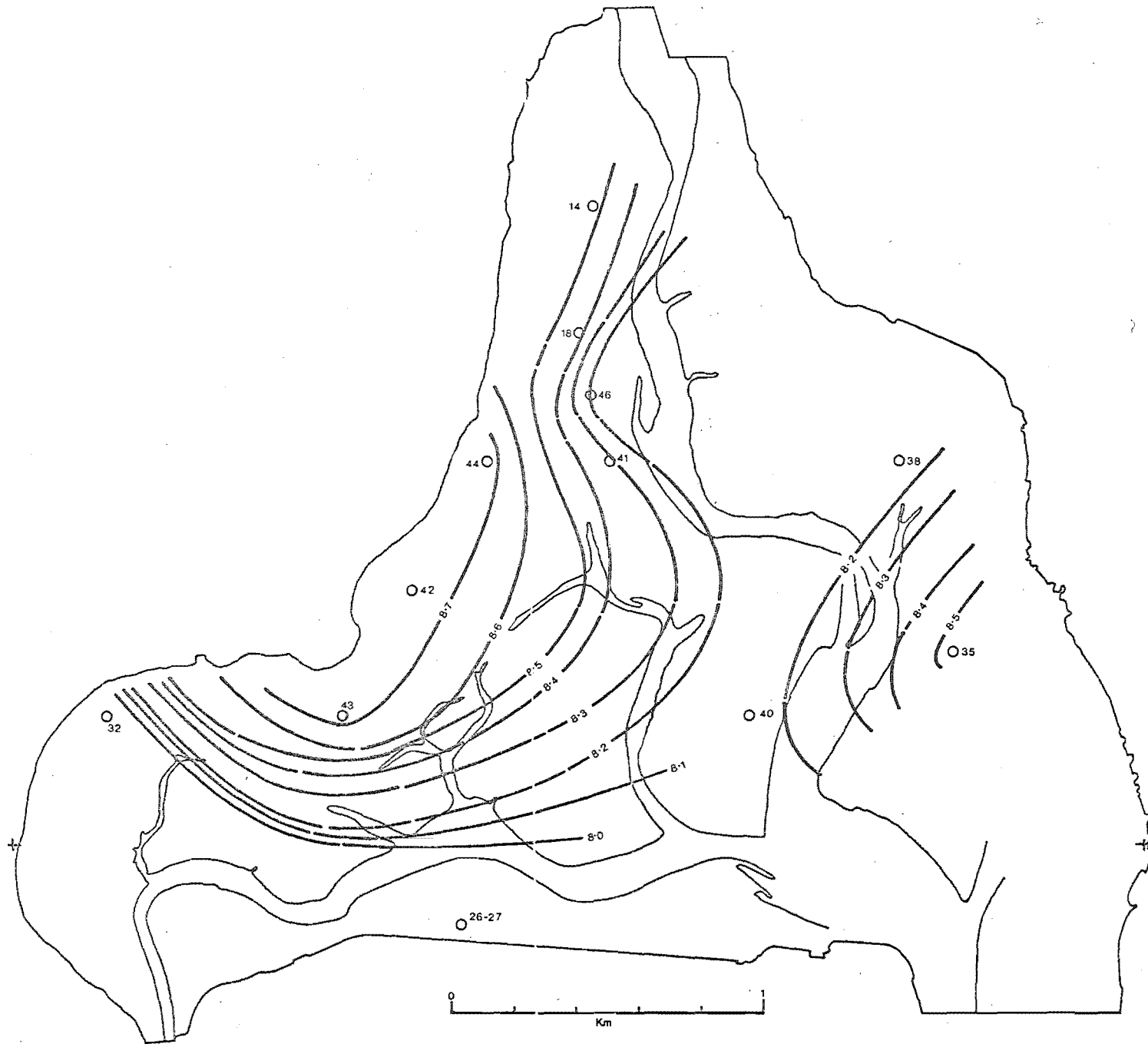
Figure 56. Contoured upper contact of subsurface sediment unit (a), in metres HAD.

than 50% mud). For example see cores 26-27 and 42, Appendix 4.

Coarsening upwards sequences also occur (as in cores 38 and 35), as do massive sequences where sand properties remain more or less uniform but muddiness either increases or decreases upwards (as in core 32). In several cores layered unit (b) sediment is overlain by massive clean or slightly muddy sand, and in others the layered sequence preserved above unit (a) is quite thin, perhaps indicating that much of the unit (b) material was eroded before deposition of overlying massive sand (cores 28-29, 35, 35 and 42). In some cases sediment interpreted as unit (b) consisted of massive and weakly plane-laminated muddy very fine sand, with minor thin muddy layers (as in 10, 13, 14, 20, 23). In some few cases it was difficult to unambiguously differentiate between units (a) and (b) - for example in core 23 below 31 cm; in core 40 below 69 cm; and in core 42, below 56 cm.

Seventy-three sediment samples were collected from unit (b) sequences (see Appendix 4 for sample locations), and the seven percentiles used to calculate Folk and Ward statistics were run through the same clustering program used to sort surface sediment into like groups. The resulting dendogram is shown in Figure 57. Four distinct cluster groups are differentiated in Figure 57, with coefficients of similarity of about 0.95 to 0.96 - about the same as the level of similarity used to differentiate cluster groups in the surface sediment analysis. The four groups are designated b1 to b4.

Representative cumulative curves for each of the groups are presented in Figure 58. Group b1 and b2 sediment consists predominantly of monolinear and curvilinear size distributions, with very similar coarse fraction properties in both (psi 5 at about 2.1 to 2.2, psi 50 at 2.5). The major differences are that most b2 curves have an inflection at about 80% to 90% (at the arrow in Figure 58), and have a finer fine tail than b1 sediments.

Sediments of Groups b3 and b4 are finer and have predominantly bilinear or sharply curvilinear size distributions, with inflections at about 3.0 psi (b3) or 2.5 psi (b4).

Also shown in Figure 58 are samples belonging to a fifth sediment group (labelled b'), which is interpreted to be a laterally equivalent, bathymetrically higher (shallower) version of b1-b4. Sediment of this sort occurs in at least 8 cores (20, 22, 23, 24, 25, 38, 40 and 42) and there are also a number of ambiguous cases - 9, 10, 30, 39 and 47.

GR. MEAN	ST. DEV.	SKEWNESS	KURTOSIS	PHI5	PHI16	PHI25	PHI50	PHI75	PHI84	PHI95	SAMPLE NO.
2.57	0.31	0.43	1.24	2.23	2.32	2.36	2.50	2.72	2.88	3.12	718
2.57	0.31	0.29	1.33	2.15	2.32	2.37	2.53	2.74	2.85	3.35	833
2.59	0.28	0.25	1.37	2.23	2.35	2.42	2.56	2.72	2.85	3.23	739
2.54	0.32	0.21	1.24	2.00	2.26	2.34	2.50	2.70	2.86	3.17	729
2.55	0.29	0.11	1.37	2.00	2.30	2.38	2.54	2.70	2.82	3.15	717
2.57	0.27	0.06	1.48	2.13	2.32	2.49	2.56	2.74	2.84	3.03	728
2.57	0.23	0.08	1.01	2.18	2.37	2.39	2.56	2.72	2.79	2.99	754
2.48	0.34	0.34	1.22	2.04	2.20	2.26	2.42	2.67	2.83	3.26	733
2.68	0.22	0.35	1.21	2.38	2.50	2.54	2.63	2.80	2.90	3.15	806
2.63	0.25	0.24	1.20	2.27	2.40	2.46	2.59	2.75	2.89	3.12	757
2.52	0.24	0.20	1.08	2.17	2.30	2.35	2.49	2.66	2.76	2.99	753
2.49	0.23	0.12	0.92	2.17	2.26	2.33	2.48	2.66	2.74	2.91	755
2.52	0.20	0.18	1.08	2.23	2.34	2.39	2.50	2.64	2.73	2.89	756
2.48	0.21	0.18	0.96	2.16	2.28	2.33	2.45	2.63	2.70	2.86	764
2.45	0.21	0.09	1.04	2.12	2.25	2.31	2.44	2.59	2.66	2.83	765
2.45	0.26	0.26	1.00	2.05	2.22	2.25	2.40	2.62	2.73	2.95	727
2.43	0.28	0.06	1.14	1.98	2.17	2.25	2.43	2.61	2.70	2.98	736
2.39	0.23	0.18	1.23	2.00	2.21	2.26	2.37	2.56	2.60	2.90	743
2.41	0.39	0.13	1.07	1.83	2.04	2.15	2.38	2.65	2.80	3.14	709
2.76	0.12	0.22	1.26	2.60	2.66	2.69	2.75	2.82	2.88	3.00	731
2.71	0.33	0.48	1.18	2.35	2.44	2.49	2.62	2.89	3.08	3.50	715
2.71	0.32	0.29	1.15	2.28	2.43	2.49	2.66	2.89	3.05	3.40	716
2.75	0.37	0.47	1.17	2.34	2.45	2.49	2.65	2.93	3.15	3.60	805
2.69	0.29	0.23	1.00	2.26	2.42	2.48	2.64	2.88	3.00	3.24	745
2.76	0.29	0.22	1.16	2.32	2.51	2.56	2.72	2.92	3.05	3.34	850
2.79	0.27	0.33	1.14	2.48	2.55	2.60	2.75	2.93	3.08	3.40	797
2.82	0.36	0.34	1.16	2.31	2.51	2.57	2.73	3.00	3.21	3.53	732
2.88	0.37	0.31	0.96	2.38	2.54	2.62	2.80	3.14	3.30	3.60	790
2.92	0.37	0.28	0.87	2.40	2.58	2.65	2.84	3.19	3.35	3.55	826
2.88	0.32	0.37	1.10	2.49	2.60	2.66	2.81	3.06	3.24	3.56	807
2.62	0.41	0.32	0.90	2.07	2.24	2.31	2.52	2.89	3.10	3.35	656
2.64	0.42	0.32	1.28	2.10	2.28	2.30	2.57	2.86	3.07	3.60	660
2.70	0.44	0.47	1.61	2.22	2.37	2.44	2.60	2.86	3.13	3.87	714
2.85	0.55	0.32	0.93	2.12	2.34	2.45	2.72	3.20	3.49	3.83	658
2.81	0.49	0.27	0.94	2.11	2.35	2.46	2.71	3.15	3.36	3.70	662
2.87	0.62	0.31	0.73	2.02	2.26	2.37	2.70	3.40	3.65	3.85	664
2.78	0.58	0.39	0.91	2.01	2.27	2.37	2.61	3.20	3.45	3.86	832A
3.34	0.35	0.12	0.74	2.89	2.97	3.03	3.32	3.60	3.73	3.92	809
3.36	0.35	0.10	0.70	2.90	2.98	3.05	3.34	3.64	3.75	3.91	793
3.34	0.37	0.08	0.78	2.80	2.96	3.05	3.32	3.64	3.75	3.92	828
3.32	0.36	0.10	0.76	2.84	2.94	3.02	3.30	3.59	3.72	3.90	841
3.37	0.35	0.07	0.78	2.88	3.00	3.10	3.36	3.66	3.76	3.94	781
3.38	0.34	0.05	0.75	2.90	3.01	3.10	3.37	3.65	3.75	3.91	796
3.38	0.36	0.29	0.77	2.82	3.05	3.10	3.28	3.70	3.80	3.95	670
3.29	0.35	0.10	0.75	2.85	2.91	3.00	3.28	3.56	3.69	3.87	676
3.29	0.35	0.15	0.78	2.80	2.93	2.99	3.25	3.55	3.68	3.87	786
3.27	0.36	0.13	0.73	2.80	2.88	2.95	3.24	3.54	3.68	3.85	798
3.29	0.32	0.14	0.73	2.86	2.95	3.01	3.26	3.54	3.65	3.81	794
3.30	0.34	0.11	0.89	2.87	2.93	3.10	3.29	3.56	3.69	3.87	677
3.26	0.39	0.15	0.72	2.70	2.83	2.93	3.23	3.57	3.72	3.90	746
3.22	0.40	0.24	0.73	2.70	2.82	2.88	3.15	3.54	3.69	3.88	816
3.27	0.42	-0.01	0.77	2.55	2.83	2.93	3.25	3.63	3.72	3.86	673
3.20	0.32	0.27	0.82	2.83	2.89	2.94	3.16	3.44	3.56	3.83	784
3.44	0.35	-0.01	0.69	2.95	3.05	3.15	3.45	3.75	3.83	3.96	671
3.43	0.34	-0.05	0.77	2.91	3.04	3.17	3.44	3.71	3.80	3.92	795
3.46	0.32	-0.01	0.82	2.95	3.12	3.20	3.46	3.70	3.80	3.95	672
3.06	0.36	0.43	0.87	2.63	2.73	2.78	2.95	3.32	3.49	3.77	843
3.07	0.37	0.38	0.93	2.60	2.74	2.80	2.97	3.32	3.49	3.78	844
3.03	0.34	0.43	0.99	2.64	2.74	2.78	2.94	3.24	3.41	3.75	783
3.10	0.33	0.36	0.87	2.69	2.79	2.84	3.02	3.34	3.48	3.75	782
3.09	0.38	0.28	0.87	2.52	2.75	2.80	3.00	3.37	3.52	3.73	663
3.06	0.34	0.19	1.05	2.57	2.75	2.83	3.02	3.27	3.41	3.70	792
2.99	0.37	0.43	0.92	2.57	2.67	2.71	2.89	3.24	3.41	3.76	845
3.12	0.42	0.20	0.90	2.49	2.72	2.81	3.05	3.42	3.59	3.83	808
3.11	0.41	0.25	0.92	2.53	2.73	2.80	3.04	3.40	3.57	3.87	827
3.13	0.39	0.18	0.80	2.65	2.74	2.82	3.10	3.43	3.56	3.84	842
3.10	0.49	0.20	0.74	2.42	2.60	2.68	3.02	3.50	3.67	3.90	659
3.12	0.48	0.11	0.84	2.35	2.65	2.75	3.07	3.50	3.65	3.88	817
3.18	0.47	0.14	0.73	2.51	2.69	2.78	3.12	3.56	3.72	3.90	705
3.02	0.56	0.06	0.82	2.15	2.43	2.60	2.98	3.45	3.64	3.85	667
3.04	0.52	0.21	0.80	2.25	2.54	2.65	2.94	3.47	3.64	3.86	815
3.00	0.50	0.06	0.73	2.24	2.48	2.59	2.97	3.44	3.55	3.75	661
2.94	0.49	0.39	0.97	2.25	2.52	2.60	2.79	3.28	3.50	3.86	657

Cluster groups (left margin): b_1, b_2, b_3, b_4

Modified Sorrensons Coefficient axis: 99 98 97 96 95 94 93 92 91 00

Figure 57. Sand fraction graphic statistics, percentile input data, and dendrogram resulting from cluster analysis of input data, unit (b) subsurface sediment.

Figure 58. Representative cumulative probability curves from groups b1-b4 and b',
unit (b) subsurface sediment.

Group b' consists of massive well sorted fine sand, physically very similar to unit (a) sediment, except slightly muddier. Group b' sediment sometimes directly overlies unit (b), as in cores 42 and 43, but more commonly occurs as a laterally equivalent, bathymetrically higher correlative of (b), as in the core series 38-23-24 (Figure 52).

Mean size vs sorting of all unit (b) samples is plotted in Figure 59, at the same scale as Figure 40 (for surface sediment). A comparison of Figures 40 and 59 indicates that sediment of units b1 and b' is analogous to Group D surface sediment, b2 is analogous to B, and b4 to C. Sediment similar to subsurface unit b3 has not been recorded at the surface. The distribution of samples in Figure 59 shows that the cluster groups b1 to b4 occupy separate sections of the diagram, and are evenly distributed within their individual fields, indicating that here also, the clustering operation has made a classification of convenience.

Figure 60 shows the depth preferences of the five groups. Groups b1 and b2 have similar depth distributions, with identical means and ranges. Group b3 sediment occurs preferentially in deeper water, never above the MTL (9.0 m), with a mean depth of 8.45 m HAD. Group B4 samples tend to occur between 8.0 m and 8.25 m, or between 8.75 m and 9.0 m, with a mean value of 8.56 m; and b' samples tend to occur preferentially above the MTL, with a mean HAD of 9.30 m.

Groups b1 and b2 have depth distributions similar to those of the series A-B-C (Figure 43) for surface sediment, b' is similar to group F, but b3 and b4 do not have surface equivalents.

Figures 61A and 61B are plots of mean size vs HAD and per cent mud vs HAD for all unit (b) sediment samples. These figures show that there is a general trend towards coarser, cleaner sediment in shallow water, and regression lines fitted to group average values (for b1-b4 only) show high coefficients of determination, indicating that the average trend is valid.

Unit (b) sediment is commonly plane-laminated and muddy, and granulometric and HAD-preference studies show that it is similar to modern, active sediment in the AHE, but quite dissimilar to unit (a) sediment beneath.

Unit (b) sand consists of single log-normal size distributions interpreted to have been deposited from saltation, or of simple mixtures of this saltation population with material interpreted to have been deposited from suspension.
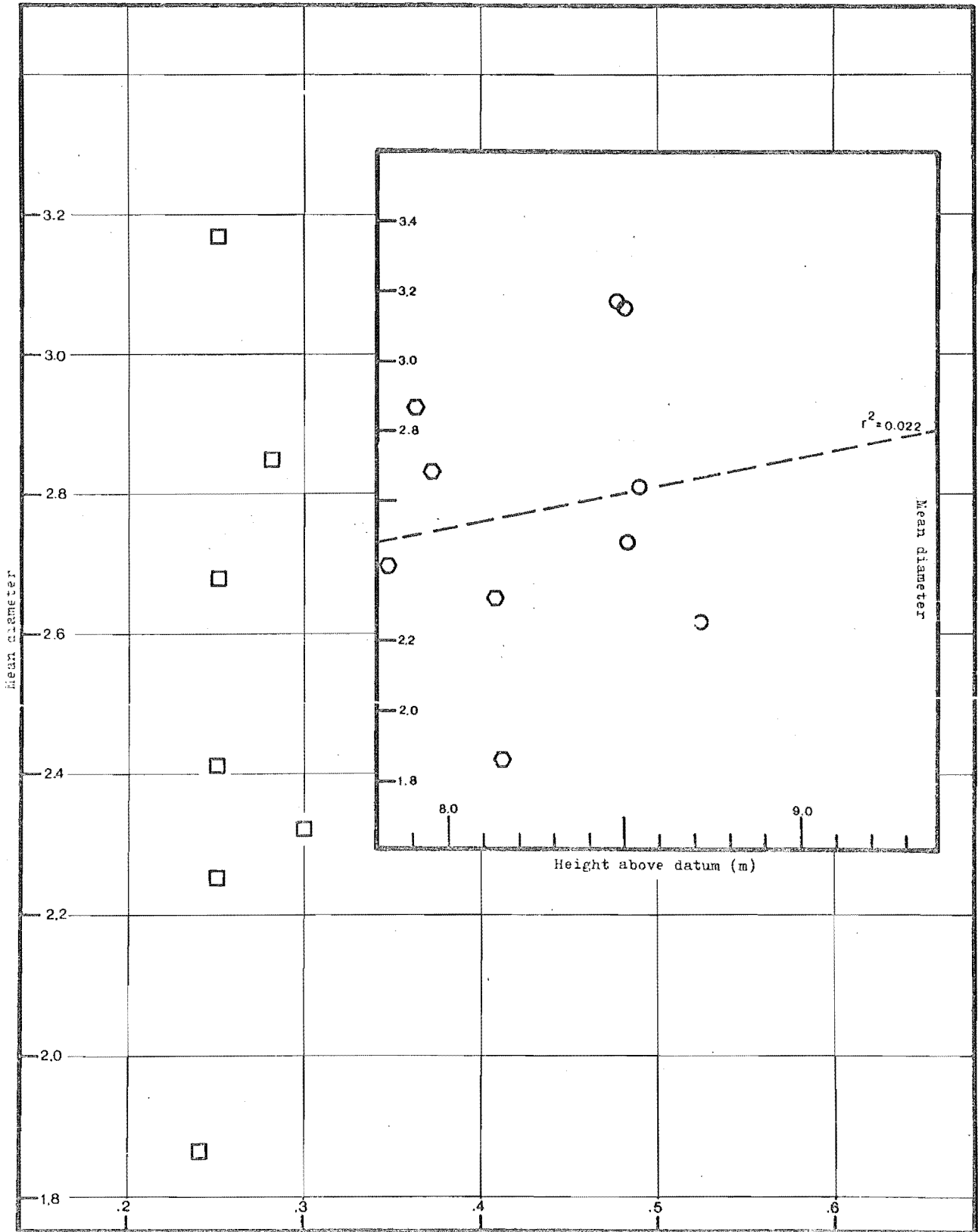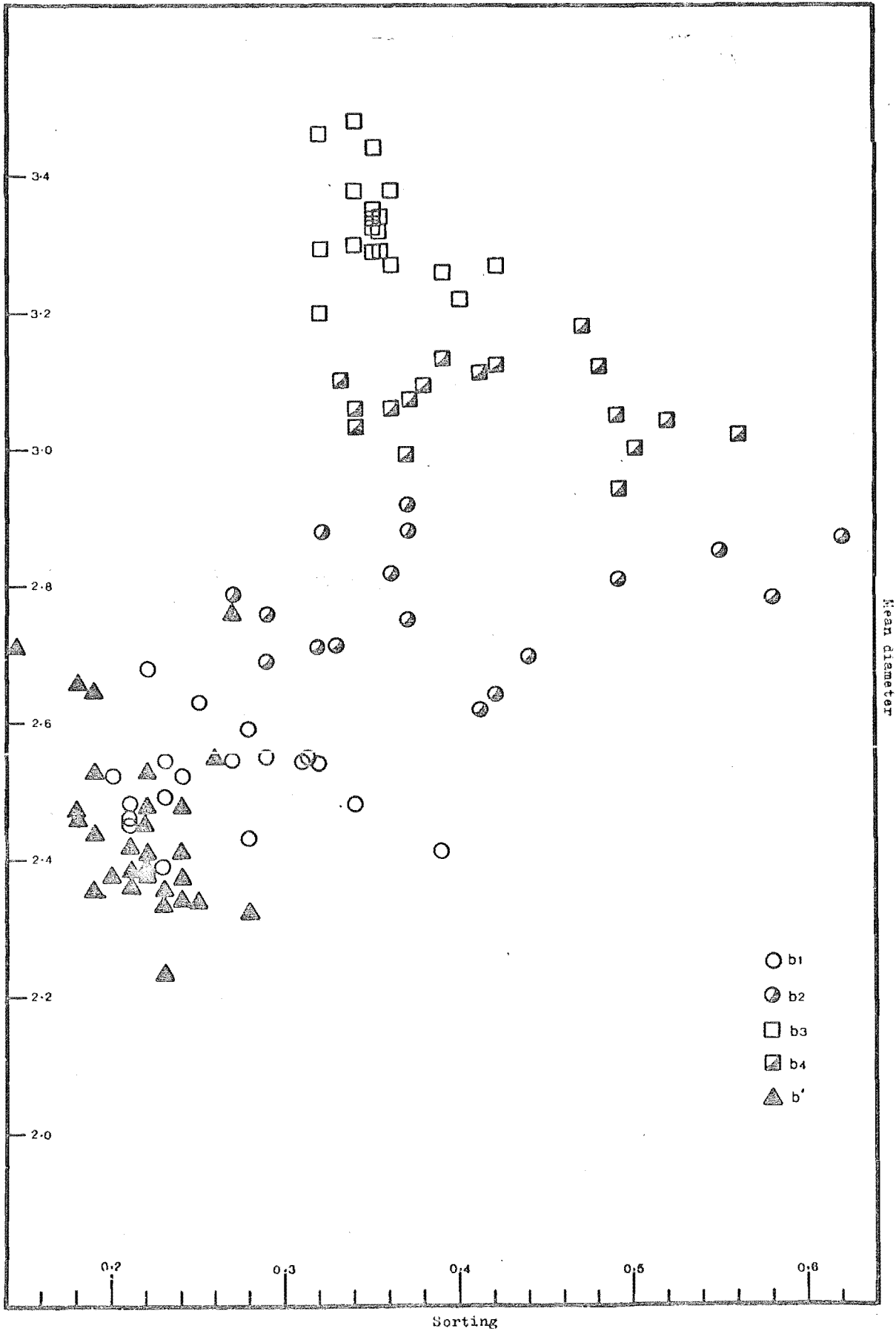
Figure 59. Scatter plot of graphic mean diameter vs graphic standard deviation for samples from unit (b), subsurface sediment.
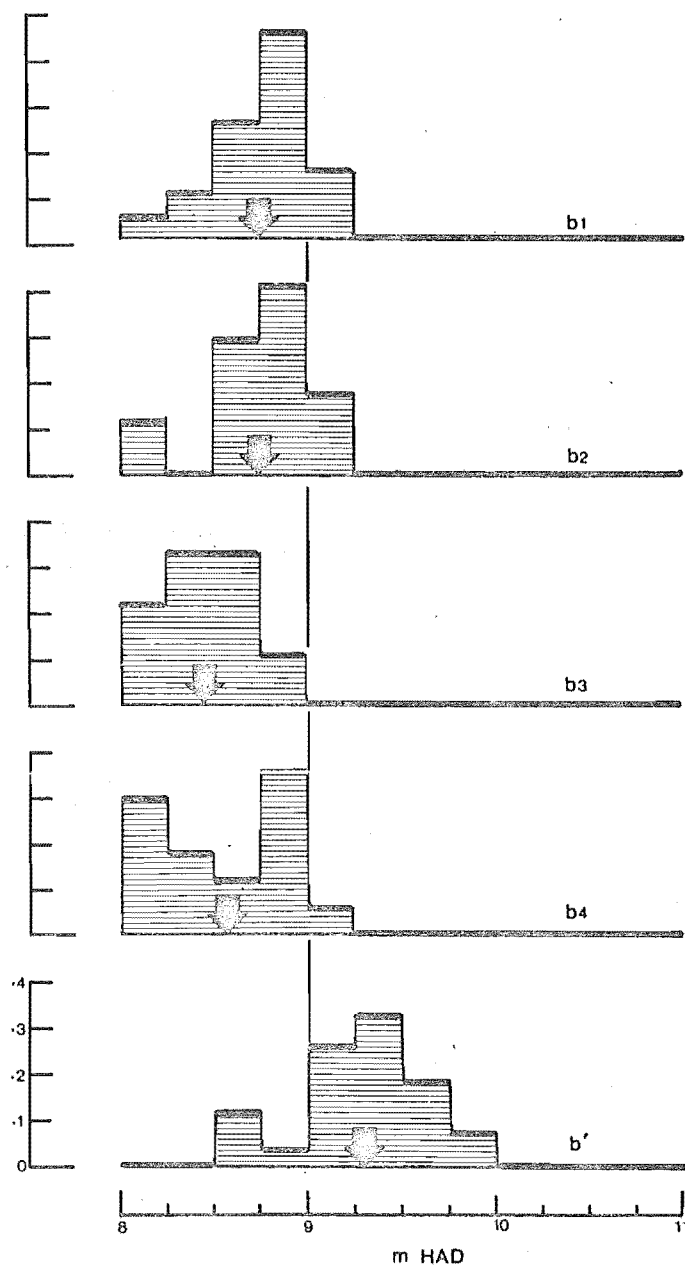
Figure 60. Sample frequency vs HAD for the groups b1-b4 and b', unit (b) subsurface sediment.
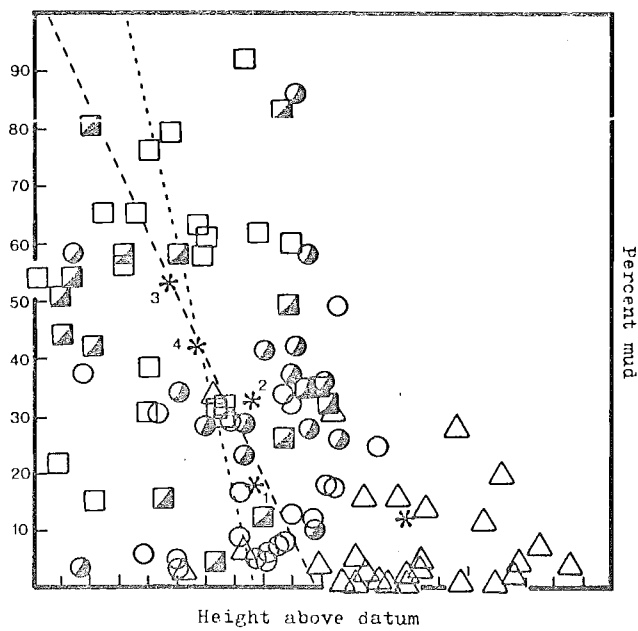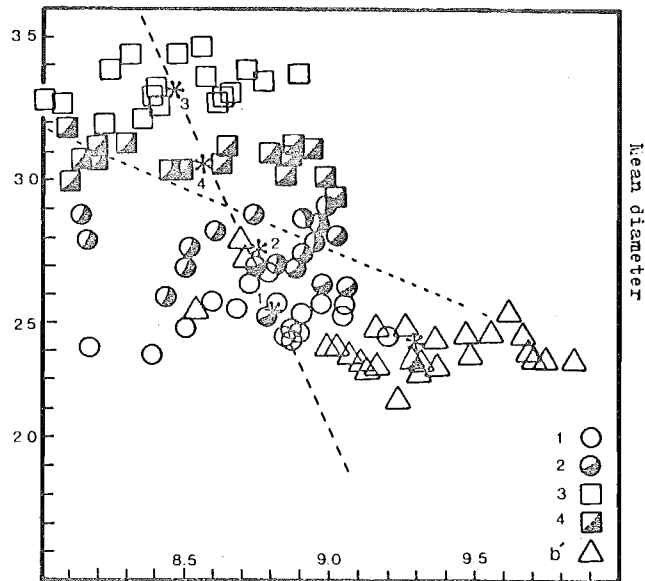
Figure 61. Scatter plots. A – Mean diameter vs HAD. B – Perecent mud vs HAD. Sample from cluster group (b), subsurface sediment.

Differences between samples are a result of various mixtures of the two basic populations, and this simple two-component model is analogous to that derived for surface sediment. However, unlike surface samples groups b3 and b4 contain more than 50% of the suspension population, and Figure 58 indicates that some b3 samples contain as much as 80%.

Unit (b) is interpreted to have been deposited after the AHE was separated from open ocean conditions, and to represent material deposited under conditions essentially similar to those which apply at present.

3. *Unit (c)*. In many cores, unit (b) sediment is overlain by a thin layer of massive olive grey plastic (buttery) mud, or very fine sandy mud – unit (c). This olive plastic mud is commonly massive and monotonous in appearance, but it may show laminations (for example, core 13), and it may be rich in coarse, leafy organic debris (probably *Zostera* leaves). The contact between units (b) and (c) is commonly sharp and abrupt, with a major textural discontinuity; in some cores the contact is gradational, with interbedded sand and mud grading up through sandy plastic mud to plastic mud (cores 37 and 41 for example).

Cores with olive plastic mud occur throughout the estuary, with the thickest sequences recorded from the north-west corner (Figure 53). There was no apparent relationship between occurrences of plastic mud and HAD, and the unit was apparently deposited throughout the estuary.

Because of its cohesiveness unit (c) is more resistant to erosion than most other sediment in the AHE, and is exposed at the surface in many locations in the estuary (Figure 62). When exposed on the higher intertidal flats unit (c) tends to be rich in coarse organic debris (leafy material, twigs and shell fragments), and as a result has a fibrous, crumbly texture.

Unit (c) has a mean mud content of 80% (s = 17%, N = 15), a sand fraction mean diameter of 3.08 psi (s = 0.16 psi, N = 10), and a mean sorting of 0.47 (s = 0.04, N = 10). The mean thickness of the unit, from four apparently complete sections (with gradational or planar contacts – cores 17, 22, 39 and 46) is 25 cm, and the average HAD of the top of the unit is 8.96 m.

While unit (c) sediment is different in appearance from both overlying and underlying sediment, it has a markedly uniform appearance from core to core, and very similar physical properties. Figures 63 and 64 show cumulative curves and summary granulometric properties of unit (c) sand, and a comparison with Figure 58 shows that it is
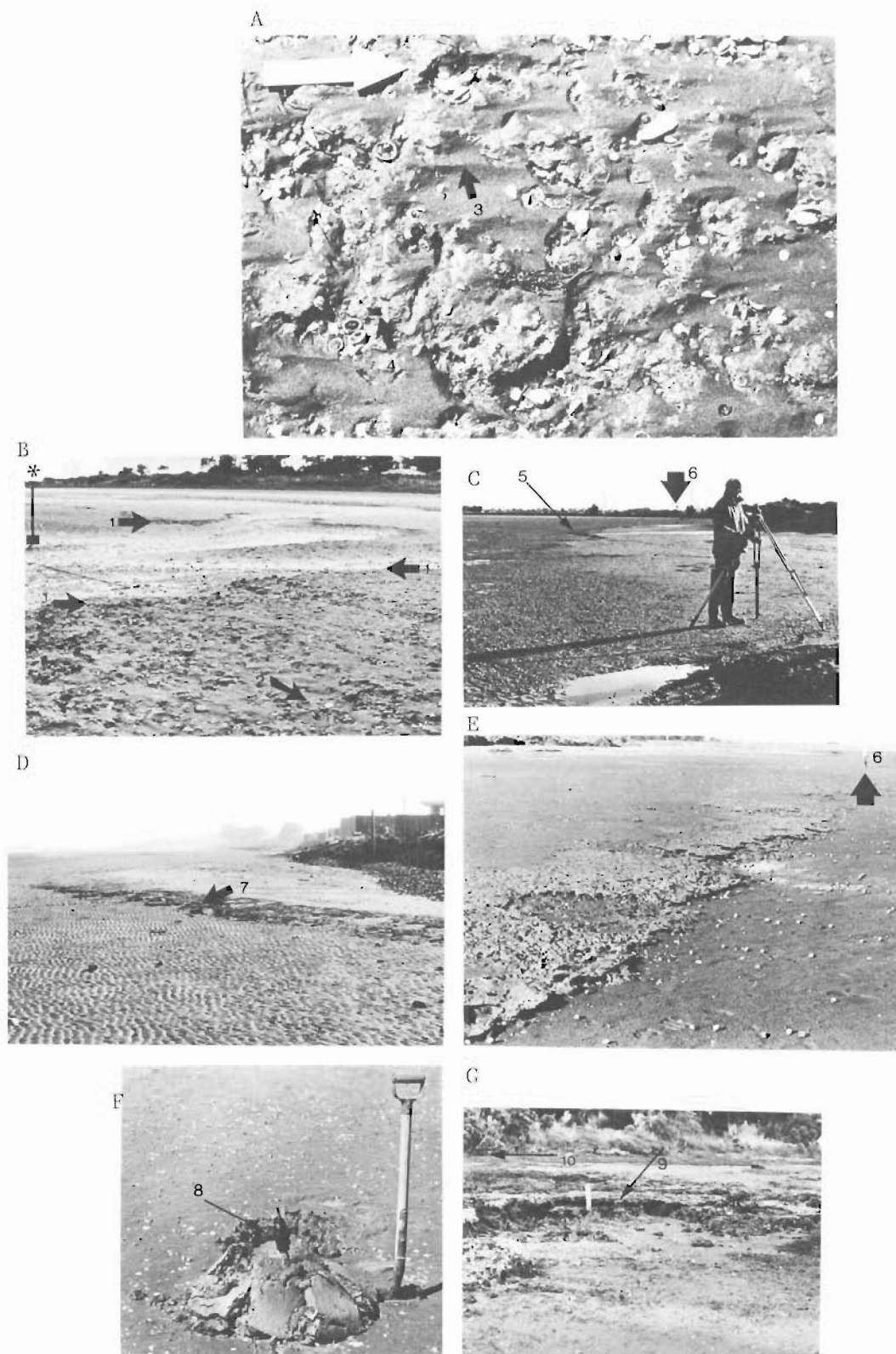
Figure 62. Surface occurrences of post-European anthropogenic mud – subsurface stratigraphic unit (c) – in the Avon-Heathcote Estuary. A, B – Unit (c) plastic mud exposed in the sides of a shallow intertidal gulley near the end of line 16, eastern high tide slopes (1). View is east north east, ebb flow is to the right (2). Spade for scale (✳). Note coarser, active clean sand (3), with lineations parallel to the ebb flow direction (arrowed), and burrows in the lumpy, cohesive erosion-resistant plastic mud (4). White arrow in A is 20cm long. C – Unit (c) fibrous, organic-rich plastic mud exposed immediately south of Sandy Point. View is west into the North Heathcote Basin (Map 1), Tom Cleary (CDB surveyor) for scale. Note scarp or eroding mud (5), shown in detail in E, below (looking east), and post (6) for location. Unit (c) mud is intensely bored, and dips offshore (to the right in E) at a slightly lower angle than the present-day sediment surface. D – Unit (c) sandy mud (7), exposed near the eastern end of line 10, Map 1. View is to the north. F – Olive plastic mud of unit (c) dug from beneath clean friable sand (8) on line 10, near the location of core 36, Figure 50 (see detailed log of core 36 in Appendix 4). G – Shelly, organic-rich unit (c) mud (9) exposed at the HW mark (10) near the east end of line 3, Map 1. Rule is 25cm long.

psi diameter
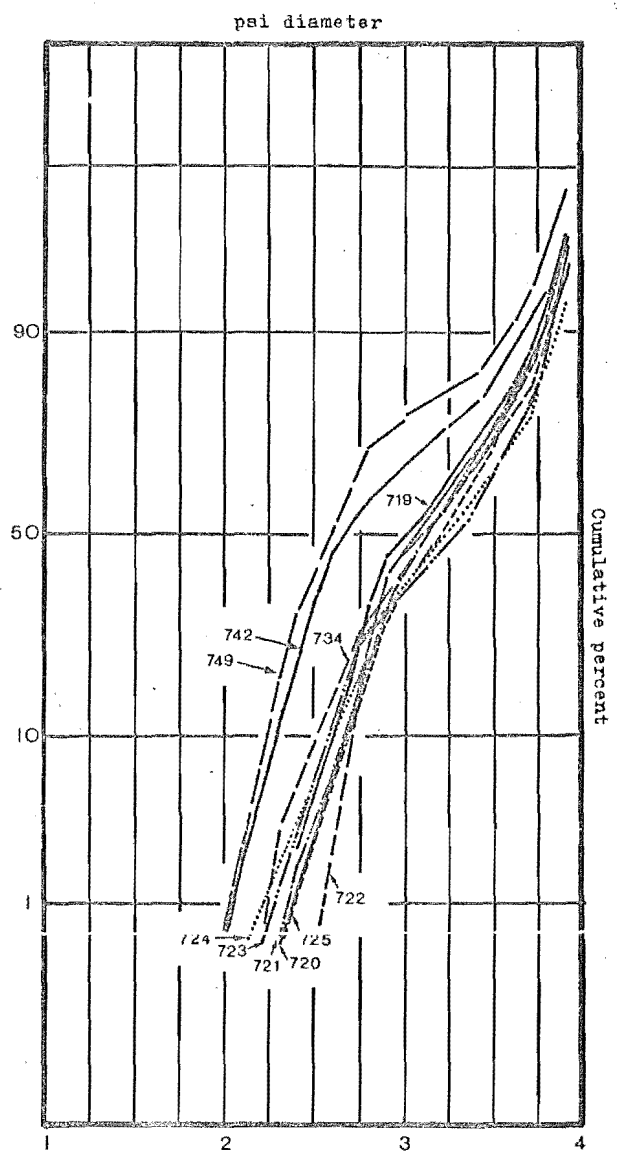
SAMPLE NO.	GP. MEAN	ST. DEV.	SKEWNESS	KURTOSIS	PHI5	PHI16	PHI25	PHI50	PHI75	PHI84	PHI95
719	3.10	0.44	0.21	0.81	2.49	2.66	2.75	3.03	3.43	3.61	3.84
720	3.14	0.44	0.25	0.83	2.54	2.72	2.80	3.06	3.47	3.65	3.90
721	3.18	0.42	0.14	0.84	2.56	2.75	2.85	3.13	3.48	3.65	3.85
722	3.18	0.42	0.22	0.70	2.60	2.75	2.80	3.10	3.53	3.68	3.85
723	3.11	0.49	0.07	0.71	2.40	2.58	2.67	3.08	3.50	3.67	3.84
724	3.11	0.50	0.17	0.80	2.36	2.61	2.72	3.03	3.50	3.70	3.88
725	3.23	0.42	-0.05	0.80	2.58	2.77	2.86	3.25	3.54	3.66	3.90
734	3.16	0.50	0.05	0.76	2.39	2.63	2.74	3.13	3.55	3.72	3.90
734	3.16	0.50	0.05	0.76	2.39	2.63	2.74	3.13	3.55	3.72	3.90
742	2.84	0.52	0.47	0.85	2.22	2.37	2.45	2.66	3.24	3.48	3.85
749	2.75	0.51	0.46	1.10	2.16	2.30	2.36	2.59	2.95	3.37	3.74

Figure 63. Representative cumulative probability curves, graphic statistics and percentile input data, unit (c) subsurface sediment.
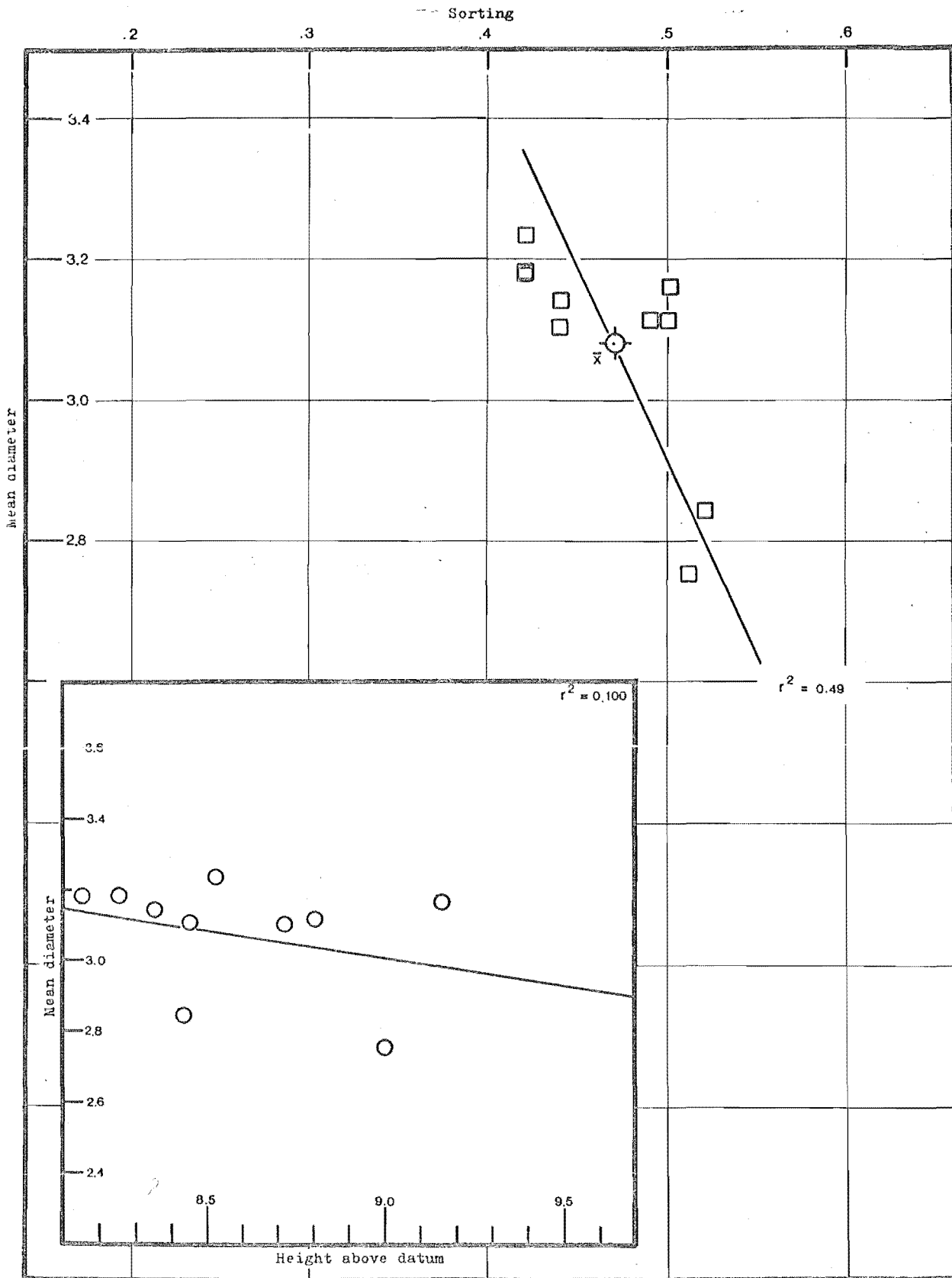
Figure 64. Scatter plots. A – Mean diameter vs graphic standard deviation, B – Mean diameter vs HAD, unit (c) subsurface sediment.

uniformly finer and poorer sorted than any of the subgroups of (b).
Figure 64 shows that there is no relationship between the sand
properties of unit (c) and water depth.

Unit (c) sediment is clearly different from all other material
in the AHE, both ancient and modern; it was deposited as a thin blanket
throughout the estuary - in many places where fine sediment had not
previously been deposited, and where it has not been deposited since.
The unit was most probably deposited during a period of very much
higher than usual suspended sediment concentrations, and was deposited
relatively rapidly and at uniform rates (hence the massive appearance,
and the independence of sand fraction properties, muddiness, and HAD).
The event most likely to be responsible for flooding the estuary with
high concentrations of mud, for periods sufficiently long to allow an
accumulation of tens of centimetres of sediment, is the urbanisation
of the catchment area of the estuary during the second half of the
19th Century. Thus unit (c) sediment is interpreted to represent
material deposited during early urbanisation of the Christchurch area,
when the tidal compartment decreased by about 30%. If this
interpretation is correct it means that the (b)-(c) contact can be
dated at about 1850, and the upper contact of (c) at about 1900.

If unit (c) was deposited with an average thickness of 50 cm
throughout the estuary, this would represent an accumulation rate of
2 cm/year for the 25 year period 1850-1900, and a total of 3.0×10^6 m^3
of sediment, which corresponds to the figure predicted in Part One
(and in detail in Appendix 1) for the decrease in the tidal compartment
during this period.

Biology and physical characteristics of sediment from above
the bioturbation interface

In many cores, cohesive muddy unit (b) or (c) sediment has an
intensely burrowed upper contact, and where thin unit (c) horizons are
exposed at the surface, they are intensely burrowed (Figure 62). The
overlying sediment is massive sand, and it commonly contains abundant
articulated (living) or coarsely fragmented bivalves. Locally there
are pebbles and blebs of soft plastic mud in this upper sandy zone
(see cores 37 and 41 in Appendix 4). If muddy horizons occur within
this upper zone, they are intensely disturbed, and consist of a few
streaky remnants of mud surrounded by sand (as in cores 26-27, 32 and
43).

Mottling and visible burrowing in subsurface sediment in marine environments is due to the myriad activities of organisms living on or in the bottom sediment, which eat, burrow through, spray out, or otherwise disturb and mix near-surface sediment (Schink and Guinasso, 1977; Rhoads, 1967). Benthic animals physically alter the sediment in which they live in a variety of ways (see Myers, 1977, for a brief, recent review of this subject). Biologically mediated sediment-water interactions involve the movement of organic matter, nutrients, and pollutants, and are significant in both the benthic and pelagic food chains (Myers, 1977; Goreau, 1977).

1. Biology. A wide variety of different animals are involved in the bioturbation of near surface and subsurface sediment in the AHE; four groups warrant detailed discussion:

(i) Polychaete worms are the most abundant animals in the AHE in both variety and numbers (Voller, 1973; Knox and Kilner, 1973). Estcourt (1967) found a total of 21 species, and one of these *(Aonides trifidus)* was found in concentrations of up to 6 000/m^2. Some are quite large, *Glycera americana* may reach 27 cm in length, and some are deep burrowers - the widespread detritus-feeding worm *Nicon aesturiensis* may be found in permanent burrows as deep as 40 cm below the surface in the AHE. Some are carnivores *(G. americana)*, some are surface detritus and deposit feeders *(N. aesturiensis)* and some are suspension feeders *(Scolecolepids benhami)*. As well as species which live in permanent burrows, there are free-living burrowing species *(Anglaophamus macroura)* and tube-building species (especially *Boccardia polynranchia* and *Axiothella quadrimaculata,* see Figure 65). The lugworm *Abarenicola affinis* constructs large and conspicuous egestion mounds on many clean sandy midtidal flats (Figure 66A, 66B).

Rhoads has shown that the North American polychaete *Clymenella torquata* is capable of producing vertical grain size gradients in near surface sediment, and of reworking all sediment to a depth of 20 cm in 1.4 to 2.4 years. Other polychaetes are also capable of reworking large volumes of sediment, and of producing subsurface biogenic layering. On the North Sea intertidal flats off Holland and Germany, the polychaete *Arenicola* (an animal which is similar to the *Abarenicola* spp. found in the AHE) produces a distinctive 20-30 cm deep concentration of gastropod shells in a manner similar to that described for *C. torquata* (Reineck and Singh, 1975, p. 135).
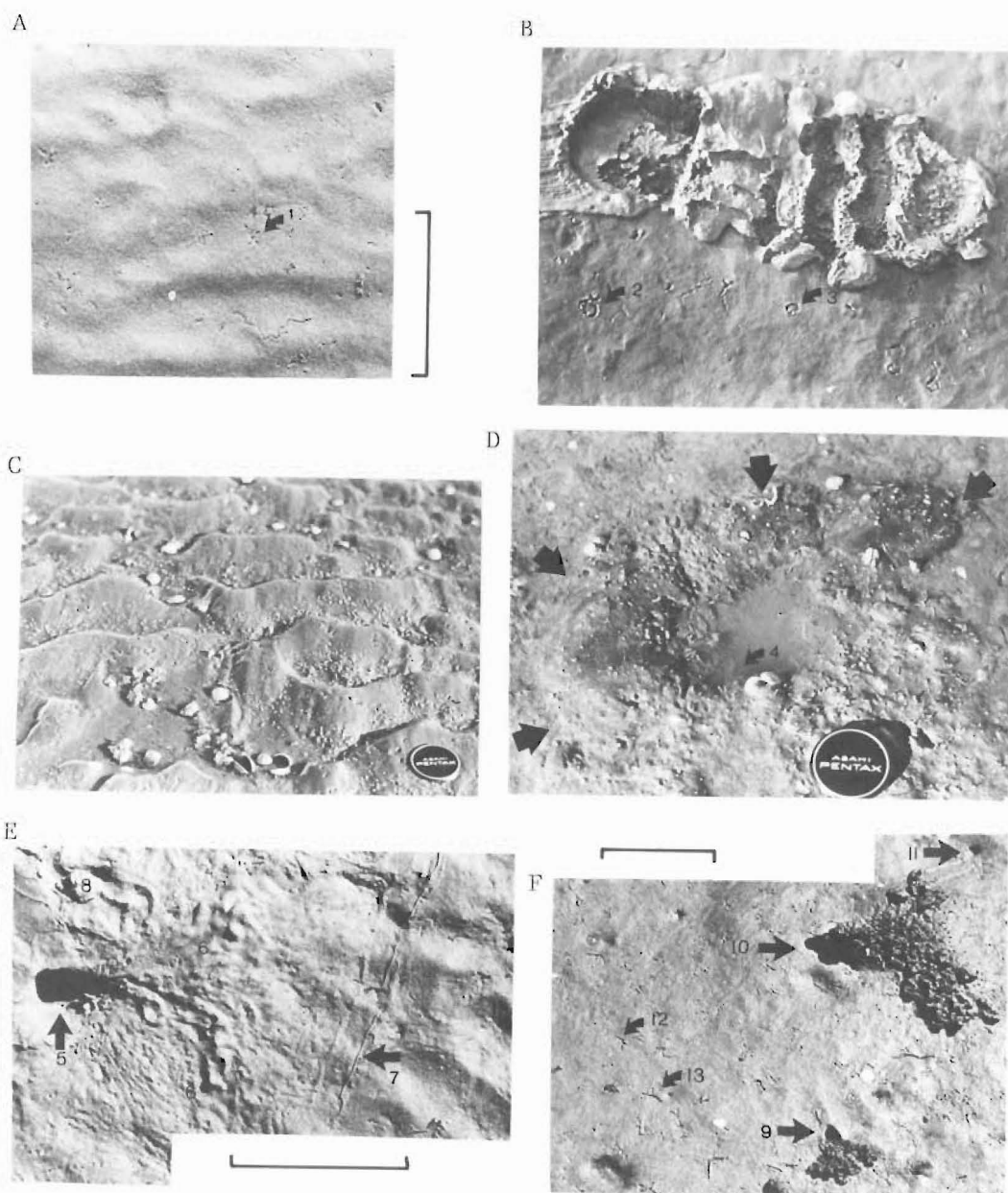
Figure 65. Surface evidence of sediment-modifying biological activity in the Avon-Heathcote Estuary. A - Holes and surface markings (1) in clean friable rippled sand near the eastern end of line 10, Map 1. Animals not identified, bar is 10cm long. B - Circular traces (2, 3) in sloppy mud near the western end of line 3, Map 1, probably due to a polychaete worm. Size 8 (NZ) boot. C - Ripples formed in slightly muddy very fine sand occupied by a dense population of the tube-building polychaete Axiothella quadrimaculata. D - Crab burrow (4) and large excavation apron (outlined by square arrows), central Heathcote Basin low tide (8.65m HAD) flats. Lense cap diameter 5cm. E - Crab burrow (5), excavation apron (6), Amphibola trail (7) and partly buried Amphibola (8), in rippled clean sand near the HW mark at the western end of line 11, Map 1. Bar is 10cm long. F - Crab burrows and aprons (9, 10, 11) and surface markings of an unidentified worm (12, 13), near the east end of line 6, Map 1. Bar is 10cm long.
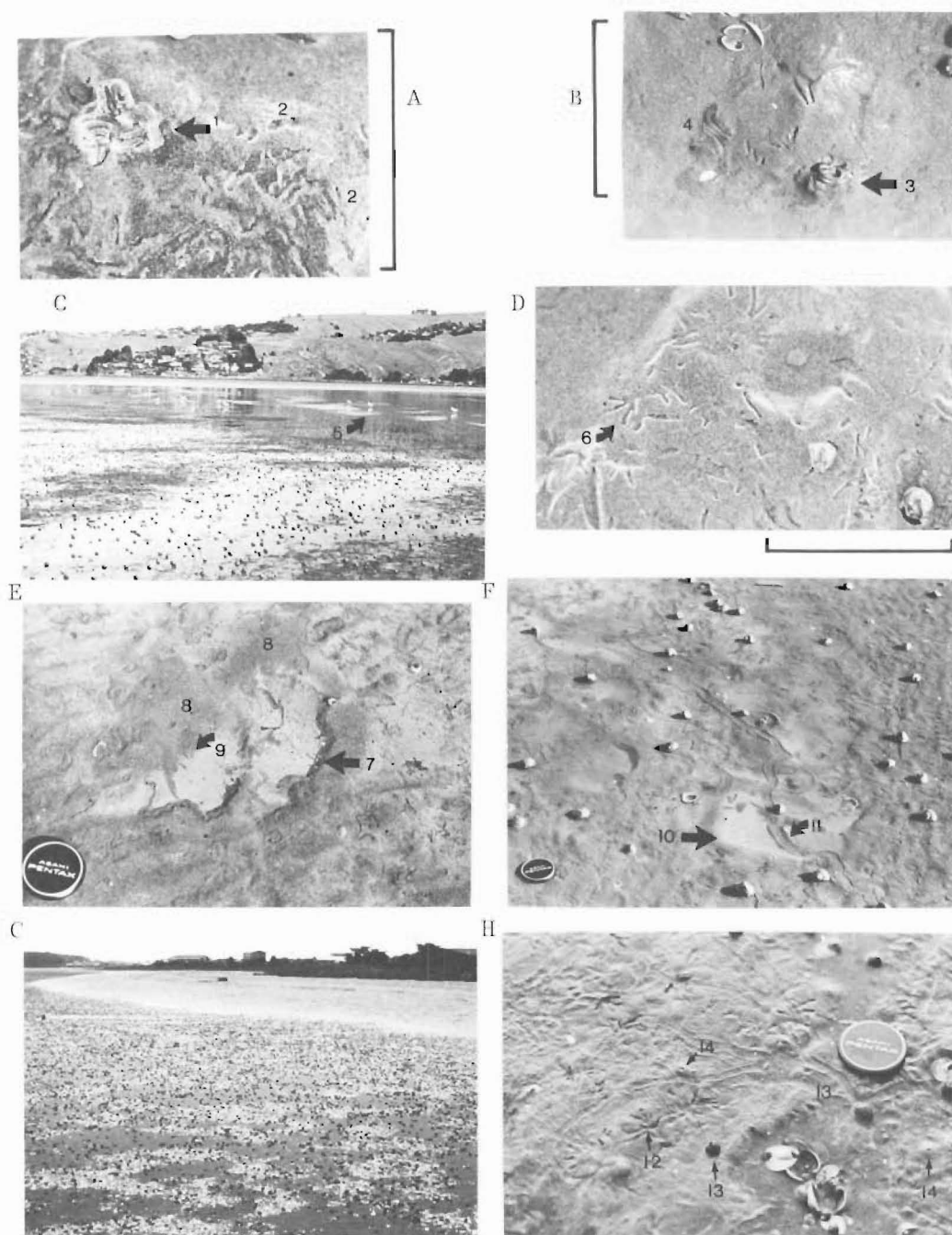
Figure 66. Surface evidence of sediment-modifying biological activity in the Avon-Heathcote Estuary. A - Egestion cast of the lugworm *Abarenicola affinis affinis* (1) and feeding traces of the bivalve *Macomona liliana* (2), southern flats 50m off the causeway. Scale is 10cm. B - Egestion casts (3, 4) of *Abarenicola*, and *Macomona* feeding traces, high tide flats near the east end of line 8, Map 1. Scale is 10cm. C - Gulls feeding near the west end of line 9, Map 1. Gulls agitate surface sediment (5) by briskly raising and lowering their feet - eating soft-bodied animals brought to the surface, and making a distinctive pattering sound. Notice the large areas of reflective standing water, and the abundant *Amphibola*. D - Characteristic birds-foot shaped feeding trace of Macomona (6). E - Hollows made by a gull from the group in C, above (7 indicates right foot mark, the bird faced away from the observer). Note lighter coloured mud on the floor of the depression, the area of coarser agitated sediment in front (8), and polychaete tubes exposed in the sides of the hollows (9). F - Larger area of gull-agitated sediment, showing fluid-mud filled depressions (10), and an *Amphibola* trail (11). Lense cap diameter 5cm. G - Dense population of Amphibola on high tide slopes (9.5 to 10.0m HAD) near the east end of line 10. H - Intensely bioturbated sediment just off the east end of the Causeway. Note *Macomona* traces (12), abundant trails of the topshell *Zediloma subrostrata* (13) and egestion casts of an unidentified worm (14).

Estimates of rates of bioturbation by polychaetes are not available for the AHE, but considering the high population densities present here, the turnover time for surface sediment may be significantly less than the 1.4 years discovered by Rhoads in Barnstable Harbour, Mass., U.S.A.

The bivalve *Chione stuchyburyi* - the cockle - is easily the most conspicuous member of the macrofauna of the AHE (Voller, 1973; Knox and Kilner, 1973), with recorded densities as high as 2 500/m^2 on some lower intertidal flats. *C. stuchyburyi* is a filter feeder, capable of filtering water at rates of 0.5 L/h for 12 h/day, and one individual may fix up to 44 g of suspended matter (dry weight) in one year (Knox and Kilner, 1973, p. 188). Cockles burrow to depths of 2-4 cm, and when present in high concentrations, may constitute from 30-40% by volume of the upper few centimetres of sediment (Figure 18). The major significance of cockles in sedimentary terms is their filtering activity, since they package suspended material into large aggregate grains, which may be transported as sand sized material, or be buried beneath the sediment surface (Haven and Morales Alamo, 1966; Myers, 1977).

The wedge shell *Macomona liliana* is common on clean sandy midtide slopes and flats in this estuary, where it lives at depths of 15 to 25 cm beneath the sediment surface. It feeds through an inhalant siphon which it extends to the surface and uses to suck sediment from an area of about 10 cm^2, leaving a distinctive, radiating, birds-foot like feeding trace (Figure 66A, B and H).

Other bivalves are relatively rare; the green mussel *Perna canaliculus* occurs in an area of about 50 × 200 m on the north side of the principal subtidal channel opposite Beachville Road, and the pipi *Amphidesma australe australe* is also found in small numbers (Knox and Kilner, 1973).

Six groups of gastropods occur in the AHE (Voller, 1973), but only two appear to be significant sediment modifiers. The large mudflat snail *Amphibola crenata* is widespread (Figure 66G, for example). *Amphibola* feed when the tide is out by passing material from a centimetre-wide, less than millimetre-deep strip of the surface through its gut, and extruding it as a continuous fecal string (see Figures 65 and 66). The long fecal strings are readily broken into shorter lengths, and the resulting millimetre-scale equant aggregate grains accumulate in shallow depressions and between ripples on the intertidal flats.

This writer has observed that where *A. crenata* is present in large numbers, up to 80% of the sediment surface may be ingested and packaged into fecal strings over a period of 3 to 4 low tides. On windy days waves sweep accumulated fecal particles from the intertidal flats, and they are preumably lost from the estuary. Thus although *A. crenata* reworks sediment by ingestion and surface displacement, its principal role in the sedimentology of the AHE is as a packager of surface sediment into readily transported, coarse aggregate grains.

The small topshell *Zediloma subrostrata* is less widely distributed than *A. crenata*, but appears to modify sediment in a similar way (Figure 66H). Other species, including the scavaging carnivore *Cominella glandiformis* (often seen converging in scores on dead animals) are apparently insignificant bioturbators.

(iii) Crabs are ubiquitous in the AHE. There are four major species: the small fleet-footed *Helice crassa*, the lower mudflat crab *Macrophthalmus hirtipes*, *Hemigrapsus crenulatus* (which Jones, 1976, found to be most abundant overall), and *Cyclograpsus lavauxi*. The two burrowers, *H. crassa* and *M. hirtipes*, are major bioturbators throughout the estuary. They both occupy permanent burrows, which may be 10-15 cm deep and up to 5 cm in diameter. During the excavation and maintenance of burrows, an apron of sediment is usually built up around the entrance (Figure 65D, E and F). Where burrows are abundant (some *H. crassa* 'colonies' contain 4-5 burrows/m²) up to 20% of the surface sediment may consist of excavation aprons, which in some cases may contain as much as 250 cm³ of unconsolidated sediment.

(iv) A burrowing Amphipod *(Paracorophium)* was found by Voller (1973) in large numbers in the north of the estuary, and a burrowing anemone *(Edwardsia leucomelos)* is common on the lower flats and slopes near the estuary inlet (Knox and Kilner, 1973). Both of these animals seem to be relatively insignificant bioturbators.

Gulls are capable of modifying large areas of surface sediment during feeding activities (Figure 66C, E and F), groups of several dozen birds are usually involved, and the result is the production of large areas of slightly hummocky agitated sediment, with feet-shaped centimetre-deep depressions or parallel tracks, floored with a layer of fluid mud. The gulls choose clean sand, in areas where a few millimetres of water remains at low tide, and in such areas surface sediment is extensively reworked to a depth of 0.5 to 1.5 cm.

These features are similar to the resting traces recorded by Hertweck (1970).

Only three plant species occur in significant numbers in the AHE. A dense zone of the eelgrass *Zostera nana* occurs in the centre of the estuary (see Knox and Kilner, 1973, p. 24; and vertical air photographs in supplementary material filed in the Department of Geology library, University of Canterbury). *Zostera* mats tend to accumulate fine sediment, and may raise the sediment level up to 10 cm above the surrounding bottom. *Zostera* was widespread prior to 1930 in the AHE, but almost completely disappeared in the 1930's (J.A. Robb, pers. comm.). Historical fluctuations in the amount of *Zostera* covering the bottom of this estuary are likely to have influenced the long-term trend discussed in Part One (and summarised in Figure 4), but the significance of this influence cannot be evaluated.

Two species of sea lettuce *(Ulva lactuca* and *Enteromorpha)* are common in the estuary, but have a negligible effect of sedimentation. The introduced cordgrass *Spartina x townsendii* (Knox and Kilner, 1973, p. 177) also occurs. *Spartina* grows as stout, erect clumps which spread laterally from horizontal rhizomes, and may cause vertical accretion of sediment at rates of up to 3.0 cm/year (Knox and Kilner, 1973, p. 179). In the AHE *Spartina* is controlled by spraying, and has so far been prevented from spreading beyond a few small colonies.

2. *Sediment analyses.* Work on bioturbation in shallow marine environments has tended to concentrate on the activities of particular animals or groups of animals, on the structures and traces left by animals, or on the vertical and horizontal distribution of animals and animal assemblages (for examples see Rhoads, 1967; Hertweck, 1970; Howard and Frey, 1972; and especially Myers, 1977). In this project it was felt that there was more to be gained by concentrating on an understanding of the physical results of bioturbation. In particular, attention was concentrated on relationships between the bioturbate zone and the uppermost active layer, and the role of bioturbation in the transportation of sediment into and out of the subsurface zone.

As a preliminary experiment, some of the granulometric properties of sand from near surface and surface (active layer) samples were compared. Figure 67 shows a plot of mean size vs sorting for 16 such pairs. In most cases core samples are of the uppermost 5 to 10 cm of sediment, although some included the upper 20-25 cm (for example;
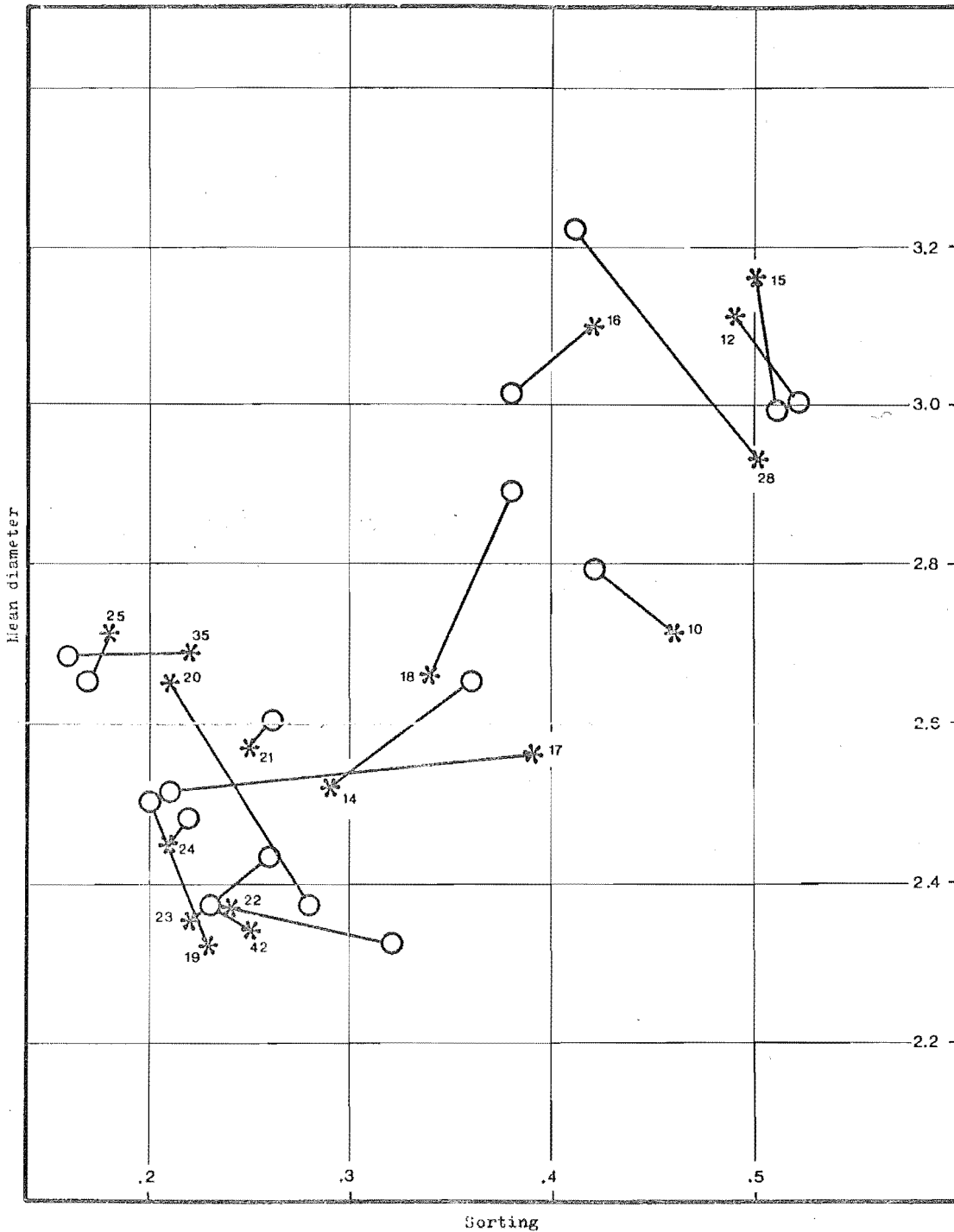
Figure 67   Scatter plot showing 17 pairs of surface sediment (active layer) samples (O) and adjacent uppermost core samples (✻) from the Avon-Heathcote Estuary. Adjacent pairs are linked.

core 18 in Appendix 4). It is clear from Figure 67 that there are significant differences between active layer and subsurface sand properties, and that these differences are apparently not systematic. This is an important discovery, because it justifies the sampling approach adopted for this project – surface sediment is more likely to reflect contemporary environmental conditions than is subsurface sediment.

To examine relationships between surface and near surface sediment, a series of samples was collected in the Heathcote Basin. The sample run began at the permanent concrete marker about 80 m east of the riprap seawall at the western end of line 12, and a surface sample (usually of the upper 1-2 mm of sediment, collected as outlined in Appendix 4) and a 5 cm-deep core were collected at CDB pegs at 100 m intervals for 1 000 m east along line 12. Deeper cores were also collected at several of these sites (core series 2-9; cores 32 and 43). Figure 68 shows the bathymetry of the western end of line 12, and the locations of all core and surface samples. All of the samples were analysed using the standard techniques previously described.

Figures 69, 70 and 71 show some of the properties of the surface and 5 cm core sample pairs. Examination of these figures reveals that some sample pairs have very similar cumulative probability curves (for example 649 and 650 in Figure 69), while others are quite dissimilar (631 and 632). In some pairs the surface samples are uniformly coarser (647-648), or uniformly finer (645-646). Other pairs have similar coarse tails, but dissimilar fine tails (629-630, 631-632). Notice that there is a fine-coarse-fine trend from left to right in Figure 69, which is apparently related to HAD. The relationships shown in Figure 69 support the conclusions drawn from Figure 67 – that surface and subsurface sediment properties are not systematically related in this estuary.

Figures 70 and 71 show some of the summary properties of the sample pairs, plotted against sample HAD. Figure 70A shows that mean grain size is uniform and independent of depth above 9.0 m, and becomes finer with increasing depth below 9.0 m. This figure emphasises the broadly similar nature of the sand fraction properties of the sample pairs, shown by the left to right trend in Figure 69. This trend is clearly related to water depth, and is probably a wave energy response, as demonstrated in Part Four. However Figure 70B shows that the mud content of the two sample types is dissimilar. Above 9.0 m sediment
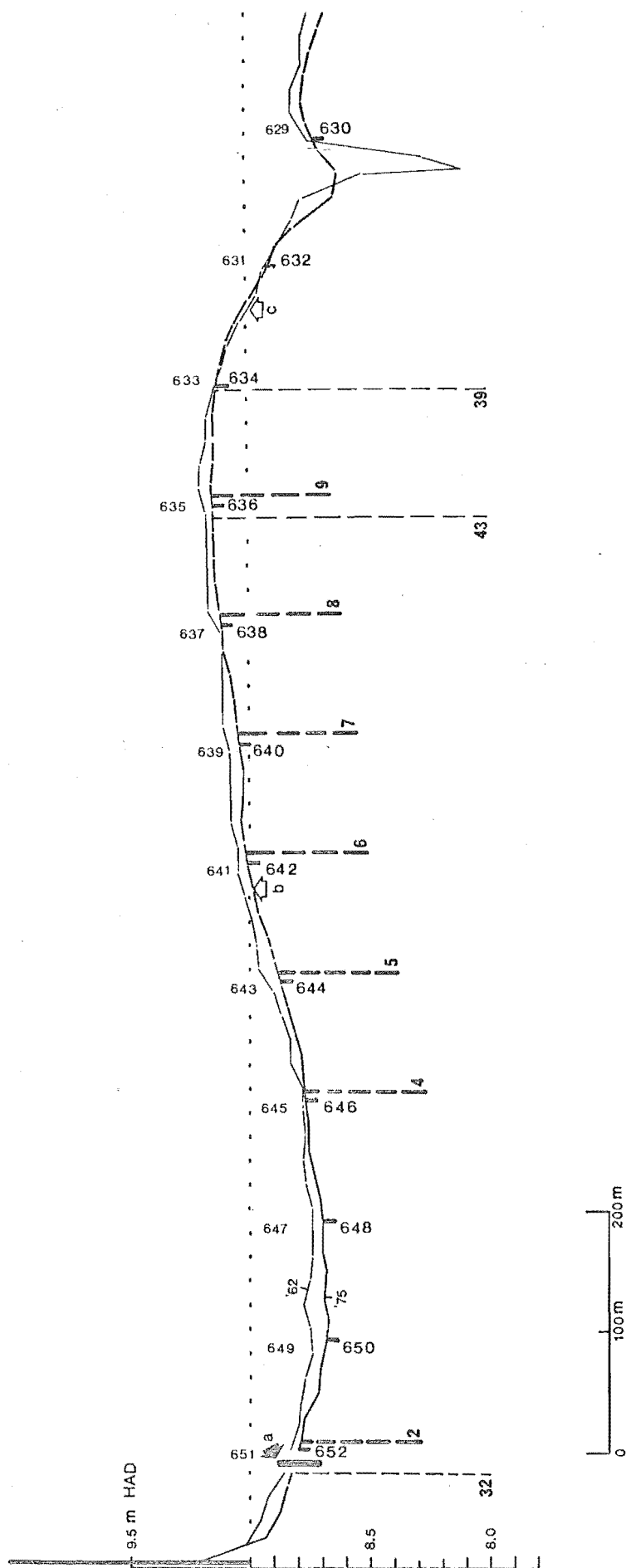
Figure 68. The western end of line 12, in the Heathcote Basin, showing the bathymetry in 1962 (thin line) and 1976 (thicker line), with the 9.0m HAD level (dashed line) and the section above 9.0m (b-c) shown for reference. Plotted on this profile are the permanent concrete marker at the end of line 12 (a), surface (odd numbers) and sub-surface (even numbers) 5cm deep core sediment samples, the locations of shallow cores 2-9 (thick dashed lines) and 3 deeper cores (thin dashed lines).
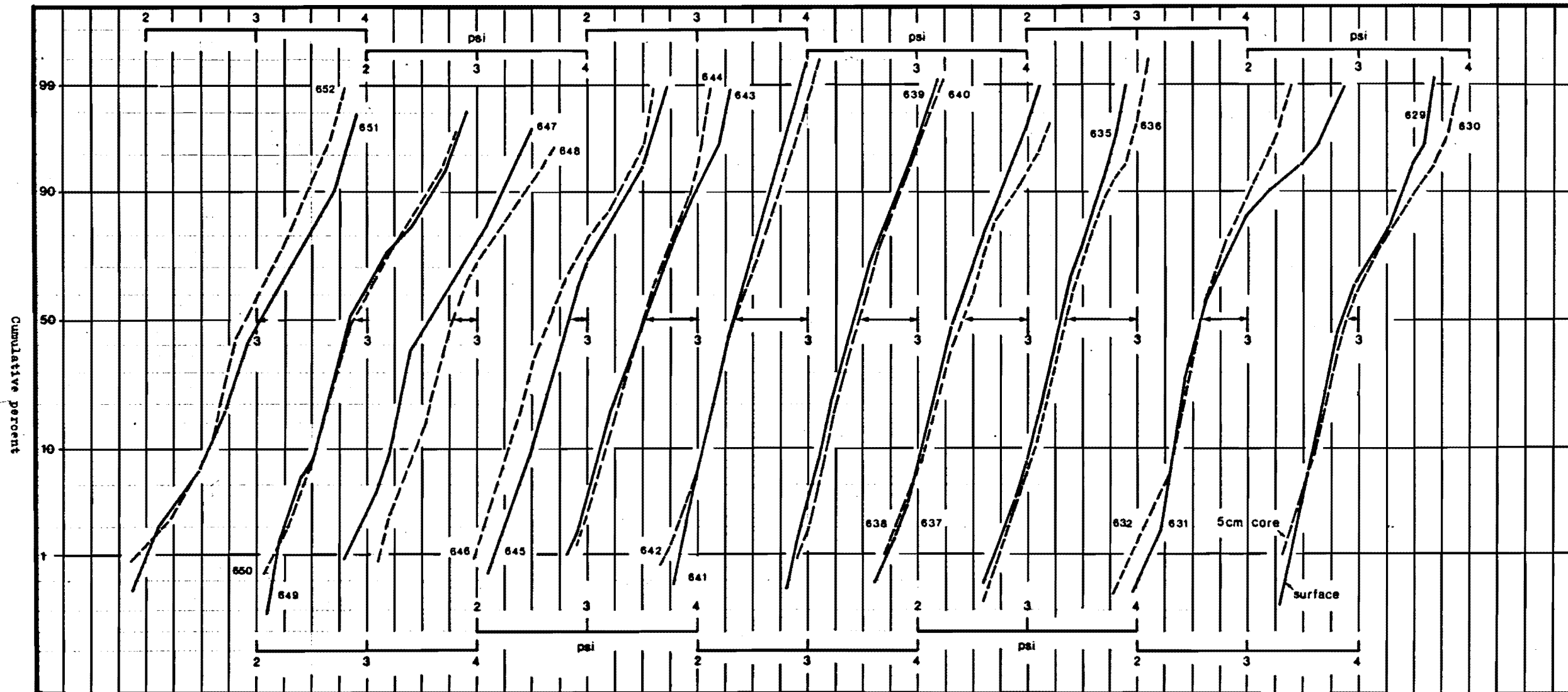
Figure 69. Sand fraction cumulative probability curves of surface and 5cm core samples collected at stations shown in Figure 66. Each pair is plotted on common axes, shown by reference to the point 3.0psi/50%.
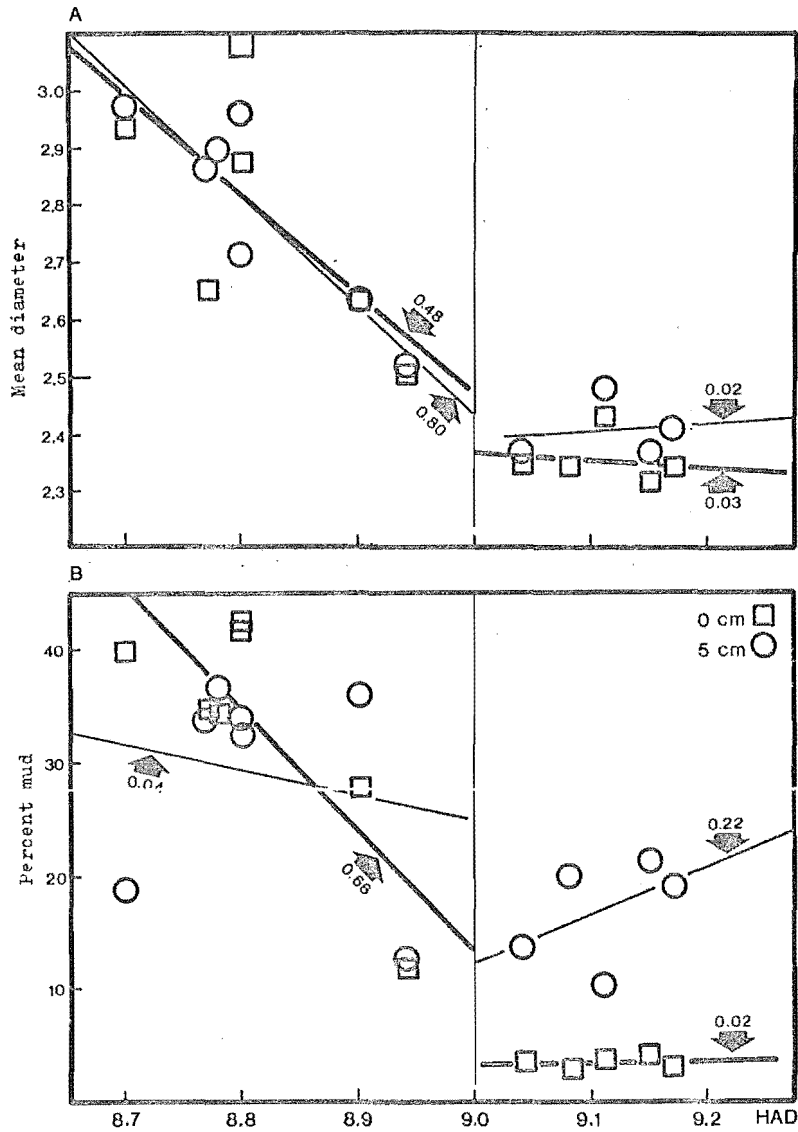
Figure 70 . Plots of sediment muddiness and graphic mean diameter of surface and 5cm core sample pairs from line 12. A - Mean diameter vs height above datum, with regression lines fitted to surface sample data (thick lines) and core sample data (thin lines), from above and below 9.0m HAD. Numbers adjacent to lines are coefficients of determination. B - Similar plot for percent mud vs HAD.
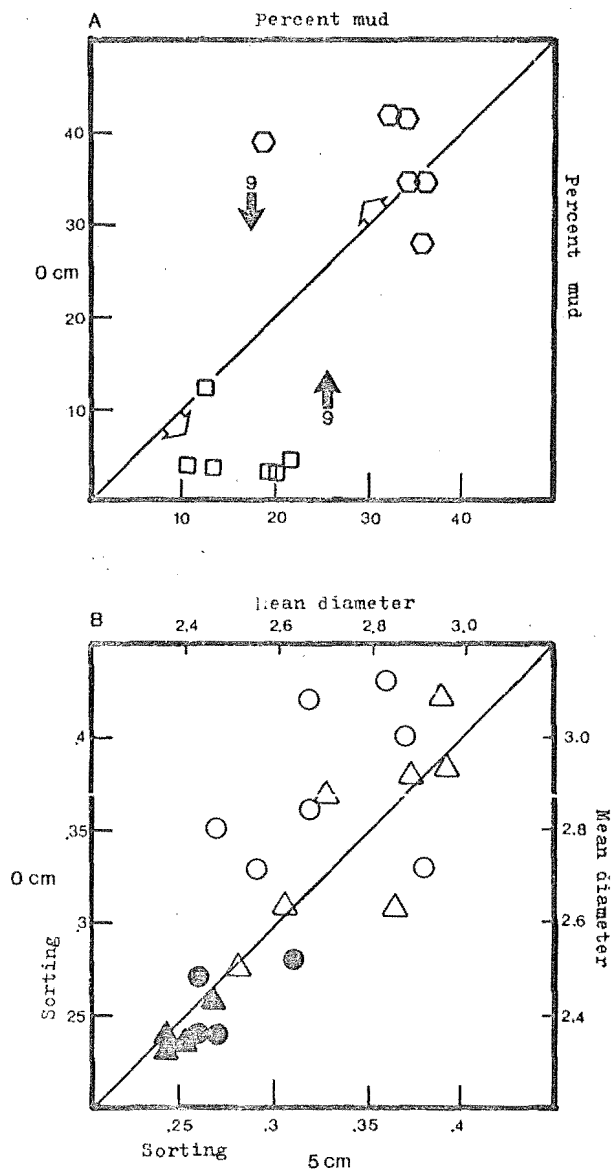
Figure 71 Scatter plots, surface sample and 5cm core sample pairs, from line 12.
A - Percent mud vs percent mud, with samples grouped into those from above 9.0m (□),
and those from below (○).   B - Mean diameter vs mean diameter (△) and graphic
standard deviation vs ·standard deviation (○) plots. Black symbols indicate samples
from above 9.0m HAD.

Figure 72. Shallow cores 2-9 from line 12 in the Heathcote Basin (see Figure 66 for locations), showing the bioturbation interface (......) and bioturbate sediment (1), massive sand and muddy sand (2), well laminated sand and moderately to weakly laminated sand and mud ((4) of subsurface unit (b). Vertical bars represent sample locations. Left vertical scale is HAD of the sediment surface, right scale refers to cores.

135
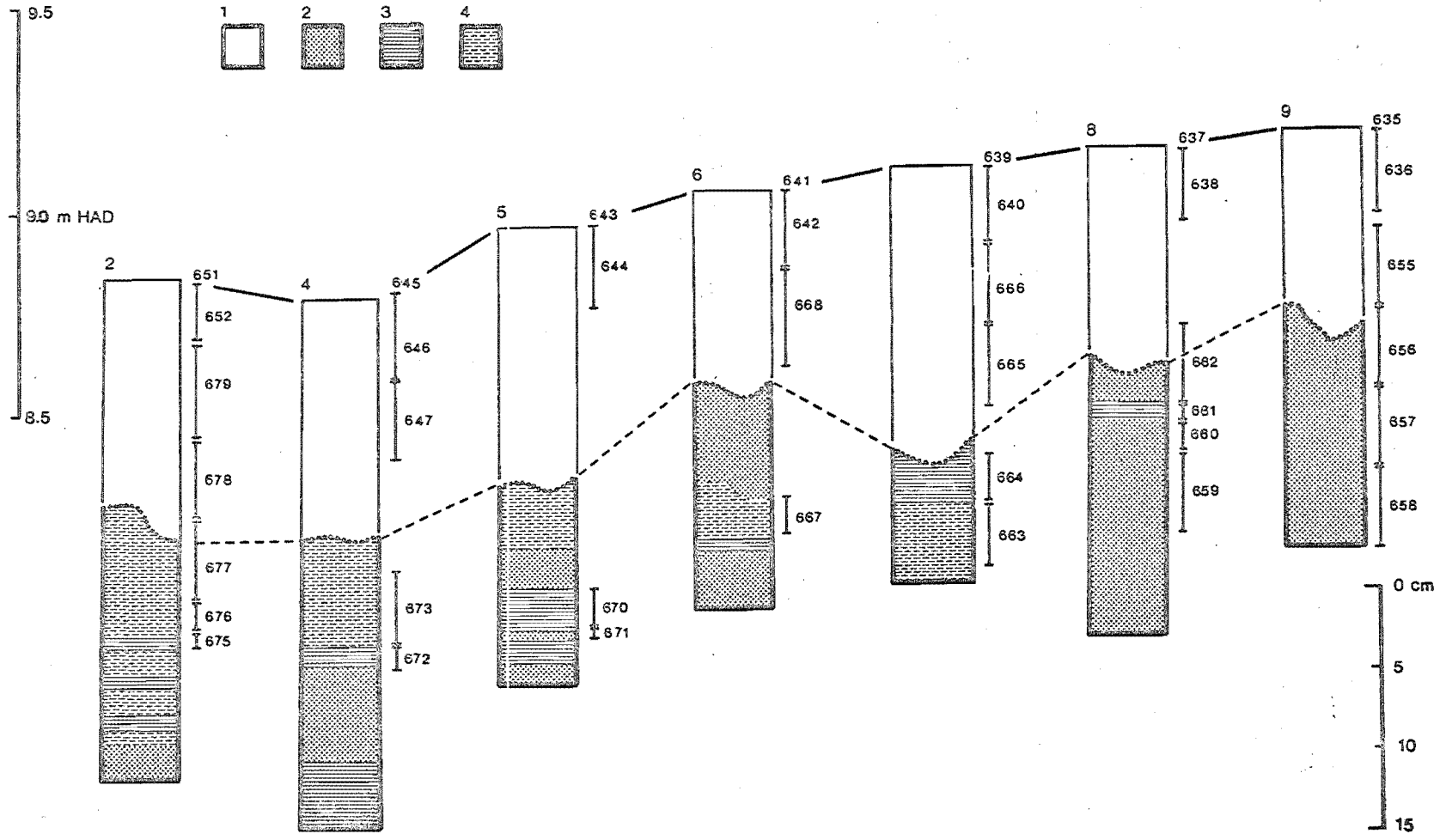
from core samples is an order of magnitude muddier than surface
sediment, and muddiness values fluctuate much more in subsurface than
in surface samples. Below the MTL, there is effectively no relationship
between water depth and muddiness of 5 cm core samples, but surface
samples do show a tendency to be muddier in deeper water.

Illustrated in Figure 72 are a series of deeper cores from
line 12 (see Figure 68 for locations) with a simplified sediment
classification modified from logs in Appendix 4. In each of the cores
in Figure 72 the base of the bioturbate zone (the bioturbation
interface) was clearly recognisable, usually about 15 cm below the
surface, and beneath the interface, plane laminated and massive unit (b)
sediment occurred.

Figures 73 and 74 illustrate cumulative curves of sand from the
samples shown in Figure 72, with samples from below the bioturbation
interface shaded for easy identification. These two figures show that
sediment from below the interface is consistently finer than sediment
from above (for example see core 2). Cumulative curves from below the
interface are commonly bilinear or multilinear, with a major inflection
at about 3.0 psi. However, curves of samples from above the interface
are commonly almost straight, and do not contain as much very fine sand.
Some curves appear to be intermediate between subinterface and near
surface curves (for example 665 in core 7, 674 in core 4), indicating
that some bioturbate sediment has properties that are intermediate
between those of the parent material – the undisturbed sediment from
below the interface – and active or subactive surface sediment.

3. Conclusions and discussion. In the AHE an active layer
occurs as a thin skin on top of a subsurface bioturbate zone. This
active layer has physical properties that reflect contemporary physical
processes, and which may be significantly different from the properties
of immediately underlying bioturbate sediment, and markedly different
from the undisturbed ancient sediment below the bioturbation interface.

Predictable gradients in sediment properties were not observed
within the bioturbate zone beneath the active layer. Sediment from
above the bioturbation interface consists of a homogeneous mixture of
constituents reworked from below, and constituents supplied from above
by contemporary physical and biological processes. The mixed,
bioturbate zone is depleted of suspendible fines (very fine sand and
mud), and enriched in a coarse lag of polygenetic sand with

Figure 73. Cumulative probability curves of samples from cores 2, 4, and 5-6.
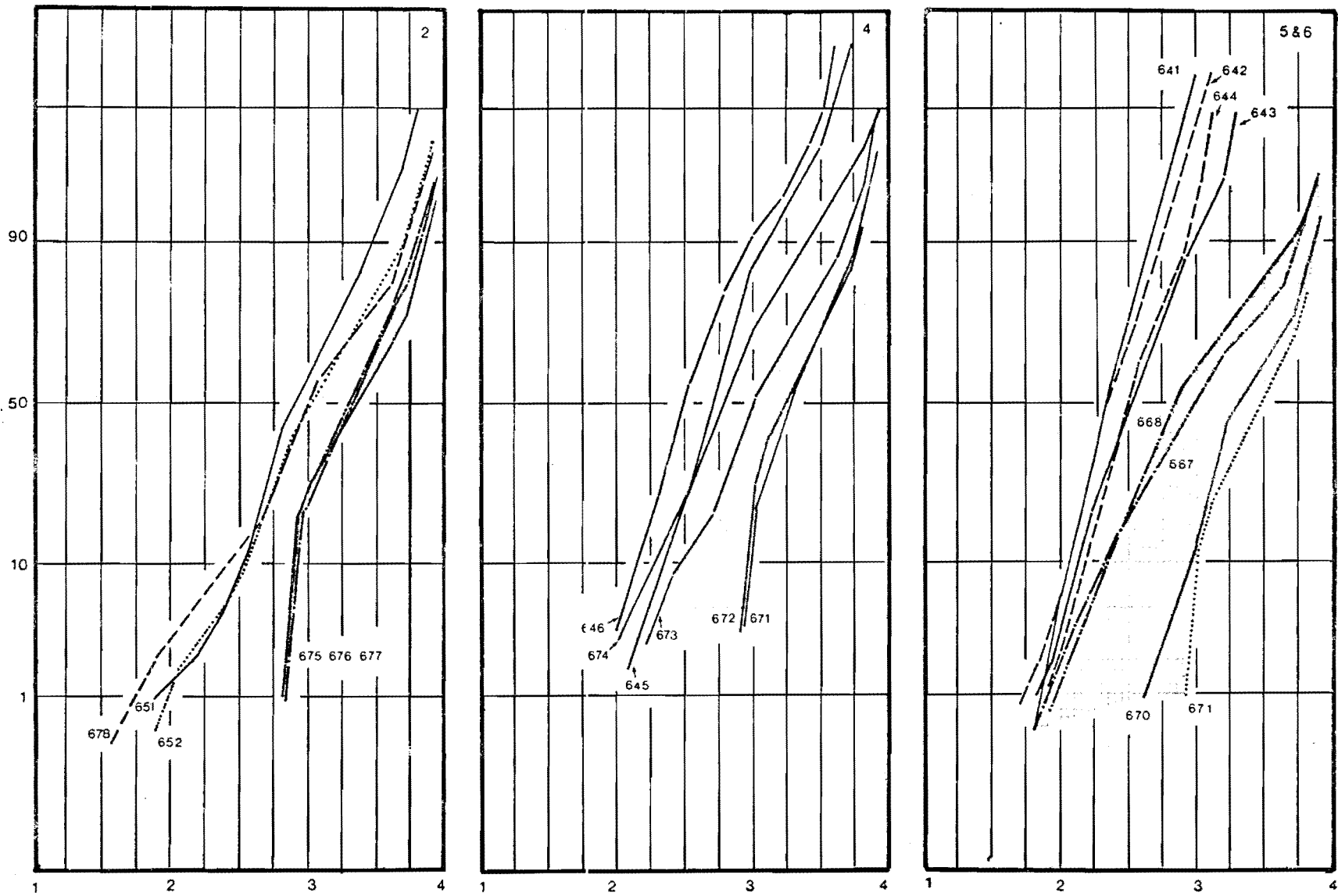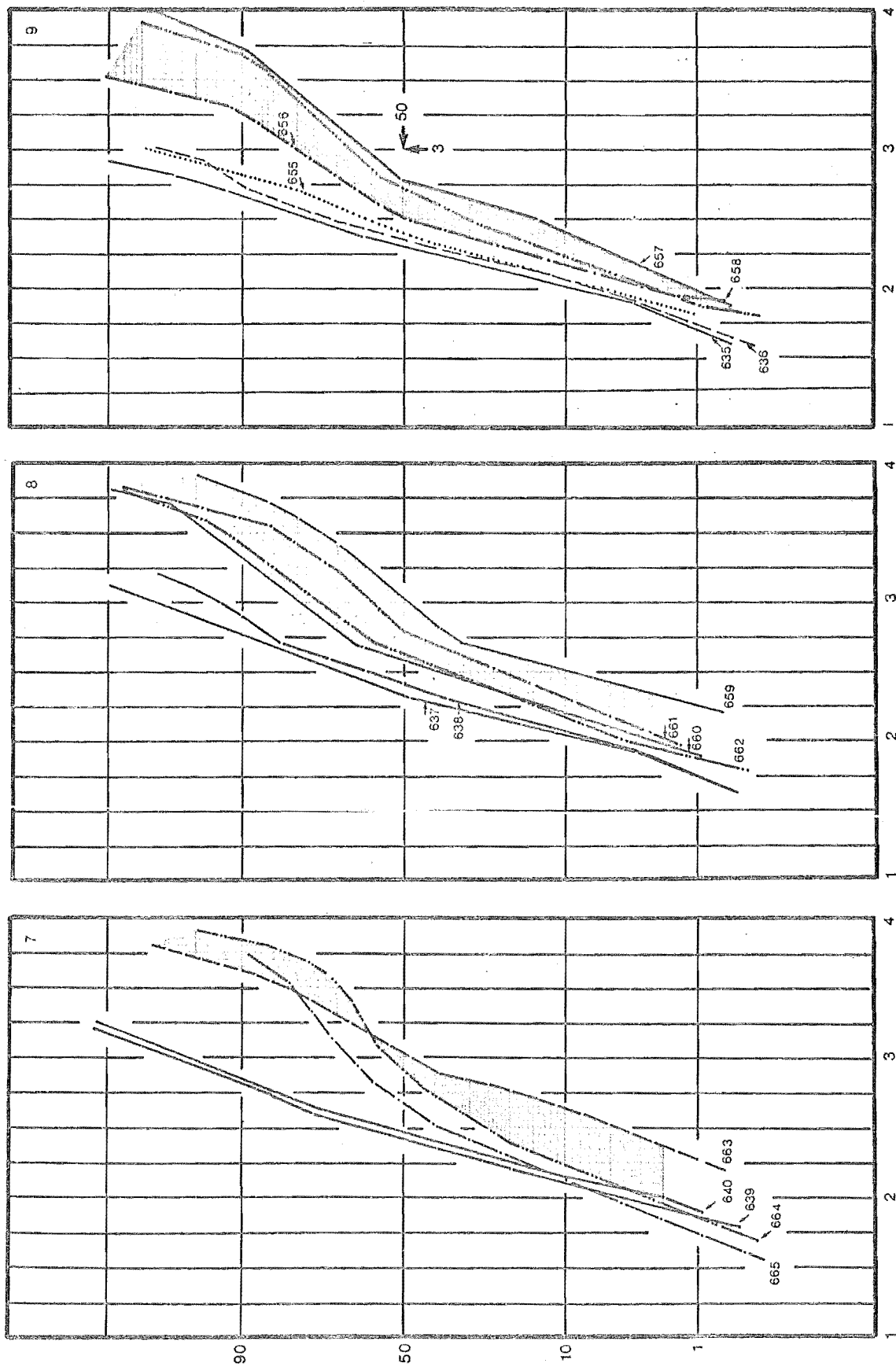
Figure 74. Cumulative probability curves of samples from cores 7, 8 and 9.

granulometric properties unrelated to any one set of physical
sedimentary processes.

The AHE is experiencing ongoing net erosion, and the sediment-
water interface is continually deepening. As a result the inhabitants
of the bioturbate zone are effectively "eating" their way downwards
into progressively older sediment, which is mixed into the bioturbate
zone (and the fine suspendible fraction is added to the water column)
at a rate equivalent to the rate of lowering of the sediment-water
interface. The rate at which a net loss of sediment occurs at a
particular location will be influenced both by the rate of reworking
(which will be related to the population densities and the species of
animals involved in bioturbation) and by the muddiness of both the
bioturbate zone and the older, undisturbed sediment beneath. If
subsurface sediment is very muddy, then a large proportion of the
material reworked on to the surface may be permanently removed. For
example the removal of all the mud from a 15 cm thick zone of 50% mud
may result in about 7-8 cm of lowering of the sediment-water interface,
all other things being equal.

It was demonstrated in Part Four that both surface mud
depositories and active surface sand have properties which are
independent of patterns of long-term erosion and deposition. This
apparent paradox is resolved if burrowing crabs, assisted by
polychaetes, bivalves and gulls, are the principal agents of sediment
erosion. If crabs excavate muddy sediment on to an equilibrium sandy
surface, then mud and sand finer than the equilibrium size will be
readily removed by tidal currents or wave activity, and over a period
of time the result will be a net loss, effectively by removing sediment
from below the surface, rather than eroding it from the top. If sandy
sediment is excavated on to a muddy surface, there will be a similar
net loss, as fines are winnowed from the hydrodynamically rough deposit.
Surface sediment will be enriched in the coarser material which remains.
As Figures 65 and 66 demonstrate, both of these processes do occur, and
one result is that a net removal of sediment proceeds without
significantly altering those surface properties that are in short-term
equilibrium with surface processes.

A repercussion of the processes outlined above is that where
subsurface sediment is very fine grained, as in the AHE (where units (b)
or (c) are usually within 15 cm of the surface), crab burrowing may be a
major supplier of mud to the modern environment. In this estuary,

subsurface mud is predominantly either pre-European or immediately post-European in origin; thus it is essentially pre-industrial 'virgin' mud, and it may be quite different from mud supplied present day, which may have properties that reflect an industrial environment. If a large amount of the mud supplied to the estuary at present is contributed by crab burrowing, it may significantly dilute modern material from external sources.

Clay mineralogy

Many estuaries show regional variations in the clay mineralogy of both suspended and deposited sediment. This may be because clay properties change as the salinity of estuarine water increases seaward, it may be because of differential deposition (through physico-chemical flocculation) as salinity increases, it may be because of a size segregation analogous to selective sorting (finer grains travel further), or it may be because seaward clays have a different (usually offshore) source than land derived, upper estuary clays (for examples see Edzvald and O'Melia, 1975; Gibbs, 1977; Meza and Paola, 1977; and Meade, 1972).

As an exploratory test to determine whether clay mineralogy showed systematic variations in either stratigraphy or location within the AHE, some 80 core samples, plus a few surface samples, were analysed for clay mineralogy.

1. *Methods.* Samples to be analysed were routinely wet sieved and the mud fraction made up to 1L. After removal of a 20 ml aliquot to determine per cent mud, the 1L suspensions were re-stirred and allowed to stand for 2 h, when a further 50 ml aliquot was taken from a depth of 10 cm, providing a sample of the finer than 8 phi size class (finer than about 4 microns). This aliquot was oven dried at $60-70^{O}C$, powdered, made into a paste with distilled water, spread thinly on a glass slide, and allowed to dry at room temperature. Slides were X-rayed from 4 to 16° 2θ with CuKα radiation, some were reX-rayed after addition of a few drops of a mixture of 9 parts ethyl alcohol and 1 part glycerol – a technique equivalent to glycolation, but more efficient (D. , McConchie, pers. comm.). A few samples were subsequently baked at $550^{O}C$ for 1 h and reX-rayed, and some glyceroled (unbaked) samples were scanned slowly (at $0.25^{O}2\theta$/minute) with narrow beam radiation over the 3.5 to 3.6$\overset{O}{A}$ kaolinite/chlorite doublet.

2. Results.

(i)   All non-glyceroled samples produced strong, sharp X-ray diffraction maxima (peaks) at 14Å, 10Å and 7Å.

(ii) A few glyceroled samples produced small, broad peaks at about 17Å, otherwise glyceroled and unglyceroled traces were identical.

(iii) The 7Å peak completely disappeared from all samples treated by baking.

(iv) Slow scanning across the 3.5 to 3.6Å area of a number of traces indicated that only one peak was present – at about 3.54Å.

These results are interpreted to mean that all analysed samples contained the non-expanding clays chlorite (with an (001) peak at 14Å, an (002) peak at 7Å, and an (004) peak at 3.5Å) and 10Å illite. Some samples contained traces of an expanding clay, probably montmorillonite, which produced the peak at 17Å (Grim, 1953; Johns and others, 1954; Martin and others, 1961; Biscaye, 1964, 1965). The absence of kaolinite was confirmed by the destruction of the 7Å kaolinite/chlorite peak on heating, the lack of a kaolinite peak in the 3.5Å area, where slow scanning will differentiate between kaolinite at 3.58Å and chlorite at 3.54Å (Biscaye, 1964), and the constant ratio between the 7Å and 14Å peak heights (Figure 77). All samples contained clay sized quartz and feldspar particles.

Following the methods outlined by Griffin (in Carver, 1971, pp. 541-571), semi-quantitative estimates of clay contents of samples were made by multiplying peak heights by Biscaye's (1964) weighting factors, such that

$$17\text{Å glyceroled peak height} = \text{montmorillonite \%}$$
$$4 \times \text{height of 10Å peak} = \text{illite \%}$$
$$2 \times \text{height of 7Å peak} = \text{chlorite \%}$$

Figure 77B indicates that 10Å illite and 7Å chlorite were present in constant proportions in almost all samples, and from the weighting factors above, the proportions are 60% illite, 40% chlorite, ± a trace of montmorillonite.

3. Conclusions. Figure 77 shows that the clay mineralogy of all analysed samples was remarkably uniform – consisting of a
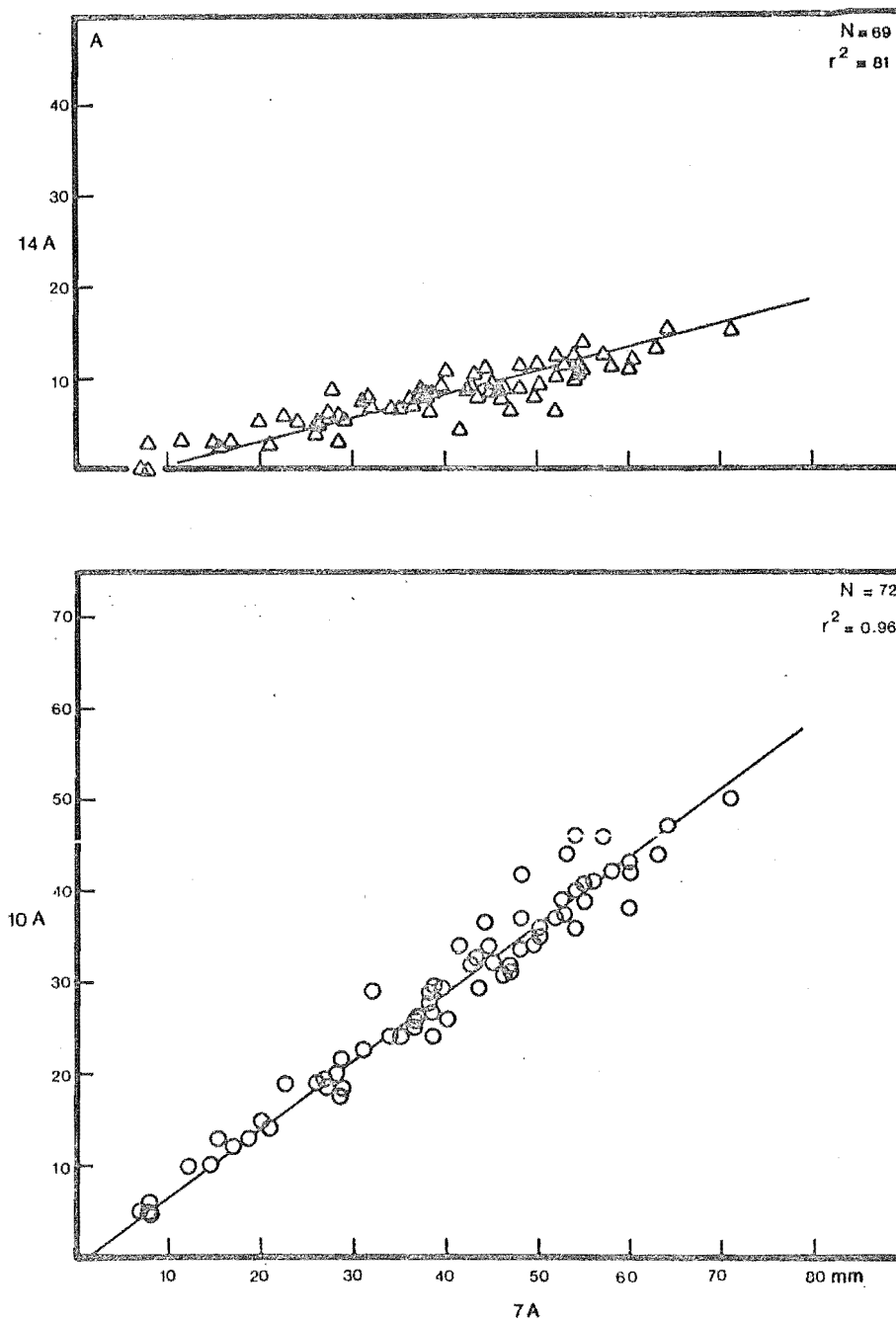
Figure 77. A — 14Å peak heights vs 7Å peak heights (in millimetres) from Xray analyses of subsurface sediment samples from the Avon-Heathcote Estuary. B — 10Å peak heights vs 7Å peak heights from the same analyses.

simple illite-chlorite ± montmorillonite assemblage, with no detected
stratigraphic or locational preferences. Samples were representative
of all stratigraphic units, and included uppermost bioturbate zone
samples from all major bathyforms. From these observations it is
concluded that clay mineralogy is of no interpretive stratigraphic or
sedimentological value in this estuary, and cannot be used to identify
sources of fine material, or to classify synchronous stratigraphic
events.

Presumably this result reflects the geology of the Christchurch
area, which consists predominantly of sands and silts deposited in
post-glacial time under shallow marine conditions. Non-marine material
(from Banks Peninsula volcanics and loess) is presumably a minor
constituent in the estuary, or perhaps only contributes small amounts
of clay minerals - loess from the northern flanks of Banks Peninsula
usually has less than 10% clay sized material, of which less than 50%
is clay minerals (McConchie, pers. comm., 1977), and thus has little
influence on the clay mineralogy of the estuary.

Sand fraction mineralogy

Reed (1951) and Harrison (1976) have both examined sandy sediment
from the AHE. Reed's samples were collected during the HMNZS Lachlan
survey in 1950 (see Part One and Appendix 1 of this report), from the
entrance area of the estuary (Reed, 1951, p. 130). Harrison's samples
were from subsurface cores collected along the western and north-eastern
edges of the estuary.

The samples analysed by Reed (1951) contained predominantly
subangular sand-sized grains of quartz, feldspar and rock fragments.
Most monocrystalline grains showed undulatory extinction, and some clear
quartz grains were polycrystalline with sutured grain boundaries. The
feldspars - acidic plagioclase and orthoclase - were commonly clouded by
alteration products such as sericite, epidote and chlorite. The
composite (rock) fragments were of sandstone (greywacke) and siltstone.
Plates of green chlorite and biotite were recorded in minor amounts by
Reed. Heavy minerals - including biotite, chlorite, magnetite, ziron
and garnet - comprised less than 0.01% of the finer than 2.0 phi
fractions of seven of his samples.

Harrison (1976) recorded that sand grains in his samples were
mainly subangular, with occasional well rounded grains. Samples

consisted mostly of quartz, feldspar and rock fragments, in the
approximate proportions 50%, 20% and 30%. The samples were classified
as feldspathic litharenites by Harrison. The present writer has
observed that many sand samples from the AHE contain 2 to 3% well
rounded, dark green glauconitic grains, and up to 5% of the coarser
sand grains in many samples are polished, highly rounded, clear quartz
grains.

Reed (1951) considered that the great majority of the sedimentary
material he examined was derived from the foothills of the Southern
Alps, and had been transported to the Pegasus Bay coastline by the
Waimakariri River. The presence of rounded glauconite grains, and
polished, anomalously well rounded quartz grains, suggests that this
Waimakariri material is diluted with small amounts of sediment from
other sources – perhaps by onshore transport of sediment from the
Canterbury Continental Shelf (see the next section, on microfauna).

Microfauna

D.G. Jenkins and K. Swanson, both of the Department of Geology,
University of Canterbury, examined samples representative of all
stratigraphic units for both foraminifera and ostracoda respectively.
Figure 78 is from Swanson (in press, in preparation). Subsamples
analysed by Swanson were 100 g splits of large samples from cores
25(773), 39(860, 40-50 cm), and 40(859, equivalent to 850; and 858,
from 100 to 120 cm). Samples were sieved into four size fractions –
coarser than 80 microns, 80-120, 120-200, finer than 200 – and all
ostracods and forams were hand picked from each fraction.

1. *Results*. A large and diverse ostracod assemblage was
identified from samples representing each of three stratigraphic
units (a) to (c) and from a sample of the bioturbate zone. Samples
contained species previously recorded from the New Zealand Continental
Shelf (by Swanson, in press) and all contained species known to live in
estuarine conditions. In addition, sample 858 contained species which
live in flowing fresh water, and sample 773 contained one specimen
(*Darwinula* sp.) known to live in marsh and swamp conditions. Unit (c),
represented by sample 860, contained only *Callistocythere neoplana*,
which was present in large numbers (102 specimens were picked from 860).
D.G. Jenkins recorded a sparse foram assemblage, including benthic and
planktonic species, some of which were of Tertiary age.
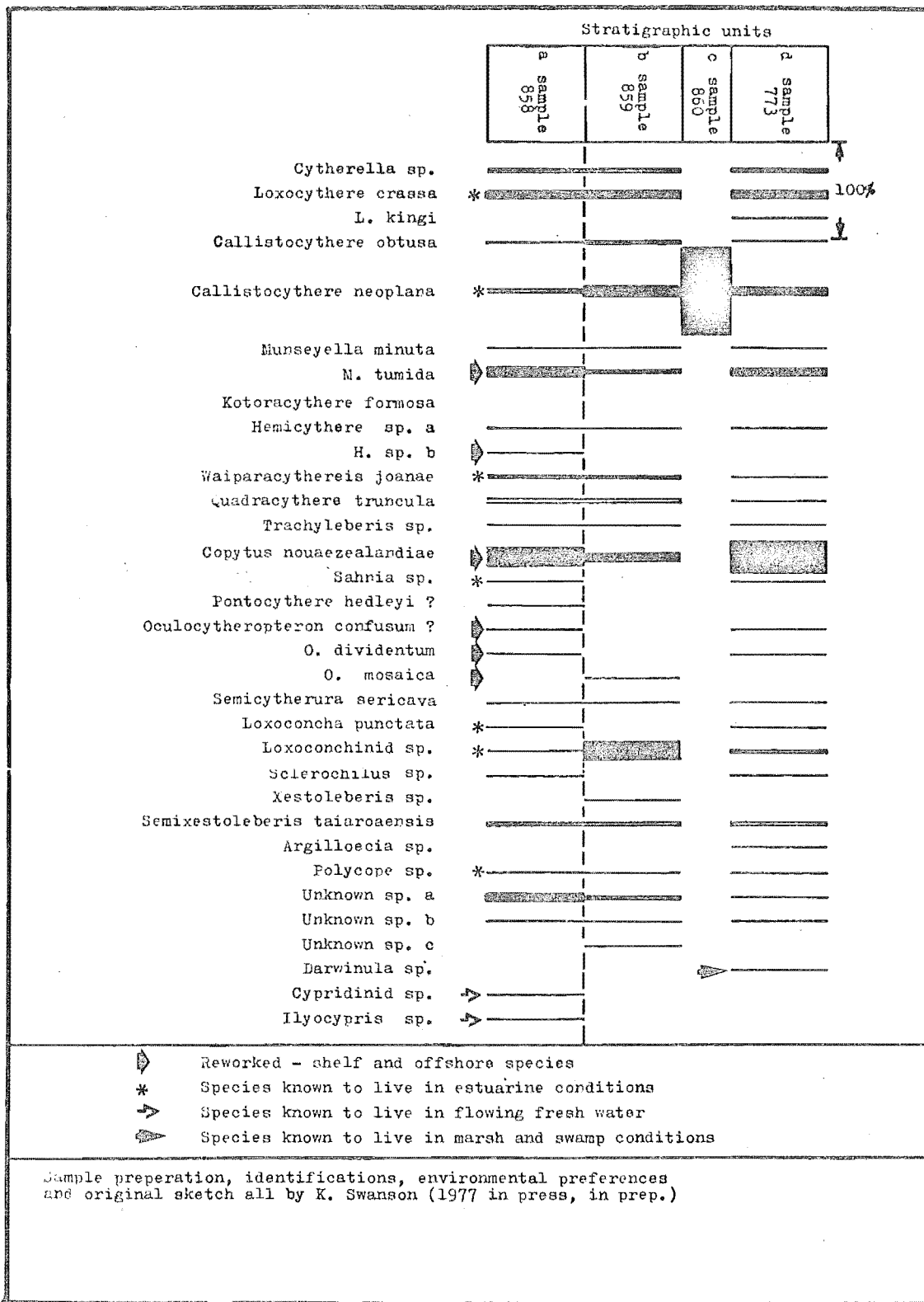
Figure 78. Relative abundances and stratigraphic distribution of Ostracoda in four core samples from the Avon-Heathcote Estuary.

2. *Conclusions.*

(i) Microfauna preserved in historic and prehistoric sediments of the AHE are derived from freshwater, estuarine and oceanic environments; both ancient and modern.

(ii) Some specimens are of Tertiary age, and may be derived from submarine erosion of Tertiary strata exposed on the sea floor of Pegasus Bay (perhaps from Pegasus Canyon, at the outer edge of the Shelf).

(iii) It is reasonable to infer that some sand present in the AHE has been transported onshore from Shelf sources, although it is not possible to judge whether this reflects contemporary processes, or whether onshore sand and microfossil transport accompanied the post-glacial transgression.

It may be that sand deposited during westward transgression of the coastline contained material from offshore sources, and that this material is currently being reworked in the modern estuary. Present day landward transportation of sand is well documented elsewhere (for example Meade, 1972). A continuous net loss of sediment from this estuary does not preclude the contemporaneous addition of sand – Boggs and Jones (1976) have recorded up-estuary sand transport distances of 800 m in one flood tide in a small Oregon estuary, and Schiedegger and Phipps (1976) record that in the Greys Harbour Estuary (Washington, U.S.A.) sand sized marine sediment is transported up to 11 km into the estuary.

(iv) If sample 860 is representative of all olive plastic mud, then Figure 78 indicates that the deposition of this material as a result of post-European flooding of the estuary with mud caused the death of all ostracod groups inhabiting the estuary, except *C. neoplana*, which thrived under those conditions. During the period of time represented by sample 860, ostracod tests from external sources were not deposited in the estuary.

It may not be unreasonable to infer that widespread mass mortality of the benthic community occurred during deposition of unit (c), probably during the years 1850-1880, and that the present community is a recolonisation assemblage.

PART SIX

SUMMARY AND SYNTHESIS

Summary history of the Avon-Heathcote estuary

The AHE is on a coastal plain which consists of Late Quaternary terrestrial and estuarine gravels, sands, peats and mud (Part One; Figure 1). The estuary probably formed between 1 000 and 2 000 yBP. When the first settlers arrived, in 1850, the area which is now Christchurch City was predominantly swamp and marsh, separated from the sea by a belt of dunes. Early urbanisation probably led to a rapid increase in the supply of fine sediment to the estuary, particularly during the period 1850-1875, when little effective drainage work was undertaken but the population grew from a few hundred to more than 10 600 people. The establishment of the Christchurch Drainage Board and a subsequent burst of drainlaying activity meant that by 1900 54 km of sewage and stormwater pipes were laid, and the quality of surface water (and public health) improved as a result. Increasing impervious cover (mainly roofs and roads) and more efficient drainage resulted in increasing volumes of storm runoff, and a reduction in the runoff lag time. In combination with a decreasing availability of erodible material, these effects caused a steep decline in the supply of sediment to the estuary.

Urbanisation and drainage modifications in the catchment of the AHE resulted in an accumulation of sediment, and a decrease in the tidal compartment. Estimates of post-European changes in the volume of the tidal compartment show that during the first 50 years it decreased by about 30% (Part One; Figure 3). However, shortly after the CDB was established, this trend slowed, then reversed, and the tidal compartment has since increased to about 30% more than its 1850 volume. The two trends were probably exponential (Figure 4). The first was due to early urbanisation and increased sediment yields; the second was probably due to a reduced sediment supply and radical changes to the hydraulics of the freshwater catchment of the estuary.

A reconstruction of historical changes that have occurred around the inlet of the estuary since 1850, based on a series of maps made at 20-30 year intervals (Figure 5), shows that these changes occurred in

three phases; from 1850 to about 1925 there was little change; from
1925 to 1955 winter storms precipitated episodic changes which resulted
in a 500 m northwards migration of the seaward section of the principal
subtidal channel, a southwards migration of the landwards section into
Moncks Bay, sympathetic adjustments of the end of Brighton Spit, erosion
of sand from Sumner Beach, and deposition of sand to form a new beach at
Clifton. From 1955 to the present the new configuration has changed
little.

The changes which occurred after 1925 were in-phase with changes
in the tidal compartment, and significant changes only occurred when
the tidal compartment increased above the 1850 (pre-European) volume.
Changes at the outlet and to the volume of the tidal compartment have
since occurred at parallel rates. The inlet has adjusted to the larger
volumes of water flowing through it, and has adopted a different
configuration as a direct result of the exponential response of the
tidal compartment of the estuary to changes in sediment yields and
runoff caused by the development of Christchurch City.

The belief that the AHE has been changed by man's activities is
fully justified. The changes which have occurred have had an
exaggerated effect in this estuary because it is small and microtidal,
and because the freshwater catchment of the estuary is so thoroughly
dominated by the Christchurch urban area. It is clear from Part One
that physical pollution of the sort that has occurred in this estuary
is not irreversible. Generalising from the results summarised above,
the indication is that estuaries are capable of adjusting and
readjusting quickly to changes in local sediment and water budgets.
Altered runoff characteristics may be the major agents of physical
pollution in urban watercourses, and in nearby water bodies.

There have been some highly visible and costly consequences of
the impact of Christchurch City on the AHE - for example the alterations
to the inlet area, and the resulting shore protection work at Sumner and
in Moncks Bay (Scott, 1955). Inevitably, other changes must also have
occurred, especially as a result of large variations in the volume of
the tidal compartment - changes in mean salinity, mean water temperature,
suspended sediment concentrations, wave characteristics, bottom sediment
properties, tidal current velocities, and so on.

A process-response link between changes in the tidal compartment
of an estuary and progressive, systematic changes in the configuration
of the inlet to the estuary has not been previously reported in the

literature. The discovery of such a link may have significant planning and engineering repercussions in areas where inlet changes threaten seaside real estate (as has happened in the Christchurch area - Part One, and as is currently happening in several other coastal areas in New Zealand). If a history of catchment landuse alterations can be reconstructed for an estuary, and especially if historical charts of the inlet are available, reasonably confident predictions of future patterns and rates of change may be possible. For another recent discussion of this subject see Reinson (1977).

Energetics

1. Wind and waves. Major conclusions reached after an analysis of the wind climate of the AHE are that effective wind stress is directionally anisotropic, that the east wind is twice as frequent as the south-west wind and four times as frequent as the north-west wind. Maximum effective fetch distances of about 1 800 m are uniformly distributed along the eastern and southern shores of the estuary, and fetch distances increase from north to south along the north-western shore. Width limitations significantly modify the distribution of effective fetch in the Heathcote Basin (Figures 6 to 10).

Because the estuary is shallow, maximum waves have periods of 1.4 s, amplitudes of 30 cm and lengths of 3.5 m. Waves reach this maximum size quickly and relatively close to the start of each fetch, so that downfetch gradients in wave energy are due to increasing wave frequencies. With increasing fetch distances, more low velocity wind events generate waves large enough to interact with the bottom. Because west winds tend to be higher velocity events, downfetch energy gradients are less well developed in areas subject to longfetch westerlies. East winds tend to be lower velocity events, and are more likely to generate downfetch energy gradients.

The application of small amplitude (Airey) wave theory (Part Two) has shown that maximum near bottom orbital velocities under waves in the AHE vary from 10 cm/s in water 1.5 m deep, to 22 cm/s in water 0.5 m deep. The amplitudes of orbital motions increase from 3 to 5 cm during the translation from 1.5 m deep water to 0.5 m deep water. Since near bottom shear stress is a function of both water depth and bottom roughness, and the presence of ripples significantly increases relative roughness values, there are very large differences between shear

stresses exerted on the bottom in water 1.5 m deep, where roughness
may be very fine sand sized, and in water 0.5 m deep, where ripple sized
roughness may occur. Shear stress values increase from 0.5 dynes/cm^2
to 2.0 dynes/cm^2 to 17 dynes/cm^2 as water in the AHE shoals from 1.5 m
to 1.0 m to 0.5 m below HWOST, and the large increase from 1.0 m to
0.5 m (almost an order of magnitude) is particularly important.

A refraction analysis (Figure 13) indicates that wave directions
are only significantly altered in water shallower than 1.2 m below HWOST
in this estuary (where the bottom is above 9.0 m HAD), and that
refraction acts to homogenise wave properties. However, in the north
and west, and in the Heathcote Basin, the shoaling transformation
reduces wave sizes, and effectively produces wave shadows.

2. *Tidal currents*. A review of current velocities measured in
the AHE indicates that probable maximum values for different water
depths range from 5 to more than 100 cm/s. Near bottom shear stresses,
calculated from the quadratic stress law with an assumed drag
coefficient (c_{100}) of 3×10^{-3}, vary from less than 0.01 dynes/cm^2 in
water shallower than 0.5 m to more than 25 dynes/cm^2 in the deeper
intertidal and subtidal channels. Even though these are probably no
better than order-of-magnitude estimates, they emphasise the surprising
discovery that tidal current shear stress values exceed wave induced
shear stresses only on the lowest intertidal flats and in the subtidal
channels of this estuary. This is true in spite of the large amounts
of kinetic energy contained in the ebbing and flooding tide. These
estimates also emphasise that in this estuary, tidal and wind induced
shear stress maxima are mutually exclusive and that the area of lowest
combined shear stress occurs at intermediate depths, midway between the
high water mark and the subtidal channels (Figure 32).

Current generated bedforms, predominantly lingoid and undulatory
straight ripples, are only found on lower intertidal flats, in the
subtidal channels, and on the flood delta in the AHE. Here tidal
velocities reach maximum values of about 60 cm/s. Larger bedforms –
megaripples and sand waves – only occur in the inlet area adjacent to
the principal subtidal channel, where velocities exceed 80-90 cm/s on
both the ebbing and flooding tides (Figure 19).

Threshold criteria indicate that tidal currents which exceed
60 cm/s are capable of entraining very coarse sand and small granules;
typical lower intertidal currents of 35 cm/s are capable of entraining

very fine sand and silt sized particles.

3. *Wind-driven currents*. The influence of wind entrainment on
large scale, cross-estuary, advection of water and suspended solids, and
on tidal current velocities, is an unexplored effect in this estuary.
Qualitative observations of wind-driven longshore currents and of
flooding due to wind setup indicate that wind forcing almost certainly
significantly modifies net circulation patterns, and influences the
transport routes of inflowing turbid water (Figure 20). If wind setup
significantly deepens water in some areas at high tide, then
contemporaneous waves will also be larger, and near bottom shear stresses
will increase. It is probable that setups and wind driven surges are
more common now than in the past, since the mean depth of the estuary
has increased over at least the past 50 years. Maximum wave sizes will
also have increased as a result of this deepening, and more stress will
be transferred from wind to the water mass during storms. Thus
supratidal flooding may be an increasingly common engineering problem
in the low-lying areas adjacent to the estuary, some of which have only
recently been built on.

Bathymetry

The AHE can be subdivided into a small number of distinctly
different and internally consistent bathyforms (Figure 21). Eastern
high tide slopes are usually low angle convex upwards features which
demonstrate clear responses to wave energy (Figures 23 and 24). Inter-
tidal channels and offshore mounds associated with the eastern high tide
slopes in the south-eastern and central eastern parts of the estuary
tend to align themselves normal to the dominant west wind and to migrate
down-wind in a shorewards direction (Figure 26). Erosion and deposition
of sediment on the eastern slopes tends to conserve their shapes, and
contributes to the trend towards a wave-normal alignment of the
bathymetry. Areas exposed to longest fetch waves exhibit quasi-stable
forms in equilibrium with wave energy, reflecting the pervasive,
macrobathymetric influence of waves in this estuary (Figure 30).

Deeper eastern flats are less well organised by waves, and
their bathymetry is a compromise between wave and tidal current energy.
Western slopes and flats also show an orderly response to wave energy,
trending from relatively high angle concave upwards curvilinear profiles
in the north, towards low angle concave upwards or nearly straight

configurations in the south, as downfetch wave energy (wave frequency) increases. Although it is likely that sediment accumulations on these western slopes are a consequence of the large volumes of effluent released from CDB outfalls, there is no conclusive bathymetric evidence to prove or disprove the possibility (Figures 28 and 29).

Tidal currents, rather than wave energy, control the configurations of the central mounds, larger intertidal channels, and subtidal channels of this estuary.

A comparison of bathymetric data from surveys completed in 1920, 1962, and 1975/77 shows that the intertidal zone of the northern half of the AHE (and probably of the whole estuary) lost up to 1 m of sediment between 1920 and 1962, and that the intertidal flats continued to lose sediment between 1962 and 1975/77, but at slower rates. Since 1962 sediment has accumulated adjacent to the two river entrances, and off the oxidation pond outfalls, but most erosion and deposition was due to slight adjustments in subtidal channel alignments (see Maps 3 and 4, Appendix 1).

Surface sediment

The surface sediment analysed in this study was collected from an uppermost layer, which is actively responding to the present energy regime and is thus a sedimentation unit (Appendix 3). Samples were separated into sand and mud (at 0.0625 mm), and sand fraction size analyses were performed with a Woods Hole-type Rapid Sediment Analyser. A brief comparison of sieve and RSA analyses of representative surface sediment samples from the AHE indicates that there were major differences between the results obtained by each method, and it is probable that if sieve analyses had been used exclusively in this project the final conclusions would have been quite different (Figures 79 and 80).

1. Mud. The muddiest sediment in the AHE occurs at the mouths of the Avon and Heathcote Rivers, where areas of $240\,000\,\mathrm{m}^2$ and $600\,000\,\mathrm{m}^2$ respectively are muddier than 40%, and reach maximum values of almost 90% (Figure 33). Trends in sediment muddiness which approximately parallel bathymetric contours, and the absence of mud above the MTL in most areas exposed to relatively long fetch waves, indicate that wave energy exerts the principal control on mud deposition in this estuary. However, close to the two river mouths, mud deposition patterns appear

to be a compromise between the rate of supply, the distance from a source, and wave energy. The resulting patterns may be quite coherent, but it has not been possible to evaluate the relative importance of each process.

That the Heathcote depository is 2.5 times larger than the Avon, and 10% muddier, is interpreted to be the result of order of magnitude differences in the rates of supply of sediment, and an indication that the mean muddiness of these depositories is influenced significantly by preferential deposition close to an essentially point source.

The evidence of widespread erosion - when a brief literature survey suggests that estuaries are often almost perfect retainers of sediment - and the presence of coherent patterns of mud deposition in areas undergoing active erosion, are both apparently paradoxical observations. The discovery of a sensible explanation of these features is a major result of the analysis of subsurface sediment in Part Five.

Since much of the mud supplied to the AHE is deposited in areas undergoing net erosion, it is probable that this mud is only in residence for a short time. As a result it is predicted that pollutants adsorbed on to mud particles will tend to have short residence times, and bottom sediment will not be enriched in mud-borne pollutants.

Finally, there is no physical, depositional evidence that the release of effluent into the estuary from CDB oxidation ponds affects the deposition of mud in any way.

2. *Sand.* A review of the literature on methods of identifying environment-specific sediment textures leads up to the conclusion that bivariate grain size plots are of no value to this study, and that there is little to be gained from this approach. Methods which follow from the work of Moss (1962, 1963) and Visher (1969) are potentially useful analytical tools, and they provide plausible explanations of sand fraction size distributions of surface samples from the AHE.

A cluster analysis was used to sort all surface samples (about 480) into like groups. Six groups were identified, and these were interpreted to be arbitrary subdivisions of a continuous spectrum of grain-size distributions, and not six discrete and natural clusters (Figures 40 and 41). Two basic grain-size distributions were recognised; the first was characterised by sharply curvilinear or bilinear cumulative curves, interpreted to represent two log-normal subpopulations, one deposited from saltation and one from suspension

(Figures 37 and 38). The second basic distribution was characterised by straight or slightly curvilinear (rarely bilinear) curves, interpreted to represent a single log-normal population deposited from saltation. Within the first basic group (cluster Groups A to C) the two subpopulations appear to have largely independent properties - the saltation population is uniformly well sorted, whereas both the sorting and mean size of the suspension population varies from Group A to C. Within the second group (Groups D to F) sorting values are consistently excellent, but mean sizes increase from D to F.

Histograms of sample height above datum vs sample frequency for each of the cluster Groups A to E (Figure 42) show that in the series A-B-C samples occur preferentially below the MTL, and only 0.5% from above the HWONT line (about 9.5 m HAD). There were no differences in the depth preferences of the three Groups A, B and C. Groups D and E occur preferentially in shallow water, but the HAD histograms of these two groups are bimodal, indicating that a significant percentage of these samples occur on the deepest intertidal flats - adjacent to the through-going subtidal channels. These results mean that sediment is only commonly deposited from suspension below the MTL, in water deeper than about 1.2 m below HWOST. Analyses presented in Part Two indicate that below the MTL, near bottom shear stresses decrease rapidly with increasing depth. The threshold for the deposition of suspended sediment (and mud) is probably about 2 dynes/cm^2 - below this value, sediment is deposited from suspension; above it, sediment is not.

A map showing the cluster group identity of all surface samples from the AHE (Map 2) indicates that the distribution of sediment deposited from suspension in this estuary is a compromise between processes which supply sediment, and those which influence its deposition and transportation within the estuary. The sequence C-B-A, which occurs with increasing distance from the river entrance in the Heathcote Basin, is interpreted to be a preferential depositional feature. In areas above the MTL (away from the river entrances), the properties of surface sediment are governed by both water depth and fetch distances, so that with increasing effective fetch distances, and thus increasing shear stress frequencies, sediment of Group E occurs in progressively deeper water. The granulometric properties of Group E sediment remain constant downfetch, indicating that sediment granulo-metrics are independent of shear stress frequency, but dependent on absolute levels of shear stress.

Cumulative curve shapes are not process-specific in this estuary, and the available evidence indicates that they are probably shear stress-specific. This result has significant repercussions for the Visher approach to cumulative curve analysis, since it indicates that a fundamental assumption of this approach - that breaks or inflections in log-probability grain size distributions are environmentally diagnostic (Visher, 1969, 1977) - may be invalid. The results of this study indicate that shear stress levels, and the properties of material supplied to a particular environment, are the main determinants of log-probability curve shapes - the processes which exert the stress are not recoverable from the resulting size distributions.

The presence of large areas of active sediment with remarkably uniform properties indicates that much of the active sediment in this estuary is in equilibrium with the physical environment, and that relict material supplied by the continuing net erosion demonstrated in Part One is not a significant modifier of surface sediment properties. A comparison of the cluster group map and maps of net erosion and deposition (Maps 2, 3 and 4) indicates that this is a valid conclusion, since the two patterns are clearly independent.

An analysis of the granulometrics of individual bathyforms indicates that where longshore energy gradients occur (as along the western slopes), longshore sediment gradients also occur. However, shore-normal trends are usually dominant, in response to the dominant shore-normal trends in water depth, wave energy and tidal current energy. Where energy is uniformly distributed longshore (as along the eastern slopes and flats), and where the bathymetry is characterised by large areas with consistent heights above datum (as on the eastern 9.0 m and 9.5 m bathyforms), sediment properties are also uniform, and exhibit an approximately shore-parallel, constant depth zonation.

Subsurface sediment

Detailed logging of 47 cores of subsurface sediment from the AHE revealed the presence of a stratigraphy consisting of pre-estuarine sand, overlain by a layered estuarine sequence, which in turn is overlain by post-European (anthropogenic) mud. The uppermost 25 cm - 30 cm of most cores consists of intensely bioturbate mottled sediment (which may be considered as a fourth stratigraphic unit) overlain by a thin, active layer.

1. Stratigraphy. Pre-estuarine sand – unit (a) – is uniformly low in mud and uniformly very well sorted, although mean grain size values vary from about 1.9 to 3.2 psi. Unit (a) sediment is interpreted to have been deposited only from saltation. It belongs to the Christchurch Formation (of Suggate, 1958), and represents the top of a 50 m thick, massive sequence of shallow marine sediment deposited during post-glacial transgression of the Canterbury coastline. Contours drawn on top of this unit indicate that the two major throughgoing subtidal channels have probably occupied their present positions since the estuary was first enclosed from the sea (Figure 56).

The estuarine sequence – unit (b) – consists of plane-laminated sand, muddy sand and sandy mud (rarely mud), and exhibits both fining upwards and coarsening upwards sedimentation sequences. A cluster analysis of all unit (b) sand samples (with the same program previously used to cluster surface sediment samples) produced four cluster groups (Figure 57). Representative cumulative curves and summary bivariate plots (Figures 58 and 59) indicate that as with surface sediment, unit (b) sand fractions are separated by the clustering operation into groups of convenience, and that there is a continuous spectrum of log-normal distributions, between end members characterised by straight curves, and by sharply curvilinear or bilinear curves. A fifth sample group (b') consists of a laterally equivalent, shallow water version of b1 to b4.

Massive olive grey plastic (buttery) mud of unit (c) overlies unit (b) sediment in many cores, and was probably deposited as a blanket throughout the estuary. Mud of this unit is interpreted to be post-European in origin, and to represent material supplied to the estuary during the early urbanisation phase of the growth of Christchurch City. Thus the lower contact of this unit may be dated at about 1850 (when settlement by European migrants first began), and the upper contact (where preserved) at about 1900. A mean accumulation of 50 cm of unit (c) sediment throughout the estuary would have been sufficient to cause the 30% decrease in the tidal compartment that probably occurred over the period 1850-1900.

2. Near-surface bioturbate sediment. A variety of infaunal and epifaunal animals in the AHE modify surface and near-surface sediment. In particular the mudflat snail *Amphibola crenata* browses across the sediment surface, converting the most recently deposited

material into readily transported fecal aggregates, and effectively
speeding the removal of fine sediment from the estuary. The bivalve
Macomona liliana alters the physical properties of surface and
subsurface sediment by burrowing to depths of about 25 cm, then
ingesting surface sediment and egesting it to form mounds on the
surface. Burrowing crabs excavate sediment from depths of up to 15 cm
below the sediment surface, dumping it as mounds adjacent to their
burrows. Polychaete worms may be present in high densities, and clearly
alter the surface roughness and compactness of the bottom of the estuary,
exerting an influence which although virtually unevaluated, must be of
major significance. Burrows, tubes, and excavation and defecation mounds
and hollows of the sort illustrated in Figures 65 and 66 create a
biogenic microbathymetry (Heezen and Hollister, 1971; Myers, 1977) which
may significantly alter near bottom shear stress values, and assist in
the removal of recently deposited (and biodeposited, or reworked),
friable sediment.

The bioturbate zone which results from the net effects of all
this biological activity is probably turned over to a depth of 10-25 cm
on a time scale of tens of days to tens of months. A thin skin of
active sediment covers the upper surface of this bioturbate zone, and
sediment below this active layer is muddier than the active layer in
shallow water (above the MTL), but less muddy than the active layer in
deeper water. While active layer muddiness is related to HAD, the
muddiness of the upper 5 cm of bioturbate sediment is not. There are
no systematic relationships between active layer sand properties and
sand properties of samples from the bioturbate zone beneath, although
the summary granulometrics of both sample types are broadly dependent on
HAD. These results indicate that if the present project had been based
on a different sampling method – perhaps 5 cm deep cores, or samples of
more casual dimensions, the information detailed in Part Four would not
have been obtained.

Recognition of the role of burrowing animals in the long- and
short-term dynamics of this estuary has provided answers to several
apparently paradoxical observations. Animals which excavate or defecate
subsurface material on to the sediment surface assist in net erosion,
and the removal of fine suspendible sediment, and generate patterns of
net erosion and deposition which are unrelated to variations in wave
or tide energy, and which are independent of present day rates of
sediment supply. Thus there may be coherent sediment muddiness

patterns, due to the deposition of mud on the sediment surface, in areas which are experiencing a net removal of sediment.

3. *Predictions*. It is probable that a net loss of sediment is occurring in this estuary because fine sediment is being exported seawards at a greater rate than it is being renewed. Thus, as long as muddy sediment is available to be mined by burrowers, a net loss will continue, the tidal compartment will continue to increase, erosion of the edges of the estuary will continue, and shore protection costs may rise, particularly where the estuary margins consist of erodible salt marsh or swamp deposits, or dune sand. Eventually a layer of uniformly clean sand will blanket much of the estuary – as is now the case in several areas, for example see cores 23, 25, 37 and 39. This layer of clean sand will act as a buffer between the ancient muddy sediment that remains, and the modern environment.

When the reservoir of biologically available virgin mud is worked out to a uniform depth – when all unit (b) and (c) sediment is buffered by a clean sandy surface layer – mud from external sources, probably reflecting a more polluted industrial source, may begin to predominate in the flux of fine sediment through the AHE. There is likely to be a steep increase in the near future, perhaps in the next 10-15 years. All remaining ancient, pre-industrial mud may be buffered by a sand layer within 25 years. The biological implications of this change in fine sediment sources may be far-reaching. Filter feeders and surface detritus-feeding animals which extract much of their food from finer particles, may decline in numbers as the reservoir of mud is mined out, and as suspended sediment concentrations decrease. Parallel adjustments to the remainder of the benthic community may result in significant long-term changes in the biological character of the Avon-Heathcote Estuary.

REFERENCES

Allen, J.R.L., 1968. Current Ripples. North Holland Publishing Co.,
Amsterdam. 432 pp.

Allen, J.R.L., and P.F. Friend, 1976. Changes in intertidal dunes
during two spring-neap intertidal cycles, Lifeboat Station Bank,
Wells-Next-the-Sea, Norfolk (England). Sedimentology, 23:
329-346.

Apfel, E.T., 1938. Phase sampling of sediments. J. Sedim. petrol.,
8: 67-68.

Amaral, E.J., and W.A. Pryor, 1977. Depositional environment of the
St. Peter sandstone deduced by textural analysis. J. Sedim.
petrol., 47(1): 32-52.

Bagnold, R.A., 1966. An approach to the sediment transport problem from
general physics. U.S. Geol. Surv. Prof. Paper 422-I: 37 pp.

Bascomb, C.L., 1968. A new apparatus for recording particle size
distribution. J. Sedim. petrol., 38: 878-884.

Biggs, L.R., 1947. The formation, control and utilization of the
coastal sand dunes between the Waimakariri River and the Sumner
Estuary. Unpub. M.A. thesis in Geog., Univ. of Canterbury.

Biscaye, P.E., 1964. Distinction between kaolinite and chlorite in
Recent sediments by X-ray diffraction. Am. Miner., 49:
1281-1289.

Biscaye, P.E., 1965. Mineralogy and sedimentation of Recent deep-sea
clay in the Atlantic Ocean and adjacent seas and oceans.
Geol. Soc. Amer. Bull., 76: 803-832.

Blake, G.J., 1964. Coastal progradation in Pegasus Bay. Unpub. M.Sc.
thesis in Geog., Univ. of Canterbury.

Bokuniewicz, H.J., R.B. Gordon, and C.C. Pilbeam, 1975. Stress on the
bottom of an estuary. Nature, 257: 575-577.

Boggs, S., and C.A. Jones, 1976. Seasonal reversal of flood-tide
dominant sediment transport in a small Oregon estuary. Geol.
Soc. Amer. Bull., 87: 419-426.

Boothroyd, J.C., and D.K. Hubbard, 1974. Bedform development and distribution pattern, Parker and Essex Estuaries, Massachusetts. U.S. Army Corps of Engineers, Coastal Engineering Research Center, Fort Belvoir, Va., U.S.A.

Bretschneider, C.L., 1958. Revisions in wave forecasting; deep and shallow water. Proc. 6th Conf. Coastal Engineering; Amer. Soc. Civil Engineers, Council on wave research.

Brown, L.J., 1975. Water well data. Sheet 576/7-8, Belfast-Styx. N.Z. Geol. Surv., Report 72.

Brown, L.J., in press. Water well data. Sheet 584/1-2, Christchurch-Sumner. N.Z. Geol. Surv. Report.

Bruce, A., 1953. Report on a biological and chemical investigation of the waters in the Estuary of the Avon and Heathcote Rivers, Christchurch Drainage Board Report, Christchurch, New Zealand. 58 pp.

Bruun, P., and F. Gerritson, 1960. Stability of coastal inlets. North Holland, Amsterdam. 123 pp.

Byrne, R.J., and J.D. Boon, 1973. An inexpensive, fast response current-speed indicator. Chesapeake Science, 14(3): 217-219.

Carter, L., and R.A. Heath, 1975. Role of mean circulation, tides and waves in the transport of bottom sediment on the New Zealand Continental Shelf. N.Z. Jl Mar. Freshwater Res., 9: 423-448.

Carver, R.E., 1971. Procedures in Sedimentary Petrology. Wiley-Interscience, New York. 653 pp.

Caston, V.N.D., 1976. A wind-driven near-bottom current in the Southern North Sea. Est. Coastal Mar. Sci., 4: 23-32.

Channon, R.D., 1971. The Bristol Fall Column for coarse sediment grading. J. Sedim. petrol., 41: 867-870.

Channon, R.D., and D. Hamilton, 1976. Wave and tidal current sorting of shelf sediments southwest of England. Sedimentology, 23: 17-42.

Clark, M.W., 1976. Some methods for statistical analysis of multimodal distributions and their application to grain-size data. Mathematical Geology, 8(3): 267-282.

Coastal Research Group, 1969. Coastal environments, N.E. Mass. and
New Hampshire, Field trip, Eastern Section Society of Econ.
Paleont. and Min., Univ. of Mass.

Cochran, W.G., F. Mosteller, and J.W. Tukey, 1954. Principles of
sampling. Jour. Amer. Stat. Assoc., 49: 13-25.

Cokelet, E.D., 1977. Breaking waves. Nature, 267: 769-774.

Consultants to the Christchurch Drainage Board, 1973. Report on
Christchurch Drainage Investigation by Royds Sutherland and
McLeay, Powell Fenwick and Partners, Consulting Engineers.
Unpub. report held by the CDB, Christchurch, New Zealand.

Cronin, L.E. (Ed.), 1975. Estuarine research, Volume II, Geology and
Engineering. Academic Press, Inc., New York. 590 pp.

Davis, J.C., 1973. Statistics and data analysis in geology.
John Wiley and Sons, New York. 550 pp.

Detwyler, T.R., 1971. Man's impact on environment. McGraw Hill,
New York. 731 pp.

Doeglas, D.J., 1946. Interpretation of results of mechanical analyses.
J. Sedim. petrol., 16: 19-40.

Drake, D.E., 1976. Suspended sediment transport and mud deposition on
Continental Shelves. *In:* Stanley, D.J., and D.J.P. Swift (Eds),
Marine sediment transport and environmental management.
John Wiley and Sons, New York. 593 pp.

Dyer, K.R., 1973. Estuaries: A physical introduction. John Wiley and
Sons, New York. 140 pp.

Edzwald, J.K., and C.R. O'Melia, 1975. Clay distributions in Recent
estuarine sediments. Clays and Clay Mins., 23: 39-44.

Emery, K.O. 1938. Rapid method of mechanical analysis of sands.
J. Sedim. petrol., 8: 105-111.

Erlich, R., 1964. The role of the homogeneous unit in sampling plans
for sediments. J. Sedim. petrol., 34: 437-439.

Estcourt, I.N., 1962. An ecological survey of the burrowing polychaetes
of the Avon-Heathcote Estuary. Unpub. M.Sc. thesis in Zool.,
Univ. of Canterbury.

Felix, D.W., 1969. An inexpensive recording settling tube for analysis
of sands. J. Sedim. petrol., 39: 777-780.

Folk, R.L., 1955. Student operator error in determination of roundness,
sphericity and grain size. J. Sedim. petrol., 25: 297-301.

Folk, R.L., 1968. Petrology of sedimentary rocks. Hemphills, Austin,
Texas. 159 pp.

Folk, R.L., and W.C. Ward, 1957. Brazos River Bar: A study in the
significance of grain-size parameters. J. Sedim. petrol.,
27: 3-26.

Friedman, C.M., 1961. Distinctions between dune beach, and river sands
from their textural characteristics. J. Sedim. petrol., 31:
514-529.

Furkert, F.W., 1947. Tidal compartments, their influence on dimensions
of harbour entrance channels. N.Z. Inst. Eng. Proc., 33:
195-211.

Galehouse, J.S., 1971. Sedimentation analysis. *In:* Carver, 1971.
pp. 69-94.

Goldberg, E.D.. 1976. Pollution history of estuarine sediments.
Oceanus, 19(5): 18-26.

Goldberg, E.D., E. Gamble, J.J. Griffin, and Minoru Koide, 1977.
Pollution history of Narragansett Bay as recorded in its
sediments. Est. Coast. Mar. Sci., 5: 549-561.

Goreau, T.J., 1977. Quantitative effects of sediment mixing on
stratigraphy and biogeochemistry: a signal theory approach.
Nature, 265: 525-526.

Gibbs, R.J., 1977. Clay mineral segregation in the marine environment.
J. Sedim. petrol., 47(1): 237-243.

Gibbs, R.J., M.D. Mathews, and D.A. Link, 1971. The relationship
between sphere size and settling velocity. J. Sedim. petrol.,
41: 7-18.

Graf, W.L., 1977. The rate law in fluvial geomorpholgy.
Am. J. Sci., 277: 178-191.

Griffin, G.M., 1971. Interpretation of X-ray diffraction data.
In: Carver, 1971. pp. 541-570.

Griffiths, J.C., 1967. Scientific method in analysis of sediments. McGraw Hill Book Co., New York. 508 pp.

Grim, R.E., 1968. Clay Mineralogy, 2nd Ed., McGraw-Hill, New York. 596 pp.

Guy, H.P., D.B. Simons, and E.V. Richardson, 1966. Summary of alluvial channel data from flame experiments 1956-1961. U.S. Geol. Surv. Prof. Paper 462-J. 96 pp.

Guy, H.P., and D.E. Jones, 1972. Urban sedimentation - In perspective. Jl. Hydraulics Div., Proc. Amer. Soc. Civil Eng., 98 (HY12): 2099-2116.

Hails, J.R., and J.H. Hoyt, 1969. The significance and limitations of statistical parameters for distinguishing ancient and modern sedimentary environments of the lower Georgia coastal plain. J. Sedim. petrol., 39: 559-580.

Harrison, S.P.A., 1976. Holocene stratigraphy of the Avon-Heathcote Estuary. Undergraduate project report, Department of Geology, University of Canterbury, 52 pp.

Haven, D.S., and R. Morales-Alamo, 1966. Aspects of biodeposition by oysters and other invertebrate filter-feedings. Limnol. Oceanogr., 11: 487-498.

Haven, D.S., and R. Morales-Alamo, 1972. Biodeposition as a factor in sedimentation of fine suspended solids in estuaries. *In:* B.W. Nelson (Ed.), Environmental framework of coastal plain estuaries. Geol. Soc. Am. Mem., 133. pp. 121-130.

Hayes, F.R., 1964. The mud-water interface. Oceanogr. mar. biol. Ann. Rev., 2: 121-145.

Hayes, M.O., 1975. Morphology of sand accumulation in estuaries: An introduction to the symposium. *In:* Gronin, L.E. (Ed.), Estuarine research, Volume II, Geology and Engineering. Academic Press, Inc., New York. 590 pp.

Heath, R.A., 1975. Stability of some New Zealand coastal inlets. N.Z. Jl Mar. Freshwater Res., 9: 449-456.

Heezen, B.C., and C. Hollister, 1964. Deep-sea current evidence from abyssal sediments. Marine Geol., 1: 141-174.

Heinemann, H.G. and R.F. Piest, 1973. Soil erosion–sediment yield. Research in progress. EOS: 149-159.

Hellstrom, B., 1970. Wind effect on lakes and rivers. Esselte AB, Stockholm, Sweden.

Hercus, A.I., 1948. A city built on a swamp – The story of the drainage of Christchurch, 1850-1903. Unpub. M.A. thesis in history, Univ. of Canterbury, Christchurch.

Hertweck, G., 1970. Das watt. Waldemar kramer, Frankfurt. 110 pp.

Howard, J.D. and R.W. Frey, 1975. Estuaries of the Georgia coast, U.S.A.: Sedimentology and Biology: I. Introduction. Senckenbergiana marit., 7: 1-31.

Hutchinson, A.H., 1972. Resource management in the estuarine environment. A case study, the Avon-Heathcote Estuary, Christchurch. Unpub. M.Sc. thesis in geog., Univ. of Canterbury.

Hydraulics Research Station, Wallingford, England, 1970. Christchurch, New Zealand. Model studies of flood alleviation. Report EX509.

Inman, D.I., 1949. Sorting of sediments in the light of fluid mechanics. J. Sedim. petrol., 19: 51-70.

Inman, D.L., 1957. Wave generated ripples in nearshore sands. Beach Erosion Board Tech. Memo., 100, 42 pp.

Ippen, A.T. (Ed.), 1966. Estuary and coastline hydrodynamics. McGraw Hill Book Co., New York. 744 pp.

Johns, W.D., R.E. Grim, and W.F. Bradley, 1954. Quantitative estimates of clay minerals by diffraction methods. J. Sedim. petrol., 24: 242-251.

Jones, M.B., 1976. Limiting factors in the distribution of intertidal crabs in the Avon-Heathcote Estuary, Christchurch. N.Z. Jl Mar. Freshwater Res., 10(4): 577-587.

Jopling, A.S., 1964. Interpreting the concept of the sedimentation unit. J. Sedim. petrol., 34(1): 165-172.

Kjerfve, B., 1975. Tide and fair-weather effects in a bar-built Louisiana estuary. In: Cronin, L.E. (Ed.), Estuarine research, Volume II, Geology and Engineering. Academic Press, Inc., New York. 590 pp.

Klein, G.D.V., 1970. Depositional and dispersal dynamics of intertidal sand bars. J. Sedim. petrol., 40: 1095-1127.

Knox, G.A., and A.R. Kilner, 1973. The ecology of the Avon-Heathcote Estuary. Unpub. report to the CDB.
358 pp.

Komar, P.D., 1974. Oscillatory ripple marks and the evaluation of ancient wave conditions and environments. J. Sedim. petrol., 44: 169-180.

Komar, P.D., and M.C. Miller, 1975. On the comparison of the threshold of sediment motion under waves and unidirectional currents, with a discussion of the practical evaluation of the threshold. J. Sedim. petrol., 45: 362-36.

Komar, P.D., 1976a. Boundary layer flow water steady unidirectional currents. *In:* Stanley, D.J., and D.J.P. Swift (Eds.), Marine sediment transport and environmental management. John Wiley and Sons, New York. 593 pp.

Komar, P.D. 1976b. The transport of cohesionless sediments on continental shelves. *In:* Stanley, D.J., and D.J.P. Swift (Eds.), Marine sediment transport and environmental management. John Wiley and Sons, New York. 593 pp.

Kranck, K., 1975. Sediment depositon from flocculated suspensions. Sedimentology, 22: 111-123.

Krumbein, W.C., 1934. Size-frequency distributions of sediments. J. Sedim. petrol., 4: 65-77.

Lee, L.P., 1953, Mean sea level and mean high water mark. N.Z. Survey Draughtsmen's Jl., 1: 325-343.

Legget, R.F., 1973. Cities and Geology. McGraw Hill, New York, 624 pp.

Leopold, L.B., 1968. Hydrology for urban land planning - A guidebook on the hydrologic effects of urban landuse. U.S. Geol. Surv. Circular 554. 18 pp.

Lindh, G., 1972. Urbanisation: A hydrological headache. Ambio, 1(6): 185-201.

Linzey, J.T., 1944. A short study of the hydrography of the Avon and Heathcote Rivers. Trans. Proc. Roy. Soc. N.Z., 73: 365-376.

Ludwick, J.C., 1975. Tidal currents, sediment transport and sand banks in Chesapeake Bay entrance, Virginia. *In:* Hayes, M.O. (Ed.), Second International Estuarine Conf. Proc. Myrtle Beach, South Carolina.

Lynch-Blosse, M.A., and N. Kumar, 1976. Evolution of downdrift-offset tidal effects: a model based on the Brigantine inlet system of New Jersey. Jl. Geol., 84: 165-178.

Macpherson, J.M., 1976. Aspects of the environmental impact of Christchurch City. N.Z. Geol. Soc. Newsletter, 16: 18-20.

Macpherson, J.M., and D.W. Lewis, in prep. What are you sampling?

Madsen, O.S., 1976. Wave climate of the continental margin: elements of its mathematical description. *In:* Stanley, D.J., and D.J.P. Swift (Eds.), Marine sediment transport and environmental management. John Wiley and Sons, New York. 593 pp.

Martens, L.A., 1966. Flood inundation and effects of urbanisation in metropolitan Charlotte (North Carolina). U.S. Geol. Surv. open file rept., 54 pp.

Mason, C.C., and R.L. Folk, 1958. Differentiation of beach, dune, and eolian flat environments by size analysis, Mustant Island, Texas. J. Sedim. petrol., 28: 211-226.

Mawson, A.H., 1972. Notes on the hydrology of the Avon and Heathcote Estuary. Unpub. paper presented to an Ecology Action seminar at the Univ. of Canterbury, 4 Aug. 1972.

McCave, I.N., 1969. Deposition of fine-grained sediment from tidal currents. Nature 224: 1288-1289.

Meade, R.H., 1972. Transport and deposition of sediment in estuaries. *In:* Nelson, B.W. (Ed.), Environmental framework of coastal plain estuaries. Geol. Soc. America Memoir 133.

Meza, M.P., and C.R. Paola, 1977. Evidence for onshore deposition of Pleistocene Continental Shelf clays. Mar. Geol., 23: M27-M36.

Miller, M.C., I.N. McCave, and P.D. Komar, 1977. Threshold of sediment motion under unidirectional currents. Sedimentology, 24: 507-527.

Millward, W.A.M., 1975. Physical characteristics of an estuarine environment. M.A. thesis, Dept. of Geog., Univ. of Canterbury.

Middleton, C.V., 1967. Experiments on density and turbidity currents, 3. The deposition of sediment. Canadian Jour. Earth Sci., 4: 475-505.

Middleton, G.V., 1976. Hydraulic interpretation of sand size distributions. Journal of Geol., 84: 405-426.

Moiola, R.J., and D. Weiser, 1968. Textural parameters: An evaluation. J. Sedim. petrol., 38(1): 45-53.

Moss, A.J., 1962. The physical nature of common sandy and pebbly deposits (Part 1). Am. J. Sci., 260: 337-373.

Moss, A.J., 1963. The physical nature of common sandy and pebbly deposits (Part 2). Am. J. Sci., 261: 297-343.

Moss, A.J., 1972. Bedload sediments. Sedimentology, 18: 159-219.

Munk, W.H., 1955. Stress on water: A hypothesis. Quart. J. Roy. Meteor. Soc., 81: 320-332.

Myers, A.C., 1977. Sediment processing in a marine subtidal sandy bottom community: 1. Physical aspects. J. Mar. Res., 35(3): 609-632.

Nelson, B.W., (Ed.), 1972. Environmental framework of coastal plain estuaries. Geol. Soc. America, Memoir 133.

Nelson, T.A., 1976. An automated rapid sediment analyses (ARSA). Sedimentology, 23: 867-872.

Norrman, J.O., 1964. Lake Vattern. Investigations on shore and bottom morphology. Geog. Annaler XLVI. 238 pp.

Officer, C.B., 1976a. Physical oceanography of estuaries. Oceanus, 19(3): 3-9.

Officer, C.B., 1976b. Physical oceanography of estuaries (and associated coastal waters). John Wiley and Sons, New York. 465 pp.

Otto, G.H., 1938. The sedimentation unit and its use in field sampling. J. Geol., 46: 569-582.

Passega, R., 1957. Textural characteristics of clastic deposition. Bull. Am. Assoc. Petrol. Geologists, 41: 1952-1984.

Passega, R., 1964. Grain-size representation by CM patterns as a geological tool. J. Sedim. petrol., 34: 830-847.

Passega, R., and R. Byramjee, 1969. Grain-size image of clastic deposits. Sedimentology, 13: 233-252.

Pearce, B.R., 1950. Recent changes in the Sumner Foreshore and Estuary. Unpub. M.A. thesis in geog., Univ. of Canterbury, New Zealand.

Poole, D.M., 1957. Size analysis of sand by a sedimentation technique. J. Sedim. petrol., 27: 460-468.

Postma, H., 1967. Sediment transport and sedimentation in the estuarine environment. *In:* Lauf, G.H. (Ed.), Estuaries, Publ. No. 83: 158-179. Amer. Assoc. Adv. Sci., Washington, D.C.

Pritchard, D.W., 1956. The dynamic structure of a coastal plain estuary. J. Mar. Research, 15: 33-42.

Pritchard, D.W. 1967. Observations of circulation in coastal plain estuaries. *In:* Lauff, G.H. (Ed.), Estuaries, Publ. No. 83: 37-44. Amer. Assoc. Adv. Sci., Washington, D.C.

Reed, J.J., 1951. Marine sediments near Sumner, Canterbury, New Zealand. N.Z. Jl. Sci. Tech., Section B, 33(2): 129-137.

Reed, W.E., R. LeFever, and G.J. Moir, 1975. Depositional environment interpretation from settling-velocity (Psi) distributions. Geol. Soc. Amer. Bull., 86: 1321-1328.

Reinson, G.E. 1977. Tide-current control of submarine morphology at the mouth of submarine morphology at the mouth of the Miramichi Estuary, New Brunswick. Can. J. Earth Sci., 14: 2524-2532.

Reineck, H.E., and I.B. Singh, 1975. Depositional sedimentary environments. Springer Verlag, Berlin. 439 pp.

Resio, D.T., R. Dolan, B.P. Hayden, and C.L. Vincent, 1977. Systematic variations in offshore bathymetry. Journ. Geol., 85: 105-113.

Rhoads, D.C., 1963. Rates of sediment reworking by *Yoldia limatula* in Buzzards Bay, Massachusetts, and Long Island Sound. J. Sedim. petrol., 33: 723-727.

Rhoads, D.C., 1967. Biogenic reworking of intertidal and subtidal sediments in Barnstable Harbour and Buzzards Bay, Mass. J. Geol., 75: 461-476.

Rizzini, A., 1968. Sedimentological representation of grain sizes.
    Mem. Soc. Geol. Italia, 7: 65-89.

Roberts, W.P., and J.W. Pierce, 1974. Sediment yield in the Patuxent
    River (Md.) undergoing urbanisatin, 1968-1969. Sediment. Geol.,
    12: 179-197.

Rogers, J.J.W., 1965. Reproduceability and significance of
    measurements of sedimentary size distributions.
    J. Sedim. petrol., 35: 722-732.

Rosin, P.S., 1975. Origin and processes of cuspate spit shorelines.
    In: Cronin, L.E. (Ed.), Estuarine research, Volume II,
    Geology and Engineering. Academic Press, Inc., New York.
    590 pp.

Sagoe, K-M.O., and G.S. Visher, 1977. Population breaks in grain-size
    distributions of sand - a theoretical model. J. Sedim. petrol.
    47(1): 285-310.

Sahu, B.K., 1964. Depositional mechanisms from the size analysis of
    clastic sediments. J. Sedim. petrol., 34: 73-83.

Sandford, R.B., and D.J.P. Swift, 1971. Comparison of sieving and
    settling techniques for size analysis, using a Benthos rapid
    sediment analyzer. Sedimentology, 17: 257-264.

Savani, I. and J.C. Kamerer, 1961. Urban growth and the water regimen.
    U.S. Geol. Surv. Water Supply paper 1591A.

Scheidegger, K.F., and J.B. Phipps, 1976. Dispersal patterns of sand in
    Gray's Harbour Estuary, Washington, J. Sedim. petrol., 46(1):
    163-166.

Schink, D.R., and N.L. Guinassa Jr., 1977. Effects of bioturbation on
    sediment - seawater interaction. Marine Geology, 23: 133-154.

Schlee, J., 1966. A modified Woods Hole rapid sediment analyzer.
    J. Sedim. petrol., 36: 403-413.

Schubel, J.R., 1971. Estuarine circulation and sedimentation. *In:*
    Schubel, J.R. (Ed.), The Estuarine Environment: Estuaries and
    Estuarine Sedimentation. Am. Geol. Inst. Short Course Lecture
    Notes. Am. Geol. Inst., Washington, D.C. pp.VI-117.

Scott, E.F., 1963. Christchurch data. Notes and comments on the Christchurch drainage and sewerage systems. Unpublished report held by the CDB, Christchurch, New Zealand.

Scott, W.H., 1955. Sea erosion and coast protection at Sumner. N.Z. Engineer 10: 438-447.

Sengupta, S., and H.J. Veenstra, 1968. On sieving and settling techniques for sand analysis. Sedimentology, 11: 83-98.

Siemers, C.T., 1976. Sedimentology of the rocktown channel sandstone, upper part of the Dakota Formation (Cretaceous), Central Kansas. J. Sedim. petrol., 46(1): 97-123.

Simons, D.B., E.V. Richardson, and M.L. Albertson, 1961. Flume studies using medium sand (0.45mm). U.S. Geol. Surv. Water Supply Paper 1498-A. 76 pp.

Spenser, D.W. 1963. The interpretation of grain-size distribution curves of elastic sediments. J. Sedim. petrol., 33: 180-190.

Sternberg, R.W., 1968. Friction factos in tidal channels with differing bed roughness. Mar. Geol., 6: 243-261.

Sternberg, R.W., 1972. Predicting initial motion and bedload transport of sediment particles in the shallow marine environment. In: Swift, D.J.P., D.B. Duane, and O.H. Piley (Eds.), Shelf sediment rransport. Dowden Hutchinson and Ross, Stroudsberg, Pa., U.S.A. pp. 61-82.

Stewart, H.B., Jr., 1958. Sedimentary reflections of depositional environments in San Miguel Lagoon, Baja California, Mexico. Am. Assoc. Petrol. Geol. Bull., 42: 2567-2618.

Suggate, R.P., 1958. Late Quaternary deposits of the Christchurch metropolitan area. N.Z. Jl. Geol. Geophys., 1(1): 103-122.

Suggate, R.P. 1968. Post-glacial sea level rise in the Christchurch metropolitan area, New Zealand. Geol. en Mijnbouw, 47(4): 291-297.

Sutherland, A.J., 1977. Wave generation and forecasting. Notes for a seminar on Coastal Engineering, Univ. of Canterbury.

Swanson, K., in press. The ostracod fauna of the Otago Shelf, New Zealand. N.Z. Oceanographic Inst. Memoir.

Swift, J.P., and J.C. Ludwick, 1976. Substrate response to hydraulic process: Grain-size frequency distributions and bedforms. *In:* Stanley, D.J., and D.J.P. Swift (Eds.), Marine sediment transport and environmental management. Wiley-Interscience. New York. pp. 159-196.

Sverdrup, H.U., and W.H. Munk, 1947. Wind, sea and swell: Theory of relations for forecasting. Publication No. 601, U.S. Navy Hydrographic Office, Washington, D.C.

Tanner, W.F. 1959. Sample components obtained by the method of differences. J. Sedim. petrol., 29: 408-411.

Tanner, W.F. 1967. Ripple mark indices and their use. Sedimentology, 9: 89-104.

Thompson, E.F., 1929. An introduction to the natural history of the Heathcote Estuary and Brighton Beach, Canterbury, New Zealand. A study in littoral ecology. Unpub. M.Sc. thesis in biol., Canterbury University College, Christchurch.

Udden, J.A., 1914. Mechanical composition of clastic sediments. Geol. Soc. Amer. Bull., 25: 655-744.

U.S. Army Coastal Engineering Research Centre, 1973. Shore protection manual. U.S. Government Printing Office, Washington, D.C.

U.S. Army, Corps of Engineers, 1962. Waves on inland reservoirs. TM-132, Beach Erosion Board, Washington, D.C.

Visher, G.S., 1969. Grain size distribution and depositional processes. J. Sedim. petrol., 39: 1074-1106.

Walton, T.L., Jr., 1977. A relationship between inlet cross-section and outer bar storage. Shore and Beach, April 1977: 9-13.

Webb, B.F., 1967. A study in the biology of the fish population of the Avon-Heathcote Estuary. Unpub. M.Sc. thesis in Zool., University of Canterbury, Christchurch.

Wigram, Sir H.F., 1916. The story of Christchurch, New Zealand. Lyttelton Times, Christchurch. 269 pp.

Wilson, D.D., in press. Hydrogeology of Metropolitan Christchurch. Jl. Hydrol. N.Z.

Wilson, W.S., 1966. A method for calculating and plotting surface wave
     rays. U.S. Army Corps of Engineers Tech. Memo. No. 17,
     Coastal Engineering Research Center, Washington, D.C.

Wright, F.F., 1974. Estuarine Oceanography. AGI/McGraw-Hill.

Zeigler, J.M., G.G. Whitney, and C.R. Hayes, 1960. Woods Hole rapid
     sediment analyzer. J. Sedim. petrol., 30: 490-495.

APPENDIX 1

Historical estimates of the tidal compartment of the AHE

1. *Predicted volumes.* The entrance of the AHE has been surveyed
a number of times since 1848 (see Scott, 1955, for a comprehensive list),
and these surveys provide a method of estimating the tidal compartment.
The method relies on work by Heath (1975) and earlier observations by
Furkert (1947), who have shown that there is a linear relationship
(here called the Furkert-Heath relationship) between the cross-sectional
area of the entrance to a tidal inlet, and the tidal compartment of the
inlet - in other words, that the amount of water flowing through an
inlet regulates its size. By making the assumptions explained in
Figure 79, it had been possible to estimate inlet cross-sectional areas
from charts made in 1854, 1874 and 1904, and then to predict the
corresponding tidal compartments from the Furkert-Heath relationship.
The results are listed in Figure 79, and they indicate that in 1854
the tidal compartment of this estuary was probably about 7.7×10^6 m^3;
by 1874 it had decreased to 5.1×10^6 m^3, and by 1904 it had increased
again, to about 6×10^6 m^3.

2. *Direct estimates.*

(i) A value of 4.85×10^6 m^3 for 1911 (from Little, 1911, in Mawson,
1962) is based on a direct estimate of the volume of water leaving the
estuary on an ordinary tide, and is of doubtful reliability, mainly
because Little apparently reported a figure of 9.5×10^6 tons of water
(9.652×10^6 m^3) as a daily outflow. Daily may mean for one tidal cycle
(about 12.5 h) or two tidal cycles (25 h), and so the appropriate figure
for the tidal compartment may be 9.652 or 4.826×10^6 m^3. Since the
latter is closer to independent estimates for 1904 and 1920 (Figure 79),
it is accepted as most likely to be correct. Other workers (Bruce,
1953; Mawson, 1962) have chosen the higher value.

(ii) Another doubtful direct estimate was made by Bruce in 1953, who
used figures for depth, width and current speed at the inlet (presumably
at or near Shag Rock - Figure 79), to calculate the amount of water
leaving the estuary during one tidal cycle (otherwise unspecified).
Bruce arrived at a figure of 360×10^6 cubic feet (10.19×10^6 m^3).

Source and date of data	Maximum depth at Shag Rock[1]	Midtide width at Shag Rock[2]	Adjusted area[3]	Tidal compartment
HMS Pandora 1854	9.14m	91.4m	460m^2	7.7$_4$ (x 10^6m^3)
Whately Elliot 1874	5.98m	70.1m	305m^2	5.1$_4$
McIntyre-Lewis 1904	5.98m	118.87m	378m^2	6.35$_4$
Joshua Little 1911	-----	-----	----	4.826$_5$
LHB/CDB Survey 1920	8.84m	100.58m	489m^2	8.18$_4$
"	-----	-----	-----	8.78$_5$
Bruce 1953	-----	-----	-----	10.19$_5$
Royds and Sutherland 1964	8.53m	118.87m	557m^2	9.15$_4$
As above	-----	-----	-----	10.80$_5$
CDB 1975	-----	-----	-----	10.928$_5$

1. Shag Rock is used because it is easily located on old charts, and because the principal subtidal channel has flowed adjacent to Shag Rock continuously since 1854 - hence data for midtide width and maximum depth can be extracted from old charts with most confidence from this locality.

2. Width across the principal subtidal channel, from midtide mark to midtide mark.

3. Depth soundings plotted on many old charts are not located accurately enough to allow the construction of detailed cross-sections, so an estimate of cross-sectional area is made by assuming a rectangular shape, such that midtide width multiplied by maximum depth equals cross-sectional area. However the survey by Royds and Sutherland (1964) did include a detailed section at Shag Rock, and the cross-sectional area calculated from that section is 55% less than the equivalent rectangular section. By assuming this relationship has held during the period 1854-1975, adjusted areas can be calculated, at 55% of the rectangular section

4. Tidal compartment predicted from the Furkert-Heath relationship (below).

5. Tidal compartment calculated from various indirect measurements, including detailed surveying of the bathymetry of the estuary (Royds and Sutherland 1964, Christchurch Drainage Board 1975-76) and measurements of velocities and cross-sectional areas at Shag Rock (Bruce 1953, Little 1911).

The Furkert-Heath Relationship (from Heath, 1975). Figures shown are the cross-sectional areas and tidal compartments tabulated above.
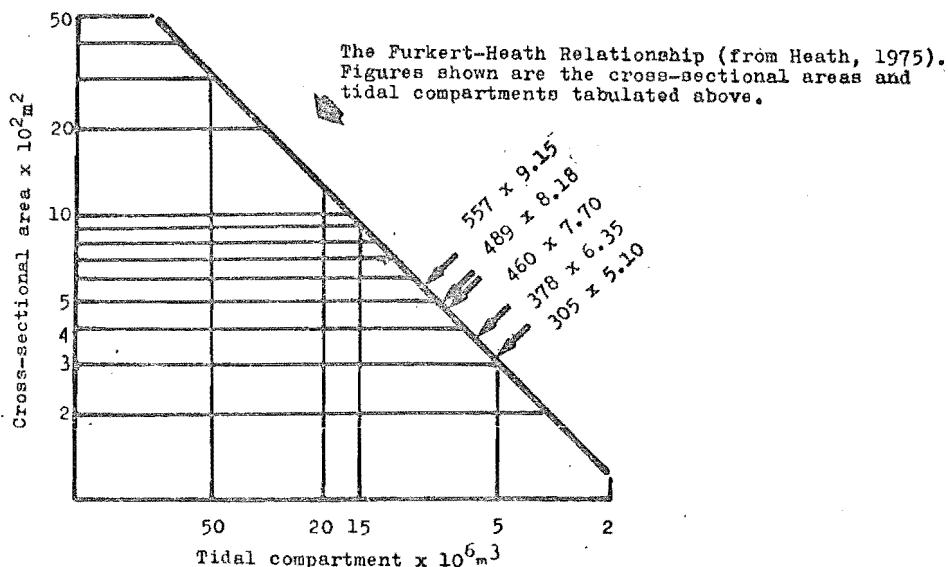
Figure 79. Cross-sectional area of the tidal entrance at mid tide and the tidal compartment at ordinary spring tide, Avon-Heathcote Estuary, 1854 - 1975.

Since she did not specify her methods, this volume has an unknown
reliability.

(iii) The three most reliable estimates in Figure 79 are based on a
survey carried out in 1962 by consultants to the CDB. This survey was
part of a comprehensive data gathering exercise (the Wallingford Report,
1970) set up to provide prototype data for a flood protection study of
the AHE by the British Ministry of Transport Hydraulics Research
Station. The consultants (Royds and Sutherland, now Royds Sutherland
Evans and McLeay) established a series of fixed, permanent stations
around the perimeter of the estuary, defining the end points of
east-west surveyed lines which formed the basis of a 200 × 20 link grid
covering the whole estuary.

Data collected from this survey was used by CDB engineers to
estimate the volume of the tidal compartment of the estuary; and the
resultant figure of 10.80×10^6 m^3 (Mawson, 1972, p. 2) for the volume
of water leaving the estuary during an ordinary spring tide is accepted
as a reliable value for the 1962 tidal compartment. The consultants
data may also be used to check the Furkert-Heath predictions for earlier
tidal compartments, since a cross-section surveyed across the principal
subtidal channel from Shag Rock to the Spit gives a 1962 cross-sectional
area of 557 m^2, or a predicted tidal compartment of 9.15×10^6 m^3.
Compared to the calculated figure of 10.80×10^6 m^3 there is a
difference of 1.51×10^6 m^3, which indicates the magnitude of error
likely to be contained in the values listed in Figure 79.

The consultants' survey design has been retained in a subsequent
resurvey of the estuary by CDB surveyors (frequently assisted by the
writer) which attempted to exactly reoccupy the 1962 grid. Data from
this 1975/77 resurvey is used here to produce a bathymetric map of the
estuary (Map 1), on which east-west lines 2 to 16 are the original 1962
lines reoccupied by the CDB team.

In 1920 the Lyttelton Harbour Board (LHB) and the CDB completed
a bathymetric survey of the estuary, and although this work was
concentrated around the inlet, some reasonably detailed data for the
northern half of the estuary was also collected (supplied to the writer
by J.A. Robb, CDB). This survey was done by boat at high tide, with
levels measured by sounding and corrected to a tide curve. The results
are less accurate and less precise than those of the 1962 and 1975/77
surveys (J.A. Robb, pers. comm.). The LHB crews collected their data

along irregular lines at low angles to the Royds and Sutherland grid, and direct comparisons of the two data sets are not possible. However an indirect comparison has been attempted (by D. Carver, CDB), by projecting 1920 stations on to the nearest 1962 survey line, for the area north of line 10, Map 1.

By comparing levels obtained in 1920 and 1975/77 with the 1962 data it is possible to calculate tidal compartments for 1920 and 1975/77, and together with Mawson's value for 1962, there are the three most reliable estimates in Figure 79.

The technique used here of estimating temporal changes in a tidal compartment by comparing sets of bathymetric data rests on four assumptions.

(i) The principal assumption is that surveyed lines represent a 100 m strip either side of each line, where lines are 200 m apart. This assumption is untested. However, north of line 12 (Map 1) bathymetric contours run more or less north-south (at right angles to the survey lines) and the profiles change little from line to line; here this assumption appears to be reasonable. In the south, lines 13-16 run subparallel to the Heathcote channel, and slight changes in the position of this channel (or slight surveying errors) may be exaggerated where profiles cross it at low angles. The $40 \, m^2$ system adopted by the writer (see below) allows this exaggeration to be compensated for, and the assumption is probably reasonably well satisfied here also.

(ii) It is assumed that sea level remains constant during the period of the analysis. Small rises or falls in relative mean sea level cause significant changes in the tidal compartment of a shallow estuary, and are of course independent of changes due to net erosion or deposition of sediment. There are few published data on the long-term stability of sea level in the Canterbury area; Lee (1953) has shown a run of mean annual levels from Lyttelton, spanning 23 years (from 1913 to 1936) which indicate that no significant change occurred over that period. Heath (1976) has published results based on a similar run of tide levels, and reached the same conclusions. Thus this assumption appears to be quite reasonable.

(iii) It is assumed also that there are no net changes in non-tidal flows into the estuary over the period considered. Changes in non-tidal inflows are equivalent to sea level changes, as they may alter the net water budget of the estuary, without altering its configuration.

Although some data on non-tidal flows into the estuary are available, no attempts have been made to estimate long-term net changes (Scott, 1963; Mawson, 1972). An assessment of the contribution that changes in non-tidal flows may have made to the post-European budget of the AHE is provided by historic data on inflows from the CDB sewage treatment plant (from Scott, 1963; Knox and Kilner, 1973). In 1929, 8×10^6 gallons/day of treated effluent was discharged (about 0.3% of the tidal compartment, then about 8.8×10^6 m^3), by 1975 this had increased to 30×10^6 gallons/day (or about 0.8% of the 1975 tidal compartment). Changes of this magnitude are probably not significant, and this third assumption appears to be reasonable.

(iv) Finally it is also assumed that no errors in surveying enter the calculations. The possibility that benchmarks may have moved between the 1962 and 1975/77 surveys, introducing widespread constant errors, appears to be slight (J.A. Robb, pers. comm., 1977).

3. Methods used to calculate volumetric changes. Data from the three most reliable surveys were plotted with large vertical exaggeration, the resulting bathymetric profiles (Appendix 2) were subdivided into 40 m sections. The vertical differences between the 1920, 1962 and 1975/77 profiles were measured at the midpoint of each 40 m section. Volumetric changes were calculated by multiplying these vertical differences by 40^2 - the resulting values effectively represent net changes in a series of 40 m^2 cells along each profile. To calculate net losses and gains for the whole estuary, the proportions of cells showing positive, negative or no change were calculated for each survey line, and a strip 100 m wide on either side of each line was subdivided into similar proportions of positive, negative and no change cells, by interpolating blocks of similar cells from line to line (Maps 3 and 4). The values for each 200 m strip were then summed to arrive at the final figures shown in Maps 3 and 4.

4. Results. If the four assumptions are valid, the volumetric changes shown in Maps 3 and 4 are equivalent to changes in the tidal compartment of the AHE. The total figure shown in Map 3, subtracted from the 1962 compartment (Mawson, 1972) gives a 1920 volume of 8.78×10^6 m^3. This represents a mean annual rate of increase of 7×10^4 m^3 for the 42 year period 1920-62. There is a difference of 0.6×10^6 m^3 between this value and the predicted value for 1920

Map 3. Sediment budget, 1920 to 1962.
Lines 2 to 10 only.

▦ Areas of sediment accumulation
  1, 2

▤ Areas of sediment accumulation – in subtidal
  channels infilled between 1920 and 1962
  3, 4

▨ Areas of sediment erosion— representing erosion
  of high-water salt marsh, causing losses of 80cm
  to 105cm of sediment (vertically) in a narrow
  strip along the NW shore of the estuary.

Unmarked squared areas – sediment erosion

Blank (unsquared) areas – subtidal channels

Intertidal volumes of sediment accumulation
  1   52 664m^3
  2   75 216m^3
  3   67 200m^3
  4   14 840m^3

              Total   209 920m^3

Intertidal volumes of sediment erosion
  1 113 321m^3

Nett loss from the intertidal zone   903 401m^3

Subtidal volumes – erosion   163 410m^3
              – deposition   55 047m^3

Nett loss from the subtidal zone   108 363m^3

Overall nett loss
(Between lines 2 and 10 only)   1 011 764m^3

Predicted overall loss, based on the assumption
that the area from lines 2 to 10 is represen-
tative of the whole estuary, and consists of
50% of the whole...
                            2 023 528m^3

Grid is arbitrarily located and aligned north-south, and
covers the same area – at the same scale – as Map 1.

Open arrows show ends of surveyed bathymetric profiles,
small solid arrows and associated thicker black lines
show locations and low tide drainage directions of inter-
tidal channels. See profiles in Appendix 2 for
vertical amounts of erosion and deposition
along individual profiles.

AREA 1

AREA 3

AREA 4

AREA 2

10
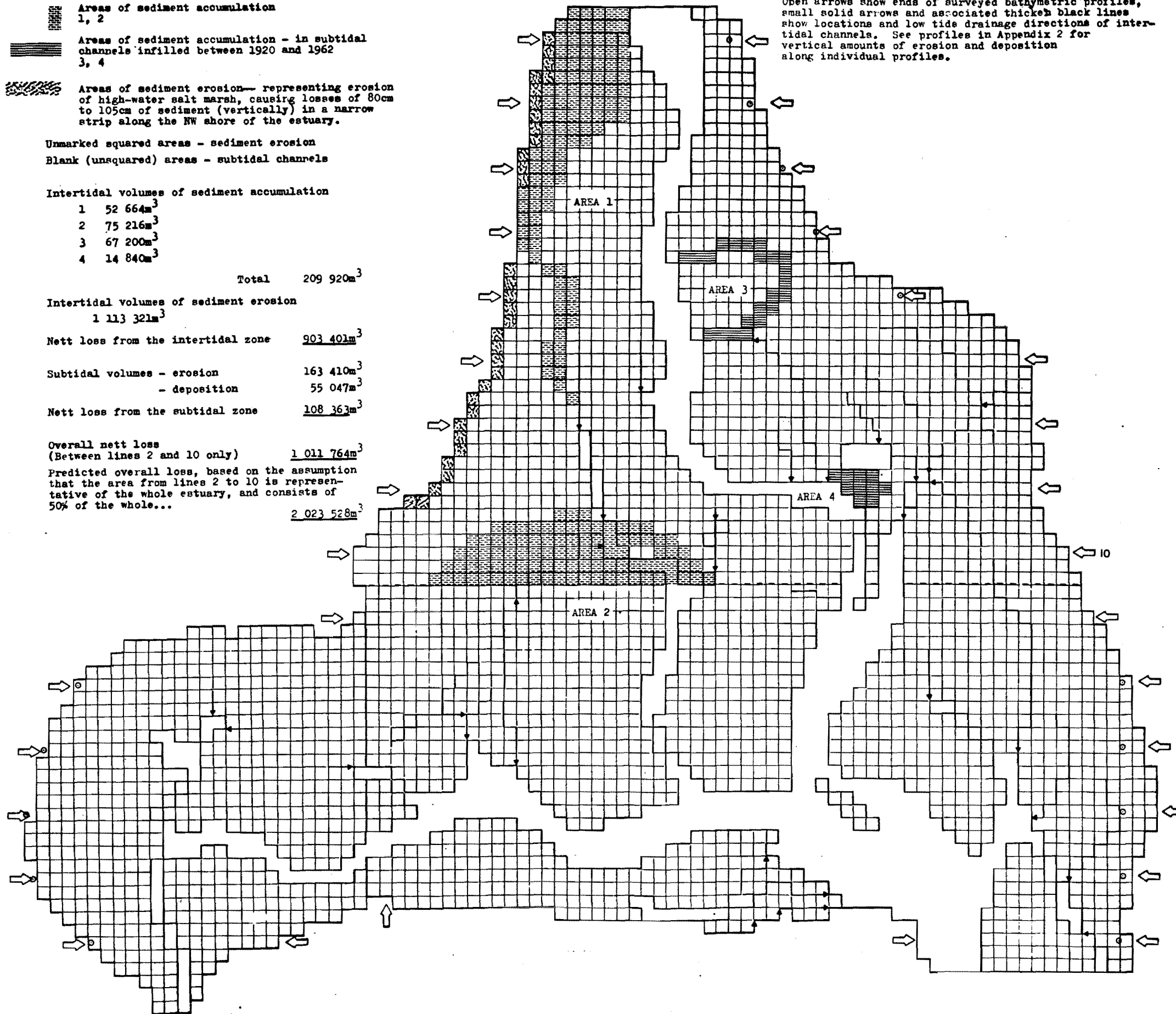
Map 4. Sediment budget, 1962 to 1975/77.

Areas of sediment accumulation
1, 2, 3, .., 8
Unmarked squared areas — sediment erosion

Blank (unsquared) areas — subtidal channels

Intertidal volumes — sediment accumulation

Area 1   6 612m^3

       2   17 400m^3

       3   41 270m^3

       4   99 680m^3

       5   28 236m^3

       6   21 793m^3

       7   6 134m^3

       8   1 706m^3

       plus scattered minor accumulation 5 179m^3

                          Total   228 010m^3

Intertidal volume — sediment erosion 286 178m^3

Nett loss — intertidal zone   58 168m^3

Subtidal volumes — erosion   328 040m^3

                   — deposition   215 872m^3

Nett loss — subtidal zone   112 168m^3

Overall nett loss   170 336m^3

AREA 8

AREA 7

AREA 3

AREA 6

AREA 2

AREA 5

AREA 1

AREA 4
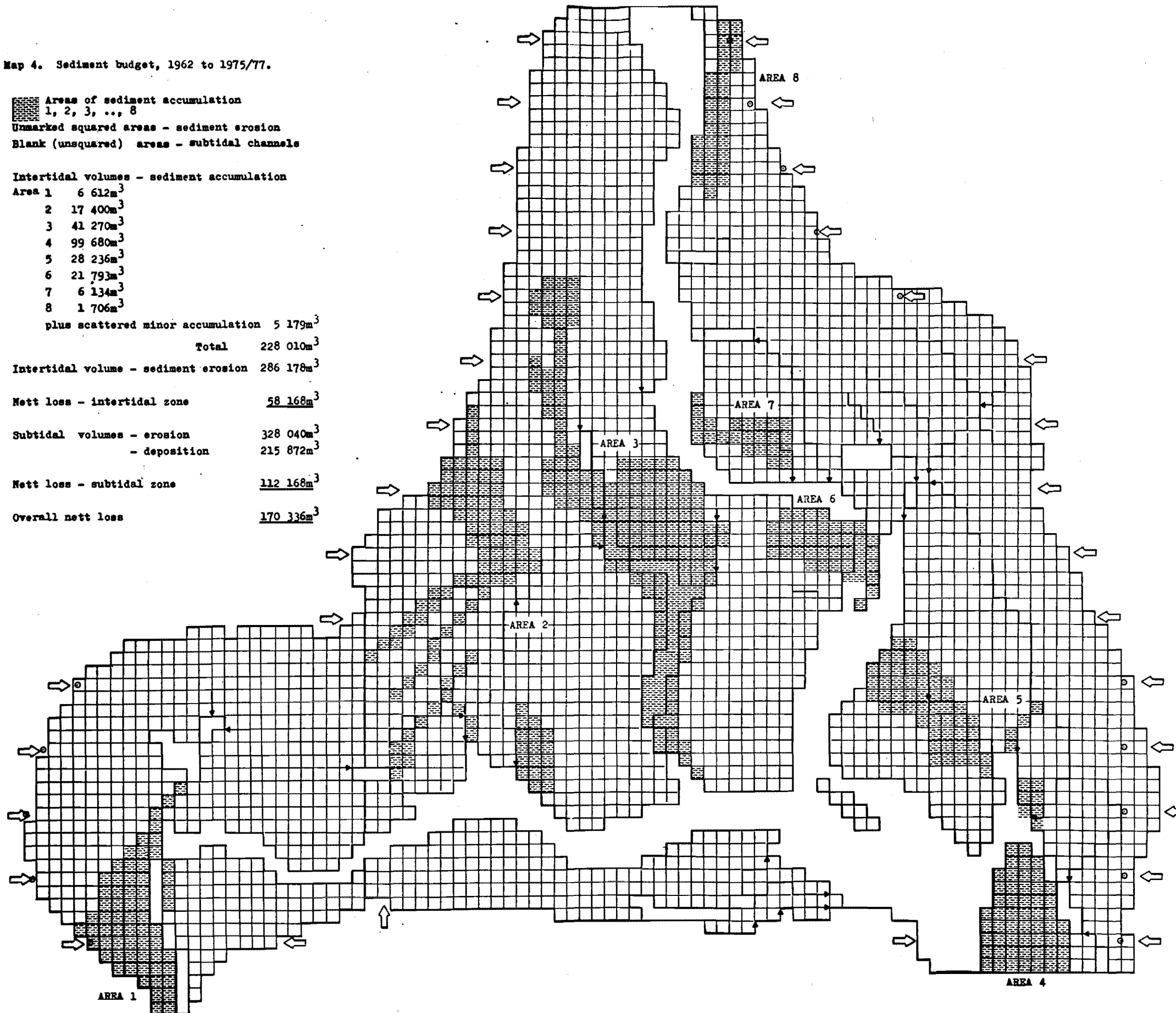
(Figure 79), which is approximately equivalent to the mean annual change for the 42 year period.

Similarly, addition of the net result of the calculations summarised in Map 4 to Mawson's 1962 volume gives a 1975/77 value of 10.93×10^6 m ^{3}, indicating a mean annual increase in the tidal compartment from 1962 to 1977 of about 9×10^3 m^3. For the 55 year period 1920-1975/77, the mean annual increase in the tidal compartment of the AHE was 18.5×10^3 m^3, or 0.34%.

CDB engineers have calculated a net loss of 1.08×10^6 m^3 for the area between lines 2 and 10 (Map 3) for the period 1920-1962 (J.A. Robb, pers. comm.). This is about 6% more than the writer's calculation of 1.01×10^6 m^3. The CDB method was based on a computer technique which integrated the vertical differences between the 1920 and 1962 surveys, and calculated a net change on the unqualified assumption that each line was representative of the 100 m strip either side of it.

Although the CDB method is more precise than the writer's, it is likely to be less accurate, since it fails to account for the exaggerations caused when survey lines cross steep-sided subtidal channels at low angles (see profiles 14 and 15 in Appendix 2).

Appendix 2. Bathymorphic profiles surveyed in 1920, 1962, and 1975/77.
Annotations show profile numbers (2 to 15), profile origins (W) and
profile ends (E). Arrows show profiles completed on a following page
(�⟩), or continued from a previous page (🔲⟩). Crosses are at 9.0m
HAD, and are spaced 100m apart. Vertical scale is indicated along the
right margin, in metres HAD.
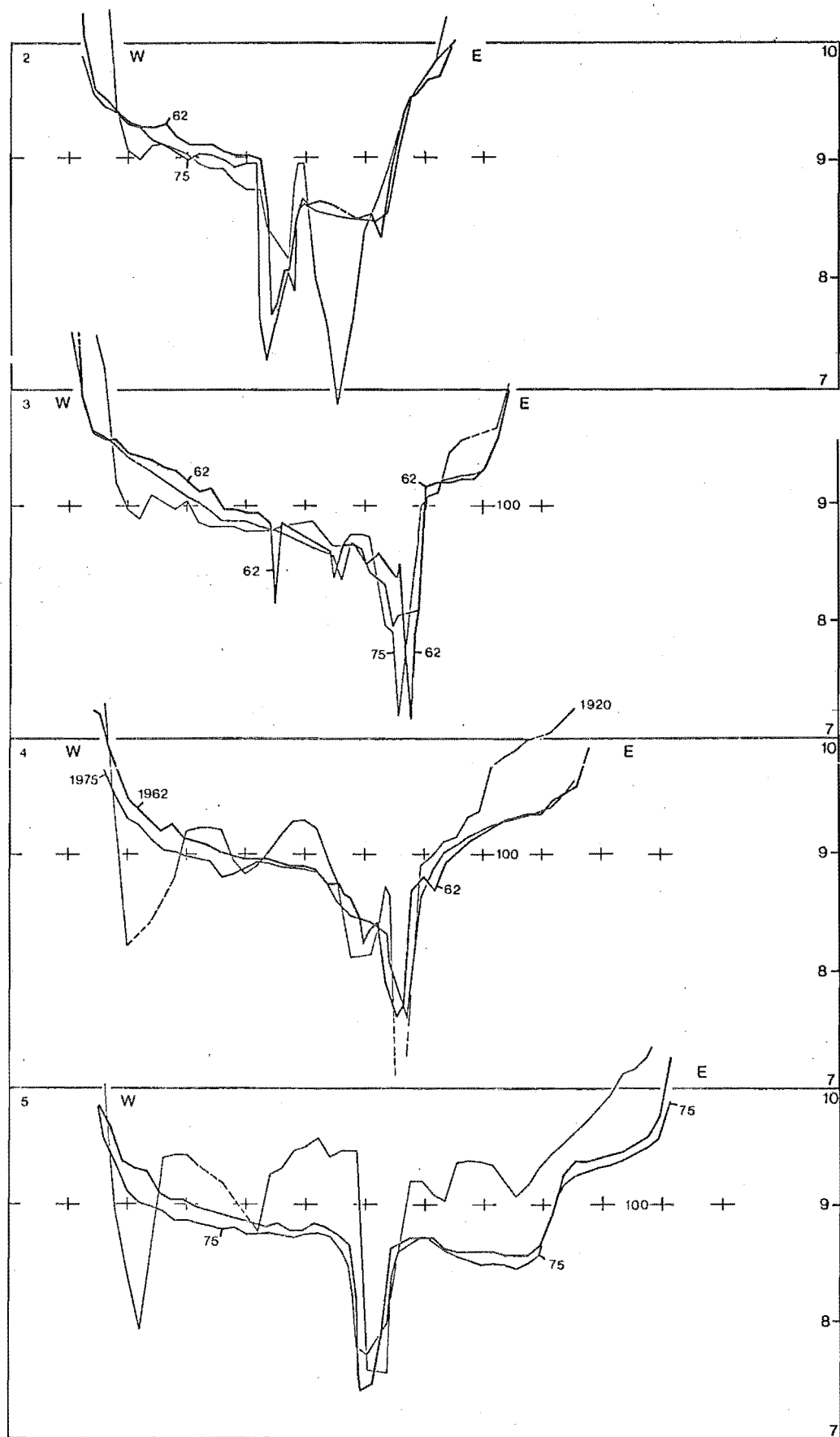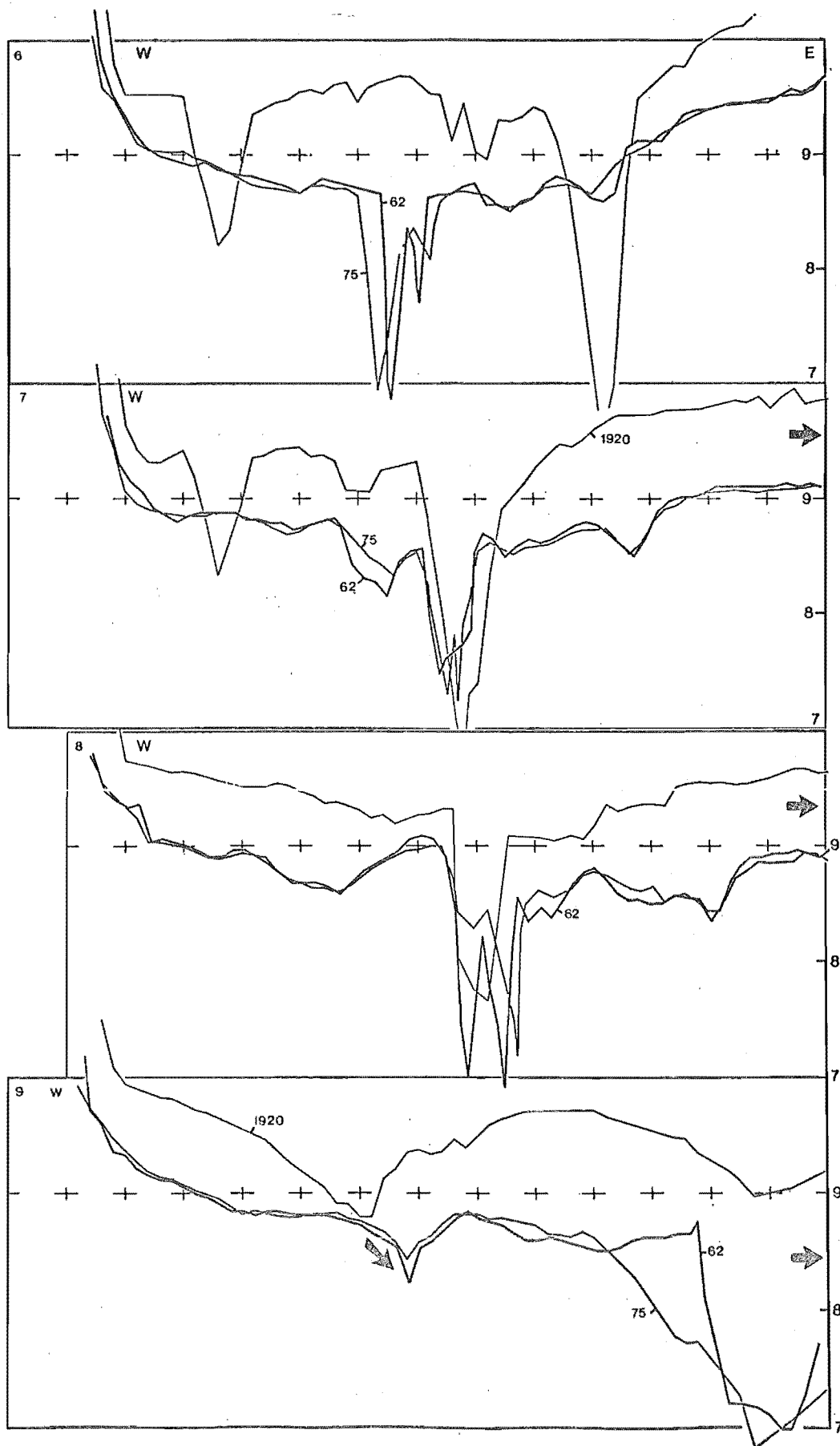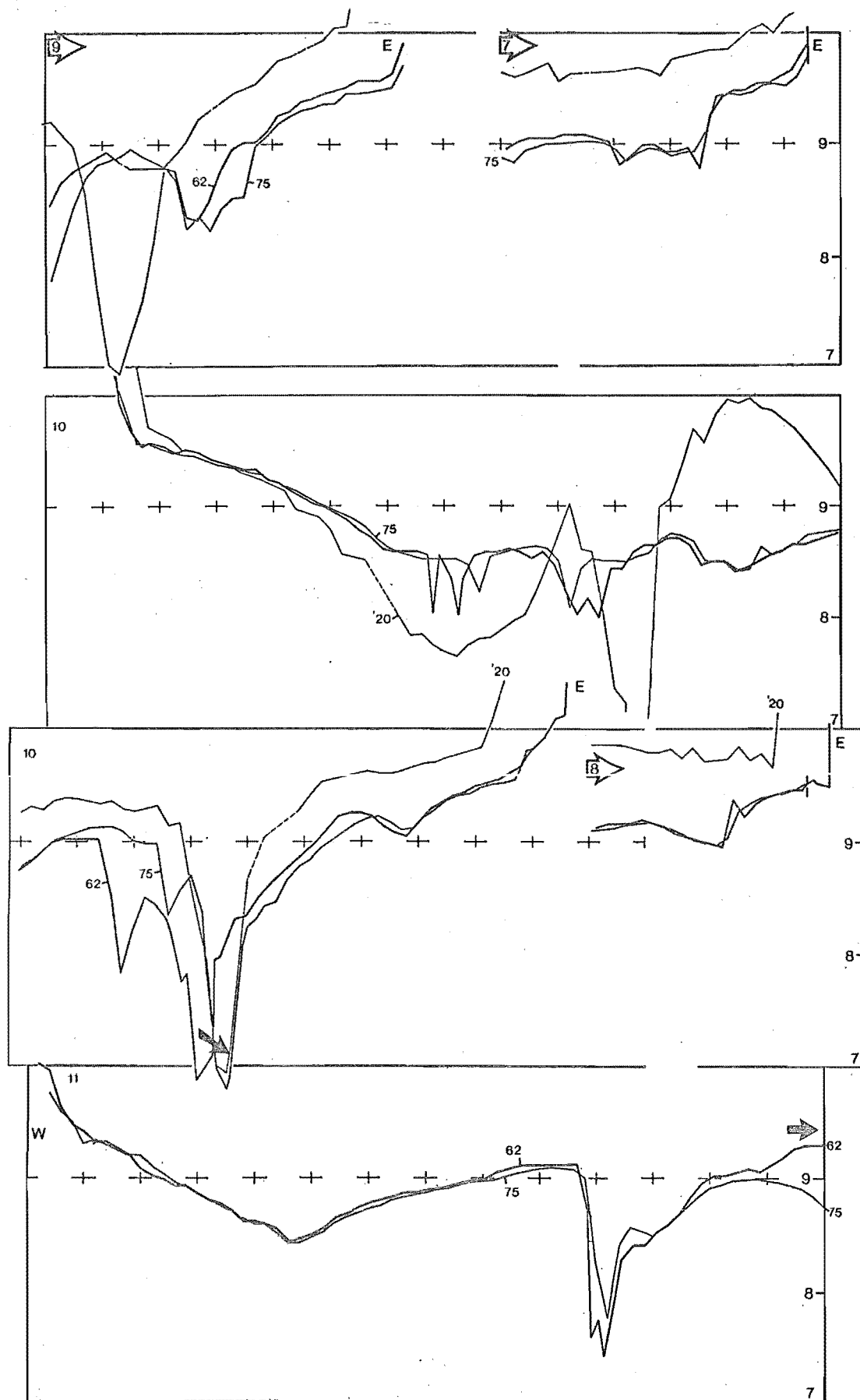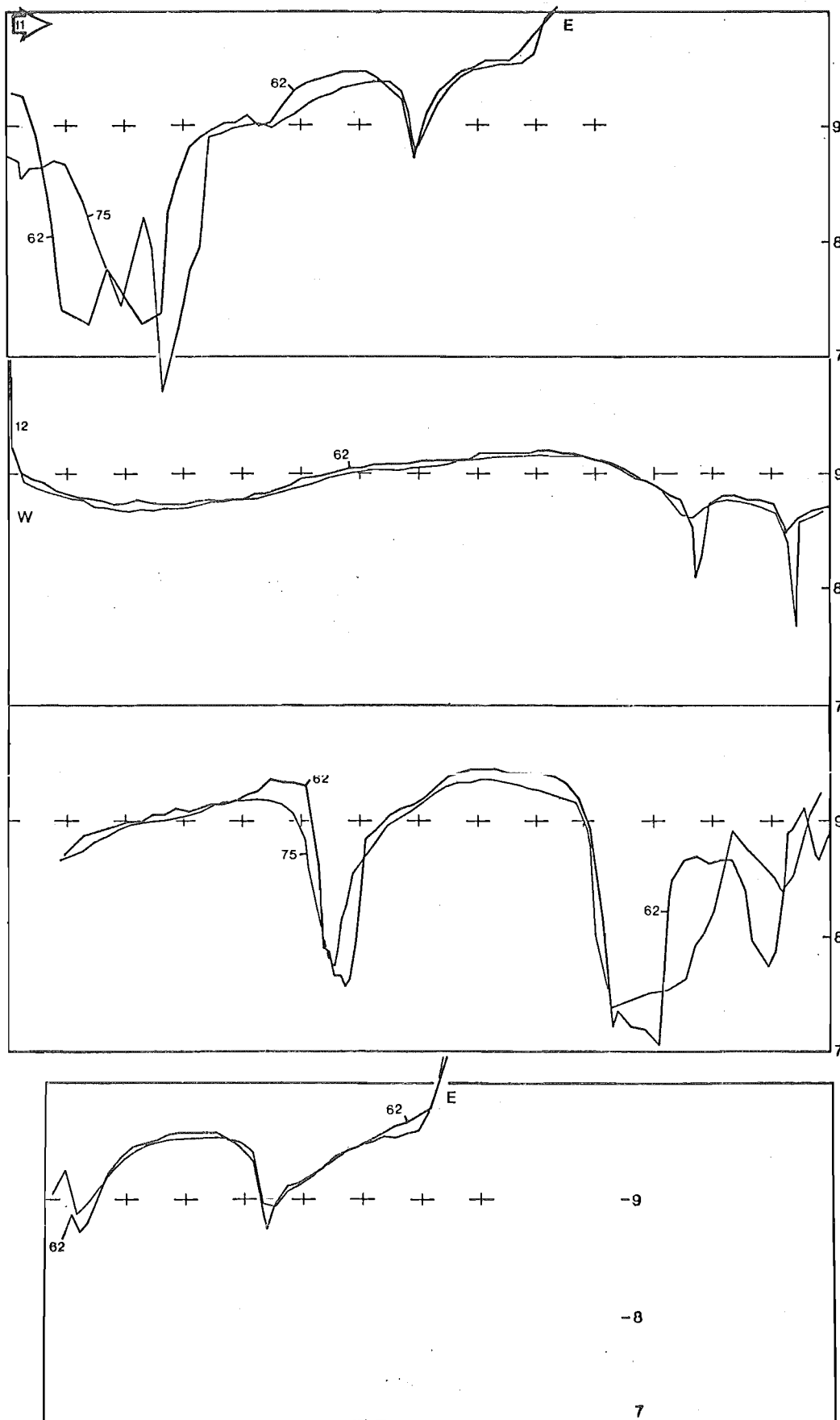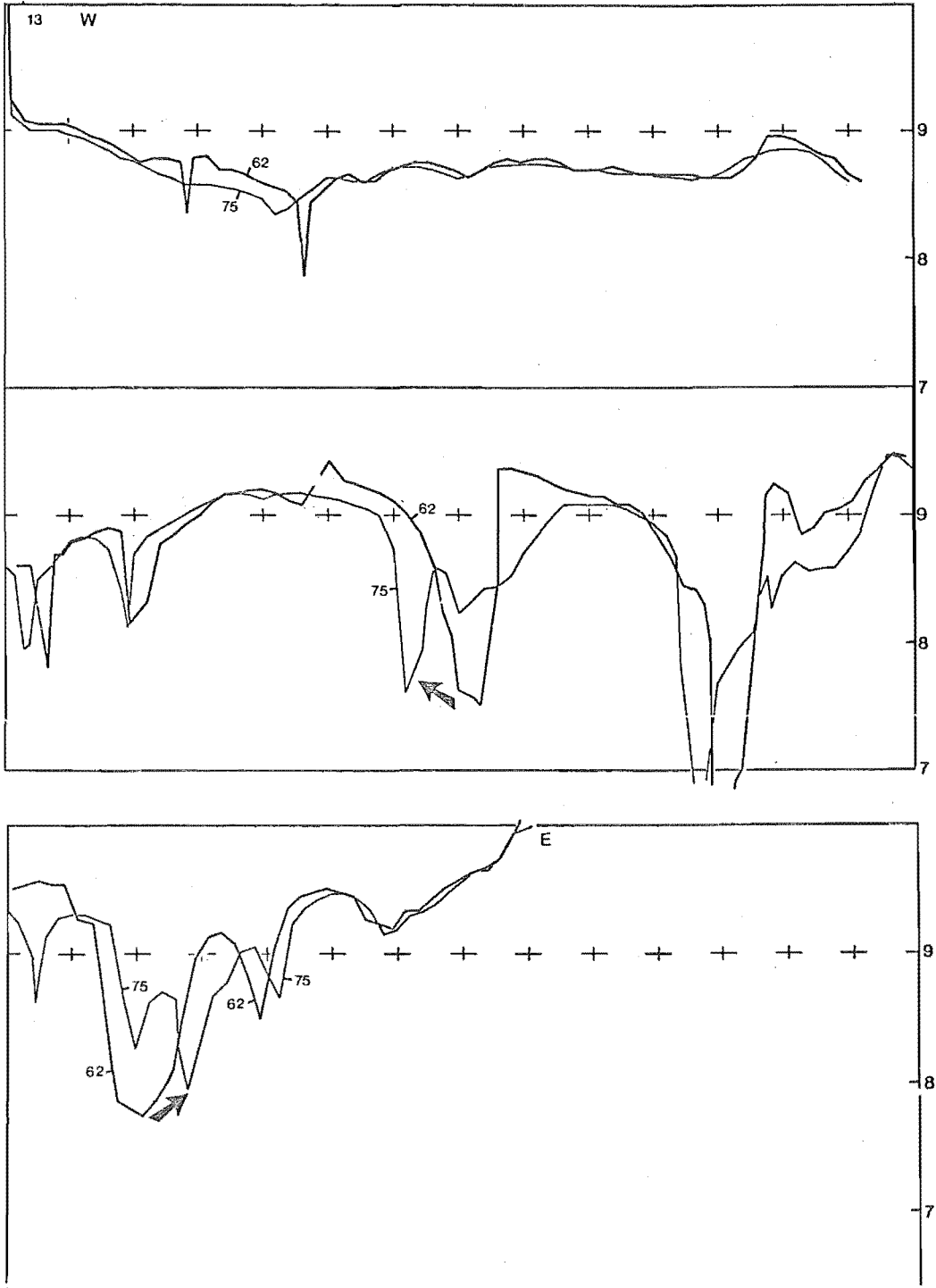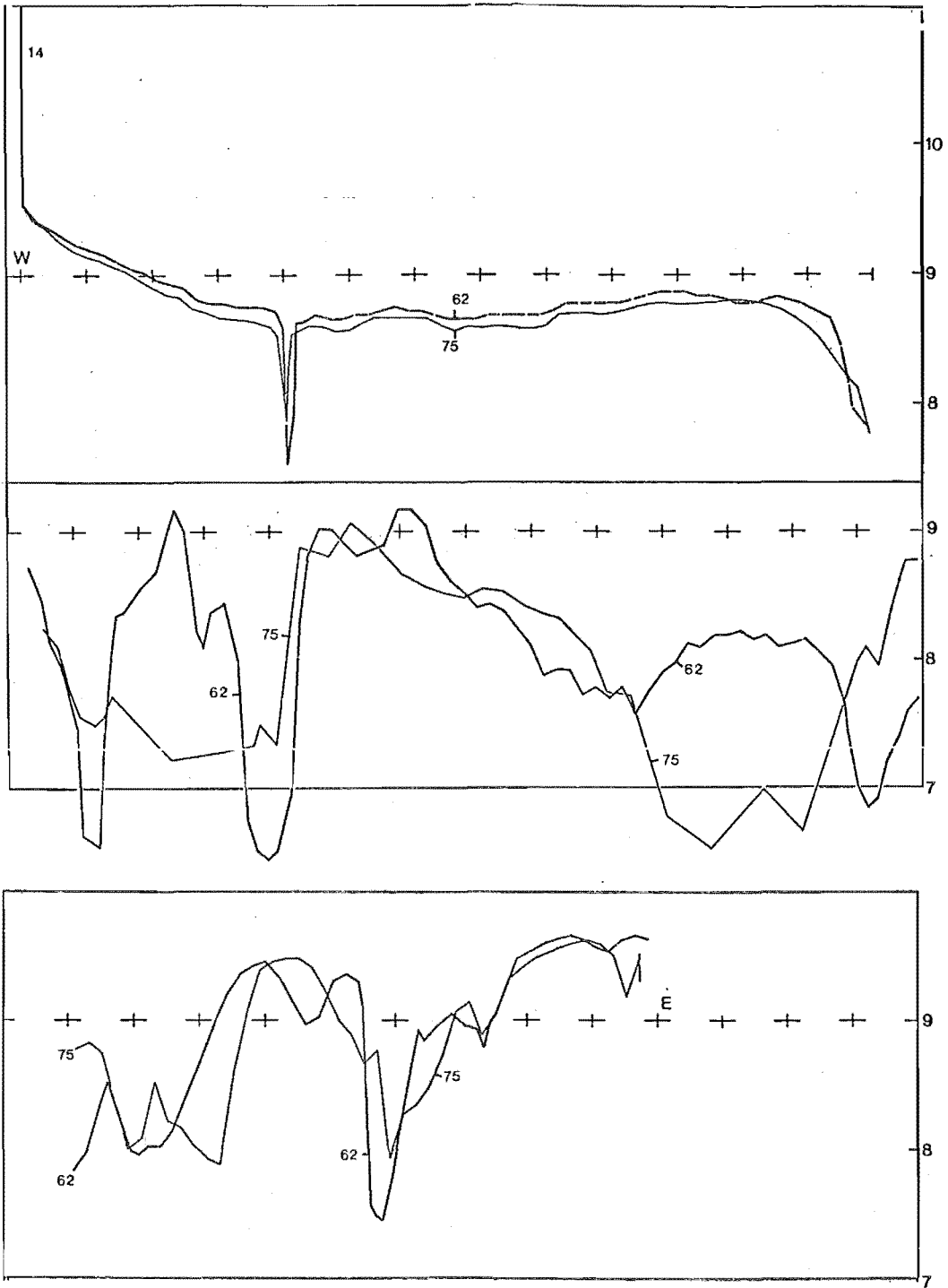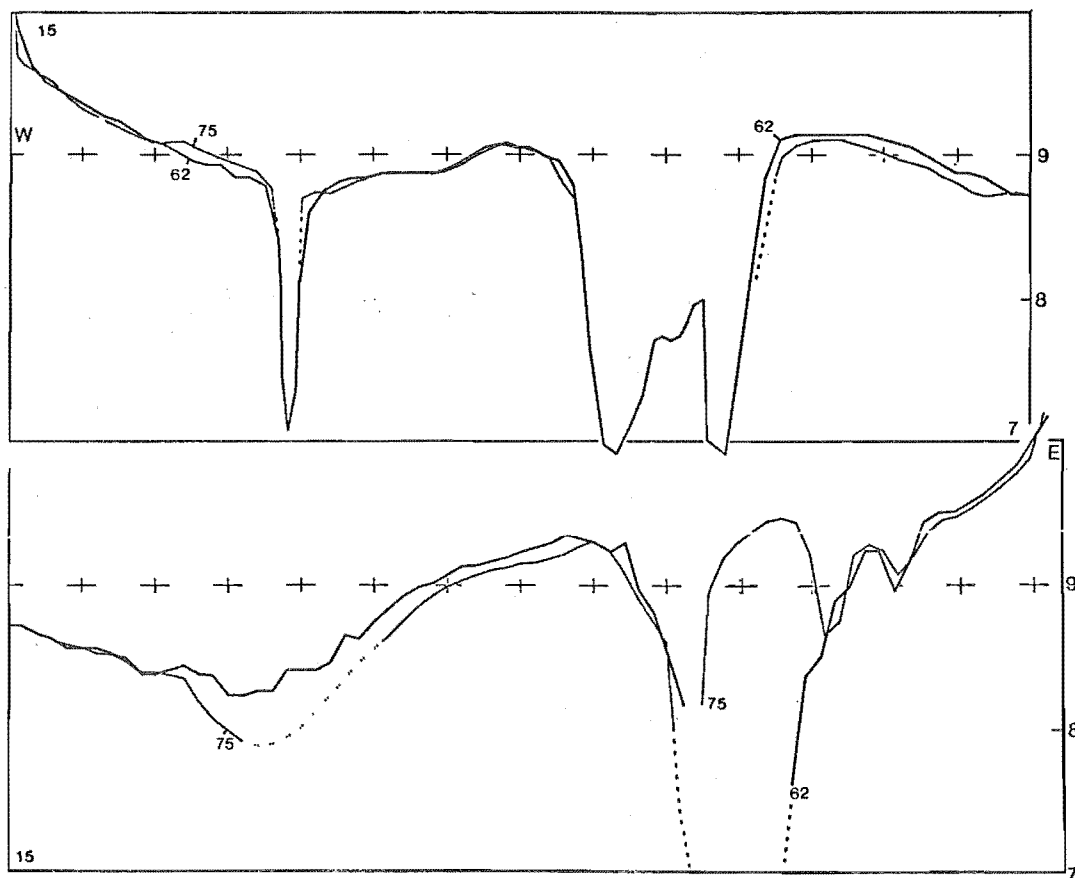
APPENDIX 3

Surface and subsurface sediment analyses. Methods and procedures.

1. Sampling design. A problem often experienced in exploratory field studies is the difficulty of estimating an optimum sampling design – one which yields maximum information for minimum effort. Since trends in sediment properties in the AHE were originally unknown, an extensive and dense sample collection was attempted.

A separate problem involves the statistical validity of sampling plans. In this study no attempt has been made to randomise the sampling design, for two reasons:

(i) The number of random samples needed to adequately represent all bathymetric subenvironments would have been prohibitively large, and the sampling design would have been unwieldy.

(ii) The CDB survey network was partly completed, and marked at convenient intervals with semi-permanent markers, before sampling began. The benefits of using these fixed sites, which could be resampled or revisited for other purposes, outweighed the theoretical benefits of a random design (Cockran and others, 1954). Unwitting bias was eliminated as much as possible by sampling only at peg locations, or at multiples of 20 m between pegs.

2. Sampling methods. If substrate properties are to be used as environmental monitors, then sample collection techniques are critically important. That no amount of analytical effort will extract meaningful results from meaningless samples is a truism apparently ignored by many recent workers (Macpherson and Lewis, in prep., 1978).

Early observations indicated that the upper few centimetres of sediment on the intertidal flats of the AHE was highly variable – sometimes massive, sometimes stratified – and almost always inhabited by a variety of benthic animals. Recognition of widespread erosion also lead to the possibility that surface sediment properties might be inherited from older sediment, and not be related to modern processes. Methods which ignored the potentially complex and polygenetic nature of this sediment would be unlikely to provide environmentally meaningful information – worse, they might be seriously misleading.

The sampling problem was tackled by assuming that there was an uppermost layer of sediment, perhaps a few grain diameters to a few centimetres thick, which was available to be modified by contemporary processes, and which owed its characteristics to those processes - in other words, that there might be an uppermost layer with the properties of a sedimentation unit (Otto, 1938; Jopling, 1964). This assumption is examined and justified in Part Five.

This uppermost layer, appropriately termed the active layer - was sampled with a soft flexible spatula (various plastic kitchen tools are suitable) by carefully scraping off the soft, unconsolidated surface sediment at each site. This method was used consistently throughout. Usually a sample of about $10 \times 10\,cm \times 1-2\,mm$ was collected, and stored in a plastic bag until analysed in the laboratory.

Samples stored in plastic bags were usually analysed within 48 hours of arriving in the laboratory. About 30 g - 50 g of each sample was wet sieved through +0.5 phi (0.7 mm) and -4.0 phi (0.0625 mm) screens, and the fraction coarser than +0.5 phi (living animals, whole shells, coarse shelly and other organic debris) was discarded.

All material passing through the 4.0 phi sieve was collected, made up to 1L, stirred vigorously, and a 20 ml aliquot was taken immediately and pipetted into a preweighed 50 ml beaker. After oven drying and cooling to room temperature, this weight of material ($\times$ 50) was accepted as the weight of mud in the original sample. Included in this figure was any salt or other dissolved solids in the sample, as well as organic material, dissolved organic material, and so on.

The sand fraction (all the material caught on the 4.0 phi sieve) was washed into preweighed 200 ml beakers, oven dried at 35-45°C, allowed to cool to room temperature and weighed. Sand and mud weights were combined to produce a total sediment weight, and per cent mud was calculated.

The dry sand was thoroughly mixed, and about 2 g extracted with a small spoon and poured into a screw-top plastic container, to make up a subsample with a weight of 2.0 ± 0.1 g. This subsample was used for subsequent RSA analysis.

The RSA used for this project has a perspex settling tube with a fall distance of 1 m, and an internal diameter of 12.7 cm (5 inches).

Recorder output consisted of a cumulative differential pressure vs time curve, traced on to squared paper as the sand grains settled past a transducer port, 1 m below the top of the tube.

From the instrument curve, elapsed times corresponding to the 95th, 84th, 75th, 50th, 25th, 16th and 5th percentiles were read off (the input percentiles for Folk and Ward graphic statistics), recalculated as settling velocities, and converted to sedimentation diameters using the data of Gibbs and others (1971).

Finally the percentile data were coded on to punched cards, and graphic statistics were calculated by the University of Canterbury Burroughs B6700 computer.

3. *Sand vs Mud*. The widely held belief that the best sediment samples are those collected from single, homogeneous sedimentation units is well supported by theoretical and experimental evidence (Otto, 1938; Apfel, 1938; Griffiths, 1962; Erlich, 1964; Jopling, 1964). Samples which amalgamate more than one such unit may contain material deposited under different physical conditions, and yield results not amenable to sensible interpretation. Yet it is still apparently common to assume that useful data can be obtained from sediment size analyses which amalgamate results of separate mud and sand size analyses - in spite of the common awareness that sand and mud are transported and deposited in different ways, and according to different physical laws.

The principal reason for considering the sand and mud fractions of a sediment as separate sedimentation units is the common observation that fine particles are almost always aggregated into larger, composite particles in nature (Kranck, 1975; Drake, 1975). Aggregate grains do not fulfil the requirements of Stokes' Law - the theoretical basis of most laboratory procedures for the size analysis of fine sediment - because they are frequently not rigid, smooth, spherical, or inelastic (Galehouse, 1971). On deposition individual aggregates will probably lose their identity; when sampled and subjected to normal laboratory procedures they almost certainly will (Kranck, 1975). And finally - as Folk (1968) has pointed out - measurements of size distributions of fine sediment may only be an indication of the efficiency of a particular dispersal technique.

In the present project 'size' analyses of surface mud were not attempted - only the total amount of mud (as defined above) was routinely determined.

4. *Sand fraction analyses by sedimentation*. Two methods are available for the size analyses of sandy sediment; sieving, and

sedimentation. Sieving separates grains according to their least cross-sectional area (Galehouse, 1971), however the behaviour of sand grains in water is a function of their volume, density, roundness and spericity. Sedimentation analyses are the only sizing techniques which take all four of these factors into account. Considering the intentions of the present study, a sedimentation method was chosen, and a Woods Hole-type Rapid Sediment Analyser (RSA) manufactured by Pelagic Instruments Inc., and owned by the Department of Geography, University of Canterbury, was used for all routine size analyses.

The particular advantages of an RSA as an analytical tool are that it is rapid, seldom requiring more than 10 minutes/sample, it is precise and accurate - replicates exhibit high reproduceability; and it provides a continuous record of size distributions, allowing fine subdivisions. Disadvantages include difficulties associated with converting settling velocities to equivalent diameters, comparing settling and sieved analyses, the under-representation of the tails of size distributions by sedimentation methods, and technical problems involving the introduction of samples into the water column. For examples see Emery (1938), Doeglas (1946), Poole (1957), Zeigler and others (1960), Schlee (1966), Bascomb (1968), Felix (1969), Nelson (1976) and Channon (19). Emery (1938), Schlee (1966), Sengupta and Veenstra (1968), Sandford and Swift (1971) and Reed and others (1975) have compared sieving and settling techniques using a variety of settling devices. Reed and others in particular found systematic and sometimes spectacular differences in grain size distributions derived from the two different methods. They attributed these to "...subtle variations in sorting with grain size, the result of an interplay between mineralogic composition and size...".

In the present study a small number of samples were both sieved and analysed with the RSA, and representative cumulative curves are shown in Figure 80. Here it can be seen that the two methods do give quite different results. In Figure 81, equivalent properties are plotted against one another, and the results mean that sieving will indicate sediment from the AHE is finer, better sorted if well sorted, poorer sorted if poorly sorted, more negatively skewed, and more leptokurtic than RSA analysis would indicate. Notice also that it is at the fine end of the curves (near 95%) that most differences occur.

There are three approaches to the problem of converting settling velocities to equivalent diameters. The first is to establish an
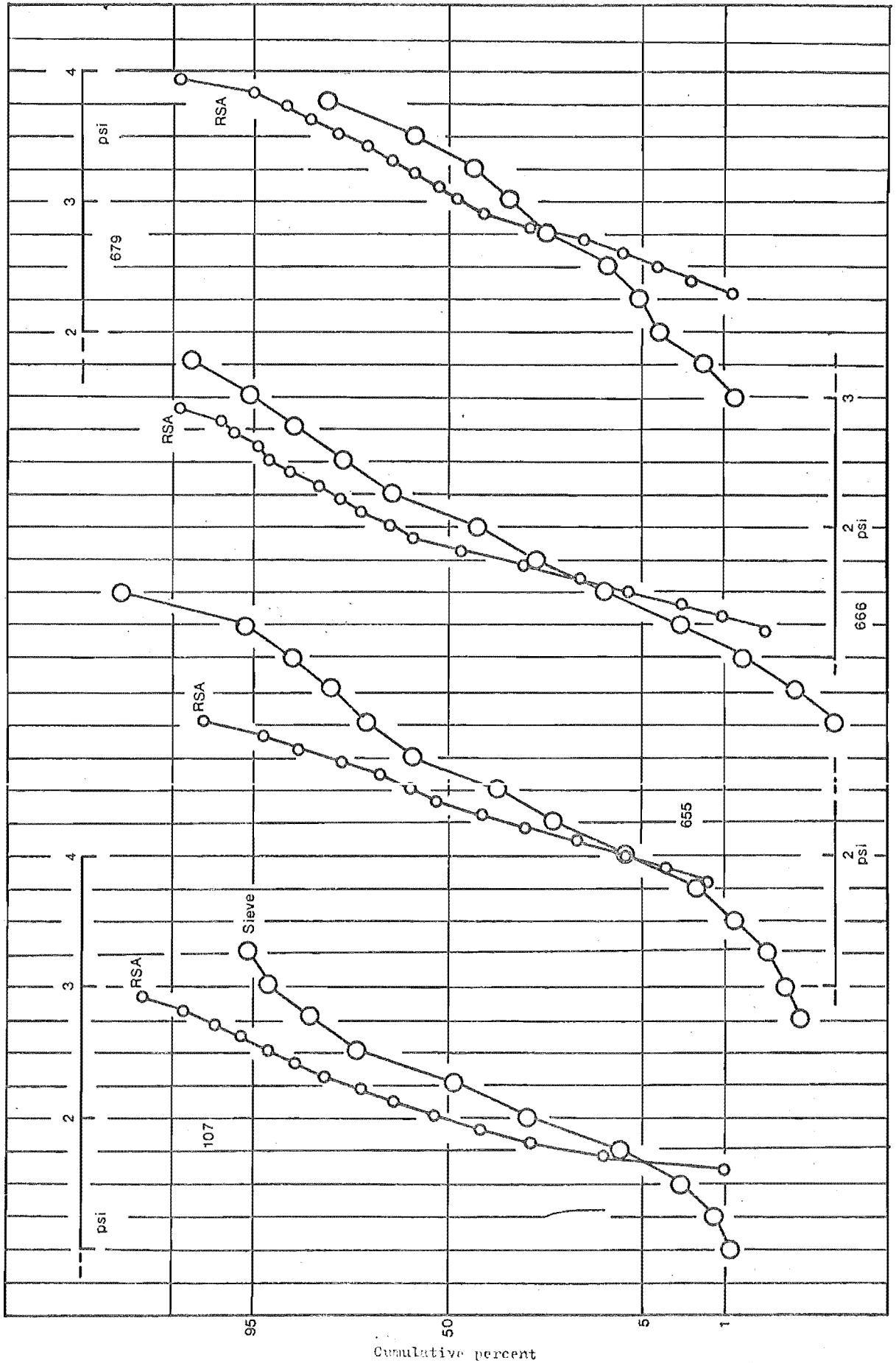
Figure 80. Comparison of cumulative probability curves of four representative sand fractions of samples from the Avon-Heathcote Estuary. Large circles are 0.25phi data points from sieve analyses, small circles are 0.1psi data points from RSA analyses.
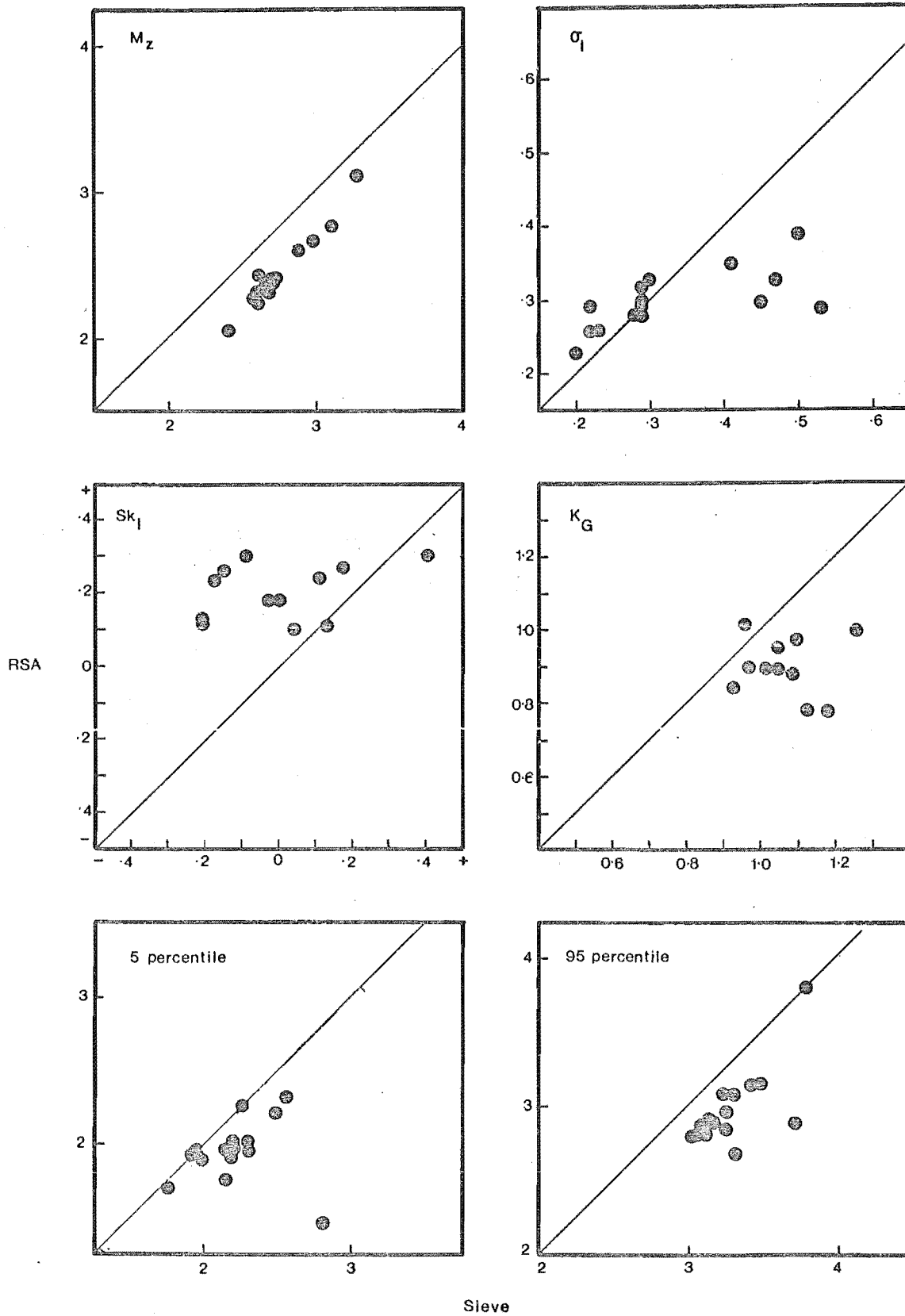
Figure 81. Scatter plots of sieve vs RSA size analyses.

apparatus-specific relationship by calibrating an instrument against particles of known sizes (Gibbs and others, 1971; Nelson, 1976).

The second approach is to convert measured fall velocities to equivalent diameters using standard relationships. Gibbs and others (1971) have published a standard settling velocity equation, derived from exhaustive experimental work, and tables of data from Gibbs and others were used in the present project to construct a standard calibration curve relating fall velocity to sedimentation diameter. *Sedimentation diameter* is defined as the diameter of a glass sphere having the same settling velocity as a natural particle. The standard curve used in the present project is filed with other supplementary material in the Department of Geology library.

A third approach is simply to express results as fall velocities. This idea is intuitively attractive, but suffers from the major disadvantage that geologists are accustomed to describing sediments in terms of grain size, not cm/second.

5. Reproducibility and reliability. The reproduceability of the analytical method for sediment muddiness was checked by taking 24×20 mℓ aliquots from a 1L cylinder and treating each as a normal subsample. Per cent mud values were calculated, giving a mean of 21.13% and a standard deviation of 0.16%. This indicates that differences greater than 0.64% mud ($\pm$ 2 standard deviations) have a probability of at least 95% of not being due to experimental error.

Although other workers have claimed that settling tubes are capable of giving results of reasonably high reliability, for example Schlee and others (1965), a simple reproduceability test was completed to ensure that the instrument used in the present study was behaving adequately. The sand fraction of sample 539 was split into $31 \times 2.0 \pm 0.1$ g subsamples, and these were run in sequence through the RSA. Figure 82 shows means and standard deviations calculated for percentile input data, and graphic statistics calculated from analyses of each of the 31 subsamples. The variability in the data of Figure 82 is an indication of the amount of experimental error likely to be introduced in the laboratory in the present study. Within the input data, extreme values (psi 5 and psi 95) have highest variability (largest standard deviations); within the graphic statistics sorting is least variable, kurtosis is most variable.

Sample	psi 1	Mean diameter	Standard deviation	Skewness	Kurtosis	psi 5	psi 16	psi 25	psi 50	psi 75	psi 84	psi 95
539 1 F	1.81	2.33	0.27	0.18	0.91	1.93	2.06	2.12	2.29	2.51	2.63	2.80
539 2 I	1.71	2.28	0.28	0.18	0.91	1.87	2.01	2.07	2.24	2.46	2.59	2.74
539 3 R	1.71	2.31	0.29	0.12	0.99	1.86	2.03	2.10	2.29	2.50	2.62	2.83
539 4 S	1.79	2.30	0.28	0.18	0.94	1.91	2.03	2.11	2.27	2.50	2.61	2.80
539 5 T	1.81	2.27	0.23	0.07	0.96	1.93	2.04	2.11	2.27	2.44	2.51	2.70
539 6	1.69	2.27	0.26	0.19	1.06	1.86	2.03	2.09	2.23	2.43	2.55	2.74
539 7 C	1.71	2.25	0.28	0.15	1.08	1.82	1.99	2.06	2.22	2.41	2.54	2.74
539 8 O	1.69	2.29	0.28	0.16	1.00	1.87	2.03	2.09	2.26	2.46	2.59	2.77
539 9 L	1.70	2.24	0.25	0.09	1.00	1.84	2.00	2.06	2.22	2.40	2.49	2.67
539 10U	1.67	2.28	0.26	0.07	0.97	1.87	2.03	2.10	2.27	2.46	2.55	2.72
539 11M	1.76	2.27	0.25	0.06	1.02	1.87	2.03	2.10	2.26	2.43	2.52	2.69
539 12N	1.67	2.24	0.28	0.08	1.11	1.82	1.97	2.06	2.23	2.40	2.52	2.74
539 13	1.66	2.24	0.23	0.18	0.95	1.86	1.97	2.03	2.21	2.41	2.54	2.74
539 14P	1.66	2.22	0.28	0.09	1.07	1.77	1.94	2.03	2.20	2.39	2.51	2.71
539 15S	1.72	2.25	0.28	0.17	0.95	1.86	1.97	2.05	2.22	2.43	2.56	2.74
539 16T	1.57	2.23	0.29	0.16	1.10	1.77	1.96	2.04	2.19	2.40	2.53	2.74
539 17	1.57	2.21	0.27	0.14	1.12	1.77	1.96	2.04	2.18	2.38	2.49	2.70
539 18O	1.68	2.28	0.28	0.12	0.93	1.85	2.01	2.07	2.26	2.43	2.58	2.78
539 19N	1.66	2.23	0.27	0.10	1.04	1.82	1.98	2.05	2.22	2.42	2.49	2.76
539 20C	1.72	2.26	0.27	0.17	1.03	1.87	2.00	2.07	2.23	2.42	2.55	2.75
539 21	1.72	2.28	0.28	0.19	1.04	1.87	2.01	2.09	2.24	2.44	2.57	2.76
539 22	1.63	2.26	0.32	0.08	1.10	1.79	1.94	2.07	2.25	2.46	2.58	2.84
539 23	1.60	2.26	0.28	0.09	0.99	1.81	1.99	2.07	2.24	2.45	2.55	2.73
539 24	1.55	2.26	0.27	0.09	1.00	1.81	2.00	2.07	2.24	2.44	2.55	2.71
539 25	1.70	2.23	0.23	-0.01	1.11	1.85	2.00	2.07	2.23	2.35	2.45	2.61
539 26	1.52	2.21	0.31	0.13	1.09	1.71	1.92	2.01	2.18	2.41	2.53	2.76
539 27	1.72	2.27	0.26	0.07	1.08	1.87	2.01	2.10	2.26	2.42	2.55	2.71
539 28	1.60	2.25	0.29	0.08	1.09	1.78	1.97	2.06	2.23	2.42	2.54	2.74
539 29	1.66	2.25	0.27	0.17	1.08	1.84	2.00	2.06	2.22	2.41	2.53	2.76
539 30	1.61	2.22	0.26	0.13	1.08	1.80	1.90	2.05	2.19	2.38	2.48	2.67
539 31	1.77	2.24	0.28	0.21	0.99	1.85	1.99	2.05	2.21	2.44	2.53	2.79

Column statistics:

psi 1

Mean diameter, $X = 2.26$ psi, $s = 0.03$ psi.

Standard deviation, $X = 0.27$ psi, $s = 0.02$ psi.

Skewness, $X = 0.13$, $s = 0.05$.

Kurtosis, $X = 1.03$, $s = 0.06$

psi 5, $X = 1.84$, $s = 0.05$

psi 16, $X = 2.00$, $s = 0.03$

psi 25, $X = 2.07$, $s = 0.03$

psi 50, $X = 2.23$, $s = 0.03$

psi 75, $X = 2.43$, $s = 0.04$

psi 84, $X = 2.54$, $s = 0.04$

psi 95, $X = 2.74$, $s = 0.05$

Figure 82. Replication exercise. Results of analyses of 31 subsamples of 539.

These results mean that differences in mean diameter greater than 0.12 psi (± 2 s) have a probability of at least 95% of not being due to experimental error. For sorting the figure is 0.08 psi, for skewness it is 0.20, and for kurtosis 0.24. These results are within the limits accepted as reasonable in experimental analyses of sediment (Folk, 1955; Rogers, 1965).

It is also instructive to examine the nature of variability at the sample site. Since exact replication of samples is not possible, the next best option is to collect a number of closely spaced samples, and test them for variability. This was done at the east end of line 9 (Map 1), where 25 samples were collected, beginning at a peg of 9.70 m HAD and progressing west. Samples were 1 m × 5 cm × 1-2 mm in size, so that a 25 m strip of the estuary bottom was continuously sampled (samples 688-712). Results are shown in Figures 83 and 84.

Figure 84 is a stack of histograms, where percentiles at 0.1 psi intervals are plotted from sample midpoint to midpoint. For example the top line in Figure 84 shows the percentage value of the 1.8 psi percentile from each analysis. A surprising result is the uniformity of the extreme values in the 25 samples, and the variability of midrange values. From sample to sample the coarse tail in particular is remarkably uniform (about 1-2% of sediment is consistently coarser than 1.8 psi). Compare this to the amount of material coarser than 2.40 psi, which varies from about 40% to about 70%. Slight variations in skewness (displacement of the mode from the mean) produce this pattern, and the effect is exaggerated because these samples are so well sorted - there is a particularly close grouping around central values.

Figure 84 also reveals that there may be two separate sand populations present in the 25 m run, represented by samples 688-700 vs 701-713. This possibility provided an opportunity to test the levels of significance established above. Mean values and standard deviations for each sample group are shown in Figure 84B, where histograms of sample graphic statistics also indicate the possible presence of the two sand populations.

The difference between the two mean diameters is 0.07 psi, and from above, this is clearly not significant. Similarly for sorting, the difference is 0.04 psi, and this is not significant. Notice that the variations in graphic values in Figure 84 are less than the variations in Figure 82. In other words the variation along this 25 m run was less than the variation expected from experimental error, and a
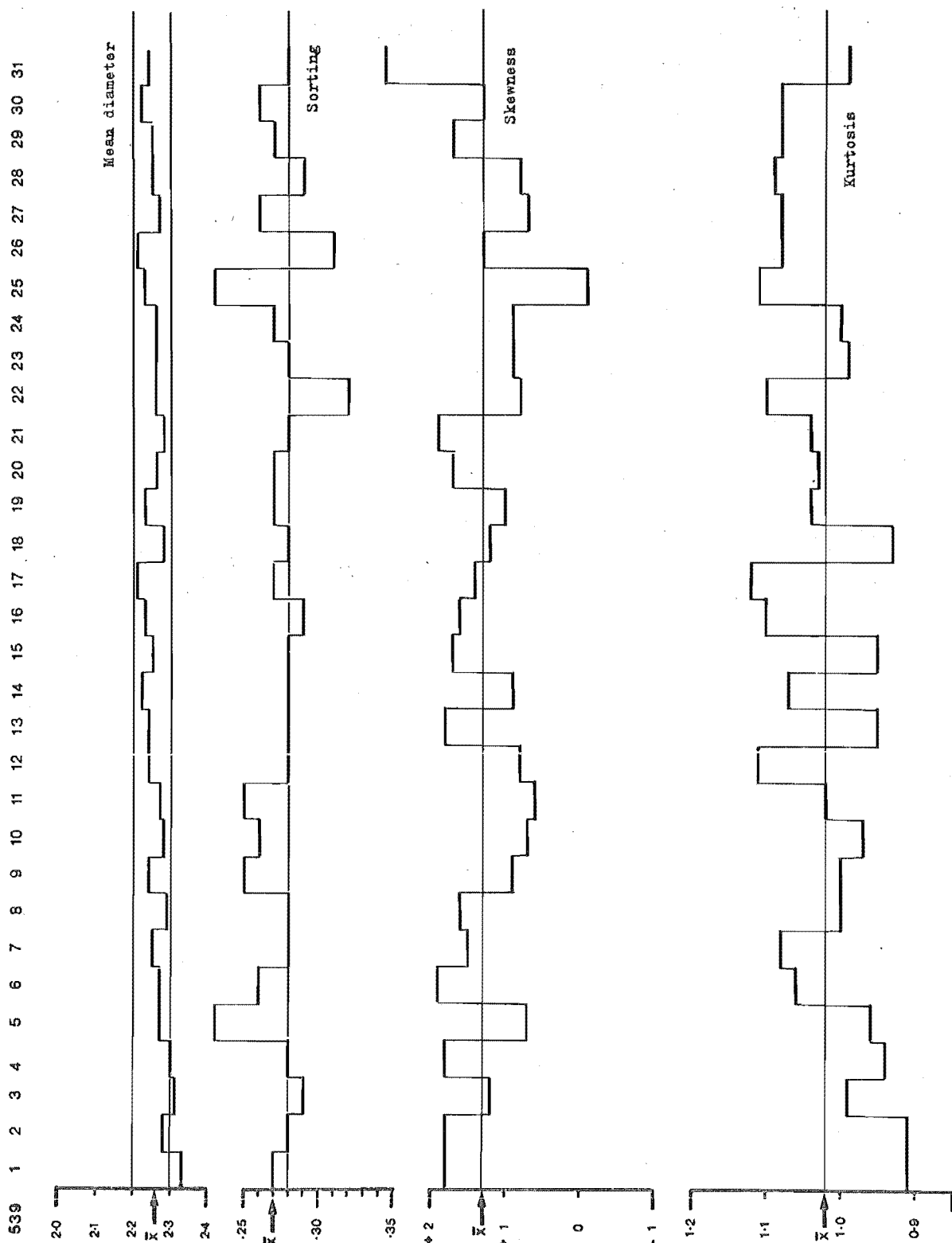
Figure 83. Replication exercise. Sequential variations in mean diameter, graphic standard deviation (sorting), skewness and kurtosis of 31 subsamples of sample 539, run in the sequence 1-31. Data from Figure 33.

Graphic statistics and input data

Sample number	Mean diameter	Standard deviation	Skewness	Kurtosis	psi 5	psi 16	psi 25	psi 50	psi 75	psi 84	psi 95
688	2.51	0.26	0.19	0.99	2.13	2.27	2.33	2.48	2.69	2.78	3.00
689	2.40	0.26	0.17	0.96	2.02	2.15	2.22	2.37	2.58	2.64	2.86
690	2.39	0.29	0.04	1.23	1.85	2.13	2.22	2.37	2.56	2.66	2.87
691	2.40	0.24	0.13	1.04	2.02	2.18	2.24	2.38	2.56	2.65	2.83
692	2.37	0.27	0.07	1.13	1.89	2.13	2.20	2.35	2.54	2.63	2.83
693	2.41	0.26	0.15	1.12	1.93	2.20	2.22	2.37	2.56	2.64	2.86
694	2.42	0.25	0.10	1.08	2.01	2.19	2.26	2.40	2.55	2.67	2.85
695	2.39	0.24	0.22	1.12	2.02	2.18	2.24	2.35	2.54	2.63	2.84
696	2.40	0.27	0.34	1.17	1.98	2.16	2.22	2.35	2.55	2.68	2.92
697	2.39	0.28	0.16	1.10	1.95	2.13	2.21	2.26	2.57	2.68	2.92
698	2.42	0.29	0.14	0.98	1.96	2.15	2.23	2.39	2.63	2.73	2.92
699	2.36	0.28	0.18	1.18	1.91	2.12	2.18	2.33	2.53	2.64	2.92
700	2.42	0.31	0.15	1.15	1.93	2.14	2.22	2.39	2.60	2.73	3.00
701	2.32	0.22	0.15	1.05	1.96	2.17	2.17	2.29	2.46	2.54	2.70
702	2.29	0.26	0.16	1.01	1.92	2.05	2.10	2.27	2.45	2.55	2.78
703	2.34	0.24	0.09	1.14	1.92	2.12	2.18	2.32	2.49	2.57	2.73
704	2.35	0.25	0.00	1.08	1.91	2.12	2.18	2.35	2.51	2.59	2.78
705	2.32	0.24	0.22	1.07	1.94	2.12	2.17	2.28	2.48	2.57	2.75
706	2.37	0.23	0.13	1.09	2.02	2.15	2.22	2.35	2.51	2.60	2.79
707	2.37	0.23	0.06	1.02	2.02	2.15	2.23	2.37	2.54	2.60	2.79
708	2.38	0.21	0.21	1.07	2.06	2.19	2.24	2.35	2.52	2.60	2.79
709	2.33	0.23	0.06	1.08	1.95	2.11	2.19	2.32	2.49	2.56	2.74
710	2.36	0.23	0.11	0.93	1.99	2.14	2.20	2.34	2.53	2.61	2.74
711	2.26	0.22	0.03	1.01	1.88	2.05	2.11	2.25	2.41	2.48	2.62
712	2.40	0.25	0.02	0.95	1.99	2.15	2.23	2.39	2.57	2.66	2.78

Figure 84. Replication exercise. Results of analyses of 25 consecutive 1m × 5cm surface sediment samples from the eastern end of line 9.
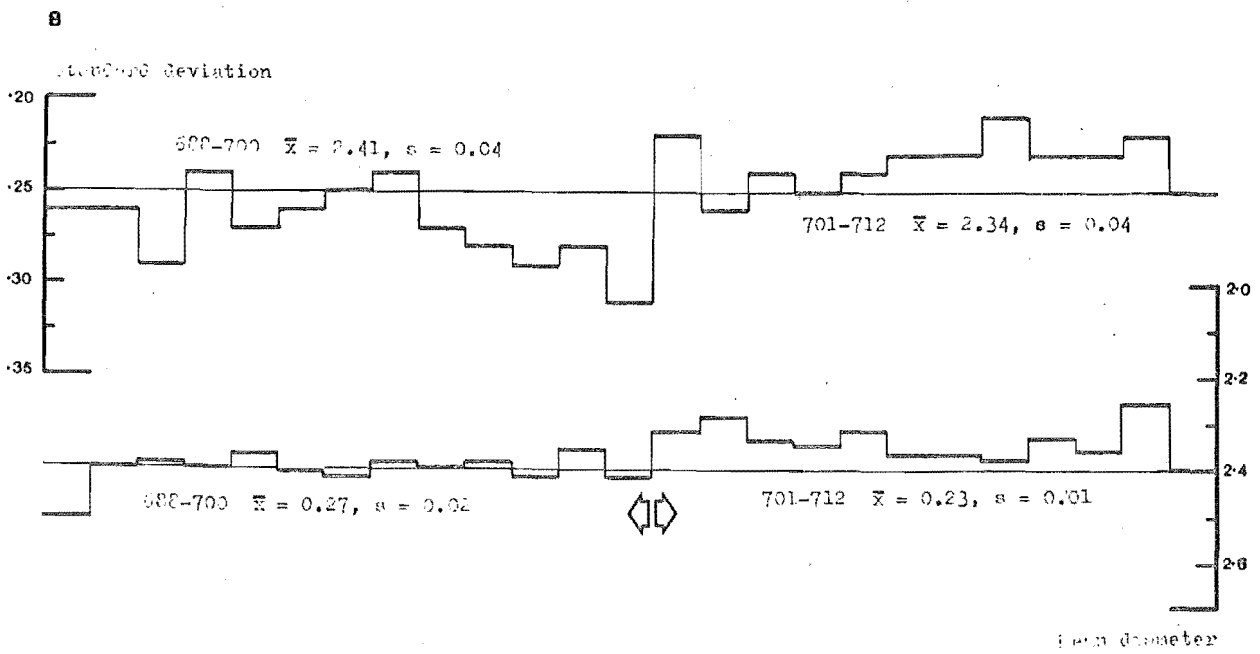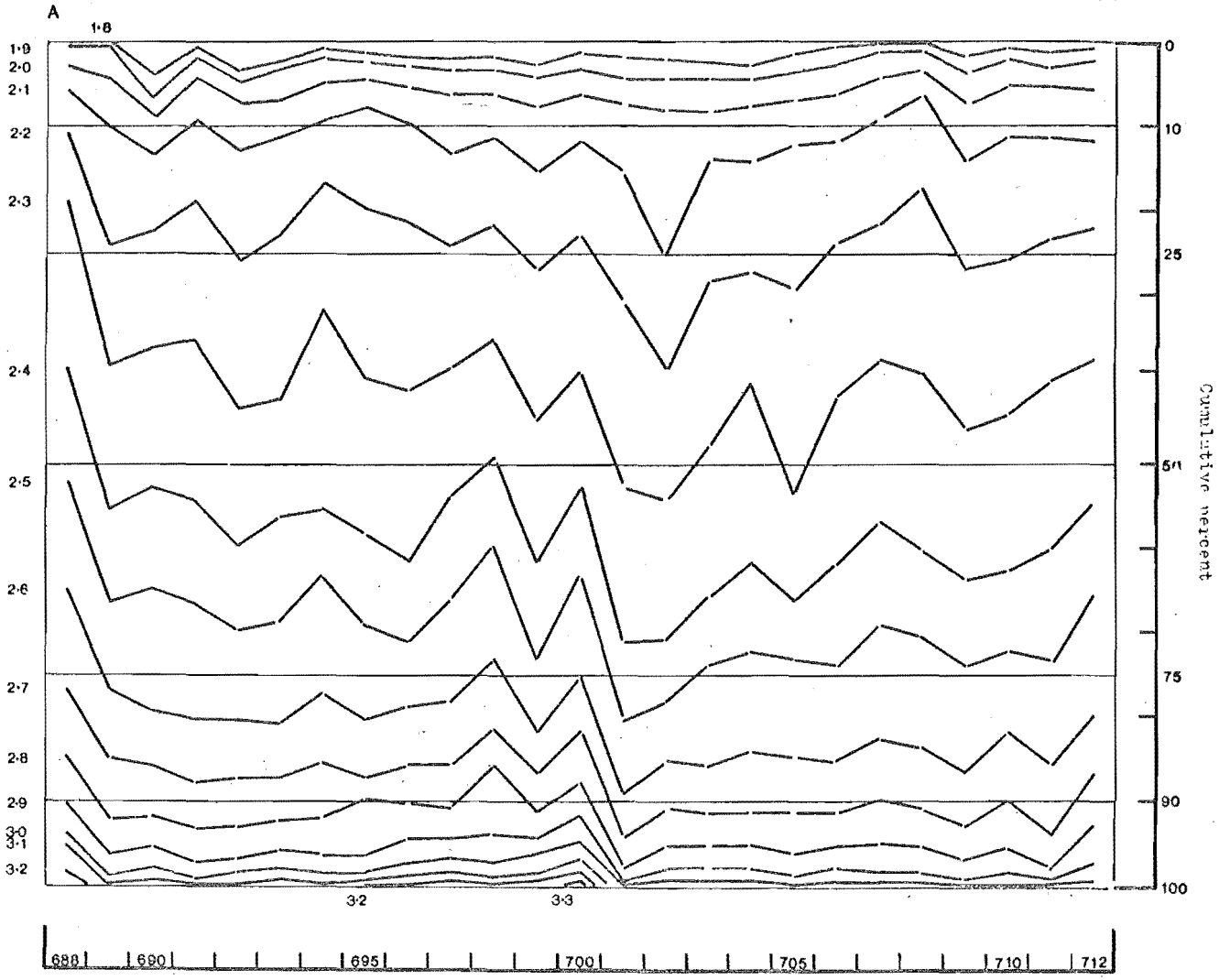
Figure 85.   Replication exercise.   Sequential variation in granulometric properties
of 25 consecutive 1m x 5cm surface sediment samples. Data from Figure 35.
A – Sequential changes in cumulative perecentages of 0.1psi intervals, from 1.8psi
to 3.3psi.   B – Sequential changes in graphic statistics.

normal 10 cm × 10 cm sample from anywhere along the run would have adequately represented it.

Appendix 4. Detailed descriptive and graphic logs, subsurface sediment cores from the Avon-Heathcote Estuary. A - Graphic log layout. B - Sediment key. Individual logs follow on subsequent pages.

cm

Graphic log

Sample location

Sample number

555

Sand fraction graphic standard deviation

Depth below surface (cm)   10

Sand fraction mean grain size

Percent mud

Medium sand ($M_z > 2.0$ psi)

Coarser fine sand (M_z 2.0-2.5 psi)

Finer fine sand (M_z 2.5-3.0 psi)

Very fine sand ($M_z < 3.0$ psi)

Sandy mud (> 50% mud)

Bioturbate sediment (mottled texture)

Olive plastic mud and sandy mud

Regularly, sparsely laminated sand and sandy mud.

Strongly laminated sand and sandy mud

Moderately laminated sand and sandy mud

Weakly laminated sand and muddy sand

Brown organic hash

Disarticulated bivalves

Articulated and living bivalves

Mud blebs comprise 1-10% of sediment

Wood fragment

Bored contact, burrows stuffed with overlying sediment

Angular or irregular bedding surface

CORE 2

651
652
679
678
677
676
675

cm

10

20

30

Percent mud	0	10	20	30	40	50	60	70
Sand fraction mean size	2·0	2·2	2·4	2·6	2·8	3·0	3·2	3·4
Sand fraction sorting		0·2		0·3		0·4		0·5

CORE 5

643
644
670
669

cm

10

20

30

	0	10	20	30	40	50	60	70
	2·0	2·2	2·4	2·6	2·8	3·0	3·2	3·4
		0·2		0·3		0·4		0·5

Text follows ▷

CORE 4

645
646
674
673
672
671

cm

10

20

30

Percent mud	0	10	20	30	40	50	60	70
Sand fraction mean size	2·0	2·2	2·4	2·6	2·8	3·0	3·2	3·4
Sand fraction sorting		0·2		0·3		0·4		0·5

CORE 6

641
642
668
667

cm

10

20

	0	10	20	30	40	50	60	70
	2·0	2·2	2·4	2·6	2·8	3·0	3·2	3·4
		0·2		0·3		0·4		0·5

CORE 7

639

640
666
665
664
663

CORE 9

635

636
655
656
657
658

Text follows ▶

CORE 10

713
714
715
716
717
718

CORE 8

637

638
662
661
660
659

Percent mud	0	10	20	30	40	50	60	70
Sand fraction mean size	2·0	2·2	2·4	2·6	2·8	3·0	3·2	3·4
Sand fraction sorting		0·2		0·3		0·4		0·5

Percent mud	0	10	20	30	40	50	60	70
Sand fraction mean size	2·0	2·2	2·4	2·6	2·8	3·0	3·2	3·4
Sand fraction sorting		0·2		0·3		0·4		0·5

	0	10	20	30	40	50	60	70
	2·0	2·2	2·4	2·6	2·8	3·0	3·2	3·4
		0·2		0·3		0·4		0·5
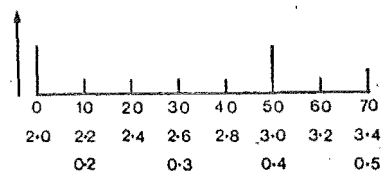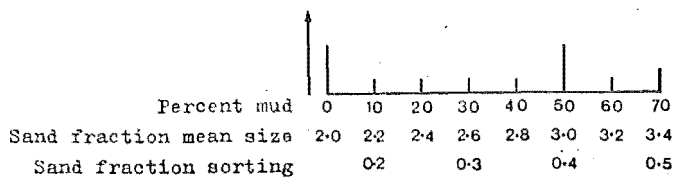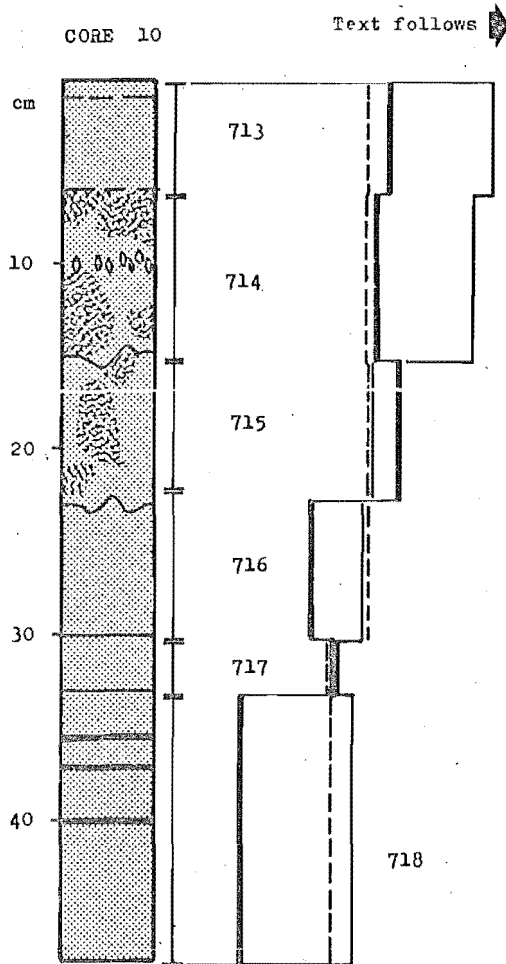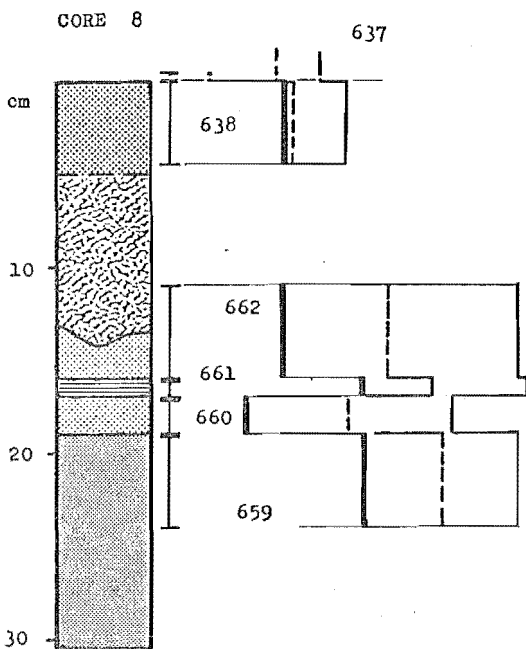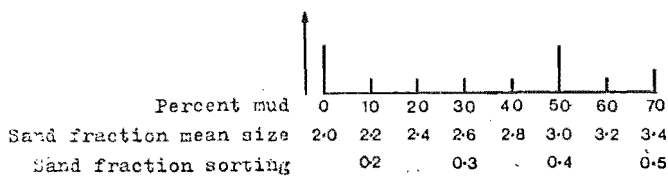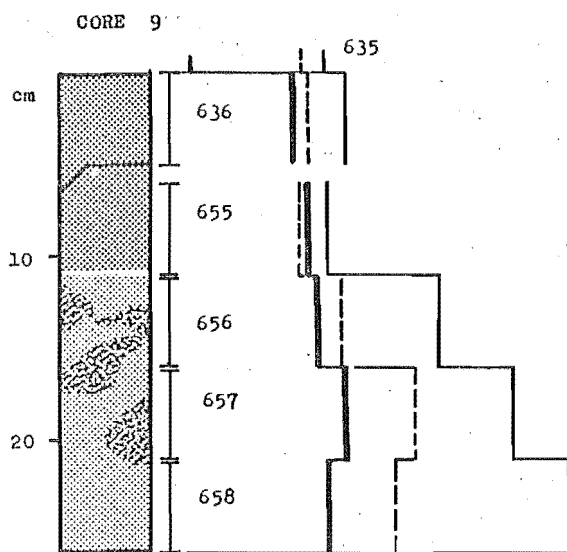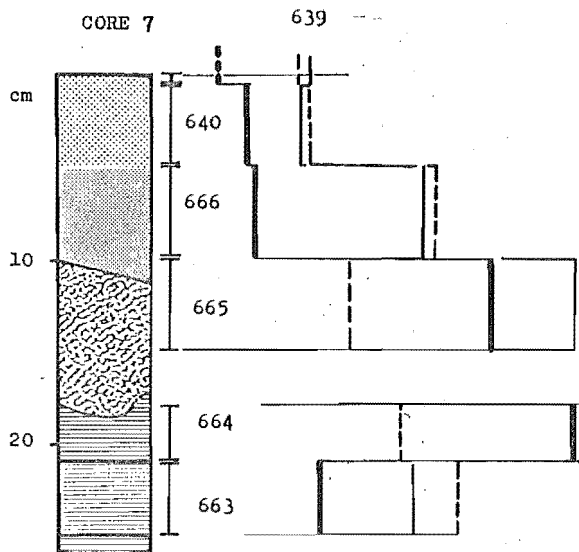
CORES 2, 4, 5, 6, 7, 8 and 9.   Heathcote Basin - Line 12.

Each of these cores can be seperated into three zones:
1. An upper, massive, shelly, sometimes muddy zone, from 2 to 3mm to about 5cm thick.
2. Below this upper layer was up to 15cm of dark grey and black mottled malodorous sediment, usually quite muddy and with a finer fine sand or very fine sand sized sand fraction. The contact between this mottled sediment and the overlying material may be gradational (as in cores 2, 4, 5 and 8), or quite sharp (cores 6, 7 and 9). The lower contact in all cases was quite abrupt.
3. A lowermost layered sequence - subsurface unit (b) sediment - of layered and massive sand and muddy sand, described in detail below:

CORE 2; 15cm-22cm, grey weakly laminated muddy very fine sand. 22cm-23cm, also at 25cm and 27cm, strongly laminated muddy very fine sand, seperated by 2cm-thick units of weakly laminated muddy very fine sand. 29cm-31cm, friable clean dark grey fine sand.

CORE 4; 15cm-22cm, weakly laminated muddy very fine sand. 22cm-23cm, strongly laminated very fine sand. 23cm-29cm, friable massive dark grey very fine sand. 29cm-33cm, very muddy strongly laminated very fine sand.

CORE 5; 16cm-20cm, weakly laminated muddy very fine sand. 20cm-22cm, clean friable fine sand, fining downwards. 22cm-25cm, strongly laminated muddy very fine sand. 25cm-25.5cm, massive muddy very fine sand. 25.5cm-27.5cm, less muddy massive very fine sand. 27.5cm-28.5cm, friable clean dark grey fine sand.

CORE 6; 12cm-18cm, weakly mottled and massive finer fine sand. 18cm-21.5cm, laminated very fine sand, grading from moderately laminated at the top to strongly laminated at the base. 21.5cm-26cm, friable clean dark grey fine sand.

CORE 7; 18cm-21cm, strongly laminated very muddy finer fine sand. 21cm-25cm, weakly laminated muddy very fine sand. 25cm-26cm, strongly laminated muddy very fine sand.

CORE 8; 14cm-16cm, muddy massive fine sand. 16cm-17cm, grey strongly laminated muddy very fine sand. 17cm-19cm, friable slightly muddy finer fine sand. 19cm-28cm, massive grey muddy very fine sand.

CORE 9; 11cm-27cm, massive and weakly mottled, sparsely shelly finer fine sand, tending to fine downwards.

CORE 10

0cm-6cm	Intermixed olive grey muddy very fine sand and dark grey and grey black muddy fine sand. Streaky vertical texture.
6cm-15cm	Mottled black and grey black muddy finer fine sand, with chalky fragile shell fragments and _in situ_ articulated shells of Cyclomactra
15cm-23cm	Grey black slightly mottled cohesive slightly plastic muddy finer fine sand.
23cm-30cm	Grey black friable finer fine sand.
30cm-48cm	Grey black friable fine sand, coarser than above, with 2mm-3mm thick cohesive mud layers at 33cm, 38cm, 39.5cm and 40cm.

CORE 11
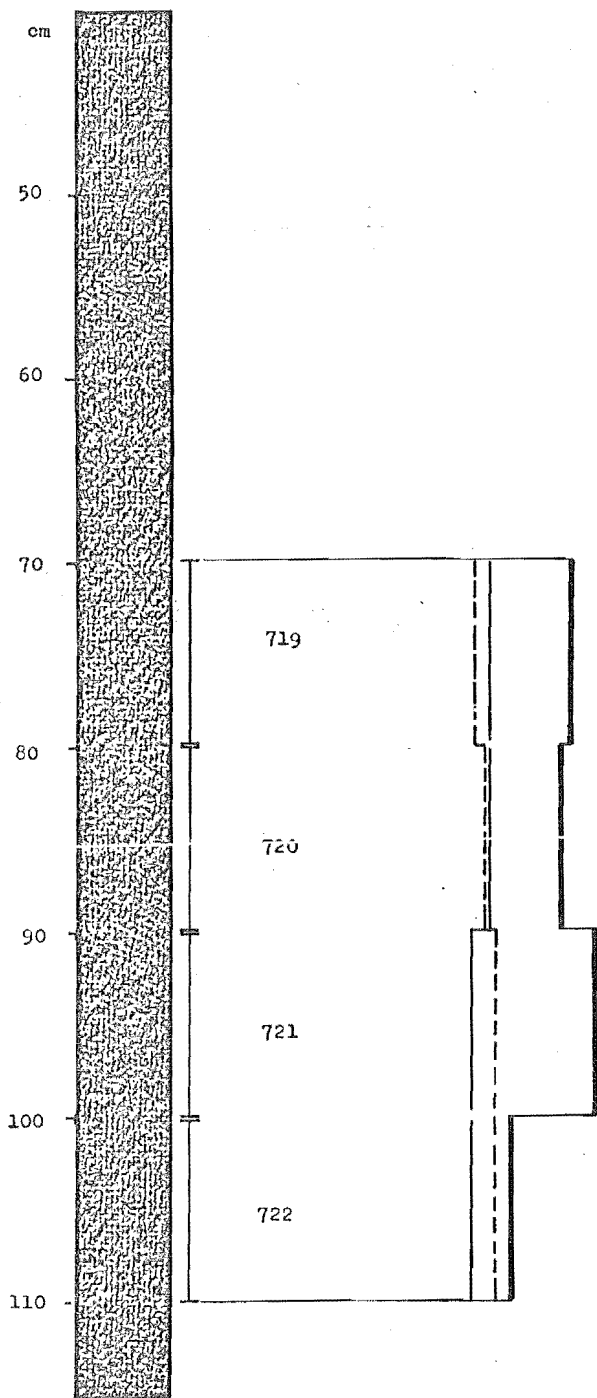
cm								
50								
60								
70								
	719							
80								
	720							
90								
	721							
100								
	722							
110								

Percent mud	0	10	20	30	40	50	60	70
Sand fraction mean size	2·0	2·2	2·4	2·6	2·8	3·0	3·2	3·4
Sand fraction sorting		0·2		0·3		0·4		0·5

CORE 12

cm								
	723							
10	724							
20								
30	725							
40								
50								
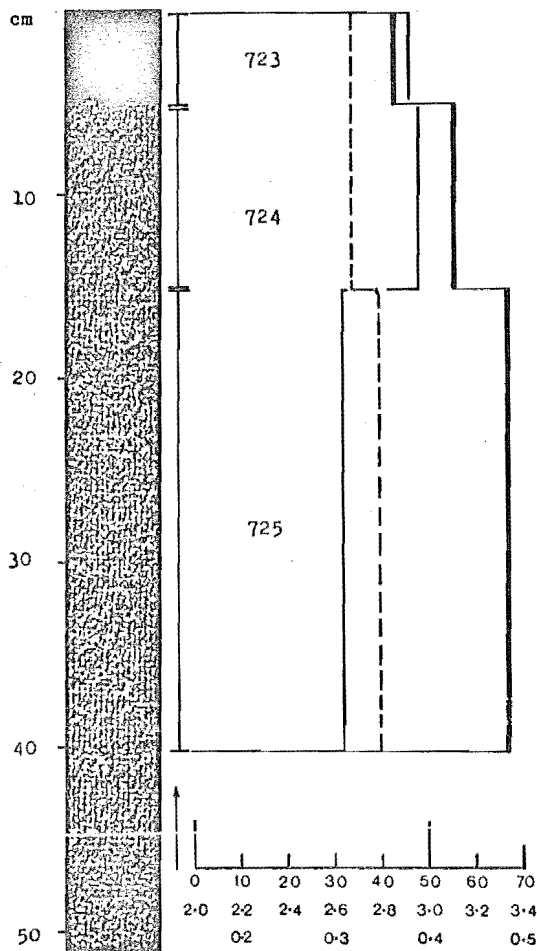
	0	10	20	30	40	50	60	70
	2·0	2·2	2·4	2·6	2·8	3·0	3·2	3·4
		0·2		0·3		0·4		0·5

CORE 12

Similar to core 11, sandier at the top,
otherwise monotonous, malodorous olive
grey mud.

CORE 11

75cm of sticky plastic medium dark grey
and olive grey mud. Slight fining upwards
trend (from 3.18 to 3.10 psi mean grain
size over the interval sampled) and slight
trend in colour, from dark grey at the base,
to olive grey near the top.

CORE 13

726

727

728

729

93%mud

Percent mud 0 10 20 30 40 50 60 70
Sand fraction mean size 2·0 2·2 2·4 2·6 2·8 3·0 3·2 3·4
Sand fraction sorting 0·2 0·3 0·4 0·5

0cm-7.5cm Olive grey weakly laminated plastic
malodorous mud. Abrupt lower contact.

7.5cm-15cm Massive friable grey sand.

15cm-35cm Mottled dark grey and medium
dark grey muddy very fine sand and fine sand

35cm-45cm Massive friable grey fine sand.

CORE 14

0-17cm Mottled medium grey and
dark grey muddy sand, apparently
fining upwards.

17cm-21cm Clean friable massive
dark grey sand.

21cm-37cm Massive or weakly mottled
very weakly laminated and plane-
bedded medium dark grey muddy sand.

37cm-44cm Clean massive monotonous
friable dark grey sand.

CORE 14

730

731

732

733

Percent mud 0 10 20 30 40 50 60 70
Sand fraction mean size 2·0 2·2 2·4 2·6 2·8 3·0 3·2 3·4
Sand fraction sorting 0·2 0·3 0·4 0·5

CORE 15

734

735

10

736

20

30

40

86% mud

93%mud
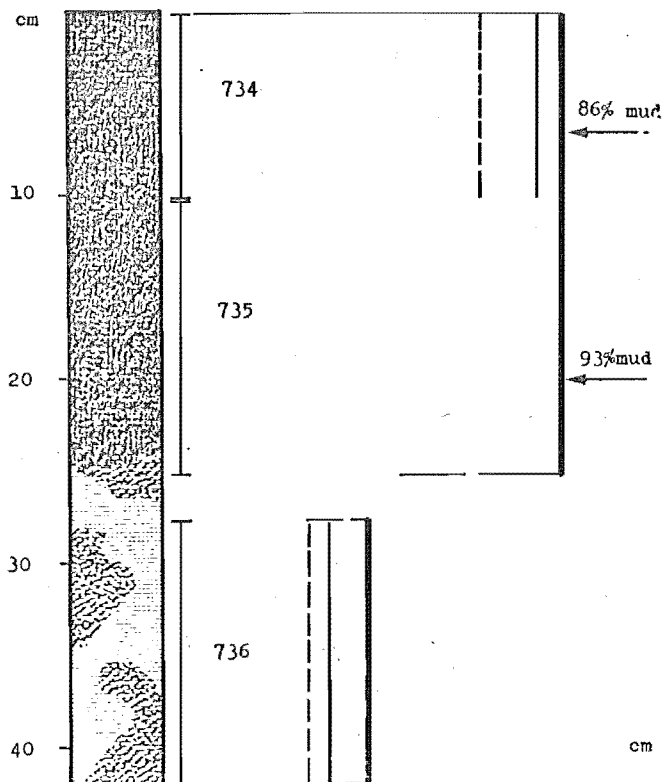
CORE 15

0-25cm Medium dark grey and olive grey
plastic malodorous mud. Weakly lamin-
ated at the top, grading down into sandy
mud and weakly laminated muddy sand.

25cm-45cm Dark grey weakly laminated
very fine sand and fine sand.
Mottled in part.

Percent mud	0	10	20	30	40	50	60	70
Sand fraction mean size	2·0	2·2	2·4	2·6	2·8	3·0	3·2	3·4
Sand fraction sorting		0·2		0·3		0·4		0·5

CORE 16

0-8cm Sandy mud and muddy very
fine sand mottled sediment.

8cm-30cm Olive grey and medium
dark grey plastic massive
monotonous malodorous mud.
Sandy layers at 30cm and 32cm,
sharp lower contact.

30cm-40cm+ Mottled muddy finer
fine sand and very fine sand.

CORE 16
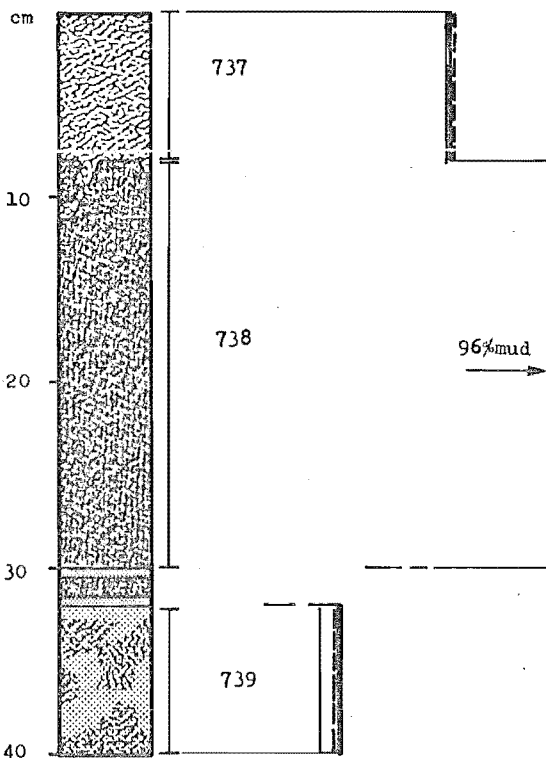
737

738

739

96%mud

Percent mud	0	10	20	30	40	50	60	70
Sand fraction mean size	2·0	2·2	2·4	2·6	2·8	3·0	3·2	3·4
Sand fraction sorting		0·2		0·3		0·4		0·5

CORE 17

cm

740

10

741

20

742

30

743

40

Percent mud   0   10   20   30   40   50   60   70
Sand fraction mean size   2·0 2·2 2·4 2·6 2·8 3·0 3·2 3·4
Sand fraction sorting   0·2   0·3   0·4   0·5
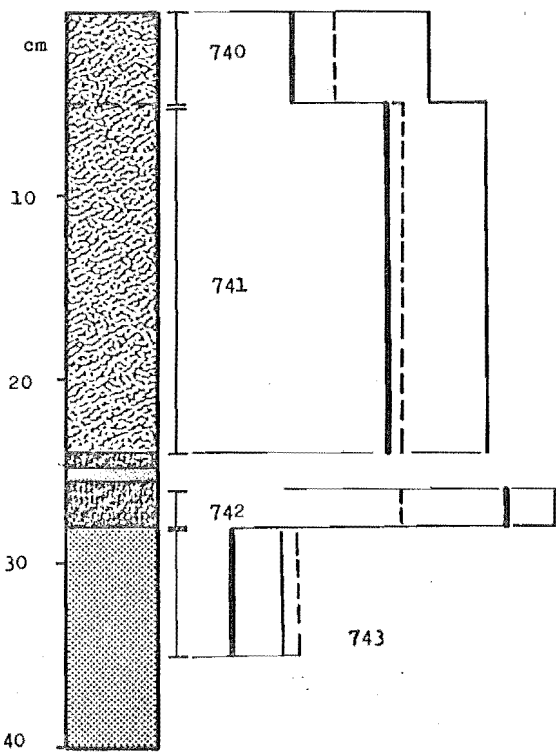
CORE 17

0–5cm Black and dark grey mottled muddy fine sand.
5cm–24cm Medium dark grey and dark grey mottled muddy fine sand.
24cm–28cm Olive grey mud and medium dark grey muddy fine sand; interbedded clean sandy zone.
28cm–40cm Dark grey clean friable massive fine sand.

CORE 18

cm

10

744

20

745

30

746

40
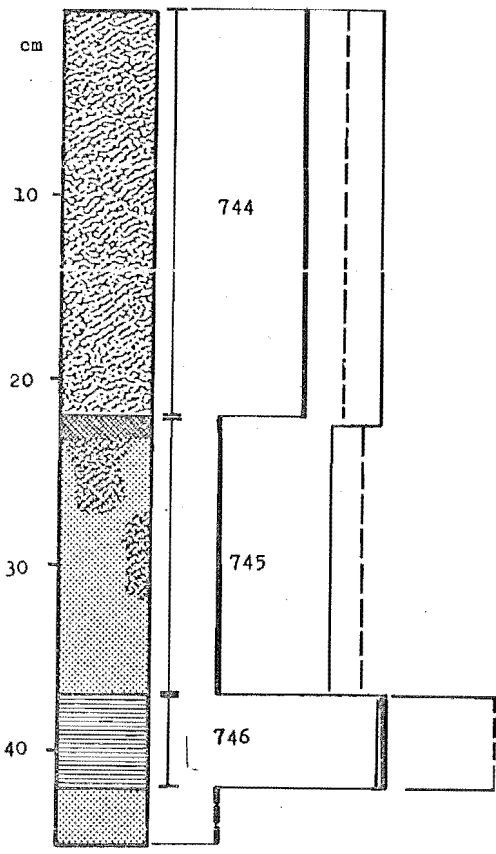
CORE 18

0–22cm Mottled black, dark grey and olive grey muddy finer fine sand.
22cm–37cm Massive dark grey friable slightly muddy fine sand, organic-rich at the top.
37cm–42cm Laminated dark grey sand and olive-grey muddy very fine sand.
42cm–45cm Massive friable clean fine sand.

Percent mud   0   10   20   30   40   50   60   70
Sand fraction mean size   2·0 2·2 2·4 2·6 2·8 3·0 3·2 3·4
Sand fraction sorting   0·2   0·3   0·4   0·5

CORE 19
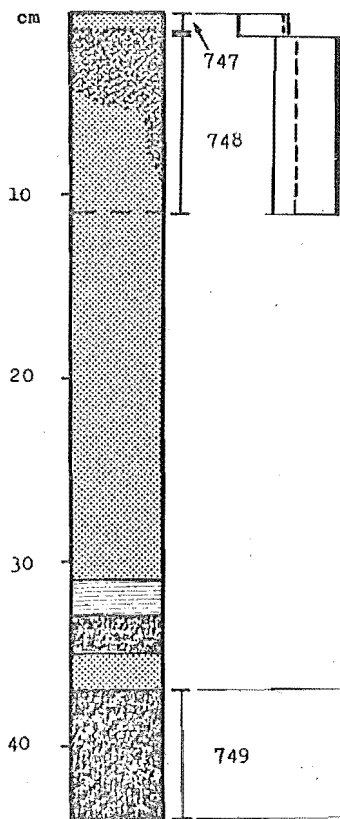
CORE 19

0-1cm	Dark grey friable massive sand.
1cm-11cm	Mottled olive grey mud and dark grey muddy sand.
11cm-31cm	Massive dark grey sand; friable and with little mud.
31cm-33cm	Weakly laminated muddy very fine sand and finer fine sand.
33cm-35cm	Mottled olive grey mud and fine sand.
35cm-37cm	Massive friable clean very fine sand.
37cm-44cm	Mottled olive grey mud and dark grey very fine and finer fine sand.

Percent mud	0	10	20	30	40	50	60	70
Sand fraction mean size	2·0	2·2	2·4	2·6	2·8	3·0	3·2	3·4
Sand fraction sorting		0·2		0·3		0·4		0·5

CORE 20

CORE 20

0-3cm	Grey friable clean massive sand.
3cm-8cm	Massive black and weakly mottled black and dark grey sand.
8cm-9.5cm	Cohesive muddy black fine sand.
9.5-13cm	Weakly laminated and sparsely mottled black and grey sand.
13cm-33cm	Weakly laminated dark grey fine sand; with a 1mm-2mm thick medium sand lamina at 13cm, intense mottling from 16cm-21cm, and fining upwards from coarser fine sand at the base.
33cm-44cm	Massive black sand, with light grey lamina at 36, 38 and 40cm. Weakly laminated from 42cm-44cm.

Percent mud	0	10	20	30	40	50	60	70
Sand fraction mean size	2·0	2·2	2·4	2·6	2·8	3·0	3·2	3·4
Sand fraction sorting		0·2		0·3		0·4		0·5

CORE 22

CORE 21

cm

681

682

683

684

685

686

687

758

759

760

cm

775

776

777

778

779

| 0 | 10 | 20 | 30 | 40 | 50 | 60 | 70 |

2·0 2·2 2·4 2·6 2·8 3·0 3·2 3·4

0·2 0·3 0·4 0·5

CORE 21

0-2.5cm Friable grey massive clean sand.

2.5cm-24cm Grey and black bioturbate
sand and muddy sand; layer of coarse
shell debris at 9cm; grading down through
a bored contact zone to structureless,
textureless, monotonous, malodorous,
plastic olive-grey mud.

CORE 22

Predominantly friable grey sand. Becomes
muddier towards the base, with muddy
zones at 24cm-29cm (20.29%), 39cm-49cm
(27.82%) and particularly at 83cm-84cm
(no sample) where plastic grey mud over-
lies a thick (1.5cm) brown organic hash
layer.

CORE 23

10cm
20
30
40cm

761
762
763
764
765

0cm-5cm Grey friable massive coarser fine sand.

5cm-13cm Weakly mottled dark grey and grey coarser fine sand, with mud blebs causing slight increase in muddiness towards the base.

13cm-27cm Massive dark grey sand with sparse fine shell debris (hash) at the top, grading to accasional disarticulated whole valves and coarse shelly debris at the base.

27cm-31cm Laminated olive-grey mud and muddy sand. Abrupt upper contact, abundant fine brown organic hash, especially at the base

CORE 24
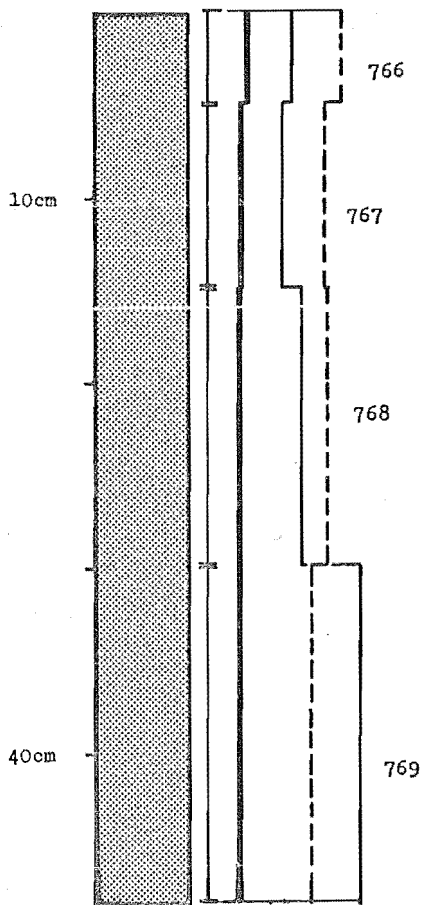
10cm
40cm

766
767
768
769

| Percent mud | 0 | 10 | 20 | 30 | 40 | 50 | 60 | 70 |
Sand fraction mean size | 2·0 | 2·2 | 2·4 | 2·6 | 2·8 | 3·0 | 3·2 | 3·4 |
Sand fraction sorting | 0·2 | 0·3 | 0·4 | 0·5 |

CORE 24

All massive grey friable sand. Slightly darker at 5cm-15cm, otherwise quite monotonous throughout.

| Percent mud | 0 | 10 | 20 | 30 | 40 | 50 | 60 | 70 |
Sand fraction mean size | 2·0 | 2·2 | 2·4 | 2·6 | 2·8 | 3·0 | 3·2 | 3·4 |
Sand fraction sorting | 0·2 | 0·3 | 0·4 | 0·5 |

CORE 26/27

cm

10

20

30

40

50

60

70

80

90

100

110

130

140

780

781

782

783

784

785

786

787

Ocm-14cm Bioturbate zone; Ocm-6cm, mottled blaxk muddy very fine sand, grading into a zone of contorted, intensely burrowed muddy layers, over 6cm-11cm, which becomeless disturbed towards the base, where weakly bioturbate muddy laminae alternate with very fine sand layers. Coarse brown organic hash layer at 14cm.

14cm-20cm Very muddy regularly laminated very fine sand with abundant brown hash, grading down into a pair of mud flasers(?), seperated by clean friable very fine sand.

20cm-25cm Massive very fine sand with sparse coarse organic hash.

25cm-38.5cm Massive and weakly laminated very fine sand. Layer of brown organic hash at 34.5cm.

38.5cm-45cm Massive very fine sand, grading up to weakly laminated muddier very fine sand.

45cm-50cm Massive very fine sand, with abundant (c. 10% by volume) fine brown hash; about 1cm of muddier very fine sand at the base.

50cm-56cm Weakly laminated slightly muddy very fine sand.

56cm-58cm Massive olive grey very fine sandy mud.

58cm-95cm Very weakly laminated muddy very fine sand; better laminated, with regular, brown hash-rich muddy laminae over the interval 80cm-90cm, and only sparsely laminated from 90cm-95cm.

95cm-96cm Massive olive grey very fine sandy mud.

96cm-104cm Massive olive grey very fine sandy mud, overlain by massive muddy very fine sand, grading up into weakly laminated, then modederately well laminated muddy very fine sand.

104cm-111cm Regularly laminated muddy very fine sand, grading up into massive very fine sandy mud.

111cm-145cm Clean friable grey massive finer fine sand, grading down into coarser fine sand.

	0	10	20	30	40	50	60	70
	2·0	2·2	2·4	2·6	2·8	3·0	3·2	3·4
		0·2		0·3		0·4		0·5

Percent mud   0   10   20   30   40   50   60   70

Sand fraction mean size   2·0   2·2   2·4   2·6   2·8   3·0   3·2   3·4
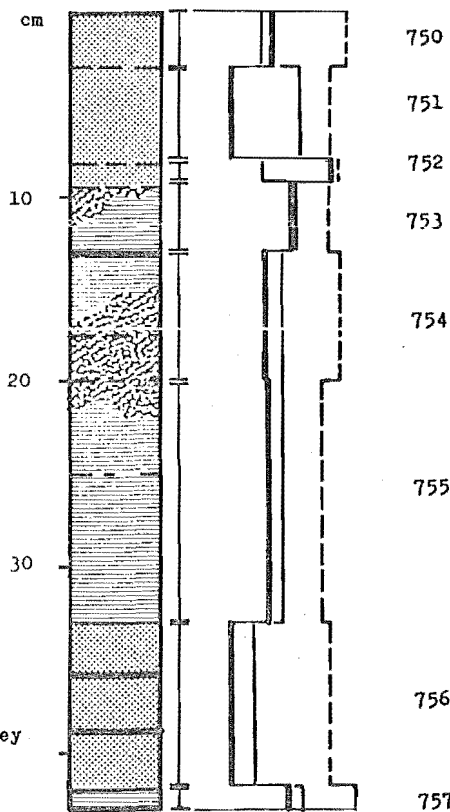
Sand fraction sorting   0·2   0·3   0·4   0·5

CORE 28/29

28/29 Ctd.

cm

788

80

10

20

CORE 46

0cm-16cm Grey friable muddy finer fine
sand at the top, grading at 5cm-6cm
into black and dark grey mottled
muddy finer fine sand and very fine
sand.

cm

16cm-64cm Mottled and patchy grey and
black muddy very fine sand, muddy
finer fine sand and coarser fine sand,
with a layer of coarser fine sand over
the interval 51cm-55cm.

30

64cm-68cm Massive muddy coarser fine
sand.

10

68cm-70cm Clean friable dark grey
coarser fine sand.

70cm-71cm Muddy massive very fine sand
overlying 0.25cm of massive olive
grey mud.

40

71cm-74cm Basal massive mud layer
overlain by weakly laminated muddy
finer fine sand.

20

74cm-80cm Mottled mud and muddy very
fine sand.

0cm-18.5cm Mottled muddy finer fine
sand and very fine sand, shelly at
about 10cm.

50

18.5cm-40cm Massive malodorous olive
grey plastic mud.

30

40cm-50.5cm Abrupt basal contact,
grading up through slightly muddy
weakly laminated finer fine sand and
very fine sand, to 2cm of massive
muddy very fine sand, at the top.

60

50.5cm-59cm Massive shelly dark grey
friable clean coarser fine sand.

789

40

790

70

50

Percent mud	0	10	20	30	40	50	60	70
Sand fraction mean size	2·0	2·2	2·4	2·6	2·8	3·0	3·2	3·4
Sand fraction sorting		0·2		0·3		0·4		0·5

CORE 30   CORE 33   CORE 34A   CORE 34B

CORE 30   0cm-15cm Mottled dark grey and black muddy very fine sand and finer fine sand.

15cm-19cm Massive clean grey friable finer fine sand.

19cm-23cm Massive clean slightly coarser fine sand.

23cm-25cm Weakly laminated slightly muddy very fine sand.

25cm-29cm Massive clean grey finer fine sand as above.

29cm-30cm Regularly laminated muddy very fine sand.

30cm-36cm Massive sand as above.

36cm-40cm Clean grey friable fine sand with 2%-5% millimetre-size very fine sandy mud blebs.

40cm-   Massive monotonous clean sand as above.

CORE 33   0cm-2cm   Friable grey fine sand.

2cm-11cm Massive black and weakly mottled black and grey-black slightly muddy fine sand.

11cm-23cm Grey mud and muddy very fine sand mottled with dark grey and black fine sand.

23cm-34cm Weakly laminated muddy very fine sand and very fine sand, grading upwards into massive medium grey muddy very fine sand.

34cm-37cm Clean to slightly muddy coarser fine sand, with sparse millimetre-size mud blebs.

37cm-   Weakly laminated slightly muddy finer fine sand and very fine sand.

CORES 34A and 34B   Both cores consist predominantly of dark grey massive, clean, friable coarser fine sand. In both there is a darker grey and grey-black mottled zone from 2cm to about 15cm. In 34A an abrupt, irregular contact at 10cm may be an erosional contact between two generations of mottled sediment. At 16cm in 34A there is abundant contorted slabs, 2cm to 3cm thick, of olive grey plastic mud, in a matrix of clean friable sand. Below this, to depths of 25cm-30cm, the sand contains blebs of millimetre-size grey plastic mud. At 25cm in 34B there is a 2mm-3mm thick light grey muddy very fine sandy layer.

CORE 32
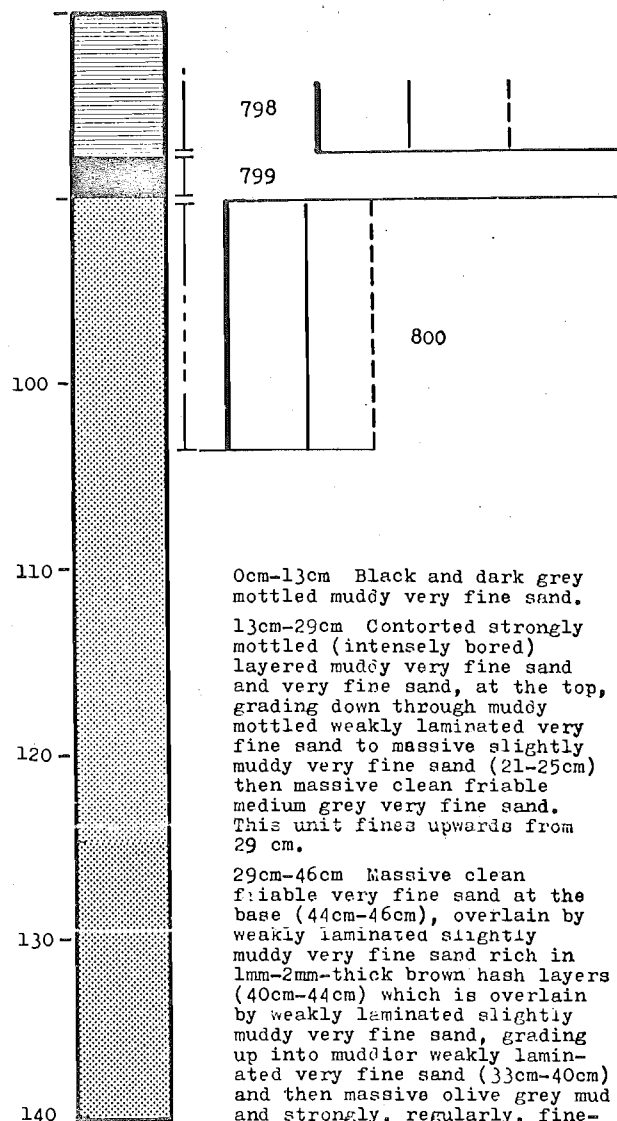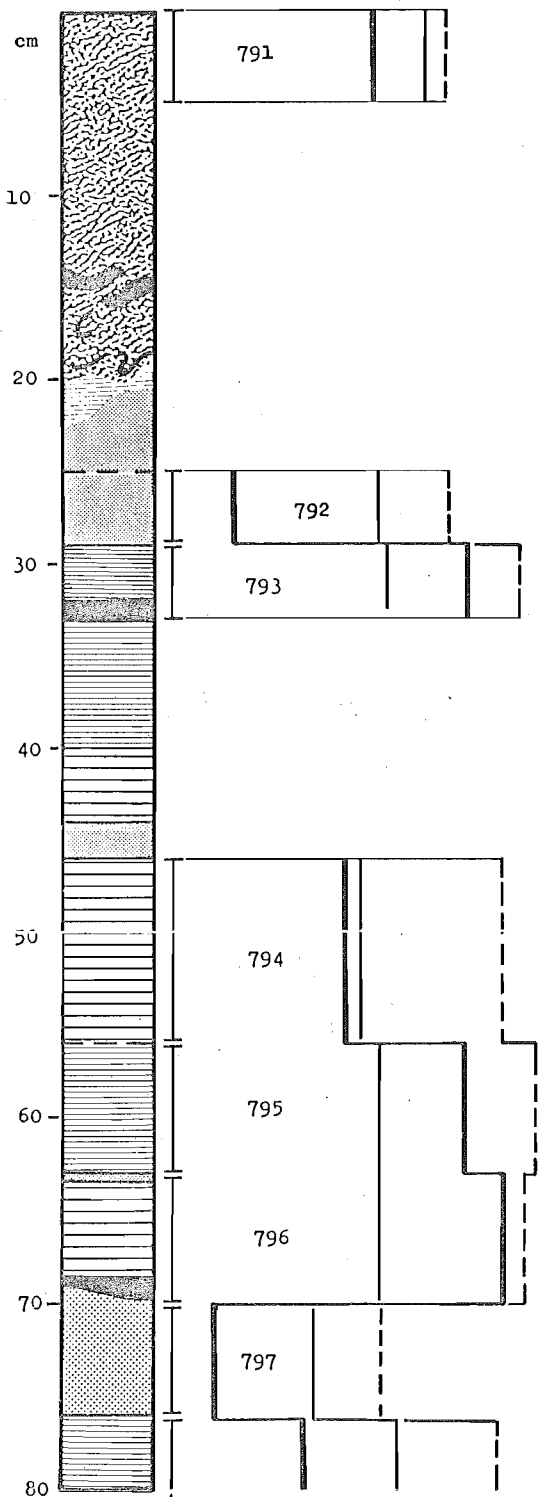
0cm-13cm Black and dark grey mottled muddy very fine sand.

13cm-29cm Contorted strongly mottled (intensely bored) layered muddy very fine sand and very fine sand, at the top, grading down through muddy mottled weakly laminated very fine sand to massive slightly muddy very fine sand (21-25cm) then massive clean friable medium grey very fine sand. This unit fines upwards from 29 cm.

29cm-46cm Massive clean friable very fine sand at the base (44cm-46cm), overlain by weakly laminated slightly muddy very fine sand rich in 1mm-2mm-thick brown hash layers (40cm-44cm) which is overlain by weakly laminated slightly muddy very fine sand, grading up into muddier weakly laminated very fine sand (33cm-40cm) and then massive olive grey mud and strongly, regularly, finely laminated very muddy very fine sand, rich in organic brown hash.

46cm-63cm Laminated muddy very fine sand, stronger, more regular lamination towrds the top, also less muddy and richer in brown organic hash towards the top. Abrupt upper and lower contacts.

63cm-69cm Olive grey massive mud grading up into regularly laminated very muddy very fine sand.

69cm-76cm Massive dark grey friable finer fine sand.

76cm-85.5cm Olive grey sandy mud gradingup into laminated slightly muddy very fine sand.

85.5cm-140cm Massive medium-dark grey, clean friable fine sand.

Percent mud	0	10	20	30	40	50	60	70
Sand fraction mean size	2·0	2·2	2·4	2·6	2·8	3·0	3·2	3·4
Sand fraction sorting		0·2		0·3		0·4		0·5

CORE 35

0cm-3cm Massive muddy friable finer fine sand.

3cm-15cm Mottled and intermixed dark grey sand and plastic olive grey mud, intensely bioturbated and rich in brown organic hash and coarse shelly debris. Gradational into:

15cm-35cm Olive grey plastic mud, weakly laminated in part.

35cm-45cm Intermixed olive grey plastic plastic mud and muddy very fine sand. 0.25cm-1.5cm-long slabs of plastic mud in a chaotic sandy matrix.

45cm-53cm Massive muddy finer fine sand, with 2-3mm-thick layers of coarse friable brown hash at 45cm and at 53cm.

53cm-70cm Abrupt angular(?erosional) basal contact, 0.5cm of olive grey very fine sandy mud at the base, grading up into weakly laminated muddy very fine sand, then into massive dark grey finer fine sand, with sparse blebs of olive grey plastic mud at 55cm-57cm.

70cm-73cm Friable massive coarser fine sand.

73cm-80cm Sequence similar to interval from 53cm to 70cm; 1cm of massive olive grey mud at the base, grading up into weakly laminated very muddy very fine sand, then up into medium dark grey massive very fine sand.

80cm-85cm Medium grey muddy very fine sand. Abrupt, angular basal contact.

85cm-133cm Massive clean dark grey friable coarser fine sand.

Percent mud	0	10	20	30	40	50	60	70
Sand fraction mean size	2·0	2·2	2·4	2·6	2·8	3·0	3·2	3·4
Sand fraction sorting		0·2		0·3		0·4		0·5

CORE 36

CORE 37

0cm-3cm Massive friable medium dark grey fine sand with abundant disarticulated shells.

3cm-6cm Black and dark grey mottled muddy fine sand.

6cm-15cm Laminated olive grey plastic mud.

15cm-26cm Clean friable slightly muddy very fine sand, with slabs and large (pebble-sized) blebs of olive grey plastic mud. Layer of sandy brown organic hash at 20cm.

26cm-40cm Massive dark grey friable coarser fine sand, with blebs of grey plastic mud from 26cm-30cm.
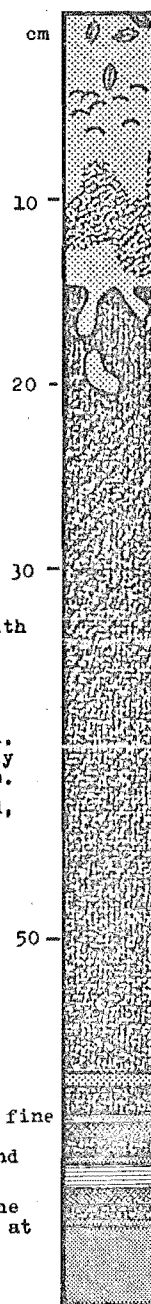
0cm-15cm Black and dark grey muddy fine sand and very fine sand, abundant living bivalves at the top; a layer of coarse (pebble-sized) plastic mud slabs at 3cm-4cm; and abundant disarticulated shells at 5cm-7cm.

15cm-65cm Massive olive grey plastic mud, bored at the top, interlaminated with sand and coarse organic hash at the base.

65cm-70cm Muddy very fine sand.

CORE 38
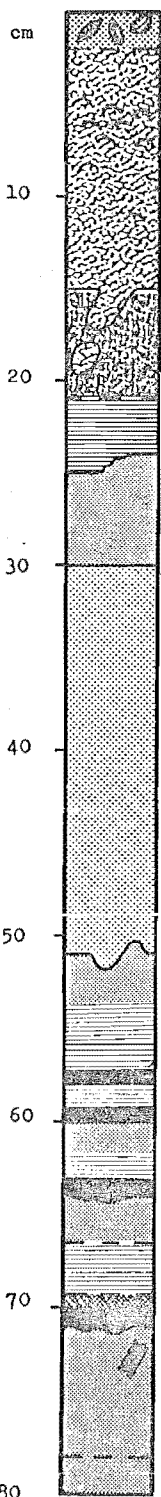
0cm-1.5cm   Grey friable coarser fine sand.

1.5cm-15cm   Mottled grey and black slightly muddy sand. Abundant coarse shell debris and disarticulated valves at 5cm-8cm.

15cm-21cm   Olive-grey massive plastic malodorous mud. Bored upper contact is sharp and abrupt, lower contact is gradational into strogly laminated mud and muddy very fine sand.

21cm-30cm   Abrupt lower contact, grading from massive muddy very fine sand, to muddier very fine sand, to laminated mud and sand at the top. Fining upwards.

30cm-51cm   Massive friable clean dark grey finer fine sand; abrupt irregular contact at the base; fining upwards to very fine sand over the upper 4cm.

51cm-71cm   Series of 4 fining downwards units (51-58, 58-60, 60-64, 64-71cm). Each with an irregular abrupt (erosional?) lower contact, 0.5-1.0cm of massive grey mud at the base, grading up into laminated muddy very fine sand, massive muddy finer fine sand, then massive clean finer fine sand. Abundant fine brown organic debris and hash layers, especially at 69cm.

Percent mud   0   10   20   30   40   50   60   70
Sand fraction mean size   2·0   2·2   2·4   2·6   2·8   3·0   3·2   3·4
Sand fraction sorting   0·2   0·3   0·4   0·5

814

817

815

818

71cm-78cm Massive slightly muddy very fine sand.

100

816

86cm-130cm Massive friable clean dark grey coarser fine sand.

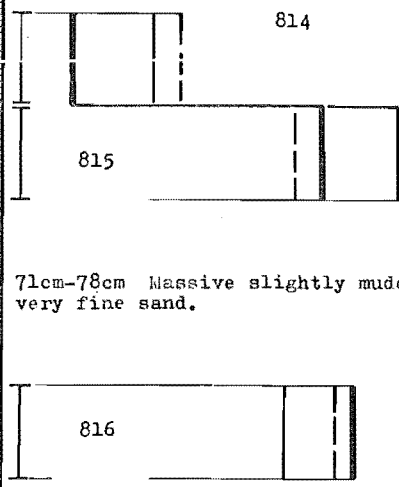78cm-86cm Strongly laminated very fine sandy mud, grading up into weakly laminated and massive very fine sand and finer fine sand.

Percent mud   0   10   20   30   40   50   60   70
Sand fraction mean size   2·0   2·2   2·4   2·6   2·8   3·0   3·2   3·4
Sand fraction sorting   0·2   0·3   0·4   0·5

CORE 39

cm

838

10 —

839 not analysed

90   843
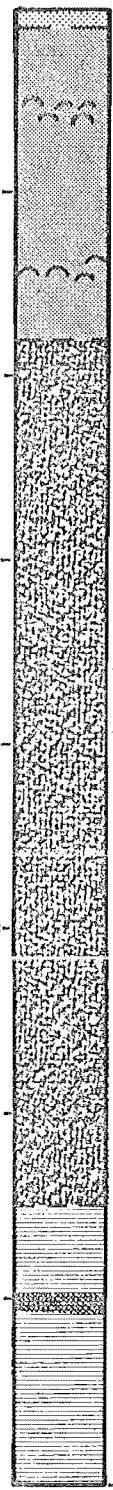
0cm-1cm Slightly muddy fine sand, with abundant living bivalves.

20 —

1cm-15cm Black and dark grey mottled, malodorous, muddy very fine sand; blebs of olive grey plastic mud and abundant coarse shelly debris at 5cm-7cm. Layer of disarticulated whole shells at 14cm.

844

845

30 —

14cm-18cm Gradation from mottled sand above, through medium grey slightly muddy very fine sand, into:

18cm-65cm Olive grey massive plastic malodorous veryfine sandy mud and mud

110

18cm-65cm Olive grey massive plastic malodorous very fine sandy mud and mud.

40 —

65cm-104cm Massive and very weakly laminated muddy very fine sand and very fine sandy mud, fining upwards from finer fine sand at the base, to very fine sand at the top. Rich in brown organic hash (c. 2-5% by volume in wet sediment) towards the top.

120

104cm-140cm Massive dark grey monotonous friable clean, coarser fine sand.

846

50 —

84% mud

60 —

840

0	10	20	30	40	50	60	70
2·0	2·2	2·4	2·6	2·8	3·0	3·2	3·4
	0·2		0·3		0·4		0·5

70 —

841

80 —   842

Percent mud

Sand fraction mean size

Sand fraction sorting

0	10	20	30	40	50	60	70
2·0	2·2	2·4	2·6	2·8	3·0	3·2	3·4
	0·2		0·3		0·4		0·5

CORE 40

cm
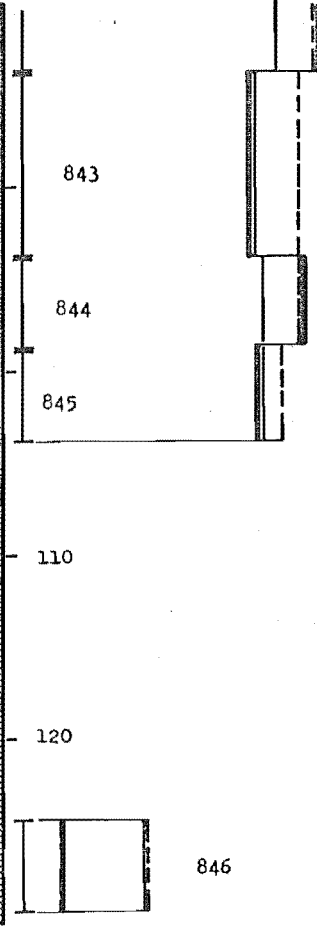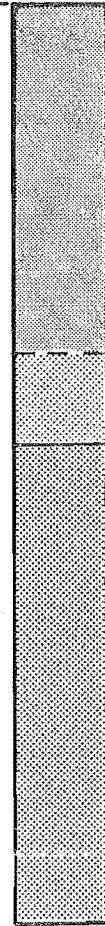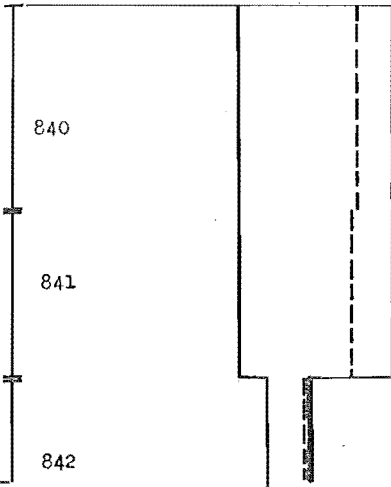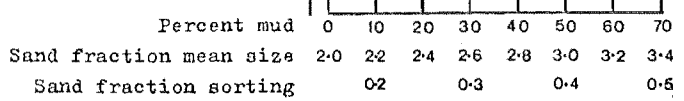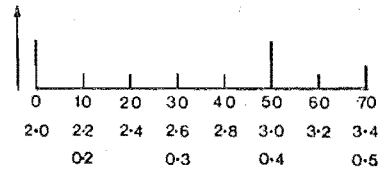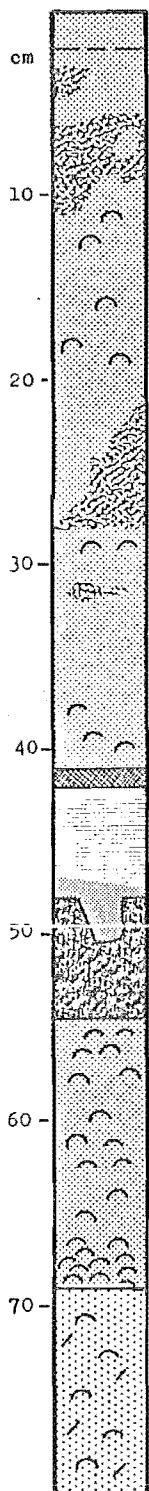
0cm-2cm Medium grey friable massive clean coarser fine sand.

2cm-41cm Mottled black and dark grey clean and slightly muddy friable fine sand. Sparsely shelly.

41cm-47cm Muddy finer fine sand, organic rich at the top, weakly laminated throughout, and slightly sandier at the base.

47cm-54.5cm Olive grey malodorous massive plastic mud.

54.5cm-69cm Shelly muddy very fine sand and fine sand, sparse millimetre-size blebs of plastic mud, otherwise massive.

69cm-96cm Massive dark grey friable medium sand, with sparse blebs of plastic mud and abundant coarse shelly debris.

96cm-140cm Massive dark grey clean friable medium sand.

80

90

852

110

120

130

140

847

848

849

850

851

Percent mud	0	10	20	30	40	50	60	70
Sand fraction mean size	2·0	2·2	2·4	2·6	2·8	3·0	3·2	3·4
Sand fraction sorting		0·2		0·3		0·4		0·5

CORE 41

CORE 47

0cm–2cm Grey friable fine sand.

2cm–35cm Olive-grey plastic massive, malodorous sparsely shelly mud. Bored upper contact with burrows stuffed with over-lying fine sand.

35cm–48cm Fining-upwards sequence, quite sandy at the base, grading up through weakly laminated very fine sand and muddy very fine sand, to weakly laminated very fine sandy plastic mud.

48cm–51cm Muddy finer fine sand with millimetre-thick grey mud ?flasers.

51cm–68cm Slightly muddy finer fine sand and very fine sand with blebs and stringers of plastic grey mud , shelly towards the base.

68cm–116cm Massive clean friable grey and medium-dark grey fine sand; sparse muddy horizons.

0cm–1cm Clean friable fine sand.

1cm–4cm Slightly muddy fine sand.

4cm–18cm Mottled dark grey and black slightly muddy finer fine sand and very fine sand. Abrupt lower contact.

18cm–33cm Massive grey muddy fine sand and very fine sand, shelly and less muddy at the base (fining upwards) and in stuffed burrows in underlying sediment.

33cm–43cm Olive-grey plastic mud as in CORE 41.

40cm

43cm–45cm Massive clean friable grey coarser fine sand.

CORE 41
continued
(80cm–116cm)

116cm

CORE 42

0-5cm Grey friable massive coarser fine sand.

5cm-35cm Medium-dark grey and black sparsely mottled friable coarser fine sand, grading from 20cm downwards into black massive coarser fine sand, and fining downwards to an abrupt lower contact.

35cm-48cm Medium grey and dark grey muddy finer fine sand. Abundant disarticulated shells, and weak sparse laminations at the top. Abrupt lower contact.

48cm-56cm Light olive grey massive muddy very fine sand.

56cm-105cm Massive clean medium grey friable fine sand, with laminated very fine sand and very fine sandy mud at 59cm-61cm, 62cm-65cm, 88cm-91cm.

Percent mud   0 10 20 30 40 50 60 70
Sand fraction mean size 2·0 2·2 2·4 2·6 2·8 3·0 3·2 3·4
Sand fraction sorting   0·2   0·3   0·4   0·5

CORE 43

2cm–5cm   Intensely bored streaky remnant of olive grey plastic mud. Overlain by 2cm of friable clean sand, and underlain by about 10cm of massive black slightly muddy, weakly mottled, sand.

15cm–41cm   Slightly muddy and muddy finer fine sand; strongly laminated at the top, where black sand, rich in fine organic hash, is stuffed into burrows and fills depressions in the bored upper contact. Less muddy and quite weakly laminated towards the base.

41cm–130cm Massive friable medium grey coarser fine sand. Quite monotonous in appearance.

832b

833

834

835

836

Percent mud   0   10   20   30   40   50   60   70
Sand fraction mean size   2·0 2·2 2·4 2·6 2·8 3·0 3·2 3·4
Sand fraction sorting   0·2   0·3   0·4   0·5

Letraset

CORE 44

cm

0cm-22cm Mottled black and dark
grey slightly muddy fine sand,
shelly at the base, and at 10cm.

22cm-33cm Muddy very fine sand
and fine sand with 0.75-1.25 cm
?flasers of massive olive grey
mud, rich in brown organic hash.

33cm-69cm Clean dark grey massive
friable coarser fine sand and
?medium sand.

0cm-5cm Grey friable massive
finer fine sand.

5cm-18cm Massive black and dark
grey friable sand, shelly at the
base.

18cm-31cm Massive and weakly
mottled black sand with blebs
of olive grey plastic mud (about
5% by volume).

31cm-43cm Friable finer fine sand;
with a layer of coarse brown and
black plant debris, small but
abundant disarticulated bivalves,
and small gastropods.

43cm-80cm Olive grey malodorous
massive plastic mud.

CORE 25

cm

770

771

772

773

774a

774b

774b is 98.1% mud
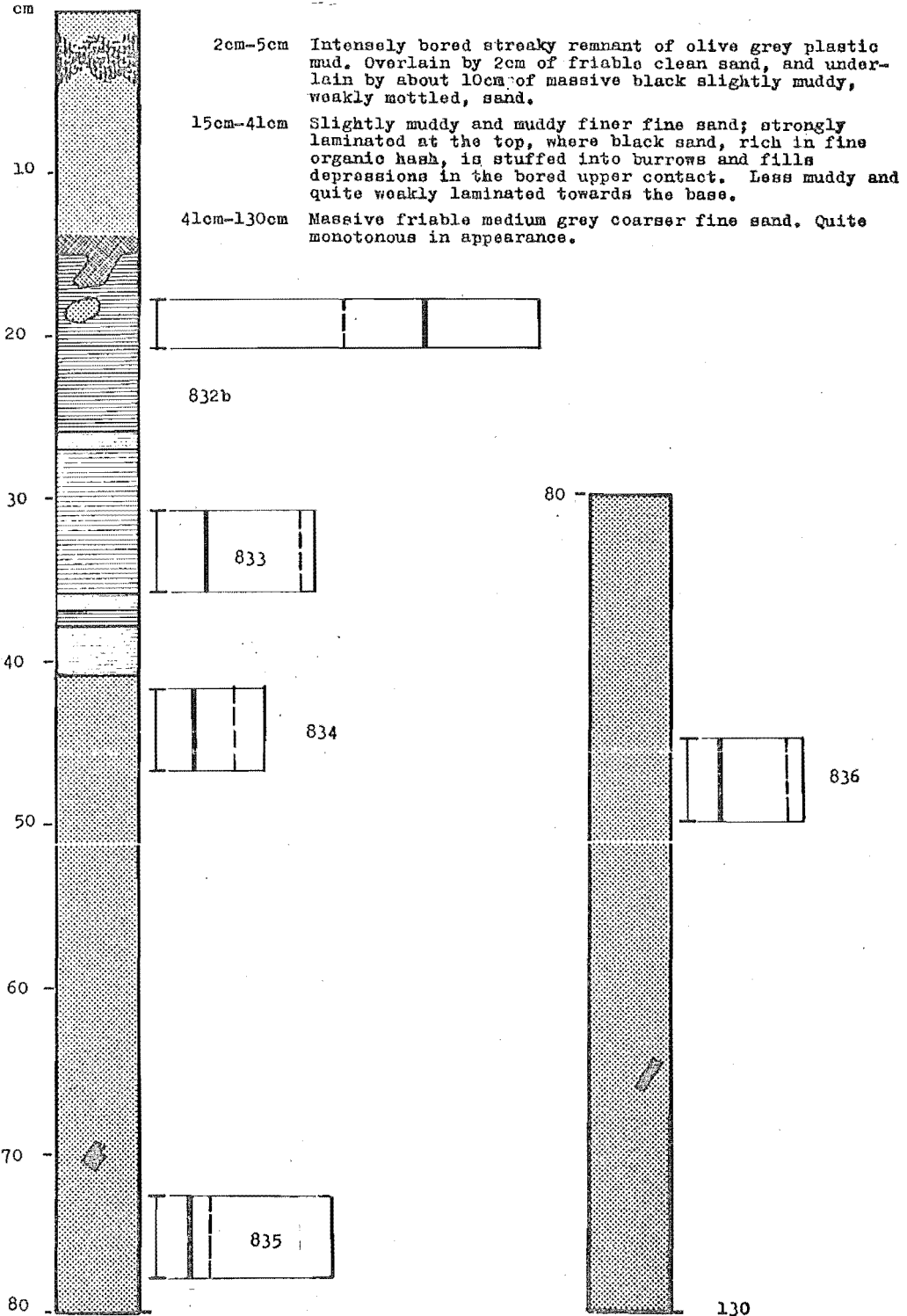
Percent mud   0   10   20   30   40   50   60   70
Sand fraction mean size   2·0   2·2   2·4   2·6   2·8   3·0   3·2   3·4
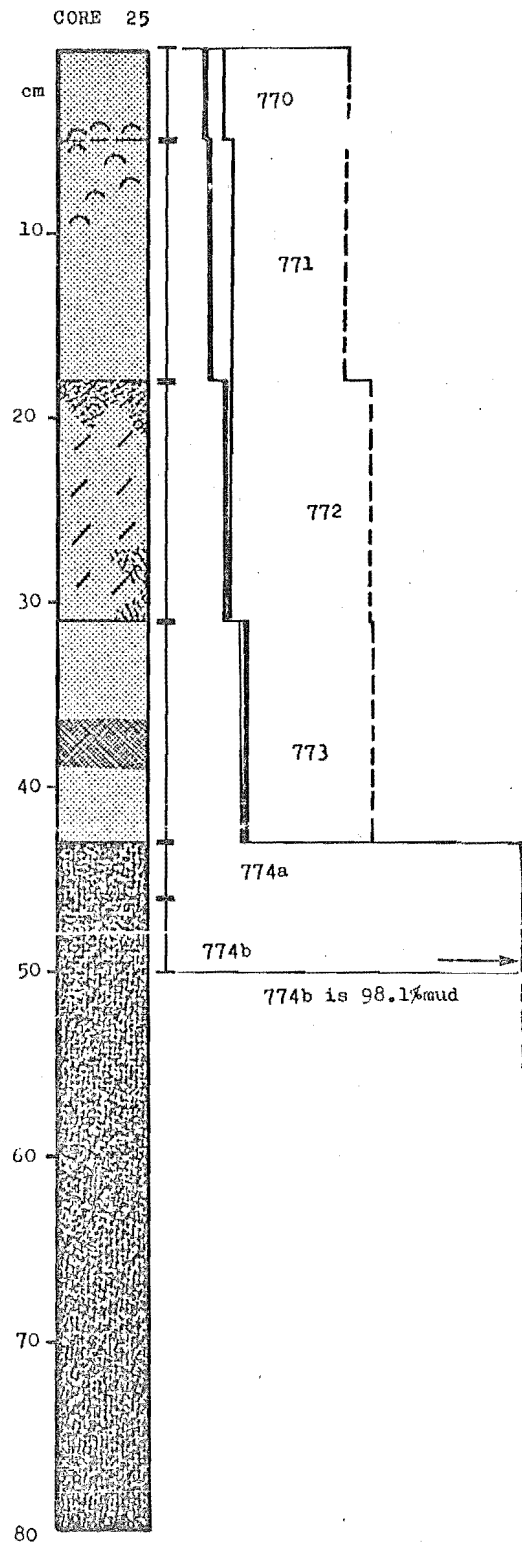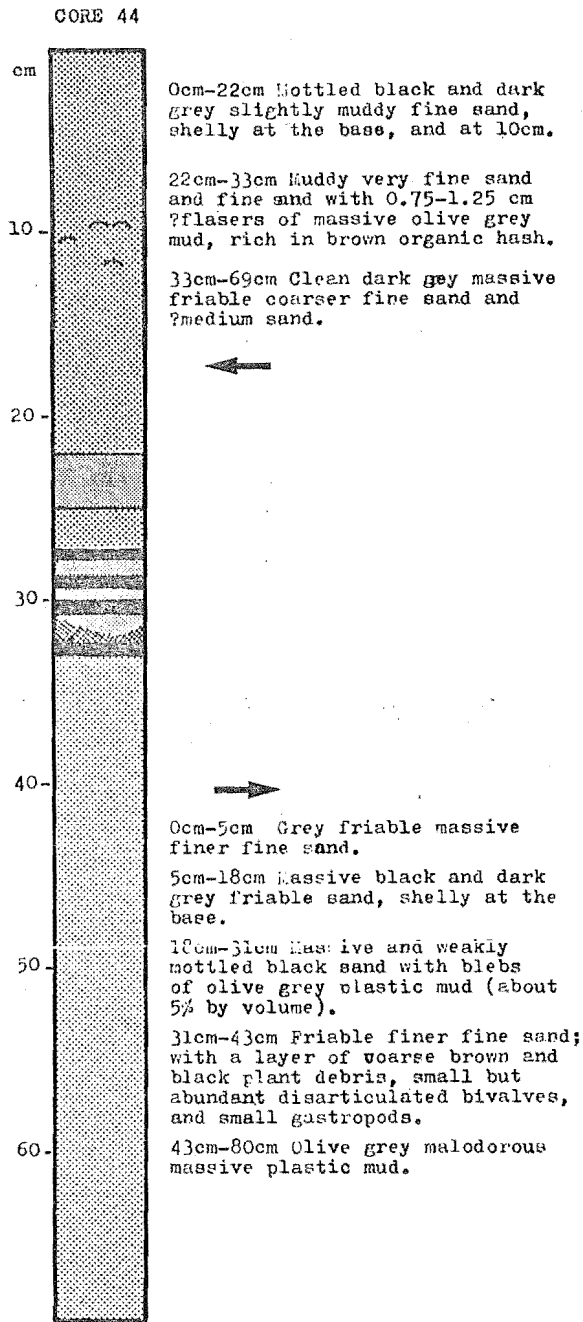Sand fraction sorting   0·2   0·3   0·4   0·5